

Unsaturated Soil Concepts and Their Application in Geotechnical Practice

Edited by
D. G. Toll

*University of Durham,
School of Engineering,
Durham, U.K.*

Reprinted from *Geotechnical and Geological Engineering*, Vol. 19(3–4). 2001



SPRINGER-SCIENCE+BUSINESS MEDIA, B.V.

Table of Contents

Preface	185–187
Papers	
A. TARANTINO and L. MONGIOVÌ / Experimental procedures and cavitation mechanisms in tensiometer measurements	189–210
DAIZO KARUBE and KATSUYUKI KAWAI / The role of pore water in the mechanical behavior of unsaturated soils	211–241
W. SCOTT SILLERS, DELWYN G. FREDLUND and NOSHIN ZAKERZADEH / Mathematical attributes of some soil–water characteristic curve models	243–283
S. S. AGUS, E. C. LEONG and H. RAHARDJO / Soil–water characteristic curves of Singapore residual soils	285–309
E. ROMERO, A. GENS and A. LLORET / Temperature effects on the hydraulic behaviour of an unsaturated clay	311–332
SANDRA L. HOUSTON, WILLIAM N. HOUSTON, CLAUDIA E. ZAPATA and CHRIS LAWRENCE / Geotechnical engineering practice for collapsible soils	333–355
D. A. CAMERON / The extent of soil desiccation near trees in a semi-arid environment	357–370
H. RAHARDJO, X.W. LI, D. G. TOLL and E. C. LEONG / The effect of antecedent rainfall on slope stability	371–399
Technical Note	
K. K. AUNG, H. RAHARDJO, E. C. LEONG and D. G. TOLL / Relationship between porosimetry measurement and soil–water characteristic curve for an unsaturated residual soil	401–416

A C.I.P. Catalogue record for this book is available from the Library of Congress.

ISBN 978-90-481-5918-5 ISBN 978-94-015-9775-3 (eBook)
DOI 10.1007/978-94-015-9775-3

Printed on acid-free paper

All Rights Reserved
© 2001 Springer Science+Business Media Dordrecht
Originally published by Kluwer Academic Publishers in 2001
Softcover reprint of the hardcover 1st edition 2001

No part of the material protected by this copyright notice may be reproduced or utilized in any form or by any means, electronic or mechanical, including photocopying, recording or by any information storage and retrieval system, without written permission from the copyright owner.



Preface

Special Issue on Unsaturated Soil Concepts and Their Application in Geotechnical Practice

This collection contains contributions from leading researchers on the engineering behaviour of unsaturated soils. Many of the major international research groups investigating these topics are represented here. It includes contributions dealing with the measurement of suction, discussions about how pore-water affects the engineering behaviour of soils and the important role played by soil–water characteristic (water retention) curves. This leads on to applications of unsaturated soil behaviour within geotechnical engineering practice, dealing with collapsible soils, foundations and slopes.

The first contribution deals with one of the most difficult areas in the investigation of unsaturated soils; the measurement of suction. Tarantino and Mongiovi (Italy) describe the experimental procedures for direct measurement of metric suction. The ability to make direct measurement of pore-water pressure below -100 kPa has been a major breakthrough in the last decade, with devices being developed at Imperial College, London, UK and at University of Saskatchewan, Canada. Tarantino and Mongiovi describe their procedure for preparing one of these devices (the Imperial College tensiometer) to restrict cavitation. Following their procedures, they were able to measure pore-water tensions greater than 2 MPa, a very major achievement indeed.

The contribution from Karube and Kawai (Japan) brings together many of the concepts developed by Professor Karube and his group at Kobe University, Japan over a long career research unsaturated soils. They look at the way pore-water is held within unsaturated soils and consider how stresses are carried by the soil skeleton and the water. They consider how these concepts can be used within an elasto-plastic model for unsaturated soil behaviour. They point out that current models cannot handle hysteresis between wetting and drying, an important feature of unsaturated behaviour. They go on to present a model for water retention (soil–water characteristic) curves that does consider hysteresis and also the effect of changes in void ratio.

Sillers, Fredlund and Zakerzadeh (Canada) continue the discussion about soil–water characteristic curves by looking at the various models that can be used to fit experimental data. They review models from Gardner's first equation in 1956 through to later, more complex models. The models are set within a consistent framework. Derivations and derivatives are presented. I am sure it will become the definitive reference for those who need to check the equations for a particular

model. They conclude that the models using three fitting parameters provide the best fit over a wide range of suctions.

Models for soil–water characteristic curves are only useful if we have experimental data on which to base them. Agus, Leong and Rahardjo (Singapore) present a large number of experimental soil–water characteristic curves determined for two types of residual soil from Singapore. They present data for eight different sites. This data set allows them to relate the parameters of the soil–water characteristic curves to index properties. They conclude that the relationships derived are suitable to provide a quick preliminary estimate of a soil–water characteristic curve.

The importance of soil–water characteristic curves is emphasized by another contribution dealing with this topic. Aung, Rahardjo, Leong and Toll (Singapore) investigate the relationship between mercury intrusion porosimetry measurements and soil–water characteristic curves. The porosimetry measurements are presented as soil–air characteristic curves. The slopes of the soil–air characteristic curves are found to be similar to the slopes of the soil–water characteristic curves. The equivalent pore diameters calculated from the mercury entry value and the air entry value appear to be related. Therefore, it is suggested that porosimetry data can be used to construct an estimate of the soil–water characteristic curve.

Romero, Gens and Lloret (Spain) look at temperature effects on both the water retention (soil–water characteristic) curves and the permeability of water (hydraulic conductivity). This is an important issue in the design of engineering barriers for radioactive waste disposal. However, experimental difficulties become even greater when the additional variable of temperature is included. From their very high quality experimental data they find that there is a shift in the soil–water characteristic curve if the temperature is increased from 22°C to 80°C. An equation is presented for fitting soil–water characteristic curves, which includes the temperature effect. They also find that water permeability is not dependent on temperature but is highly dependent on void ratio and degree of saturation.

The first application of unsaturated soil mechanics in the collection is presented by Houston, Houston, Zapata and Lawrence (USA). They review the problems associated with unsaturated collapsible soil with particular reference to the impact of urbanisation in arid regions. They use their considerable experience of identifying and characterising collapsible soils to give very practical guidelines on how to tackle the problem. They note that estimating the extent and degree of wetting is the most difficult task and suggest ways to do this. They also discuss possible mitigation measures.

Cameron (Australia) investigates an equally difficult problem; design of shallow footings on expansive/shrinkable soils. He looks particularly at the effects of trees and the influence they have on suction profiles in the ground. He reports on measured suction profiles adjacent to trees in a semi-arid region of Australia. It is shown that the drying effect due to trees extends below what would normally be considered as the zone within which movements occur. He presents preliminary design guidelines for estimating the extra settlement caused by the proximity of trees.

To complete the collection, Rahardjo, Li, Toll and Leong (Singapore) examine the effect of antecedent rainfall on slope stability. They present a case study on the Nanyang Technical University campus in Singapore where a spate of twenty landslides occurred following a single large storm event. However, they contrast this with similar size storm events that had not led to landslides. The difference in the case that did produce landslides was the amount of rain that had fallen on preceding days. Numerical modelling showed that the additional antecedent rainfall was sufficient to lower the factor of safety of a slope to close to unity, consistent with the failures that occurred.

I hope this collection is seen to be valuable both in contributing to the research effort on unsaturated soil behaviour and also in showing how unsaturated soil concepts can be applied within geotechnical engineering practice. We still have much to learn about unsaturated soils. Nevertheless, we are making significant headway in establishing rational approaches to dealing with these complex circumstances.

David Toll

Editor



Experimental procedures and cavitation mechanisms in tensiometer measurements

A. TARANTINO and L. MONGIOVÌ

Dipartimento di Ingegneria Meccanica e Strutturale, Università degli Studi di Trento, Trento, Italy (Fax: ++39 0461 882599; e-mail: tarantin@ing.unitn.it)

(Received 23 August 2000; revised 18 January 2001; accepted 1 May 2001)

Abstract. In recent years tensiometers for direct measurement of matric suction have been developed at Imperial College and later on at the University of Saskatchewan. The major drawback of these instruments is water cavitation which may occur before pressure equalisation. A better understanding of the mechanisms that control cavitation inside the tensiometer may therefore help optimise their design and define adequate experimental procedures. This paper presents some of the experiences gained over the past four years using three tensiometers manufactured by Imperial College. Some of the anomalous responses recorded by tensiometers are first discussed. These were probably due to inadequate saturation of the porous ceramic rather than malfunctioning of the instruments. The results from a series of tests conducted with two or three tensiometers positioned on the same sample are then presented. These were helpful in defining suitable experimental procedures. Finally, the history of tension breakdown of each tensiometer is examined to identify some of the factors that affect the maximum sustainable tension as well as measurement duration. On the basis of data recorded before and after cavitation, a possible mechanism of cavitation in a tensiometer is described.

Key words: cavitation, suction, tensiometer, unsaturated soil

Introduction

Instruments for measuring matric suction fall into two main categories, those that measure directly and others that measure indirectly. With indirect measurement, instruments need to be calibrated against known values of matric suction. A common method for controlling and measuring matric suction is the axis translation technique. Unfortunately, the validity of this method has not yet been satisfactorily assessed. Calibration data obtained by raising ambient air pressure might not be accurate for estimating matric suction of soils in the field.

The disadvantage of calibration is eliminated when matric suction is measured directly. Recent advances in the understanding of the direct measurement of soil matric suction have extended the range of such measurements to about 1.8 MPa (Ridley and Burland, 1993). Tensiometers have been developed at Imperial College (Ridley and Burland, 1996) and later on at the University of Saskatchewan (Guan and Fredlund, 1997). These instruments seem to provide an affordable, easy to use and reliable means of direct measurement of matric suction.

The major drawback of these instruments is water cavitation. Water may cavitate before pore pressure equalisation is reached thus causing test interruption and requiring instrument re-saturation. In some cases, cavitation occurs almost instantaneously and tensiometers are not able to function (Harrison and Blight, 2000). A better understanding of the conditions leading to cavitation is thus essential to determine adequate procedures for long term measurements and to optimise design of new instruments.

This paper presents some of the experiences gained at the University of Trento over the past four years using three tensiometers manufactured by Imperial College, London. Measurements of negative pore water pressure have been carried out during oedometer tests (Tarantino and Mongiovi, 2000), during null-tests (Tarantino et al., 2000b) and also on unconfined air dried kaolin samples.

Some of the anomalous responses recorded by this type of tensiometer are first discussed. These responses are believed to be indicators of an insufficient saturation of the porous ceramic rather than malfunctioning of the instrument. Then, the results from a series of tests conducted with two or three tensiometers positioned on the same sample are presented. These tests were helpful in defining suitable experimental procedures. Finally, the results of measurements where cavitation occurred are examined. In particular, the history of the tension breakdown of each tensiometer is recorded to investigate the factors controlling the process of cavitation in the tensiometers. On the basis of data recorded before and after cavitation, a possible mechanism of cavitation in the tensiometer is described.

Measurement of Water Tension and Cavitation

Several models have been presented in the literature to explain the occurrence of cavitation in water subjected to tensile stresses. The most widely accepted is that proposed by Harvey et al. (1944). They assume that cavitation originates from undissolved gas nuclei existing in the interstices in the container's wall rather than from free cavities in the liquid. A free spherical gas nucleus is usually unstable and tends to go into solution. On the contrary, a gas nucleus in a cavity in the wall of the container may remain undissolved even under a high water pressure. When pressure is decreased to negative values, these nuclei can expand and eventually trigger cavitation. This process is controlled by gas diffusion across the gas-liquid boundaries and creeping of the gas-liquid-solid junction determined by the advancing and receding of contact angles.

Water tensile stress has been measured by physicists using glass and steel Berthelot tubes. The tube is initially almost completely filled with water while the remaining volume is occupied by a mixture of air and water vapour. The tube is then heated to expand the enclosed liquid and force the air into solution. On subsequent cooling the liquid adheres to the wall of the tube and becomes subjected to gradually increasing tension until it breaks down at the onset of cavitation. It has been shown that pre-pressurisation is needed before water tension is produced in the tube. High posi-

tive pressures cause the majority of gas nuclei to dissolve and enable the liquid to sustain tension. Moreover, it was found that only a few heating-cooling cycles were necessary to enable some tension to be generated (Chapman et al., 1975) and that the breaking tension increased with repeated heating-cooling cycles (Jones et al., 1981).

The pre-pressurisation of water has been considered essential to saturate the tensiometer both at Imperial College and at the University of Saskatchewan. Some differences however exist between the two pre-pressurisation procedures. Guan et al. (1998) suggests that tension breakdown is affected primarily by the number of cycles and the magnitude of pre-pressurisation pressure. In particular, they applied six pre-pressurisation cycles that began with a positive pressure of up to 12000 kPa followed by a vacuum of -85 kPa.

The advantage of cyclic pre-pressurisation to enhance the ability of water to withstand tensions might be argued. It has been suggested by Marinho and Chandler (1995) that this procedure may help dissolve potential cavitation nuclei, according to the experience gained by physicists using the Berthelot tube (e.g. Chapman et al., 1975). However, it is worth noting that cycles of pressurisation in the Berthelot tube, which are induced by the heating-cooling process, inevitably result in water cavitation in the tube and, hence, cycles of cavitation and subsequent pressurisation are actually applied. On the contrary, in the procedure adopted by Guan et al. (1998) cavitation is not triggered and the absolute water pressure always remains positive during the cycles of pre-pressurisation.

Ridley and Burland (1999) assert that the pre-pressurisation procedure is less important and that the initial saturation of the porous stone plays a more important role. Provided that the suction probe is adequately saturated, the stress required to cause breakdown would be uniquely related to the air entry value of the ceramic. In contrast to the procedure adopted at the University of Saskatchewan, they saturated the tensiometer by applying a pressure of only 4000 kPa, which was maintained constant for at least 24 hr. The pre-pressurisation system was not cycled from positive to subatmospheric pressure.

IC Tensiometer

The tensiometer used in the experimental programme was manufactured at Imperial College and has been previously described by Ridley and Burland (1996). Compared to the first prototype (Ridley and Burland, 1993), this tensiometer has an integral strain gauged diaphragm and a water reservoir of reduced size. It carries a porous ceramic with a 1.5 MPa air entry value, which is glued within the tensiometer's body (Figure 1).

A saturation pressure chamber, also manufactured at Imperial College, was used to re-saturate the suction probes after cavitation. The chamber is equipped with a screw piston for manual pressurisation. Although cheap and safe, this system shows a disadvantage. It requires continuous adjustment of the screw piston to main-

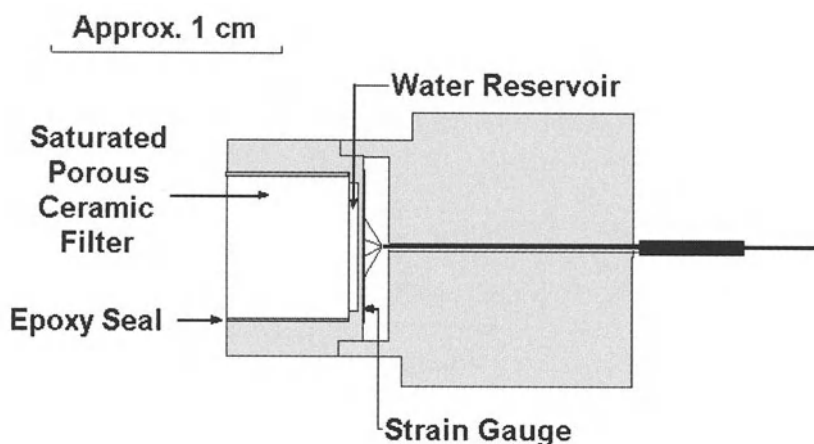


Figure 1. The IC tensiometer (after Ridley and Burland 1999).

tain the water pressure in the range required to saturate the porous stone. In fact, once a pressure is applied, air cavities are forced into solution causing expansion of water in the chamber and the pressure drops. Such a drop was found to be significant when the system was left overnight and is believed to be a critical drawback of the experimental procedure.

To ensure a constant 4 MPa water pressure during the 24 hr pressurisation period, a different pressurisation system was devised. An air/water bladder cell was connected to the pressure chamber as shown in Figure 2. The upper compartment was filled with nitrogen so as to increase gas pressure up to 4 MPa. Nitrogen was used because of the availability of high pressure nitrogen cylinders in the laboratory. Water volume changes induced by air dissolution were thus compensated by the expansion of the nitrogen in the cell. Because of the high compressibility of nitrogen, the pressure in the upper compartment, and hence the water pressure, could be maintained constant over a period of time. This pressurisation device was preferred to an automatically controlled water pump to avoid overpressure in case of failure of the control procedure. Water has a low compressibility and even a small volume change can cause a sudden pressure variation. Clearly all precautions were taken to make the high pressure system safe.

The tensiometers in use at the University of Trento have a low sensitivity, approximately $0.7 \mu\text{V/kPa}$. Therefore, special attention was given to the energy supply system and the data acquisition system. A resolution of $1\text{--}2 \mu\text{V}$ was required for the electronic system. An AC energy supply was specifically designed at the Physics Laboratory of the University of Trento and it was coupled with a 16-bit A/D board. This instrumentation permitted a resolution of about $1 \mu\text{V}$.

Calibration data for the tensiometers was derived for positive pressures. Tensiometers were positioned in the saturation chamber and known pressures were

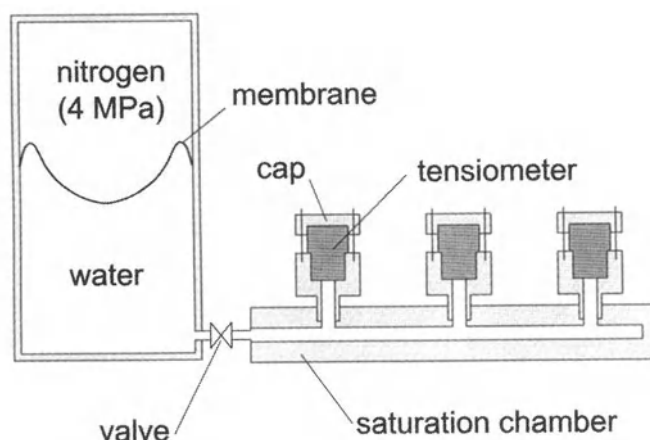


Figure 2. Schematic layout of the saturation chamber and the pre-pressurisation system.

applied using a dead-weight calibration device. The bolts that hold the tensiometers in place were only slightly tightened to avoid deformation of the measurement diaphragm and, hence, false changes in pressure. Calibration consisted of two cycles of pressure increase and decrease between 0 and 1500 kPa in steps of 50 or 100 kPa. In each step, water pressure was maintained constant for some minutes to account for the low permeability of the porous ceramic. This procedure was repeatedly performed throughout the experimental programme. Measurement accuracy, in terms of maximum output deviation with respect to the applied value, was found to be better than 1.5 kPa (0.1% full-scale output).

To determine negative pore water pressures the calibration curve was then extrapolated to the negative range, assuming a symmetric response of the measurement diaphragm.

Experimental Procedure

One of the key elements for measuring soil water tension is the high air entry porous ceramic. This interface inhibits the passage of air into the water reservoir as a separate phase, thus delaying cavitation in the tensiometer. However, the porous ceramic needs to be adequately saturated to achieve this goal. This is the reason why the experimental procedure plays such an important role.

An insufficiently saturated porous ceramic is believed to have produced anomalous responses in the tensiometer. These have been generally observed after the instruments have just been put into operation or have been used after being left unused for a long period of time. For example, a significant drift has been occasionally recorded when leaving the tensiometers in free water, the initial zero pressure has not been always recovered after a rapid drop in pressure or after suction

measurement, and a change in the calibration line has been in some cases observed after cavitation and subsequent pressurisation.

The reason why poor saturation of the ceramic would cause these anomalous responses is not clear. They probably could be caused by relatively large air cavities present in the ceramic since anomalous responses were no longer observed after the porous ceramic had been adequately saturated. Adequate saturation was achieved by cycles of cavitation and subsequent pressurisation (Tarantino et al., 2000a).

Insufficient saturation of the porous ceramic is believed to lead to measurement inaccuracy, which might be difficult to detect. It is in fact not possible to calibrate the tensiometer in the negative range. The use of indirect methods such as filter paper and thermal conductivity sensor to assess reliability of tensiometer measurements (Marinho and Chandler, 1994; Guan and Fredlund, 1997) is also questionable. It is a direct measurement of matric suction that should be used to calibrate indirect methods and not vice versa.

A straightforward way to assess measurement reliability and, hence, the suitability of a particular experimental procedure, is to compare the response of more than one tensiometer positioned on the same sample. A series of tests were therefore conducted with three tensiometers positioned on unsaturated kaolin samples. The results from these tests made it possible to progressively adjust the experimental procedure, which is described in the following paragraphs.

Before each measurement, possible changes in the slope of the calibration line were first checked. A new calibration would be unpractical since the calibration procedure lasts many hours. An indirect and swift manner to detect possible variations was to modify the pressure in the saturation chamber using the screw piston. Each tensiometer was then expected to record the same change in pressure. If any discrepancies were observed, calibration was repeated following the procedure previously described.

After removal from the saturation chamber, tensiometers were placed in free water. If pressure equalisation was not attained within 1 hour, tensiometers were not considered ready for measurement. They were then positioned on a dry sample in order to trigger cavitation and re-saturated for at least 24 hr.

Once equalisation in free water was completed, the porous stone was wiped and left to dry out until a water pressure of approximately -1000 kPa was attained. The tensiometer was then immediately replaced in free water to check whether the water pressure regained the same initial value. If this was not the case, the tensiometer would again be considered not suitable for measurement and re-saturated after triggering cavitation.

The reading was then reset and a saturated paste was placed on the porous ceramic to improve contact with the soil sample. Typically, water pressure would tend to equalise within minutes if the tensiometer was properly 'connected' to the soil sample. In the experimental study presented herein, the samples along with the tensiometers, were placed in a plastic bag to prevent soil water evaporation. A string

was used to tighten the plastic bag around the electric wires of the tensiometers. Temperature was recorded using two thermoresistors with a resolution of 0.01°C .

After measurement, saturation of the porous ceramic was checked again. Measurement data were discarded if the pressure did not drop to about -100 kPa upon cavitation or did not return approximately to zero when cavitation had not occurred. A residual pressure within a range from -10 to 0 kPa was considered acceptable.

Measurement of Soil Water Tensile Stress

The results from test no. 10 are shown in Figure 3. The water pressures recorded by the three tensiometers as well as the temperature are plotted versus time. For simplicity, the tensiometers used in this study are referred to as *pr2*, *pr3*, *pr4*.

In this measurement, cavitation occurred after only 200 min (about 3 hours) for tensiometer *pr3* whereas *pr4* was able to function for almost 4 days. Tensiometer *pr2* did not cavitate and was replaced in free water after measurement. Small fluctuations were recorded by *pr4*, which appear in phase with temperature changes (Figure 3(b)–(c)). These are partly attributed to expansion of gas nuclei in the porous ceramic that remain stable in the water under tension. A similar response has been reported by Tarantino and Mongiovì (2000).

The three tensiometers showed good agreement since the maximum difference in pressure did not exceed 10 kPa. This level of precision (± 5 kPa) is considered acceptable for this type of measurement and was found to be typical for tensiometers with good saturation of the porous ceramic.

It is worth focusing on the response of the tensiometer before and after measurement. Initially, pressure was rapidly dropped twice to about -1000 kPa. The difference recorded before and after this pressure drop was less than 10 kPa upon the first cycle, and negligible upon the second cycle, as illustrated in Figure 4(a)–(b) for tensiometers *pr2* and *pr3*. This response was generally observed for tensiometers exhibiting a good level of precision. On the other hand, tensiometers generally exhibited unsatisfactory performance if the change in pressure recorded after the second cycle was greater than 5–10 kPa.

Upon cavitation, water pressure dropped to about -100 kPa as would be expected. However some differences should be noted. Water pressure remained almost constant over about 400 min for *pr3* whereas it slowly increased for *pr4* (Figure 4(c)–(d)). The former response was generally observed for cavitation occurring after a short period of time and at a relatively low suction. The latter was shown after a prolonged measurement. This different behaviour would result from different degrees of saturation of the porous ceramic, which is likely to be lower in the first case. A possible mechanism is suggested later in this paper.

After measurement, the pressure recorded by *pr2* regained the initial zero value (Figure 4(e)). This is likely to indicate adequate saturation of the porous ceramic. However, pressures less than zero may be recorded after measurement despite a good measurement performance. This is illustrated by the results from test no. 18

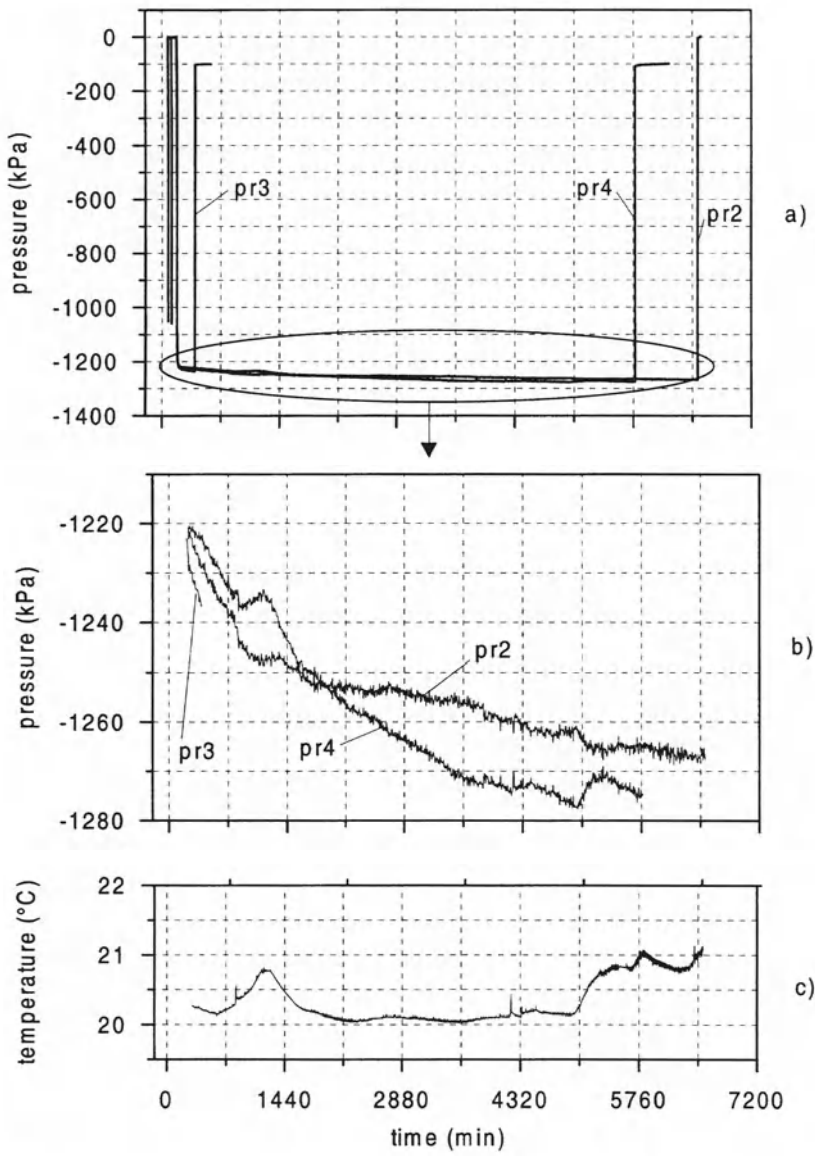


Figure 3. Test no. 10. (a) initial zero check, suction measurement, and cavitation; (b) enlargement; (c) temperature changes.

(Figure 5). In this test, the plastic bag was initially kept open and then repeatedly closed to analyse the tensiometer response to a relatively rapid change in suction. After measurement, *pr2* recorded a pressure of -20 kPa although the three tensiometers recorded a difference in pressure within 10 kPa.

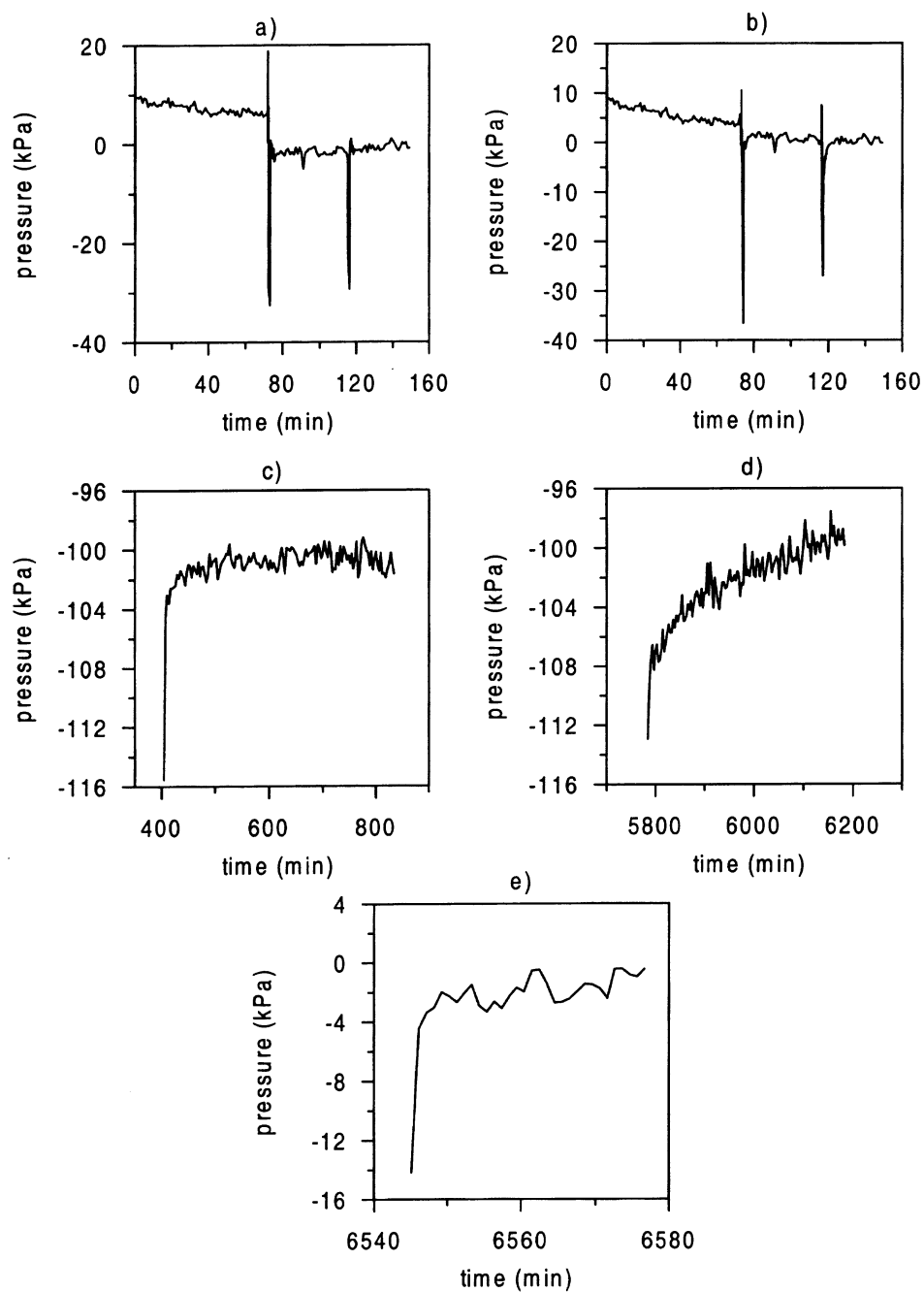


Figure 4. Test no. 10. (a) initial zero check for pr_2 ; (b) initial zero check for pr_3 ; (c) cavitation of pr_3 ; (d) cavitation of pr_4 ; (e) equalisation after measurement of pr_2 .

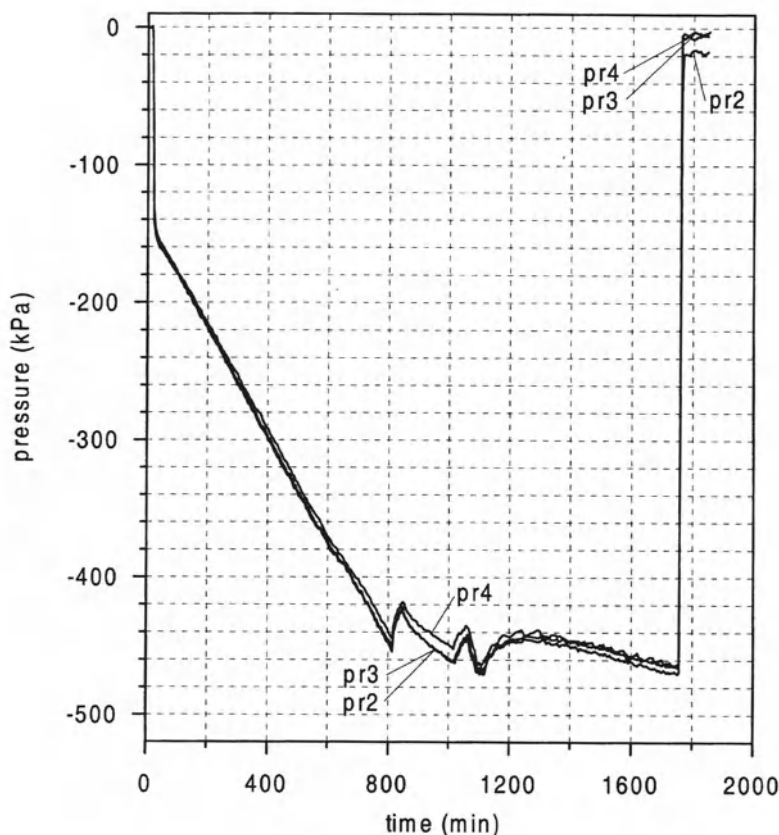


Figure 5. Test no. 18.

An example of poor performance of the tensiometer, probably due to inadequate saturation of the ceramic, is given in Figures 6 and 7. Figure 6 shows the response of tensiometers *pr2* and *pr4* when placed on a sample having a suction of about 1000 kPa. Before measurement, possible changes in the slope of the calibration line were checked in the saturation chamber. As shown in Figure 6(a), the two tensiometers recorded the same pressure change while modifying the pressure in the chamber using the screw piston. The porous stone of both tensiometer was then wiped twice, and the pressure regained the initial zero value when replacing the tensiometer in free water. The maximum difference in pressure recorded during the measurement was about 10 kPa. The tensiometers recorded significant fluctuations since the air conditioner was not functioning (Figure 6(b)).

After the measurement, the tensiometer *pr4* was placed on a dry sample in order to trigger cavitation. The tensiometer was then positioned in the saturation chamber at a pressure of 4 MPa, along with the tensiometer *pr2*. The two tensiometers were kept in the chamber only for 100 min and not for 24 hr as recommended. This was aimed at inducing inadequate saturation in the tensiometer *pr4*.

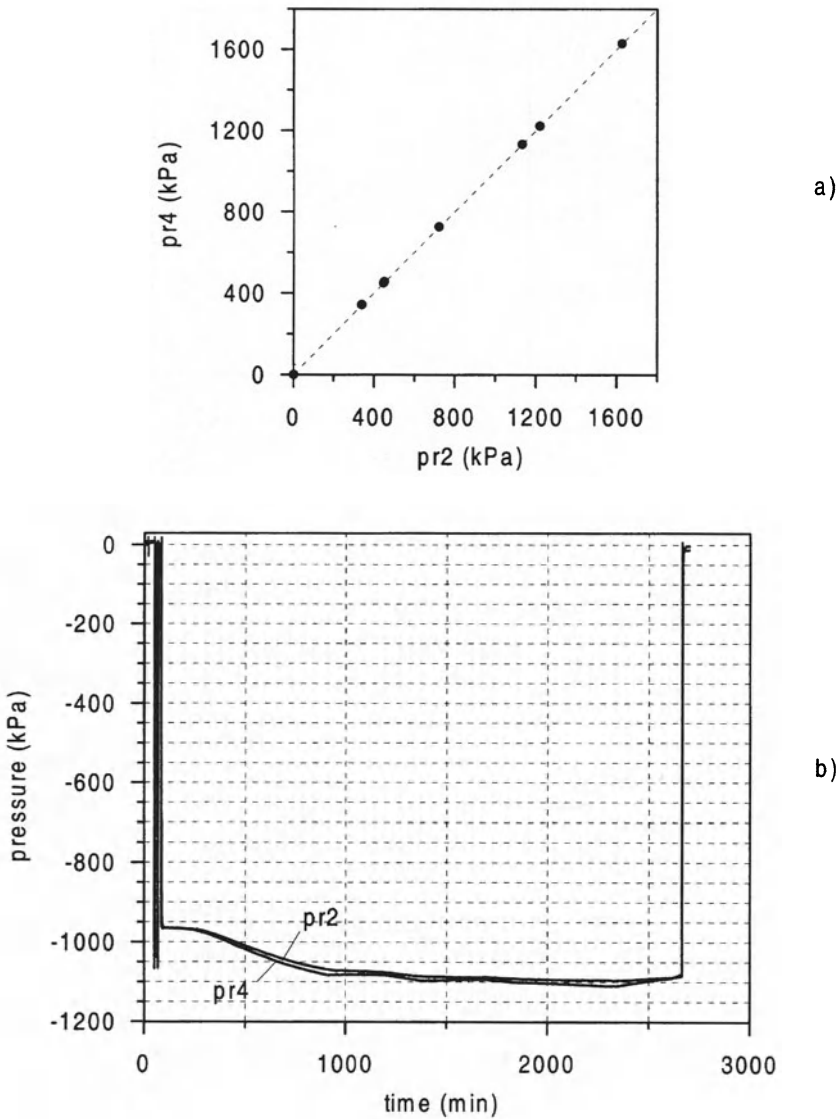


Figure 6. Response of tensiometers thought to be adequately saturated. (a) Initial calibration check; (b) Measurement of the two tensiometers placed on the same sample.

Before removing the tensiometers for the new measurement, the calibration was checked again in the saturation chamber as shown in Figure 7(a). The difference in pressure recorded by the two transducers was about 120 kPa at 1600 kPa and reduced when the pressure in the chamber decreased towards zero. It is worth noting that these differences were much greater than the measurement accuracy.

The two tensiometers were first placed on sample with a suction of about 400 kPa, then on a sample having a suction of about 1000 kPa (Figure 7(b)). The difference in

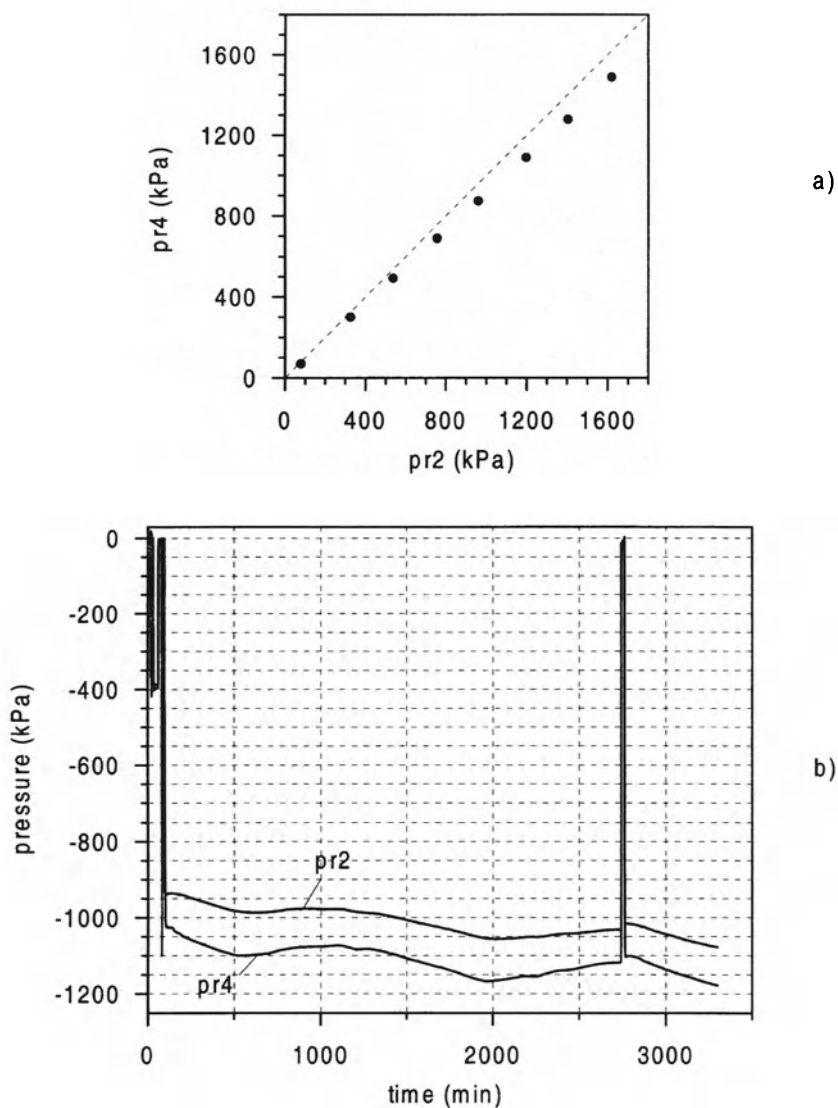


Figure 7. Response of tensiometers thought to be inadequately saturated. (a) Initial calibration check; (b) Measurement of the two tensiometers placed on the same sample.

pressure recorded in the latter case was about 100 kPa. This result was surprising because the two tensiometers had previously showed good agreement (Figure 6(b)). Possible errors due to a non-uniform distribution of soil water content were therefore checked for. The tensiometers were removed from the sample and placed again on it, but the difference in pressure remained unchanged. Possible irreversible changes in the calibration line were also checked for after the measurement. The tensiometers were kept for three days in the saturation chamber, and the calibration checked

again. The response observed was similar to that observed in Figure 6(a), indicating that the calibration line had not changed.

The significant difference shown in Figure 7(b) is therefore likely to be due to inadequate saturation of the porous ceramic, which would also be the reason for the anomalous response of the tensiometer *pr4* during the calibration check (Figure 7(a)). It is worth noting that, although the tensiometer *pr4* exhibited a poor performance in terms of precision, the pressure returned to zero when placing the tensiometer in free water after wiping the porous ceramic. This did not always occur during the first measurements following the first saturation of the tensiometer, probably because of a lower degree of saturation of the porous ceramic.

The results from these series of tests have shown that tensiometers are capable of a measurement precision of ± 5 kPa provided the porous ceramic is adequately saturated. Saturation should be properly checked throughout the experimental procedure, in particular before measurement. Changes in the calibration parameters, the time required for equalisation after removal from the saturation chamber, and the response of the tensiometer upon a rapid drop in pressure are assumed to be adequate indicators of the saturation of the porous ceramic. It was observed that the tensiometers would not perform satisfactorily if some of these initial tests failed. When this happened, the tensiometer was re-saturated after triggering cavitation.

Cycles of cavitation and subsequent pre-pressurisation were found to be the key factor to improved saturation of the porous ceramic. This experimental procedure was indeed suggested by Steve Ackerley (pers. comm.) as it had been earlier observed at Imperial College that repeated cycles of cavitation significantly improved the performance of the probes. The advantage of this experimental procedure can be better emphasised if the cavitation history of each tensiometer is examined.

Cavitation History

The three tensiometers that had been used in the experimental programme described herein remained stored inside the saturation chamber for 1 year, since they were not used during this time. The air/water bladder cell ensured a constant pressure of 4 MPa and there was no need to refill the system or restore the nitrogen pressure. After 1 year saturation the three tensiometers were calibrated in the saturation chamber and then used for suction measurements.

Table 1 lists the tension breakdowns of *pr2* during the five-month experimental programme. The two types of samples used in these tests had matric suctions in the range 1200–1500 kPa and 2400–2600 kPa respectively. It can be seen that in the first test cavitation occurred after just 1 min at a very low tensile stress.

Such a result was totally unexpected. The tensiometer was assumed to be fully saturated after the one year period of pressurisation. However, it can also be observed that after this first cavitation and subsequent pressurisation the probe was capable of measuring a remarkable suction, much higher even than the nominal air entry value of the porous stone. In fact, cavitation occurred at -2260 kPa (test 8).

Table 1. Tension breakdown history for tensiometer *pr2*

Test No.	Samples A ¹ Tension breakdown (kPa)	Duration (min)	Samples B ² Tension breakdown (kPa)	Duration (min)
1	-655	1		
8			-2260	490
13			-2584	885
17			-2403	200

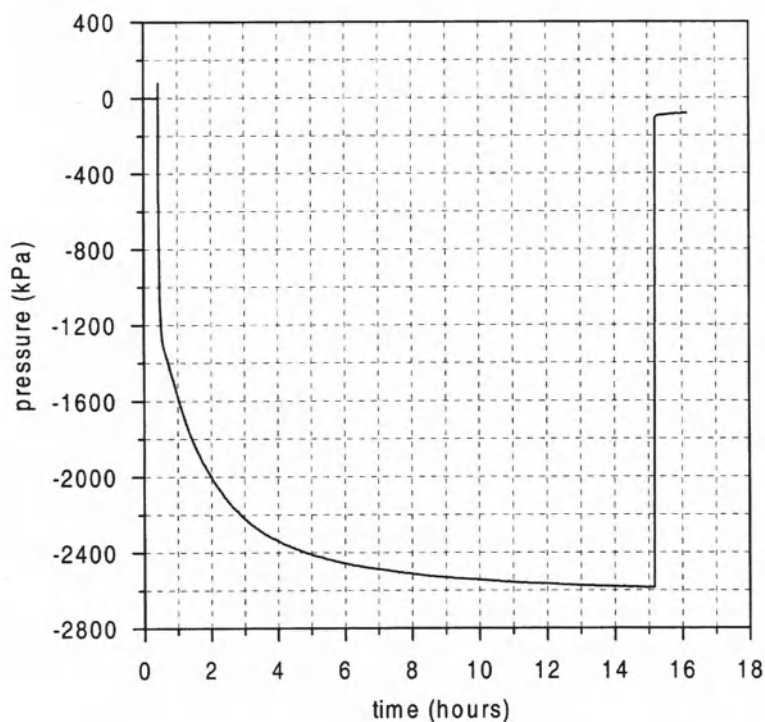
¹Suction range 1200–1500 kPa.²Suction range 2400–2600 kPa.

Figure 8. Test no. 13: measurement of soil water tension of about 2600 kPa.

This result was also unexpected since direct measurement of suctions greater than 2 MPa have not previously been reported in the literature. Also during test 13, equalisation was almost attained before activation occurred after 15 hours, as illustrated in Figure 8. It would thus appear that cycles of cavitation and subsequent pressurisation help to improve saturation of the porous ceramic and, hence, produce an increase in the maximum sustainable tension.

Table 2. Tension breakdown history for tensiometer *pr3*

Test No.	Samples A ¹	Duration (min)	Samples B ²	Duration (min)
	Tension breakdown (kPa)		Tension breakdown (kPa)	
1	-1306	10		
2	-1270	14		
3	-1299	8		
4	-948	2		
5	-1225	47		
6	-1238	475		
7	-1230	162		
8			-1886	74
9	-1258	396		
10	-1236	220		
11			-1876	80
14			-2137	113
17			-2049	100
21*	-1275	2000		
23*	-1240	2049		

*oedometer testing

¹Suction range 1200–1500 kPa.²Suction range 2400–2600 kPa.

The importance of these cycles is better emphasised by the cavitation history of *pr3* and *pr4*. Their porous stones accidentally dried out during shipping and were resaturated at the University of Trento following the procedure described by Ridley and Burland (1999). The vacuum chamber was obtained by adapting a triaxial cell chamber. It is possible that the large volume of the cell did not allow the air pressure inside the chamber to be reduced as much as necessary. This would have produced an inadequate saturation of the porous ceramic, thus explaining the different performance of *pr3* and *pr4* (Tables 2 and 3) when compared to probe *pr2*.

For the case of *pr3*, it can be observed that tension breakdown for samples A (suction range 1200–1500 kPa) generally occurred in the same range of pressure. However, measurement duration increased progressively with the number of cavitation–pressurisation cycles, with a variation of two orders of magnitude. There is a certain scattering in the data, which might be expected considering that water under tension is in a metastable condition. Nevertheless, a trend can be clearly observed. Similar observations can be made from the data from B-type samples (suction range 2400–2600 kPa).

For the case of the tensiometer *pr4*, it is also important to note that a significant increase in the measurement duration occurred after the first time that the pressure in the tensiometer dropped to about -2000 kPa (test no. 8). Similar behaviour was also observed for tensiometer *pr3* after a series of cavitation at high suctions (tests 11, 14, and 17). It is assumed that bringing the water to very high suction

Table 3. Tension breakdown history for tensiometer *pr4*

Test No.	Samples A ¹		Samples B ²	
	Tension breakdown (kPa)	Duration (min)	Tension breakdown (kPa)	Duration (min)
1	-1400	12		
2	-1268	64		
3	-1500	380		
5	-1215	22		
6	-1190	10		
7	-1255	1270		
8			-1995	145
10	-1275	5600		
11			-1870	70
14			-2040	100
17			-2110	60

¹Suction range 1200–1500 kPa.²Suction range 2400–2600 kPa.

causes a large amount of very small gas nuclei to enlarge. Upon cavitation, these nuclei are drawn into the large cavity that forms within the ceramic with the result that the number of potential cavitation nuclei is reduced.

Data Interpretation

At the outset, it is important to consider where cavitation takes place. It has been generally assumed that cavitation is triggered by a small amount of gas trapped in the tiny crevices in the wall of the container or in undissolved dust particles in the water (Ridley and Burland, 1994; Marinho and Chandler, 1995; Guan et al., 1998). However, it seems reasonable to expect that there will be cavitation nuclei trapped in the small pores of the high air entry ceramic rather than in the crevices of the water reservoir walls. Accordingly, cavitation would take place in the porous ceramic and not in the water reservoir of the tensiometer.

This assumption is supported by an anomalous response that was often recorded while increasing the water pressure after cavitation. A typical result is shown in Figure 9, where the pressurisation of *pr3* after cavitation is reported for test no. 14. The tensiometer had cavitated after 113 min to a pressure of -100 kPa. It was then left on the sample for about 200 min and during this time the water pressure slowly increased to -95 kPa. After installing the tensiometer in the saturation chamber the valve connecting the chamber with the air–water bladder cell was opened to increase water pressure. It can be noted that the pressure recorded by the tensiometer did not increase instantaneously but dropped by about 35 kPa prior to rising towards 4000 kPa. The drop in pressure would indicate that a tensile stress was still transmitted to the measurement diaphragm and hence water still completely filled the reservoir.

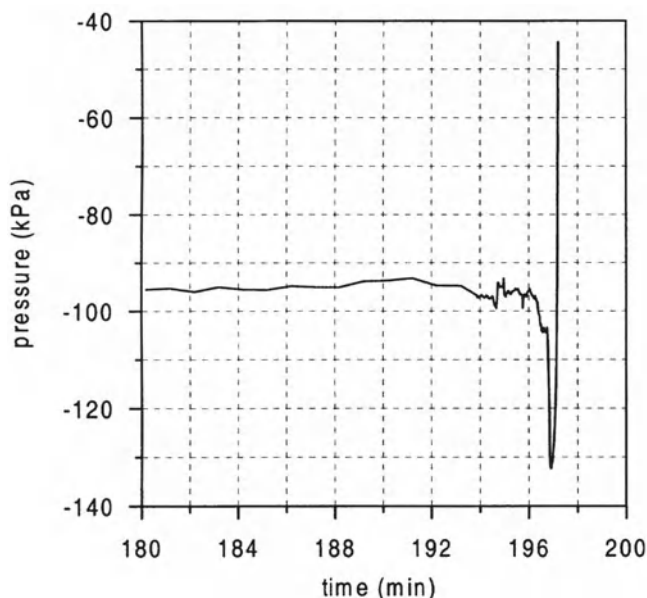


Figure 9. Pressure drop upon pressurisation.

The reason for this pressure drop is not clear. However, it is possible that the positive pressure applied on the porous stone produces a change in the configuration of the menisci inside the ceramic and a temporary drop in pressure. This phenomenon was commonly observed when cavitation occurred after a relatively short period of time or after the application of a very high suction. In both cases, a large air cavity is expected to have formed within the porous ceramic.

The occurrence of cavitation within the ceramic would explain the different response recorded by the tensiometers as illustrated in Figure 4(c)–(d). After cavitation, air diffuses towards the cavity from outside the tensiometer and the pressure increases towards zero. For the case where the degree of saturation is low, a large air cavity would develop in the ceramic. A large amount of air would be required to increase the pressure in the cavity, which would therefore remain almost constant during the first hours after cavitation (Figure 4(c)). On the contrary, when small air cavities form in the ceramic upon cavitation, the same amount of diffused air is able to increase more rapidly the pressure in the tensiometer (Figure 4(d)).

Another point which is worth emphasising is that small air cavities would remain inside the porous stone even though water is under tension. This assumption is supported by another interesting result obtained while carrying out measurement no. 11 using tensiometer *pr2*. After measuring a water tensile stress of 2530 kPa for 315 min, this tensiometer was removed from the sample and placed in free water. As shown in Figure 10 the water pressure increased very slowly to zero and 10 min passed before complete equalisation was reached. Commonly 3 min were sufficient

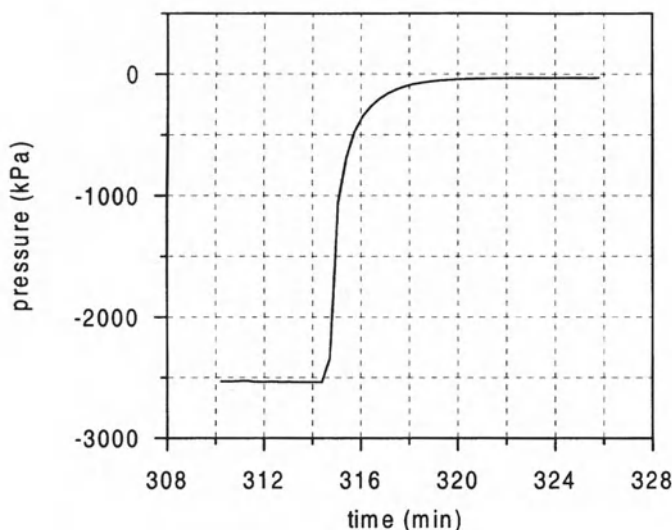


Figure 10. Slow equalisation after suction measurement of about 2.5 MPa.

for pressure equalisation. This time lag was probably caused by the growth of the small gas nuclei existing inside the porous stone. The tensiometer had experienced for the first time that value of water tension and this caused the small nuclei in the ceramic to enlarge. As a result, the permeability of the porous stone decreased, thus delaying equalisation.

The presence of air cavities in the porous ceramic would account for the anomalous responses observed after the tensiometers had been put in operation or had remained unused for a long period of time. Because of relatively large air cavities in the ceramic, the pressure transmitted to the measurement diaphragm would differ from that applied externally to the ceramic. This difference in pressure would be caused by capillary effects. This mechanism would explain why the initial zero pressure is not recovered. Air cavities would grow in the water under tension and would not reduce in size once the tensiometer was placed again in free water. The change in the slope of the calibration line would also result from a change in the configuration of menisci in the porous ceramic.

Concerning the factors that affect the maximum sustainable tension, the tension breakdown history shows that a mere pressurisation is not sufficient to dissolve cavitation nuclei. This is proved by the almost instantaneous cavitation experienced by *pr2* after 1 year of uninterrupted pressurisation at 4 MPa. However, still holding the same pre-pressurisation pressure, it was possible to record water tensions greater than 2 MPa after the first cavitation. Thus, the number of cavitation and subsequent pressurisation cycles seems to be one of the factors affecting the maximum sustainable tension. This is in agreement with the results obtained by physicists using

the Berthelot tube. In the same manner as water tension was found to increase with repeated heating-cooling cycles, it can be assumed that cycles of pressurisation and cavitation increase the tension breakdown pressure.

The pre-pressurisation pressure in itself does not seem to affect significantly the maximum sustainable tension. This differs from the conclusions drawn by Guan and Fredlund (1997), who recognised that the magnitude of the pre-pressurisation plays a fundamental role. In the authors' opinion, it is not necessary to apply very high positive pressures (10–12 MPa) to achieve good saturation of the porous ceramic. However, no data are available to prove this assertion and this issue remains open.

Cavitation Mechanisms

According to the data collected so far, a mechanism of cavitation inside the tensiometer may be proposed. Small gas nuclei exist in the porous ceramic interstices. These are not dissolved by the high pressures applied because of the curvature of the air-water meniscus (Figure 11(a)). If the tensiometer is left for a long period under high pressure, not only would these small gas nuclei remain stable but air might diffuse towards those nuclei where the pressure is lower. These are likely to trigger cavitation when water pressure is reduced to negative values. Such a mechanism would explain why cavitation occurred after just 1 min in *pr2* despite 1 year of pre-pressurisation.

When the water pressure dropped to negative values, the curvature of the air-water meniscus is reversed and stable gas nuclei may enlarge without triggering cavitation (Figure 11(b)). These expanded air cavities have probably caused the reduction in the permeability of the ceramic as illustrated in Figure 10.

A large air cavity would form inside the tensiometer when tension breakdown occurs (Figure 11(c)). In this large cavity the absolute pressure is almost zero and, hence, the surrounding small gas nuclei are driven towards this cavity. In addition, the newly formed large cavity would directly incorporate other cavitation nuclei (Figure 11(d)). On subsequent pressurisation, the large cavity could be easily forced into solution as opposed to the small gas nuclei in the interstices which can remain stable under high water pressures.

In other words, the gas nuclei that remain undissolved upon pressurisation might be eliminated through cavitation followed by pressurisation. Accordingly, tension breakdown and measurement duration increase.

This cavitation mechanism would also explain why it has been possible to measure water tensions much greater than the nominal air entry value of the ceramic. The ceramic within the tensiometer is saturated by repeated cycles of cavitation. Its degree of saturation would be higher than that in the ceramic tested by the manufacturer. This is presumably saturated by simply applying a high positive pressure. It is assumed that the air entry value is not only related to the porosity

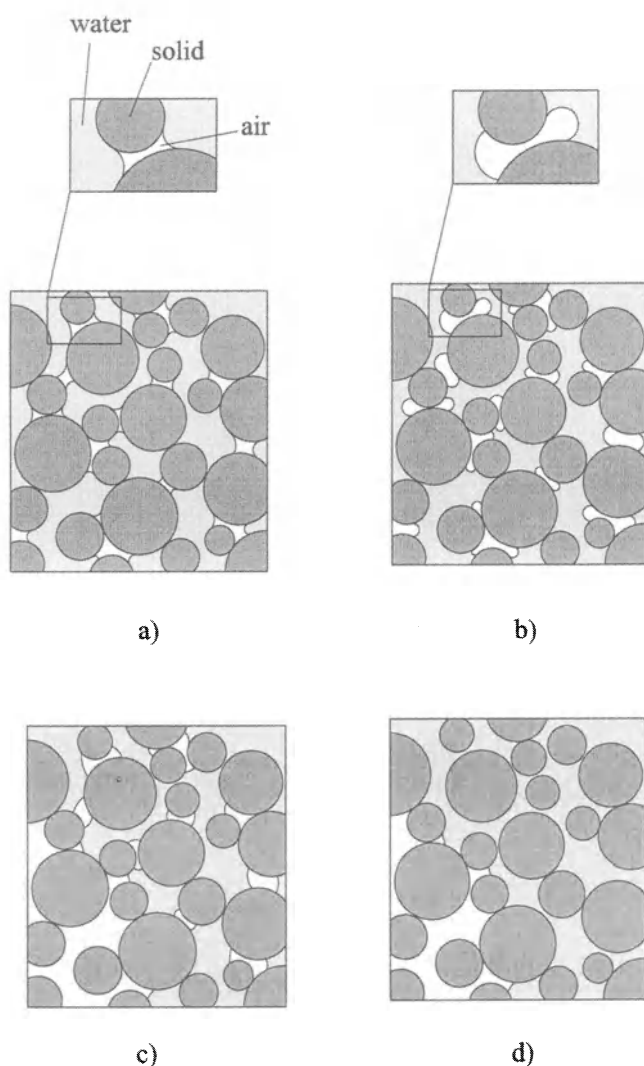


Figure 11. A possible cavitation mechanism inside the tensiometer. (a) pre-pressurisation; (b) measurement; (c) cavitation; (d) air diffusion.

of the ceramic but also to its degree of saturation. The higher the degree of saturation, the higher would be the air entry value.

However, it is also possible that the air entry value indicated by the manufacturer is just a nominal value, and that the actual air entry value is much greater.

Conclusions

Tensiometers for direct measurement of matric suction have been developed at Imperial College, London and later on at the University of Saskatchewan. These

instruments are well suited for laboratory and in situ soil suction measurements. Their major drawback is water cavitation which may occur before pore pressures equalise. A better understanding of the cavitation mechanisms may therefore help to optimise instrument design and define adequate experimental procedure.

Anomalous responses of the tensiometers recorded after the instrument had just been put into operation or had remained unused over a long period of time are first described. These were probably due to inadequate saturation of the tensiometer porous stone rather than malfunctioning of the instrument. Such responses were then taken as an indication that tensiometers were not ready for measurement and needed to be re-saturated.

A series of tests were performed to define suitable experimental procedures. The results have shown that tensiometers have a satisfactory level of precision (± 5 kPa) provided the porous ceramic is adequately saturated. Saturation should be properly checked throughout the experimental procedure, in particular before measurement.

Finally, the tension breakdown history of three tensiometers has been discussed. Based on the experimental data presented herein it can be inferred that a mere pre-pressurisation of the water in the probe is not sufficient to dissolve potential cavitation nuclei within the probe. Instead, the experiments indicated that cycles of cavitation and subsequent pressurisation can produce a significant increase in the maximum sustainable tension. In particular water tension greater than 2 MPa was recorded by all three tensiometers used in this programme. Cycles of repeated cavitation also increased the measurement duration.

To interpret the response of the tensiometers it has been assumed that small gas nuclei are difficult to dissolve by applying a pre-pressurisation pressure. In fact in this case dissolution is prevented by the cavity air-water interface, which is convex on the air side and carries the high water pressure. On the contrary the large cavities which form inside the tensiometer after cavitation are capable of sucking out the air from the small cavitation nuclei. Air from the nuclei is driven into the larger cavities by their nearly zero absolute pressure. As opposed to the small gas nuclei, the large cavities can be easily forced into solution by the subsequent pressurisation.

It would appear that small air cavities remain in the porous stone even if water is under tension. Cavitation would be triggered by these nuclei and therefore would take place in the porous stone.

Acknowledgements

The authors wish to thank Dr. John McDougall for commenting on the paper. They also wish to thank Dr. Andrew Ridley for his suggestions and advice. The help of Mr. Steve Ackerley in solving many of the experimental problems encountered is gratefully acknowledged.

References

- Ackerley, S. (1997) Personal communication.
- Chapman, P.J., Richards, B.E. and Trevena, D.H. (1975) Monitoring the growth of tension in a liquid in a Berthelot tube, *J. of Physics E: Scientific Instruments*, **8**, 731–735.
- Guan, Y. and Fredlund, D.G. (1997), Use of tensile strength of water for the direct measurement of high soil suction, *Canadian Geotechnical Journal*, **34**, 604–614.
- Guan, Y., Fredlund, D.G. and Gan, J.K.M. (1998) Behavior of water subjected to high tensile stresses, In *Proceedings of the 2nd International Conference on Unsaturated Soils*, Vol. 1 Beijing 1998, International Academic Publishers, Beijing, pp. 356–361.
- Harrison, B.A. and Blight, G.E. (2000) A comparison of in-situ soil suction measurements, in *Unsaturated Soils for Asia, Proceedings of the Asian Conference on Unsaturated Soils*. Singapore, 2000, H. Rahardjo, D.G. Toll and E.C. Leong (eds), Balkema, Rotterdam, pp. 281–285.
- Harvey, E.N., Barnes, D.K., McElroy, W.D., Whiteley, A.H. Pease, D.C. and Cooper, K.W. (1944) Bubble formations in animal, 1-Physical Factor, *J. Cellular and Comparative Physiology*, **24**(1), 1–22.
- Jones, W.M., Overton, G.D.N. and Trevena, D.H. (1981) Tensile strength experiments with water using a new type of Berthelot tube, *J. of Physics D: Applied Physics*, **14**, 1283–1291.
- Marinho, F.A.M. and Chandler, R.J. (1994) Discussion: A new instrument for the measurement of soil moisture suction, *Géotechnique*, **44**(3), 551–556.
- Marinho, F.A.M. and Chandler, R.J. (1995) Cavitation and direct measurement of soil suction, in *Unsaturated Soils, Proceedings of the 1st International Conference on Unsaturated Soils*. Vol. 2 Paris, 1995, E.E. Alonso and P. Delage (eds), Balkema, Rotterdam, pp. 623–630.
- Ridley, A.M. and Burland, J.B. (1993) A new instrument for the measurement of soil moisture suction, *Géotechnique*, **43**(2), 321–324.
- Ridley, A.M. and Burland, J.B. (1994) Discussion: A new instrument for the measurement of soil moisture suction, *Géotechnique*, **44**(3), 551–556.
- Ridley, A.M. and Burland, J.B. (1996) A pore pressure probe for the in situ measurement of soil suction. In *Advances in Site Investigation Practice*, London, 1995, C. Craig (ed), Thomas Telford, London, pp. 510–520.
- Ridley, A.M. and Burland, J.B. (1999) Discussion: Use of tensile strength of water for the direct measurement of high soil suction, *Canadian Geotechnical Journal*, **36**, 178–180.
- Tarantino, A. and Mongiovi, L. (2000) Experimental investigations on the stress variables governing unsaturated soil behaviour at medium to high degrees of saturation. In *Experimental Evidence and Theoretical Approaches in Unsaturated Soils, Proceedings of an International Workshop*, Trento, 2000, A. Tarantino and C. Mancuso (eds), Balkema, Rotterdam, pp. 3–19.
- Tarantino, A., Bosco, G. and Mongiovi, L. (2000a) Response of the IC tensiometer with respect to cavitation. In *Unsaturated Soils for Asia, Proceedings of the Asian Conference on Unsaturated Soils*, Singapore, 2000, H. Rahardjo, D.G. Toll and E.C. Leong (eds), Balkema, Rotterdam, pp. 309–314.
- Tarantino, A., Mongiovi, L. and Bosco, G. (2000b) An experimental investigation on the independent isotropic stress variables for unsaturated soils, *Géotechnique*, **50**(3), 275–282.



The role of pore water in the mechanical behavior of unsaturated soils

DAIZO KARUBE¹ and KATSUYUKI KAWAI²

¹*Graduate School of Science and Technology, Kobe University, Japan*

²*Faculty of Engineering, Kobe University, Japan*

(Received 16 June 2000; revised 12 January 2001; accepted 21 May 2001)

Abstract. Deformation and failure of soils are governed by the stresses acting on the soil skeleton. The isotropic stress acting on the soil skeleton can be divided into two components. One is the stress component which is transmitted through the soil skeleton. This skeleton stress is influenced by the pore water (“bulk water”) in the soil. The other is the internal stress component which does not contribute to equilibrium with a given external force. The internal stress is induced by the capillary tension of meniscus water clinging to the contact point of soil particles and acts so as to connect the soil particles tightly. Therefore, in modeling the stress and strain relations for unsaturated soils, it is of much importance to quantitatively evaluate how the pore water exists in the soil. This paper discusses the role of pore water on the mechanical behaviour of the soil. In particular, the significance of the water retention curve is emphasized from a mechanical viewpoint. Essential features required in modeling of the constitutive relations for unsaturated soils are discussed and presented.

Key words. constitutive equation, suction, unsaturated soil, water retention curve.

Introduction

One of the most important subjects of soil mechanics is to predict the deformation of the ground. When a soil mass is loaded, it deforms and then a counter force is generated so as to balance the load. Although soil consists of a soil skeleton and pore fluid, the latter does not play a principal role in the shear behaviour, that is, the pore fluid does not resist the shear force. The pore water migrates within the soil skeleton subjected to hydraulic boundary conditions.

In such saturated soils, Terzaghi's effective stress component is applicable. However, for unsaturated soils, where the pore space is occupied by both air and water, this may no longer hold.

Bishop et al. (1960) initiated the study of mechanical behaviour of unsaturated soils. They performed suction controlled triaxial compression tests and examined the roles of net normal stress $\sigma_{net} = (\sigma - u_a)$ and matric suction $s = (u_a - u_w)$ in the stress-strain and strength characteristics of unsaturated soils. Since their pioneering work, the volume change characteristics of unsaturated soils have been investigated and the applicability of their effective stress equation, has been examined by many researchers. To date, some elasto-plastic stress-strain models

have been proposed. In the paper, Bishop's effective stress is reviewed and representative elasto-plastic models are introduced. It is discussed how the change of degree of saturation can be introduced into the constitutive relations in terms of the stress components. An elasto-plastic model proposed by the authors is introduced. Finally, current studies of the water retention curve are introduced as the water retention curve plays an important role in the relationships.

Stress components in unsaturated soils

In saturated soils, Terzaghi's effective stress concept is applicable

$$\sigma = \sigma' + u_w \quad (1a)$$

therefore

$$\sigma' = \sigma - u_w \quad (1b)$$

where, σ = total stress, σ' = effective stress and u_w = pore-water pressure. Equation (1a) implies that the pore-water pressure u_w is generated so as to balance directly a part of the applied load (total stress). The remainder of the applied load contributes to deform the soils as the effective stress σ' . In other words, the effective stress is a component of stress which is transmitted through the soil skeleton from one boundary surface to another.

Even in the unsaturated state, Terzaghi's effective stress equation is satisfied as long as the air exists in the form of bubbles that are isolated from the soil skeleton. However, when the air exists as a continuous phase in the soil pore space, the pore-water pressure u_w in Equations (1a) and (1b) should be replaced by the pore air pressure u_a :

$$\sigma = \sigma_{net} + u_a \quad (2a)$$

therefore

$$\sigma_{net} = \sigma - u_a \quad (2b)$$

σ_{net} is the set normal stress and is the stress component which is conducted through the soil skeleton. Bishop (1959) tried to explain "effective stress" for unsaturated soils in a similar fashion with Equations (2a) and (2b), therefore

$$\sigma = \sigma^* + \chi_m \cdot u_w + (1 - \chi_m)u_a \quad (3a)$$

therefore

$$\sigma^* = (\sigma - u_a) + \chi_m(u_a - u_w) = \sigma_{net} + \chi_m(u_a - u_w) \quad (3b)$$

where, σ^* = effective stress for unsaturated soil proposed by Bishop, and χ_m denotes the ratio of sectional area of meniscus water to that of the soil mass.

Figure 1 explains the difference between Equation (2b) and (3b). In the figure N^* is the contact force consisting to two types of forces, one is the force N_{net} that is

transmitted through soil particles constituting the soil skeletons and the other is the internal force N_m that is induced by the meniscus of the water surrounding the contact points of the soil particles. The net normal stress σ_{net} and Bishop's effective stress σ^* are expressed as follows.

$$(N_{net}/A) = \sigma_{net}, (N^*/A) = \sigma^* \text{ and } (N_m/A) = \chi_m(u_a - u_w) \quad (4)$$

where, A = cross sectional area of a soil mass, N = internal force. The stress component $\chi_m(u_a - u_w)$ of Equation (4) is called meniscus stress, which is not propagated through the soil skeleton. Unsaturated soils usually remain in the intermediate states between the two extreme states described by Equation (1a) and Equation (2a). The pore water first exists around the contact points of soil particles as meniscus water at the highly unsaturated state. Then, when the pore water is introduced, some of the meniscus water around the soil particles combines together to form a larger mass of pore water containing some contact points of soil particles as shown in Figure 2. Such pore water is called "bulk water" in this paper. Since the bulk water contains some contact points between soil particles, it can bear an external load together with the soil skeleton. The bulk water in unsaturated soils is thought to be equivalent to the pore water in saturated soils. Therefore, the equilibrium of total stress with stresses which are generated inside the soil mass can be expressed as,

$$\sigma = \sigma_{skel} + \chi_b \cdot u_w + (1 - \chi_b) \cdot u_a \quad (5)$$

where, σ_{skel} = normal stress component acting on the soil skeleton, $\chi_b = (A_b/A)$, A_b = cross-sectional areas of bulk water. When one substitutes Equation (5) into Equation (2a), σ_{skel} can be expressed as,

$$\sigma_{skel} = \sigma_{net} + \chi_b(u_a - u_w). \quad (6)$$

Equation (6) indicates that the mechanical action of bulk water is characterized by

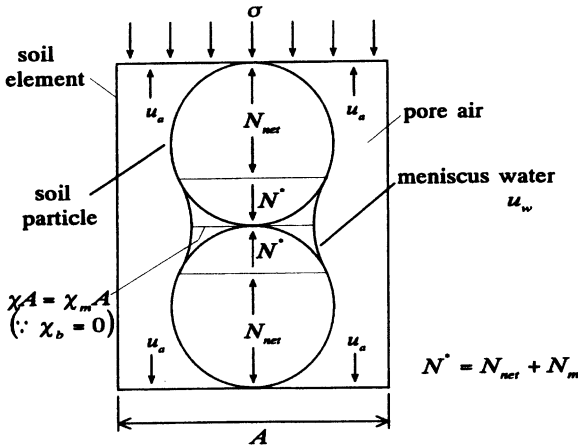


Figure 1. Equilibrium of stress components at surface and inside of soil element.

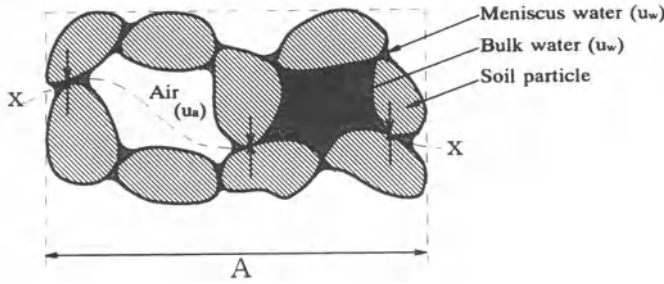


Figure 2. Wavy section of general unsaturated soil.

the term, $\chi_b(u_a - u_w)$. In deriving Equation (3a) from the equilibrium of forces at contact points of soil particles, the bulk water has not been taken into account. χ_m in Equation (3a) is the ratio of the cross-sectional area of meniscus water, as shown in Figure 1. Therefore, for the general case of unsaturated soils where some meniscus water is annexed into a mass of bulk water, the stress allotment role should be as follows:

$$\sigma = \sigma^* + (\chi_m + \chi_b) \cdot u_w + [1 - (\chi_m + \chi_b)] \cdot u_a \quad (7a)$$

therefore

$$\sigma^* = \sigma_{net} + (\chi_m + \chi_b)(u_a - u_w) \quad (7b)$$

or

$$\sigma^* = \sigma_{net} + \chi(u_a - u_w) \quad (7c)$$

where,

$$\chi = \chi_m + \chi_b \quad (7d)$$

Furthermore, substituting Equation (6) for σ_{net} into Equation (7b), one obtains,

$$\sigma^* = \sigma_{skel} + \chi_m(u_a - u_w). \quad (8)$$

Equation (8) implies that the normal stress σ^* acting on the plane at a contact point is given by the sum of the stresses, σ_{skel} and $\chi_m(u_a - u_w)$. Both σ_{skel} and σ^* are normal stress components but their mechanical actions on the soil skeleton are different. The stress σ_{skel} acts so as to compress the soil skeleton, and the stress σ^* acts so as to increase the shear resistance at the contact point of soil particles resulting in increasing rigidity of the soil skeleton. In the case of saturated soils, both stress components become exactly the same and correspond to Terzaghi's effective stress. However, in unsaturated soils, the value of σ^* is higher than that of σ_{skel} because of the additional term $\chi_m(u_a - u_w)$. The mechanical behaviour of unsaturated soils are influenced by these internal stress components; Terzaghi's effective stress concept becomes inapplicable. It can be understood from the above consideration that these stress factors, $(u_a - u_w)$, χ_b and χ_m should be taken into account in formulating

the stress–strain relationships for unsaturated soils. In fact, almost all stress–strain models proposed in the past consider the pore pressure difference ($u_a - u_w$) using matric suction s :

$$s = (u_a - u_w). \quad (9)$$

Once s is introduced, the coefficients of χ_b and χ_m have to be determined. These coefficients may be given as functions of the degree of saturation S_r , which is defined by,

$$S_r = \left(\frac{e_w}{e} \right) \times 100 = \frac{w \cdot G_s}{e} \quad (10)$$

where, e_w = relative void ratio introduced by Toll (1995), w = water content in percent and G_s = specific gravity of soil particles.

Since the degree of saturation S_r is described in term of the strain component as in Equation (10), it is then necessary to express S_r as a function of stress components instead. Usually the water retention curve is used to express S_r in terms of stress components as,

$$\chi_m = g_m(S_r) = g_m[h(s)] \quad (11a)$$

$$\chi_b = g_b(S_r) = g_b[h(s)] \quad (11b)$$

$$S_r = h(s) \quad (11c)$$

where, g_m and g_b are the functions which relate S_r to χ_m and χ_b , respectively. However, usually, it is not easy to obtain exact descriptions of the equations g_m and g_b , because the water retention curve of Equation (11c) is essentially stress-history dependent and shows heavy hysteretic response between drying and wetting processes.

Discussion of preceding works from the viewpoint of role of pore-water

BISHOP'S EFFECTIVE STRESS EQUATION

Bishop (1957) proposed the equation of effective stress expressed in Equation (3b) and Equation (7c).

Substituting Equation (7c) into the Mohr–Coulomb equation, one can express the shear strength of a soil mass as,

$$\tau_f = c' + [(\sigma - u_a) + \chi(u_a - u_w)] \tan \phi' \quad (12)$$

where τ_f = shear strength, c' = cohesion and ϕ' = friction angle. As to the parameter χ for shear strength, many shear test results (Karube et al., 1996; Vanapalli et al., 1996) suggest that

$$\chi = S_e = \frac{S_r - S_{r0}}{100 - S_{r0}} \quad (13)$$

where S_e = relative degree of saturation, S_r = degree of saturation in percent and $S_{r0} = (S_r)_{s \rightarrow \infty}$. Substituting Equation (13) into Equation (7c), one obtains;

$$\sigma^* = (\sigma - u_a) + \frac{S_r - S_{r0}}{100 - S_{r0}}(u_a - u_w). \quad (14)$$

In Equation (14), Bishop's effective stress, σ^* contains both matric suction s and degree of saturation S_r . The applicability of Bishop's effective stress equation should be examined based on test results obtained from a series of stress probe tests on the p - s plane (where p is net stress $(\sigma - u_a)$). Figure 3 shows typical test results. In Figure 3a, four stress paths employed in the experiment are indicated. All four specimens are loaded up to the stress point A and then a different load increment (as indicated by the arrows in the figure) is applied to each of the four specimens.

Figure 3b shows the changes of void ratio, Δe_1 , Δe_2 , Δe_3 and Δe_4 or $\Delta e_{4'}$ for load increment correspond to $A \rightarrow 1$, $A \rightarrow 2$, $A \rightarrow 3$ and $A \rightarrow 4$, respectively. (Note that the path $A \rightarrow 4'$ is followed by a collapsible soil.) The parameter χ in Bishop's effective stress equation can be evaluated from test results as:

$$\chi_{1,2} = \frac{\Delta e_2}{\Delta e_1} \quad (15a)$$

$$\chi_{3,4} = \frac{\Delta e_4}{\Delta e_3} \quad \text{or} \quad \chi_{3,4'} = \frac{\Delta e_{4'}}{\Delta e_3}. \quad (15b)$$

If the value of $\chi_{1,2}$ is found to be equal to $\chi_{3,4}$ or $\chi_{3,4'}$, it implies that the Bishop's effective stress equation is acceptable. However, it seems that there is not such experimental evidence (e.g. Jennings and Burland, (1962). It is certainly the case that, when a negative value of $\chi_{3,4'}$ is obtained by collapsing, Bishop's effective stress equation never holds.

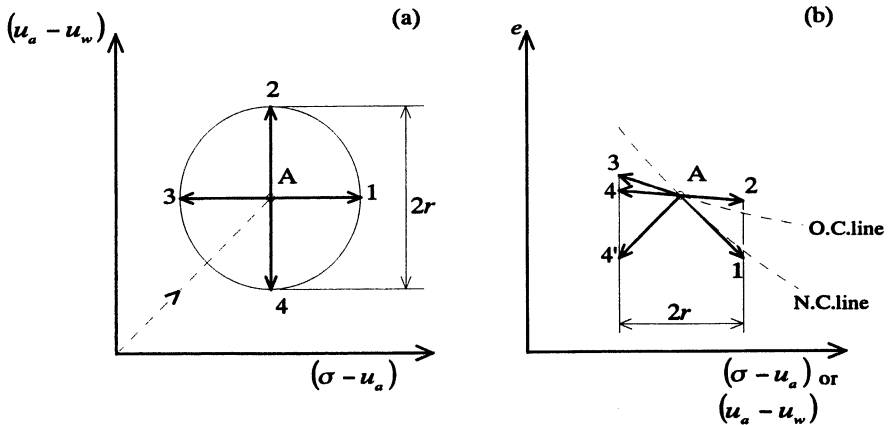


Figure 3. Stress probe test, (a) stress probe, (b) induced void ratio change.

ELASTO-PLASTIC MODEL BY ALONSO *ET AL.*

Alonso et al. (1987, 1990) have proposed an elasto-plastic constitutive model. First, the stress-strain relationships of their model under isotropic stress condition are discussed. The isotropic net stress p_0 is given by,

$$p_0 = p_{0T} - u_a \quad (16)$$

where p_{0T} = isotropic total stress. The volumetric compression characteristics of unsaturated soils under the condition of constant suction is assumed as shown in Figure 4 and can be formulated as;

$$(1 + e) = N(s) - \lambda(s) \ln \frac{p_0}{p_0^c} \quad (17)$$

where $\lambda(s)$ = the gradient of $(1 + e)$ and $\ln(p_0/p_0^c)$ relationship, that is,

$$\lambda(s) = \lambda(0)[(1 - r) \exp(-\beta s) + r] \quad (18a)$$

where p_0^c = reference net isotropic stress, $\lambda(0)$ = gradient of the above relation at saturated state, $N(s) = (1 + e)$ of soil mass at $s = s$ and $p_0 = p_0^c$, β = the parameter which controls the rate of increase of soil stiffness with suction, and

$$r = [\lambda(s \rightarrow \infty) / \lambda(0)]. \quad (18b)$$

Among these parameters, r is thought to be a material parameter but β would be influenced by the value of S_r . Since $\lambda(s)$ is given as a function of β , $\lambda(s)$ would be also affected by degree of saturation, S_r . The value of S_r strongly depends on the water retention characteristics. The water retention curve is heavily dependent on the loading path and shows strong hysteresis loops. Therefore it is not easy to uniquely specify the value of S_r .

For an anisotropic stress state, Alonso et al. introduced the modified Cam-Clay model to determine the shape of the yield surface. Figure 5 shows the elliptic yield

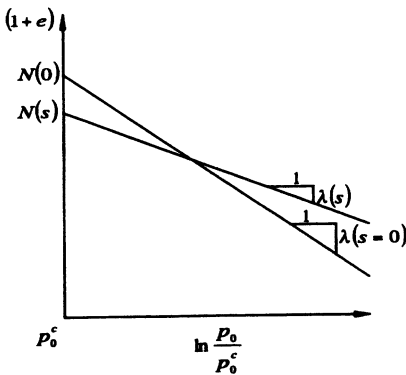


Figure 4. Isotropic compression line under constant suction.

surface and critical state line (CSL) on the constant suction plane. The effect of suction is taken into account by introducing an additional net stress p_s , which is defined as $p_s = (\text{difference of compression strengths between unsaturated and saturated specimens}) / (\text{inclination of critical state line, } M)$, and it will be influenced by S_r .

It is felt that such a formulation should be based on the energy balance for unsaturated soils. Specification of the yielding surface should be based on the formulation of dissipation energy balance because the yield surface of the modified Cam-Clay model was derived from dissipation energy balance for saturated soils. This will be introduced in the new model described later.

ELASTO-PLASTIC MODEL BY KOHGO ET AL.

Kohgo *et al.* (1993a, b) defined the effective stress as shown in Figure 6, that is: when $s \leq s_A$,

$$\sigma' = \sigma - u_w \quad (19a)$$

when $s > s_A$,

$$\sigma' = (\sigma - u_a) + s_c - \frac{a_e(s_c - s_A)}{a_e + (s - s_A)} \quad (19b)$$

where s_A = air entry value (AEV) of a given unsaturated soil. Equation (19a) assumes that the pore air exists as bubbles suspended in the pore-water, isolated from the soil skeleton. However, when the soil is wetted from a dry state to the state of $(0 < s \leq s_A)$, some pore air remains by clinging to soil skeletons. Equation (19a) does not consider such a state. In Equation (19b), the value of parameter a_e , which gives the initial gradient of σ' against s as in Figure 6, is difficult to be uniquely specified, as it depends on the hysteresis of the water retention curve. Moreover, for soils on the dry side of the optimum water content, the gradient

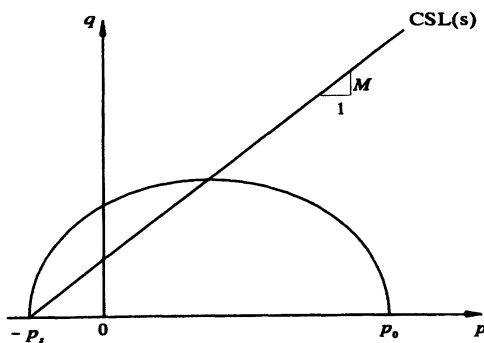


Figure 5. Yield surface in p - q - s space (p_0 is the trace of the yield line on p - s plane).

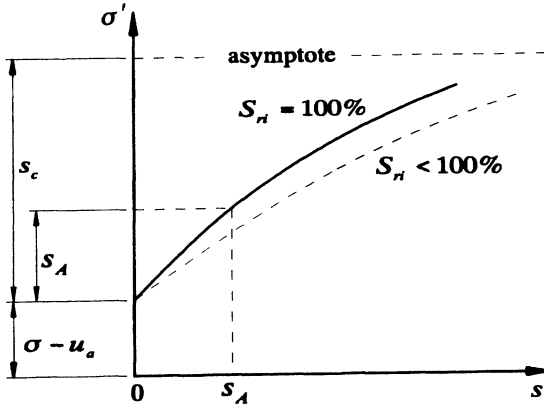


Figure 6. Effective stress by Kohgo *et al.* (1993a, b) (S_{ri} : initial degree of saturation)

of the water retention curve gets smaller resulting in a small value of a_e . Such effect of degree of saturation on the parameter a_e has to be taken into account.

The effective stress defined by Kohgo *et al.* can be regarded as a variation of Bishop's definition. Therefore, the loading-path dependent characteristics of volume change as shown in Figure 3 still cannot be explained.

Kohgo *et al.* introduced the flow surface expressed in $e - p'_0 - s$ space, where p'_0 denotes an isotropic effective stress, that is,

$$e = \Gamma(s) - \lambda(s) \log p'_0 \quad (20a)$$

where,

$$\Gamma(s) = \frac{\Gamma(0) + e_0^0 y}{1 + y} \quad (20b)$$

$$\lambda(s) = \frac{\lambda(0)}{1 + y} \quad (20c)$$

$$y = \frac{s - s_A}{a_s} \quad (20d)$$

In the above equations, $\lambda(s)$ in Equation (20a) corresponds to that used by Alonso *et al.* (Equation 17) and therefore the parameter a_s would still be influenced by the degree of saturation.

For anisotropic stress conditions, Kohgo *et al.* defined the yielding surface and plastic potentials in $p' - q$ space. In their model, since the effective stress state can be uniquely specified once the parameter a_s is determined, models for saturated soils such as the model of Cam clay type can be employed. They adopted the modified Cam-Clay in their model to describe the yielding surface.

Modeling based on stress components induced by suction

Karube (1987, 1988) performed a series of triaxial compression tests for low-plasticity clays compacted on the dry side of optimum water content. He could construct an elasto-plastic model which explains the test results obtained. In his modeling, it was assumed that the pore-water consists of the adsorbed water covering the surface of the soil particles and the water menisci at contact points of soil particles. The bulk water was tentatively left out for simplicity. The model obtained, however, could not apply to soils on the wetter side in which consolidation was induced by increasing suction.

In order to deal with the wide range of unsaturated soils from perfectly saturated to absolutely dry states, the idealized model was extended into a more general form (Karube and Kato, 1994, Karube, 1997, Karube et al., 1998). Namely, bulk water was taken into consideration. When a part of the bulk pores within the soil skeleton is occupied by pore water, the water is called the bulk water. The mechanical role of bulk water is thought to be the same as that of pore-water in saturated soils. Namely, it can support the external total stress in cooperation with the soil skeleton.

The broken line x-x in Figure 2 represents a wavy section of an unsaturated soil mass, of which the gross area is A and the cross-sectional areas of pore air, bulk water, meniscus water and adsorbed water are A_a , A_b , A_m and A_0 , respectively. Then, the following relation is satisfied.

$$(A - A_a) = A_b + A_m + A_0. \quad (21)$$

If it can be assumed that each cross-sectional area in the right hand side of Equation (21) is proportional to the equivalent degree of saturation which is provided by each form of pore water, the following decomposition can be introduced,

$$S_r = S_{rb} + S_{rm} + S_{r0} \quad (22)$$

where,

$$\frac{S_r}{100} = \left(1 - \frac{A_a}{A}\right), \frac{S_{rb}}{100} = \frac{A_b}{A}, \frac{S_{rm}}{100} = \frac{A_m}{A} \quad \text{and} \quad \frac{S_{r0}}{100} = \frac{A_0}{A}. \quad (23)$$

The mechanical behaviour of unsaturated soils is governed by each term of Equation (22). However, it should be noted that the adsorbed water is not part of the pore-water in the case of unsaturated soils. The bulk water and the meniscus water play dominant roles in the mechanical behaviour of unsaturated soils. Their contributions are evaluated by the parameters χ_b and χ_m as,

$$\chi_b = \frac{A_b}{A - A_0} = \frac{S_{rb}}{100 - S_{r0}} \quad (24)$$

$$\chi_m = \frac{A_m}{A - A_0} = \frac{S_{rm}}{100 - S_{r0}} \quad (25)$$

Since the contribution of meniscus water is described by Equation (25), the definition

of meniscus stress, p_m , defined by Equation (4) would be extended as,

$$p_m = \frac{S_{rm}}{100 - S_{r0}} \cdot (u_a - u_w) = \chi_m \cdot s \quad (26)$$

Likewise, the bulk stress p_b which is an isotropic stress induced by bulk water would be defined as,

$$p_b = \frac{S_{rb}}{100 - S_{r0}} \cdot (u_a - u_w) = \chi_b \cdot s \quad (27)$$

These two stress components were previously defined by Equations (5) to (8) as normal stresses. However, the strict definitions are provided by Equations (26) and (27). The meniscus stress p_m and the bulk stress p_b are defined as isotropic stresses applicable to the multi-dimensional situation. The bulk stress can be treated as the same as the pore-water pressure in the case of saturated soils. Namely, the following equation is introduced.

$$\begin{aligned} p_{skel} &= p' = p + p_b = p + \chi_b \cdot s \\ &= (p_T - u_a) + \frac{S_{rb}}{100 - S_{r0}} (u_a - u_w) \end{aligned} \quad (28)$$

where p_{skel} is the stress component (skeleton stress) which is conducted through soil skeletons and the symbol of p' is used instead of p_{skel} for simplicity. The isotropic meniscus stress p_m is an internal stress working so as to stiffen the soil skeletons but does not contribute to bear the external force. It just internally equilibrates with the suction and surface tension of meniscus water at every contact point of soil particles. As consequence, the isotropic stress for unsaturated soils consists of two components of $p' = p_{skel}$ and p_m . The constitutive equation has to be described using these two components.

EVALUATION OF MENISCUS STRESS

The meniscus stress p_m can be evaluated by comparing compressive strengths of saturated and unsaturated specimens as follows.

The critical state line of saturated specimens is expressed as,

$$q_f = c_{ir} + p' M \quad (29)$$

where $q'_f = (\sigma'_1 - \sigma'_3)_f$; compressive strength with surface energy correction,

$$p' = \frac{\sigma_1 + 2\sigma_3}{3} - u_w; \text{ effective mean stress (for triaxial conditions, } \sigma_2 = \sigma_3)$$

c_{ir} = intercept of critical state line on q_f -axis

M = inclination of failure line with respect to p' -axis (30)

In the case of unsaturated soils, Equation (29) becomes,

$$q_f = c_{tr} + M(p' + p_m) \quad (31)$$

The term of $(p' + p_m)$ can be described as

$$p' = p_m = p + p_b + p_m = (p_T - u_a) + (\chi_b + \chi_m) \cdot s \quad (32)$$

where, the parameters χ_b and χ_m are expressed from Equations (22), (24) and (25) as,

$$\chi_b + \chi_m = \frac{S_r - S_{r0}}{100 - S_{r0}} = S_e = \chi \quad (33)$$

Then, substituting Equations (32) and (33) into Equation (31), one obtains,

$$q_f = c_{tr} + M(p + \chi \cdot s) \quad (34)$$

The parameter χ can be determined from triaxial tests using Equation (33) in terms of degree of saturation or can be evaluated from the shear strength using Equation (34). Figure 7 shows values of χ obtained by different methods of calculation (Karube *et al.*, 1996). As for the shear strength, it is found that the bulk stress and the meniscus stress equally contribute to the shear strength mobilization (Karube *et al.*, 1996). Thus it is convenient to introduce the following stress parameter as,

$$p_s = p_b + p_m \quad (35)$$

where, p_s is the suction stress.

EQUATION OF ISOTROPIC COMPRESSION

The relationship of void ratio and isotropic stress for saturated clays in normally consolidated state is given by

$$e = e_1 - \lambda \ln(p'_0/p'_{0i}) \quad (36)$$

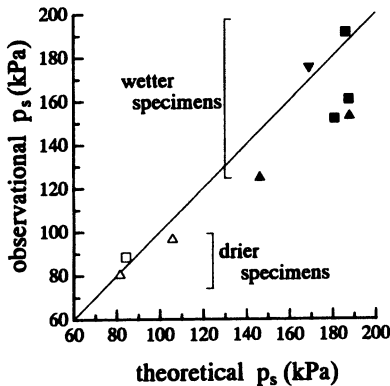


Figure 7. Parameter χ from theory and observation.

therefore

$$-\frac{dp'_0}{de} = \frac{1}{\lambda} p'_0 \quad (37)$$

where, λ = compression index in natural logarithm scale, p'_0 is isotropic stress ($q = 0$), e_i = void ratio at $p'_0 = p'_{0i}$.

The left hand side of Equations (37) is a stiffness. For saturated soils the stiffness is proportional to the magnitude of effective stress. In unsaturated soils, meniscus stress acts as an internal stress at every contact point in addition to net stress. Therefore the stiffness of unsaturated soil would be evaluated as;

$$-\frac{dp'_0}{de} = \frac{1}{\lambda} (p'_0 + ap_m) \quad (38)$$

where, a = contribution ratio of meniscus stress to the stiffness of the soils. The plastic incremental volumetric strain is calculated by;

$$dv^p = \frac{\lambda - \kappa}{1 + e_i} \frac{dp'_0}{p'_0 + ap_m} \quad (39)$$

where, κ = swelling index in natural logarithm scale, e_i = void ratio at $v^p = 0$. Assuming plastic volumetric strain v^p is a state function of the isotropic net stress p_0 and the meniscus stress p_m , Equation (39) can be integrated as follows:

$$v^p = \frac{\lambda - \kappa}{1 + e_i} \ln(p'_0 + p_m) + B \quad (40)$$

where, B = integration constant.

To determine the constant B , the initial yield locus is introduced based on the hypothesis that the soil mass is initially saturated and then becomes unsaturated by increasing suction with an increase of the meniscus stress p_m , that is,

$$p'_0 = p'_{0y} + ap_m \quad (41)$$

where, p_{0y} = yield stress in the saturated state.

Therefore, the plastic volumetric strain under the unsaturated state is expressed as

$$v^p = \frac{\lambda - \kappa}{1 + e_i} \ln \left(\frac{p'_0 + ap_m}{p'_{0y} + 2ap_m} \right) \quad (42)$$

The parameter a in Equation (38) must be determined experimentally. By considering a micro-mechanism of plastic deformation of soil skeleton, one can roughly estimate a as one-half ($a \cong 0.5$) (based on Mindlin, 1949). Figure 8 shows the iso-stiffness lines and the initial yield locus on the $p - p_m$ plane. Furthermore, the contour of plastic strain is obtained from Equation (42), that is,

$$p_m = \frac{p'_0 - Hp'_{0y}}{a(2H - 1)} \quad (43a)$$

where,

$$H = \exp \left[\left(\frac{1 + e_i}{\lambda - \kappa} \right) v^p \right] = \frac{p'_0 + ap_m}{p'_{0y} + 2ap_m}. \quad (43b)$$

The obtained contours of plastic strain are shown in Figure 9. A family of straight lines radiates from the point $(p'_0 = p'_{0y}/2, p + m = -p'_{0y}/2a)$. According to Equation (42), plastic volumetric strain does not develop when suction increases. This is consistent with experimental data for soils having relatively low degrees of saturation (Matyas and Radhakrishna, 1968).

Next, consider an initial yield locus of a specimen compacted on the dry side of the optimum water content. As a soil is compacted, the number of contact points between soil particles increases. It results in a decrease of the meniscus water per contact point and leads to an increase of suction. Therefore, since the suction s and the compression stress p increase simultaneously during compaction, it is thought that the initial yield locus should be drawn on the right hand side and the gradient of the yielding line gets smaller than that shown in Figure 9. Then, Equation (41) is rewritten as;

$$p'_0 = p'_{0y} + a'p_m \quad (44)$$

where, a' = gradient of initial yield locus relative to p_m axis, $a' > a$. The plastic

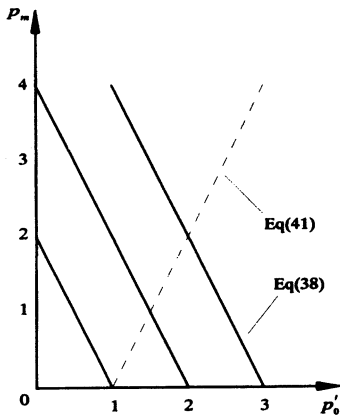


Figure 8. Example of equi-stiffness (in full line) and initial yield locus (in broken line) when $a = 0.5$, $p'_{0y} = 1$.

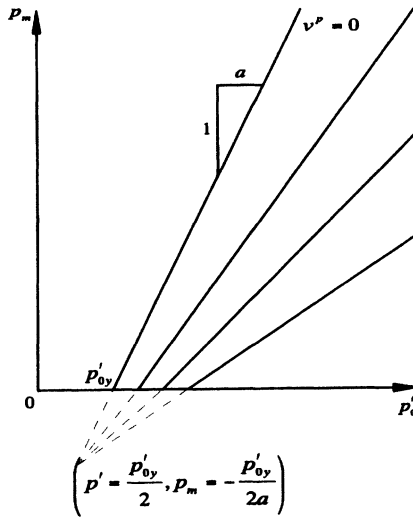


Figure 9. v^p -contours of initially unsaturated soil.

volumetric strain and the meniscus stress p_m are expressed as;

$$v^p = \frac{\lambda - \kappa}{1 - e_i} \ln \left[\frac{p'_0 + ap_m}{p'_{0y} + (a + a')p_m} \right] \quad (45)$$

$$p_m = \frac{p'_0 - Hp'_{0y}}{a[1 + (a'/a)]H - 1} \quad (46)$$

Figure 10 shows the contours of plastic volumetric strain represented by Equation (46).

It should be noted that the plastic volumetric strain expression can also be obtained by considering the shear yield surface in $p' - p_m - q$ space. The following differential equation can be introduced for the condition of triaxial compression (justification for this equation is provided later in the paper).

$$\frac{dq}{dp'} - \frac{q}{p'} + \frac{M(p' + p_m)}{p'} = 0 \quad (47)$$

where, $q = \sigma_1 - \sigma_3$; deviator stress. Honda (2000) integrated Equation (47) under the following stress condition as;

when $p' = p'_{sat}$,

$$q_y = Mp_m \quad (48)$$

where; p'_{sat} = intersect of yield surface on p -axis, that is, p' of yield surface for

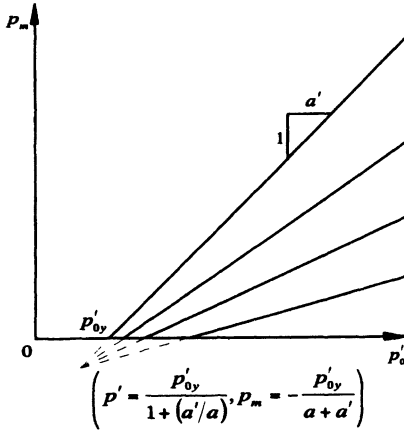


Figure 10. p^p -contours of compacted soil.

saturated soil at $p = 0$ as shown in Figure 11. Thus the yield surface is obtained as

$$q = Mp' \left(\ln \frac{p'_{sat}}{p'} + \frac{p_m}{p'} \right) \quad (49)$$

The yield locus for the $p' = p_m$ relation is obtained from Equation (49) as

$$p'_0 = p'_{sat} + p_m - \frac{p_m^2}{2p'_{sat} + p_m} \quad (50)$$

According to Equation (50), the yield loci (equivalent to the contour of plastic volumetric strain) are described as a family of nearly parallel straight lines which cross the p axis at 45° . This does not agree with experimental data by Matyas and Radhakrishna (1968), however, Equation (49) is easy to handle because of its clean-cut form.

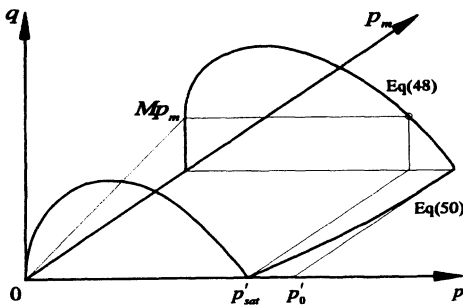


Figure 11. Shear yield point (Equation (48)) and resultant yield locus (Equation (50)).

CONSTITUTIVE EQUATION

An elasto-plastic model for unsaturated soil was developed by referring to the original Cam-clay model for saturated soils by Roscoe et al. (1963). The energy equation of the original Cam-clay model is,

$$p' dv^p + q d\varepsilon^p = Mp' d\varepsilon^p \quad (51)$$

where, $\varepsilon^p = \frac{2}{3}(\varepsilon_1^p - \varepsilon_3^p)$; plastic shear strain. Since the stress p' appearing in the left hand side of Equation (51) is the stress component which is conducted through the soil skeleton, it can be replaced by the skeleton stress p' in the case of unsaturated soils. The stress p' on the right hand side of Equation (51) is the normal stress component which contributes to shear resistance and it would correspond to the stress component $(p' + p_m)$ in the unsaturated state. Therefore, the energy equation for unsaturated soils can be extended to,

$$p' dv^p + q d\varepsilon^p = M(p' + p_m) d\varepsilon^p \quad (52)$$

therefore

$$\frac{dv^p}{d\varepsilon^p} = \frac{M(p' + p_m)}{p'} - \frac{q}{p'} \quad (53)$$

If an associated flow rule is applied, $(dv^p/d\varepsilon^p)$ can be replaced by $(-dq/dp')$ and Equation (47) is derived. Equation (47) can be integrated under the condition that $p' = p'_0$ when $q = 0$ and then the yield surface is obtained as follows,

$$\frac{q}{Mp'_0} = -\frac{p'}{p'_0} \ln \left[\frac{p'}{p'_0} \right] + \frac{p_m}{p'_0} \left(1 - \frac{p'}{p'_0} \right) \quad (54)$$

where, $p'_0 = (p')_{q=0}$.

The plastic volumetric strain v^p in terms of $p' - p_m - q$ is obtained by substituting p'_0 of Equation (54) into Equation (42) or (45). However, Equation (54) cannot be solved by p'_0 . When Equation (54) is approximated to a parabolic equation, the plastic volumetric strain is expressed as;

$$v^p = \frac{\lambda - \kappa}{1 + e_i} \ln \frac{\frac{q}{M} + \sqrt{\left(p' + p_m - \frac{q}{M} \right)^2 + \frac{2ap'}{M}} - (1 - a)p_m}{p'_{0y} + 2ap_m} \quad (55)$$

On the other hand, since p_{sat} in Equation (49) introduced by Honda is given by

$$v^p = v^p_{sat} = \frac{\lambda - \kappa}{1 + e_i} \ln \frac{p'_{sat}}{p'_{0y}} \quad (56)$$

the plastic volumetric strain is obtained by substituting p_{sat} of Equation (56) into

Equation (49) as,

$$v^p = \frac{\lambda - \kappa}{1 + e_i} \left[\ln \left(\frac{p'}{p'_{0y}} \right) + \frac{q - Mp_m}{Mp'} \right] \quad (57)$$

Next, the shear strain increment is derived from the energy Equation (53) as,

$$d\varepsilon^p = \frac{p' dv^p}{M(p' + p_m) - q} \quad (58a)$$

where,

$$dv^p = \frac{\partial v^p}{\partial p'} dp' + \frac{\partial v^p}{\partial p_m} dp_m + \frac{\partial v^p}{\partial q} dq \quad (58b)$$

Equation (58b) is easily calculated from either Equation (55) or (57).

If the components of degree of saturation S_{rm} , S_{rb} and S_{r0} are not determined, the stress components, p_m and p_b are not specified. The method of determination of the components is discussed later in the paper.

Water retention curve evaluated by Brooks and Corey's equation

Throughout the paper, the authors have emphasized the significance of the water retention curve and the effect of suction history on the curve. Such a suction-history dependent water retention curve should be incorporated into the formulation of the stress-strain relationships for unsaturated soils. In other words, the relationship between suction and degree of saturation has to be examined thoroughly. The water retention curve has been studied for many years in irrigation engineering. However, in the engineering field (see, intensive review by Leong and Rahardjo, 1997), the water retention curve for the engineering use has not been sufficiently explored. The logarithmic scale is often used to plot the suction value of the water retention curve. However, natural scale is sometimes more convenient when the suction does not reach very high values (not more than 500 kPa). This is advantageous if the curve is to be extrapolated, even in the negative region.

If the water retention curve under constant net stress is considered, two bounding (ultimate) water retention curves are defined as shown in Figure 12. The upper curve (curve (1)) is the drying curve starting from the saturated state and it converges asymptotically to $S_r = S_{r0}$. The lower curve (curve (2)) is the wetting curve starting from the asymptote and it crosses the S_r axis at a point below $S_r = 100\%$. In this paper, two series of laboratory tests which have been carried out to obtain the drying and wetting curves are introduced first. The influence of void ratio on the water retention curve is examined. The water retention curves obtained from experiments are evaluated here using the empirical model by Brooks and Corey (1966). The correlations between void ratio and parameters used in the model are investigated.

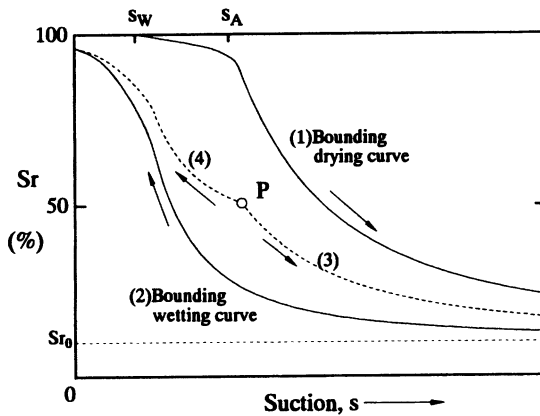


Figure 12. Concept of water retention curves, (1) Drying curve from $S_r = 100\%$, (2) Wetting curve from $s = \infty$, (3) Drying curve starts from P, (4) Wetting curve starts from P.

EXAMPLES OF WATER RETENTION CURVE

The water retention curves in Figure 13 were obtained from initially saturated low plasticity clays, where material properties are summarized in Table 1. In Test A, the specimen was consolidated under an isotropic stress of 19.6 kPa with both pore-water and pore-air pressures kept at zero. After that, the pore-air pressure was increased to 490 kPa and then it was released stepwise with the pore-water pressure kept at zero. Isotropic stress was applied to the specimen so as to keep the net constant. Likewise, Test D was conducted under the condition of constant net stress of 98 kPa. The void ratio of both test specimens was found to decrease in the earlier stages of suction loading. The water retention curves in terms of the degree of saturation and the water content are shown in Figures 13(a) and (b), respectively.

In order to examine the influence of net stress, a series of oedometer tests was also performed with control of net vertical stress and suction. Soil specimens were

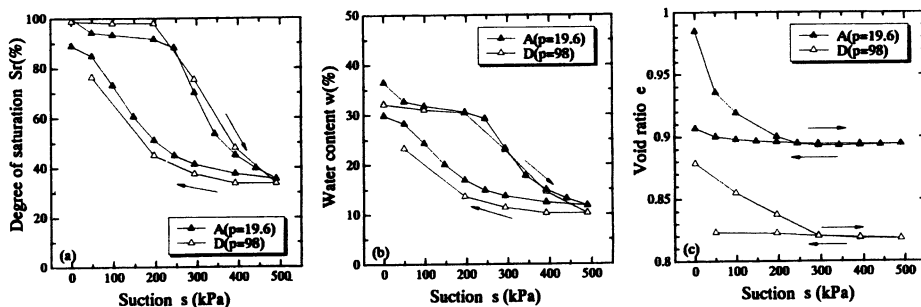


Figure 13. Effect of net stress on water retention curve, (a) Degree of saturation, (b) Water content, (c) Void ratio.

Table 1. Physical properties of tested soil.

G_s	w_L (%)	w_p (%)	$< 2 \mu\text{m}$ (%)	d_{max} (μm)
2.70	43.0	29.6	17	30

Table 2. Initial condition.

Test	Void ratio e	Water content w (%)	Degree of saturation S_r (%)
● a	2.11	23.2	29.7
■ b	1.62	30.2	50.5
⊙ c	1.59	17.5	29.7
○ d	1.20	23.1	52.0
□ e	0.99	30.4	82.9

prepared from soil powder whose water content had been controlled to specific values in advance. The soil specimens were statically compacted in the oedometer apparatus under a vertical stress of 169 kPa. Table 2 shows material properties and test conditions. Vertical load and air pressure were gradually increased and the negative pore-water pressure was measured. Loading was continued until the pore-water pressure reached zero and the vertical net stress attained 196 kPa. After that, the suction was increased to 490 kPa and then released to zero. During suction increase and decrease, the vertical net stress was kept at 196 kPa. Figure 14(c) shows the change in void ratio. The void ratio did not change much but collapse was found in some specimens having initially higher values of void ratio when the suction was released to less than 50 kPa. As for the water content (figure 14b), it seemed to converge to a point as the suction increased.

Many models describing the water retention curve have been proposed. The air entry values s_A and the volume of residual (adsorbed) water S_{r0} are usually adopted as input parameters of the models. When suction is gradually applied to initially

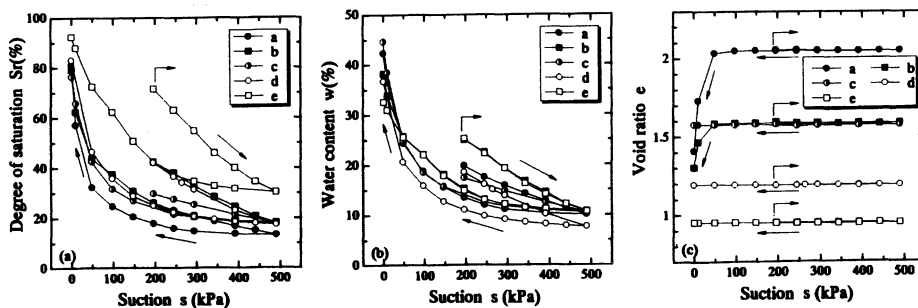


Figure 14. Effect of initial water content on water retention curve, (a) Degree of saturation, (b) Water content, (c) Void ratio. (See Table 2 or initial conditions.)

saturated soils, the air entry value (AEV) can be recognized as the point at which drainage begins to proceed faster. However, for the soil specimens compacted on the dry side, it is difficult to recognize such a point as seen in Figure 14. In such a case, it is difficult to recognize such a point as seen in Figure 14. In such a case, the air entry value (AEV) is graphically determined by fitting the model to the curve obtained from experiments. Brooks and Corey's model was used to determine the AEV. Brooks and Corey's model is expressed as,

$$S_r = (100 - S_{r0}) \left(\frac{s_A}{s} \right)^2 + S_{r0} \quad (59a)$$

Curve fitting work was performed using relative degree of saturation S_e on log-log scale as,

$$\log S_e = \lambda (\log s_A - \log s) \quad (59b)$$

where,

$$S_e = \frac{S_r - S_{r0}}{100 - S_{r0}} \quad (59c)$$

Firstly, data obtained from experiments are plotted in $\log s$ – $\log S_e$ space. Assuming an appropriate value of S_{r0} , one can apply Equation (59b) and draw a straight line starting from s_{\max} as shown in Figure 15. Then, λ is determined as the gradient of the straight line and s_A (AEV) is given by the value of suction when $\log S_e = 1$.

Likewise, Brooks and Corey's model can be applied to the wetting curve as,

$$S_r = (100 - S'_{r0}) \left(\frac{s_W}{s} \right)^{\lambda'} + S'_{r0} \quad (60a)$$

And,

$$S'_e = \frac{S_r - S'_{r0}}{100 - S'_{r0}} \quad (60b)$$

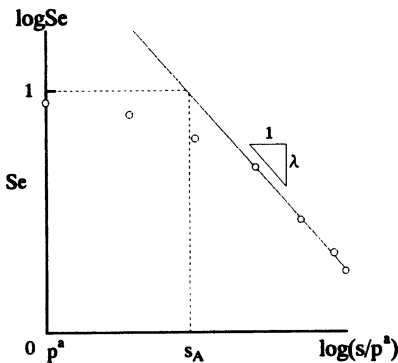


Figure 15. Fitting Brooks and Corey's equation to suction test.

The water entry value s_W (WEV) is given as the value of suction when $S'_e = 1$. The parameters determined in such a manner are tabulated in Table 3. For details, see Kawai et al. (2000).

FACTORS AFFECTING THE PARAMETERS OF WATER RETENTION CURVE

When suction is applied to an unsaturated soil, the suction increase creates the tendency for the pore water (which is held by meniscus tension within the soil skeleton) to migrate. Then, the bulk water begins to drain away when the suction reaches the air entry value. Since it is thought that the bulk water begins to flow when the suction exceeds the capillary tension stress, AEV (s_A) would reflect the magnitude of capillary tension in the soil. The capillary tension is in inverse proportion to the size of bulk pore and the size of the bulk pore is in proportion to the void ratio. Therefore, AEV is thought to be in inverse proportion to the void ratio e of the soil. Figure 16(a) indicates the relationship between the value of AEV and the void ratio, obtained from experiments by Kawai *et al.* (2000). The relationship between WEV and degree of saturation is plotted in Figure 16(b). It was found that the experimental data can be explained by the broken lines drawn in the figures as,

$$s_A = A \cdot e^{-B} \tag{61a}$$

$$s_W = A' \cdot e^{-B'} \tag{61b}$$

where, A , B , A' and B' are constant parameters. When the suction increases beyond, AEV, virtually all bulk water is removed from the soil. The pore-water consists of the meniscus water clinging to the contact points of soil particles and the absorbed water covering the soil particles. Under such a state, the quantity of meniscus water would be in proportion to the number of contact points and also be in inverse proportion to

Table 3. Brooks and Corey's approximation of water retention curves.

test	e ($s > s_A$)	Drying process				Wetting process			p (kPa)
		S_{r0} (%)	e_{w0}	s_A (kPa)	λ	S'_{r0} (%)	s_W (kPa)	λ'	
● a	2.05	9.21	0.199	33.3	0.73	0	4.9	0.41	196
■ b	1.58	11.77	0.185	85.3	0.94	0	19.6	0.47	
● c	1.57	12	0.188	13.7	0.46	0	7.8	0.36	
○ d	1.19	15.86	0.189	101.9	1.10	11.1	28.4	0.87	
□ e	0.95	19.93	0.189	163.7	107	0	39.2	0.47	
▲ A	0.895	21.13	0.189	223.4	1.72	29.2	90.2	1.80	196
(B)*	(0.895)	—	—	—	—	41.7	78.4	1.74	
(C)*	(0.895)	—	—	—	—	70.5	86.2	3.54	
△ D	0.819	0	0	246.0	1.57	0	15.7	0.33	98

Note: *Test B and C: see Kawai *et al.* (2000)

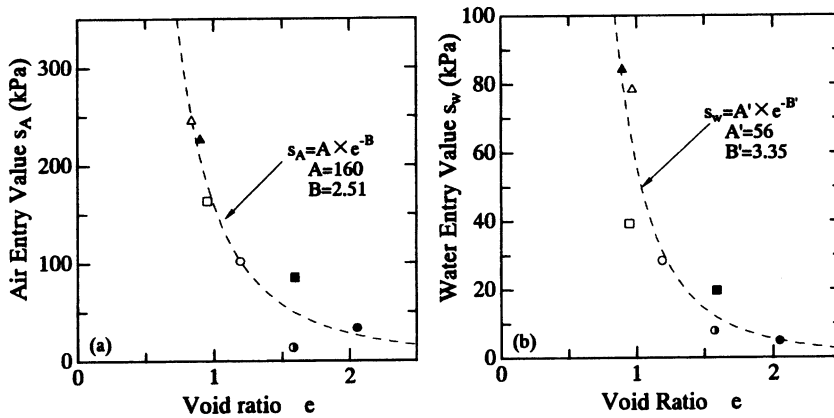


Figure 16. Relationship between void ratio and (a) air entry value, (b) water entry value.

void ratio. The quantity of adsorbed water would be determined by the total surface area of soil particles. Therefore the residual relative void ratio and the residual water content would be constant.

As summarized in Table 3, the values of residual relative void ratio e_{w0} obtained from experiments of Test to a Test e coincides and is independent of test conditions. This is in contrast with the values of S_{r0} which are fairly scattered. Herein, S_{r0} is calculated from

$$S_{r0} = \frac{e_{w0}}{e} 100 \quad (62)$$

where, $e_{w0} = w_0 \cdot G_s$, residual relative void ratio, w_0 = residual water content. The experimental results support the above inference.

CORRELATIONS BETWEEN PARAMETERS OF A DRYING CURVE

Both air entry value s_A and residual degree of saturation S_{r0} can be expressed as functions of void ratio e as given by Equation (61a) and (62). Eliminating e from both the equations, one obtains

$$s = A(e_{w0})^{-B} \cdot (S_{r0}/100)^B \quad (63)$$

Figure 17 shows the relationship between s_A and S_{r0} , in which the solid line is given by Equation (63) with $A = 160$, $B = 2.51$ and $e_{w0} = 0.0019$. Experimental data shows good agreement with the theoretical prediction by Equation (63) except the data obtained for Test D. It is shown that the value of residual degree of saturation becomes higher as the air entry value becomes larger. Such a soil has a steep gradient of water retention curve resulting in a larger value of λ as defined in Equation (59a). Figure 18 shows the correlation between s_A and λ . The broken line indicated in

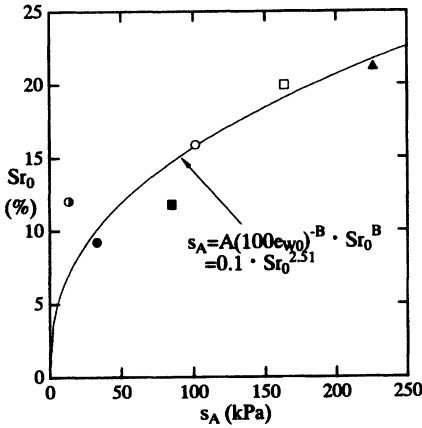


Figure 17. Relationship between air entry value and residual degree of saturation.

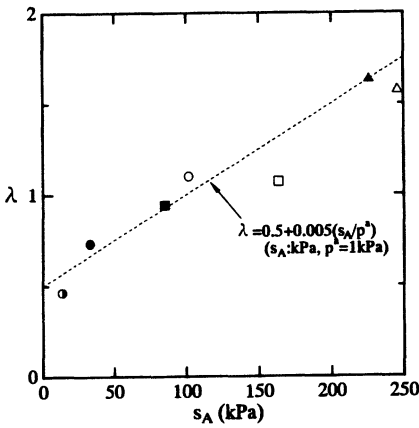


Figure 18. Parameter λ plotted against air entry value.

Figure 18 is expressed as

$$\lambda = 0.5 + 0.05(s_A/p^a) \quad (64)$$

where p^a = unit stress of s_A , 1 kPa.

It is concluded that the water retention curve can be described as a function of void ratio based on experiments in which the change of void ratio is measured during suction increase.

PARAMETER OF A WETTING CURVE

Figure 19 illustrates typical wetting curves. When the wetting curve is described using Brooks and Corey's model, three fitting parameters λ' , S'_{r0} and s_w have to

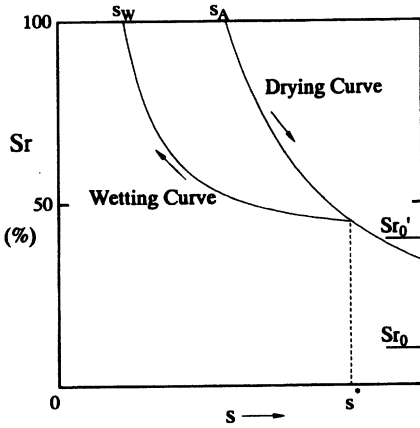


Figure 19. Wetting curve rebounding from a point on drying curve.

be determined. When the wetting curve starts from the point (s^*, S_r) as shown in Figure 19, the following relationship, from Equations (59a) and (60a), is satisfied.

$$\left(1 - \frac{S_{r0}'}{100}\right) = \frac{1 - (s_A/s^*)^\lambda}{1 - (s_W/s^*)^{\lambda'}} \left(1 - \frac{S_{r0}}{100}\right) \quad (65)$$

Since the drying curve is known, then the parameters s_A , S_{r0} , λ , s_W and s^* are obtained. Therefore Equation (65) implies a theoretical relationship between S_{r0}' and λ' when the wetting curve passes through the point of (s^*, S_r) . The points A, B and C in Figure 20 are obtained from the wetting curves A, B and C in Figure 5 of Kawai et al. (2000) and curves drawn using a solid line indicate the possible equations corresponding to the wetting curves.

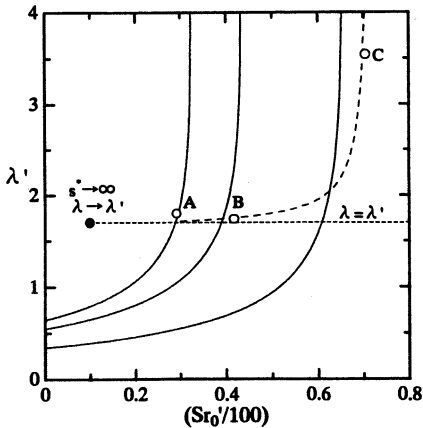


Figure 20. Relationships among s^* , λ' and S_{r0}' .

It is found that since the value of λ' quickly approaches to that of λ with suction increase, λ' can be assumed to be equal to λ . Then, the parameter S'_{r0} can be calculated from Equation (65). Note that the parameter s_W has been defined by Equation (61b) as a function of void ratio.

EXPRESSION OF WATER RETENTION CURVE STARTING FROM A GIVEN POINT

The wetting curve starting from an arbitrary point can be approximated as

$$S_r = (100 - S'_{r0}) \left(\frac{s_W}{s} \right)^\lambda + S'_{r0} \quad (66a)$$

where, s'_{r0} is the parameter determined from the condition that the wetting curve passes through a given point P (s_P, S_{rP}), that is,

$$S'_{r0} = \frac{S_{rP} - 100 \times (s_W/s_P)^\lambda}{1 - (s_W/s_P)^\lambda} \quad (66b)$$

The family of wetting curves is outlines in Figure 21(a).

Next, consider drying curve passing through a given point P. Such a drying curve is located between two ultimate drying curves indicated as (1) and (2) in Figure 12. Since both ultimate drying curves have the same asymptote at $S_r = S_{r0}$, any drying curve located between two limitation curves is thought to have the same asymptote at $S_r = S_{r0}$. Also the gradient λ of a drying curve can be chosen as the same value as that of two ultimate drying curves. Such a drying curve has the air entry value s_{AP} expressed as

$$s_{AP} = s_P \left(\frac{S_{rP} - S_{r0}}{100 - S_{r0}} \right)^{1/\lambda} \quad (67)$$

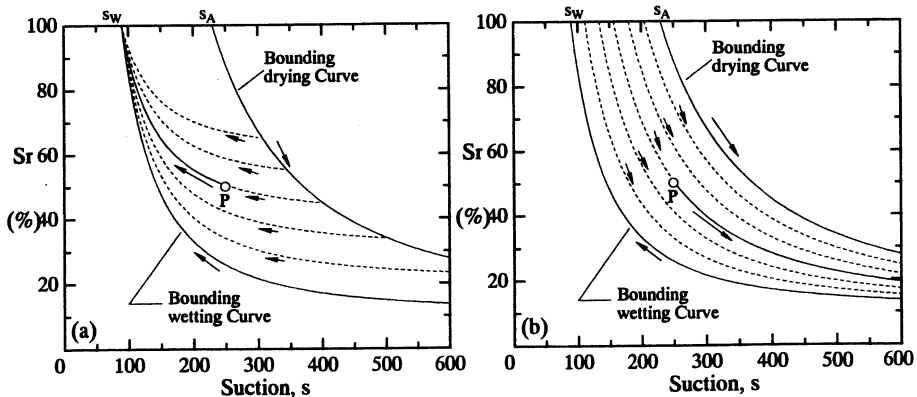


Figure 21. Water retention curve from a given point P, (a) Wetting curve, (b) Drying curve (Example: $S_{r0} = 10\%$, $s_A = 230$, $s_W = 90$).

The family of drying curves is illustrated in Figure 21(b). Equation (67) implies that each drying curve has a different air entry value, s_{AP} . Apparently, it seems to be contradictory that the air entry value should be uniquely specified for a soil. Therefore, the parameter s_{AP} is introduced to specify the location of the drying curve and is valid only for the drying curve in the range where suction is higher than s_P . Consequently, it is understood that the wetting curve and the drying curve can be described by the parameters used in the two ultimate water retention curves.

The driest curve to estimate the components of degree of saturation

The stress–strain equations introduced in this paper have been developed based on the assumption that the degree of saturation consists of three components as shown by Equation (22). In order to specify each component, a conceptual water retention curve named “the driest curve” (Karube et al., 1998 and Wheeler and Karube, 1995). The driest curve is defined as a water retention curve which the driest soil can possibly trace in the $s - S_r$ space. Once the driest curve is introduced, three components constituting the degree of saturation can be specified as follows.

portion of bulk water:

$$S_{rb} = \frac{(100 - S_{r0})(S_r - S_{rd})}{100 - S_{rd}} \quad (68)$$

portion of meniscus water:

$$S_{rm} = S_r - (S_{r0} + S_{rb}) \quad (69)$$

portion of adsorbed water:

$$S_{r0}$$

where, S_{rd} = degree of saturation on the direct curve.

Since the wetting curve starting from S_{r0} means the water retention curve of soils contains less bulk water, this ultimate wetting curve (indicated by (2) in Figure 12) in this sense, can be regarded as the driest curve in the region of higher suction. On the other hand, since the bulk water begins to rapidly increase when the suction value falls below AEV s_A , the ultimate wetting curve cannot be used to express the driest curve. In the region of suction lower than s_A , it is assumed that the driest curve is expressed by the quadratic equation tangential to the ultimate wetting curve at s_A . Then, the driest curve is described as follows:

$s \geq s_A$:

$$S_r = S_{rd} = (100 - S_{r0})\left(\frac{s_W}{s}\right)^\lambda + S_{r0} \quad (70a)$$

$s < s_A$:

$$S_r = S_{rd} = (100 - S_{r0}) \left(\frac{s_W}{s_A} \right) \left\{ -(\lambda + 1) \left(\frac{s}{s_A} \right)^2 + (\lambda + 2) \left(\frac{s}{s_A} \right) \right\} + S_{r0} \quad (70b)$$

Figure 22 shows the driest curve together with the bounding wetting and drying curves.

Summary and conclusion

In this paper the essential features required in the stress-strain modeling for non-expansive unsaturated soils are discussed from the viewpoint of role of pore-water in the mechanical behaviour of soils. The isotropic stress acting on the soil is clarified into three kinds of stresses, that is, total mean stress, pore air pressure and pore water-pressure. The sum of these isotropic stresses is decomposed into isotropic net stress and suction from a mechanical viewpoint. Such decomposition is widely employed in the research on unsaturated soils. This paper also adopts this decomposition of the isotropic stress. However, the suction is not used directly but treated as a function of the degree of saturation as the isotropic compressive stress induced by suction is dependent on the degree of saturation. Conclusions are summarized as follows:

- (1) Pore-water in unsaturated soils is classified into bulk, meniscus and adsorbed water. The bulk water is easily drained out and is immediately replaced by air when suction increases, particularly in the case of soils having high degrees of saturation. On the contrary, when the suction is released, all bulk water does not recover in the pores. This is a major reason why the water retention curve shows heavy hysteresis depending on suction history.

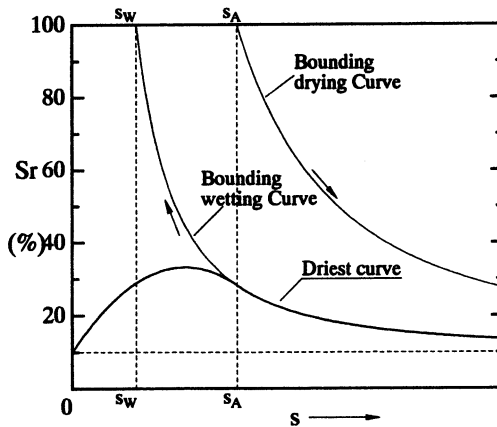


Figure 22. Composition of the driest curve.

- (2) Each form of pore-water classified above can be assigned to specific mechanical actions. Bulk water induces 'bulk stress' with suction, which is equivalent to the pore-water pressure in the case of fully saturated soils. Therefore the sum of net stress and bulk stress can be defined as the skeleton stress, which is transmitted through the soil skeleton just like the effective stress in saturated soils. The meniscus water induces 'meniscus stress' with suction, which works at the contact points between soil particles but does not contribute to equilibrium with the external applied force. The meniscus stress works internally so as to stiffen the soil skeleton. The adsorbed (residual) water influences the forms of bulk water and meniscus water in the soils but does not induce any stress component itself. The sum of skeleton stress and meniscus stress is called contact point stress, corresponding to Bishop's effective stress. Therefore, it is understood that Bishop's effective stress does not have unique linear relationship with the skeleton stress.
- (3) Constitutive models for unsaturated soils described in terms of net stress and suction are briefly reviewed. The basic assumptions used in modeling are examined. Modeling for unsaturated soils has been carried out by simple referring to the models proposed for fully saturated soils without considering irreversible characteristics of unsaturated soils. In particular the hysteresis of the water retention curve has hardly been taken into consideration in the constitutive modeling.
- (4) In order to consider the hysteresis of the water retention curve in modeling the constitutive relationship for unsaturated soils, some ideas are presented in this paper.
 - The prediction method of a water retention curve passing through any given arbitrary point on the plane of the suction s and the degree of saturation S_r is examined. Herein, Brooks and Corey's model is employed to interpolate the water retention characteristic obtained from experiments. However, it is found that Brooks and Corey's model cannot explain well the water retention characteristic in the low suction range.
 - The change of void ratio has a dominant influence on the water retention curve. In this paper a formulation to consider the influence of void ratio has been presented introducing the relative void ratio originally proposed by Toll (1995).

A method to quantitatively evaluate each of the three components based on an equivalent degree of saturation has been proposed based on the idea of the driest water retention curve.

Acknowledgements

The authors appreciate many graduates of the Geomechanics Group in Kobe University. They are indebted especially to Prof. S. Kato and Dr. M. Honda for their continuous support. The authors are also grateful to Prof. A. Iizuka for

valuable comments on this paper. Finally the financial support provided from the Ministry of Education, Science and Culture are gratefully acknowledged.

References

- Alonso, E. E., Gens, A. and Hight, D. W. (1987) Special problem soils. General Report. *Prod. 9th European Conf. Soil Mechanics and Foundation Eng.*, **00**, 1087–1146.
- Alonso, E. E., Gens, A. and Josa, A. (1990) A constitutive model for partially saturated soils. *Geotechnique*, **40**(3), 405–430.
- Bishop, A. W. (1959) The principle of effective stress, *Teknisk Ukeblad* no. 39, pp. 859–863.
- Bishop, A. W., Alpan, I., Blight, G. E. and Donald, I. B. (1960) Factors controlling the strength of partly saturated cohesive soils. *Proc. Conf. Shear Strength of Cohesive Soils*, ASCE: 503–532, 1027–1042.
- Brooks, R. H. and Corey, A. T. (1966) Properties of porous media affecting fluid flow. *Proc. ASCE*, 92. IR(92): 61–88.
- Honda, M. (2000) Method of predicting mechanical behavior of unsaturated foundation ground (in Japanese). *Ph.D thesis*, Kobe University.
- Jennings, J. E. and Burland, J. B. (1962) Limitation to the use of effective stress in partly saturated soils, *Geotechnique*, **12**(2), pp. 125–144.
- Kraube, D. (1987) Basic stress–strain relations of unsaturated soil. *Proc. 8th Asian Conf. Soil Mechanics and Foundation Eng.*, **1**, 49–52.
- Kraube, D. (1988) New concept of effective stress in unsaturated soil and its proving test. *Advanced Triaxial Testing of Soil and Rock*, ASTM STP977: 539–552.
- Kraube, D. and Kato, S. (1994) An ideal unsaturated soil and the Bishop's soil. *Proc. 13th Int. Conf. Soil Mechanics and Foundation Eng.*, **1**, 43–46.
- Kraube, D. (1997) Stress analysis of unsaturated soil based on the driest curve. *Proc. 14th Int. Conf. Soil Mechanics and Foundation Eng.*, **1**, 333–336.
- Karube, D., Kato, S., Honda, M. and Kawai, K. (1998) A constitutive model for unsaturated soil evaluating effects of soil moisture distribution. *Proc. 2nd Int. Conf. on Unsaturated Soils*, Beijing, **1**, 485–490.
- Kraube, D., Kato, S., Hamada, K. and Honda, M. (1996) The relationship between the mechanical behaviour and the state of pore-water in unsaturated soil. *J. of Japanese Society of Civil Eng.*, no. 535/111–34, pp. 83–92 (in Japanese).
- Kawai, K., Karube, D. and Kato, S. (2000) The model of water retention curve considering effects of void ratio. *Proc. Asian Conf. on Unsaturated Soils*, Singapore, pp. 000–000.
- Kohgo, Y., Nakano, M. and Miyazaki, T. (1993a) Theoretical aspects of constitutive modeling for unsaturated soils. *Soils and Foundations*, **33**(4), 49–63.
- Kohgo, Y., Nakano, M. and Miyazaki, T. (1993b) Verification of the generalized elasto-plastic model for unsaturated soils. *Soils and Foundations*, **33**(4), 64–73.
- Leong, E. C. and Rahardjo, H. (1997) Review of soil water characteristic curve equations. *J. of Geotechnical and Geoenvironmental Engineering*, **123**(12), 1106–1117.
- Matyas, E. L. and Radhakrishna, H. S. (1968) Volume change characteristics of partially saturated soils. *Geotechnique*, **18**, 432–448.
- Mindlin, R. D. (1949) Compliance of elastic bodies in contact, *J. of Applied Mechanics*, **16**, pp. 259–268.
- Toll, D. G. (1995) A conceptual model for the drying and wetting of soils. *Proc. 1st Int. Conf. on Unsaturated Soils*, Paris, **2**, 805–810.
- Roscoe, K. H., Schofield, A. N. and Thuraijah (1963) Yielding of clays in the state wetter than critical, *Geotechnique*, **13**(3), 211–240.

- Vanapalli, S. K., Fredlund, D. G., Pufahl, M. D. and Clifton, A. W. (1996) Model for prediction of shear strength with respect to soil suction, *Canadian Geotechnical Journal*, **33**(3), pp. 379–392.
- Wheeler, S. J. and Karube, D. (1995) Constitutive modeling. State of the Art Report. *Proc. 1st Int. Conf. on Unsaturated Soils*, Paris, **3**, 1323–1356.



Mathematical attributes of some soil–water characteristic curve models

W. SCOTT SILLERS,¹ DELWYN G. FREDLUND² and
NOSHIN ZAKERZADEH³

¹*Vemax Management Inc., Edmonton, Alberta, Canada, T6B 2L5.*
e-mail: scott.sillers@vemax.com

²*Department of Civil Engineering, University of Saskatchewan, Saskatoon, Sask., Canada, S7N 5A9. e-mail: D.Fredlund@engr.usask.ca*

³*Department of Civil Engineering, University of Saskatchewan, Saskatoon, Sask., Canada, S7N 5A9. e-mail: Noshin_zakerzadeh@engr.usask.ca*

(Received 17 August 2000; revised 29 January 2001; accepted 1 May 2001)

Abstract. Numerous mathematical models have been proposed in the research literature to represent soil–water characteristic curve data. A number of proposed mathematical models are summarized and the significance of each of the associated soil parameters is illustrated. The advantages and disadvantages of the various mathematical models are outlined. The derivatives for each of the model equations are presented along with comments regarding the efficiency of the best-fit regression procedures.

The models using three soil parameters models proved to be superior for representing the wide range of soil suctions required in solving geotechnical problems. Regression analyses using three soil parameters were shown to be numerically more stable, converging with a reasonable number of iterations.

Key words: pore size distribution, pressure plate test, soil suction, soil–water characteristic curve, unsaturated soil, water content.

1. Introduction

The soil–water characteristic curve (SWCC) is the relationship between the amount of water in the soil (i.e. gravimetric or volumetric water content) and soil suction (i.e. matric suction at low suctions and total suction at high suctions). The soil–water characteristic curve contains vital information for deriving unsaturated soil property functions for the coefficient of permeability, shear strength and volume change.

The soil–water characteristic curve contains important information concerning the amount of water contained in the pores at any suction, the pore size distribution and the stress state in the soil–water. Figure 1 shows three stages related to the process of desaturation (i.e. increasing soil suction) that can be described as follows:

- 1 Capillary saturation zone: the pore-water is in tension in this zone, however, the soil remains essentially saturated due to capillary forces. The capillary saturation

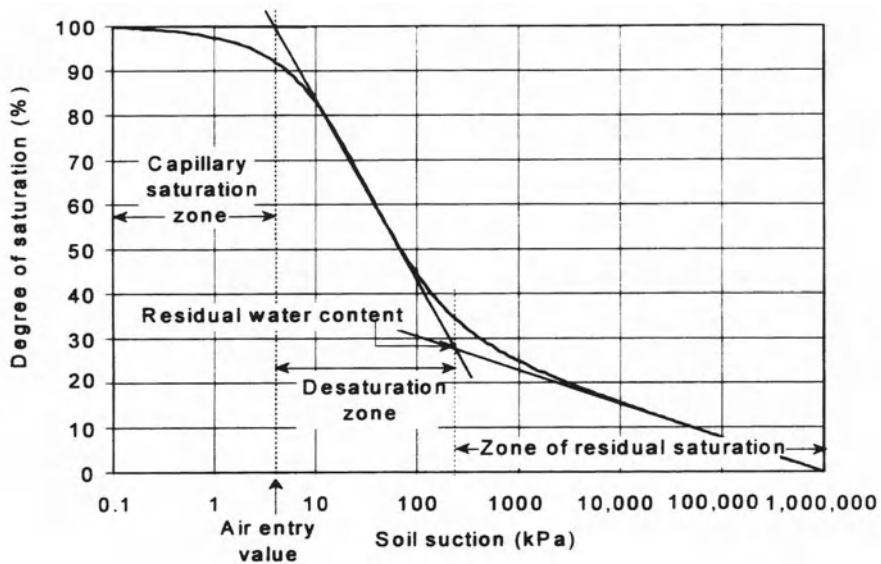


Figure 1. Soil-water characteristic curve illustrating the regions of desaturation.

- zone continues up to the air entry value or bubbling pressure, $(u_a - u_w)_b$ of the soil where air starts to enter the largest size pores.
- 2 Desaturation or funicular zone: the liquid water within the pores is increasingly displaced by air in the desaturation zone. The desaturation zone ends at the residual water content, θ_r , where pore-water becomes essentially immobile within the soil matrix. Increases in soil suction do not result in significant changes in water content.
 - 3 Zone of residual saturation: the liquid water is tightly held to the soil and moisture movement occurs mainly as vapor flow. There is little hydraulic flow of water through the pores; however, there may be some water movement in the form of film flow (Huang et al. 1994). In the residual zone, the term soil suction loses its physical significance and can then better be regarded as an equivalent term for the energy required for the withdrawal water from a unit mass of soil. The zone of residual saturation is terminated at oven dry conditions (i.e. water content equals zero), corresponding to a soil suction of approximately 1,000,000 kPa (Croney and Coleman, 1961). Water not driven off under these conditions is chemically bonded to the soil and should not have a significant effect on the engineering behavior of the soil (Mitchell, 1976).

Figure 2 shows three typical soil-water characteristic curves for a clay, silt and sand. The air entry value for the soils tends to increase as the soil particles become finer. Also, the slope of the curve in the desaturation zone tends to become flatter as the soil particles become finer.

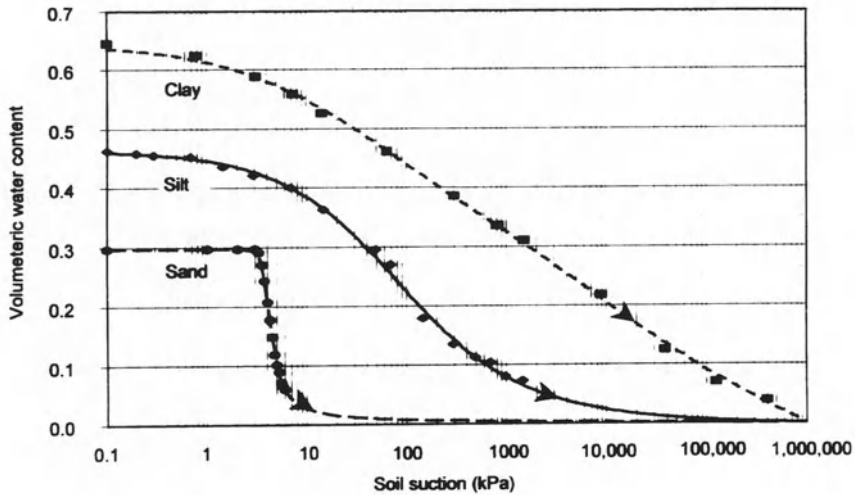


Figure 2. Three typical soil–water characteristic curves for a clay, silt and sand.

Experimental data for the soil–water characteristic curve can be obtained from laboratory tests. A mathematical function can then be fitted to the soil–water characteristic data. Many mathematical models have been proposed in the literature for representing the soil–water characteristic curve. The objective of this paper is to present the mathematical attributes of a number of the equations that have been proposed for the soil–water characteristic curve. Each attribute is illustrated for the mathematical models in terms of the manner in which the model parameters affect the shape of the soil–water characteristic curve (Sillers, 1997).

The relationship between the effective pore size and soil suction is called the pore size distribution. The pore size distribution can be acquired from the soil–water characteristic curve. Conversely, a pore size distribution function and the capillary theory can be used to derive a model for the soil–water characteristic curve. Models derived from the pore size distribution are termed statistical or micromechanical approaches. Numerous investigators have derived models for the soil–water characteristic curve using this approach (van Genuchten, 1980; Kosugi, 1994; Fredlund and Xing, 1994).

Unsaturated soils are assumed to consist of capillary pores. Under equilibrium conditions at a particular water content, the air–water interfaces are assumed to have the same constant overall curvature throughout the free pore-water (Fairbridge and Finkl, 1979). The pore size distribution provides an approximation of the pore radius of the soil pores in accordance with the capillary theory. The pore size distribution does not take into account the adsorptive nature of water onto soil particles. It would appear that a model for the soil–water characteristic curve should include a principle that compliments capillarity to fully account for the adsorptive water.

2. Pore Size Distribution and its Relationship to the Soil–Water Characteristic Curve

Soil consists of a series of interconnected pores that are randomly distributed between a maximum and a minimum value (Brutsaert, 1966; Kosugi, 1994; Fredlund and Xing, 1994). These pores can be characterized for mathematical simplicity as an equivalent spherical pore with a radius, r . A statistical distribution describing the pore radius density function, $f(r)$, along with the capillary theory can be used to derive models for the soil–water characteristic curve.

The accuracy and complexity of the soil–water characteristic model depends on the flexibility of the pore radius density function, $f(r)$. The derivation of a micromechanical model requires a statistical distribution to represent the pore radius density function $f(r)$, where r is a variable representing the equivalent pore radius or radius of curvature as defined by the Laplace equation. The volume of pores having radii ranging from r to $r + dr$ is $f(r)dr$ per unit of volume of medium. Therefore, the function $f(r)$, is equal to $d\theta/dr$ where θ is the volumetric water content. The sum of these elementary volumes gives the volume of pores that are filled with water.

$$\theta(R) = \int_{R_{\min}}^R f(r)dr + C_r \quad (1)$$

where:

- R = a specific value of r
- R_{\min} = the minimum pore size that is available for storage, either corresponding to the residual water content or to a suction of 1,000,000 kPa, and
- C_r = a constant related to the residual water content.

The largest pore size that is filled with water is R_{\max} , corresponding to a volumetric water content, $\theta(R_{\max})$ that is equal to θ_s . R_{\min} corresponds to the smallest pore size within the soil and a volumetric water content, $\theta(R_{\min})$, equal to residual water content, θ_r . In the case where $\theta(R_{\min})$ is equal to 0, and C_r is equal to 0, Equation (1) becomes:

$$\theta_s = \int_{R_{\min}}^{R_{\max}} f(r)dr \quad (2)$$

where:

- θ_s = saturated water content.

The radius of curvature of a water surface (i.e. equivalent pore radius) is related to the soil suction in accordance with the capillary theory.

$$r = \frac{C}{\psi} \quad (3)$$

where:

$$\begin{aligned} C &= \text{a constant equal to } \frac{2T_s \cos \alpha}{g\rho_w}, \\ T_s &= \text{surface tension of water,} \\ \alpha &= \text{angle of contact between soil and water, and} \\ \psi &= \text{soil suction.} \\ g &= \text{acceleration due to gravity} \\ \rho_w &= \text{density of water} \end{aligned}$$

The pore radius density function, $f(r)$, can be transformed into a pore size distribution, which is a function of soil suction rather than pore radius. The maximum suction in the soil, ψ_o , can be written as,

$$\psi_o = \frac{C}{R_{\min}} \quad (4)$$

and the air entry value, ψ_{aev} is,

$$\psi_{\text{aev}} = \frac{C}{R_{\max}} \quad (5)$$

where:

$$\begin{aligned} \psi_o &= 1,000,000 \text{ kPa at oven dry conditions (Croney and Coleman, 1961;} \\ &\quad \text{Fredlund and Xing, 1994), and} \\ \psi_{\text{aev}} &= \text{air entry value, kPa.} \end{aligned}$$

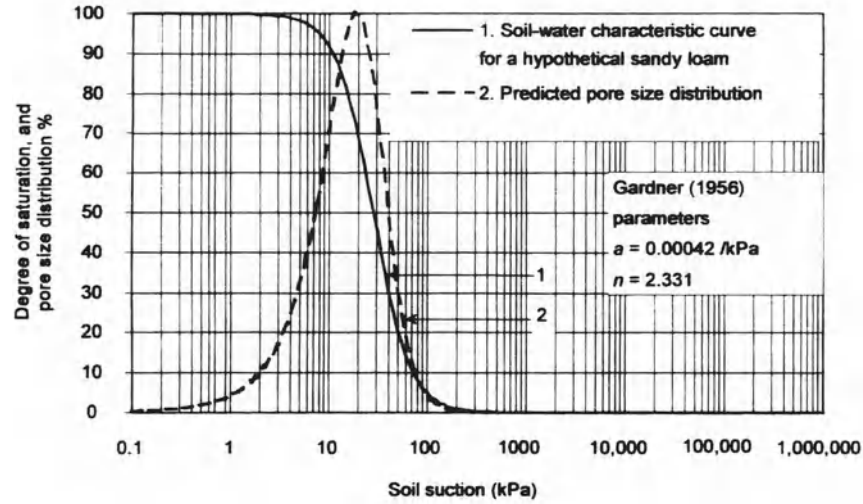
The pore radius density function, $f(r)$, is transformed to the pore size distribution, $f(\psi)$, by the relationship between pore size and soil suction.

$$f(\psi) = f(r) \frac{dr}{d\psi} \quad (6)$$

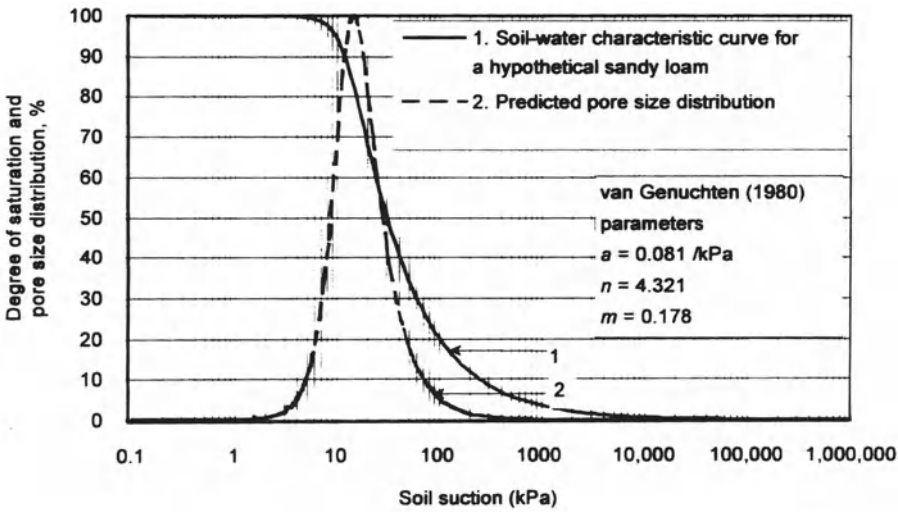
A change in the pore radius with a change in soil suction can be written as follows:

$$\frac{dr}{d\psi} = -\frac{C}{\psi^2} \quad (7)$$

The pore size distribution is closely related to the shape of the soil–water characteristic curve. Figure 3(a) shows that the pore size distribution is symmetrical about the inflection point for the Gardner (1956) model. Figure 3(b) shows that the pore size distribution is unsymmetrical about the inflection point for the van Genuchten (1980) model. The same is true for the Fredlund and Xing (1994) model which shows asymmetry (Figure 3(c)) except for the case where m is equal to 1.

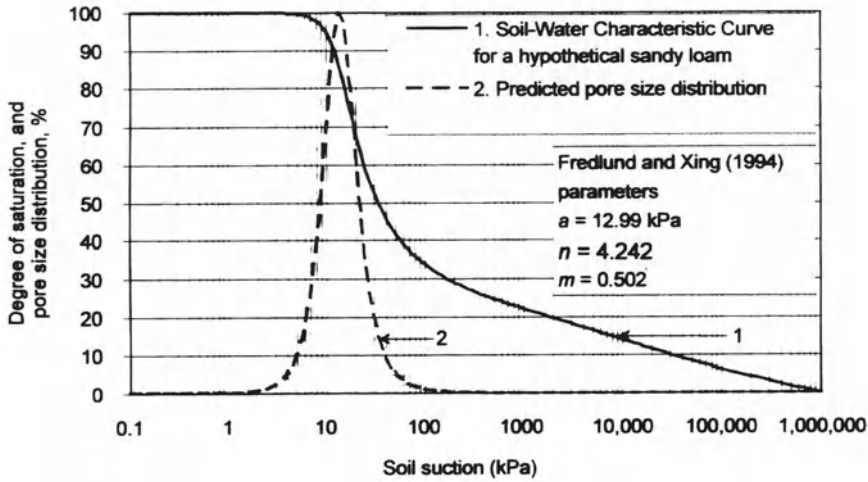


(a) Best-fit using the Gardner (1958) model.



(b) Best-fit using the van Genuchten (1980) model.

Figure 3.



(c) Best-fit using the Fredlund and Xing (1994) model.

Figure 3. Soil–water characteristic curve and pore size distribution for a hypothetical sandy loam soil (a) best-fit using the Gardner (1956) model; (b) best-fit using the van Genuchten (1980) model; and (c) best fit using the Fredlund and Xing (1994) model.

Let us suppose that soil suction can be represented by the variable, h . Substituting the equation for pore radius, r , into Equation (1) gives,

$$\theta(\psi) = \theta_s \int_{\psi_0}^{\psi} f\left(\frac{C}{h}\right) d\left(\frac{C}{h}\right) \quad (8)$$

Rearranging Equation (8) as a function of the variable, h , gives,

$$\theta(\psi) = \theta_s \int_{\psi}^{\psi_0} f\left(\frac{C}{h}\right) \frac{C}{h^2} dh \quad (9)$$

Equation (9) forms the mathematical basis for deriving soil–water characteristic models.

A measure of pore size distribution can also be obtained using mercury intrusion porosimeter tests (Praparahan et al., 1985, Olson, 1985, Kong and Tan, 2000). Mercury has a contact angle greater than 90° and the injection of mercury into the pores is similar to ejection of water from the pores. The use of mercury as the fluid requires the use of external pressure to intrude the soil pores. This pressure can be measured and the capillary pressure for water can be estimated. The volume of pores not intruded by mercury should be used to calculate the water content corresponding to a particular pressure (Praparahan et al., 1985). Mercury porosimetry provides a measure of the pore size distribution but the accuracy to which the results represent the actual pore distribution has not been fully verified.

Table 1. Soil-water characteristic curve models and corresponding pore size distribution.

Model name	Model*	Pore size distribution $f(\psi)^*$
Gardner (1922)	$\theta = \frac{B}{\psi} - D$	constant pore size
Linear function representing water content (from Fredlund and Xing, 1994).	$\theta = B - D\psi$	$\frac{A}{\psi^2}$
Brooks and Corey (1964)	$S = B - D\psi^m$	$\frac{A}{\psi^{(m+1)}}$
Brutsaert (1966) model	$S = \frac{1}{1 + \left(\frac{\psi}{a}\right)^n}$	$\frac{\frac{n}{a} \left(\frac{\psi}{a}\right)^{n-1}}{\left[1 + \left(\frac{\psi}{a}\right)^n\right]^2}$
Normal distribution	$S = \frac{1}{2} \operatorname{erfc}\left(\frac{\psi - \mu}{\sqrt{2}s}\right)$	normal distribution
van Genuchten (1980)	$S = \frac{1}{(1 + (a\psi)^n)^m}$	$\frac{mna(a\psi)^{n-1}}{[1 + (a\psi)^n]^{m+1}}$
McKee and Bumb (1987) (Boltzman)	$S = \exp\left(-\frac{\psi}{B}\right)$	exponential distribution
Fredlund and Xing (1994)	$S = \frac{1}{\left(\ln\left(e + \left(\frac{\psi}{a}\right)^n\right)\right)^m}$	$\frac{mn\left(\frac{\psi}{a}\right)^{n-1}}{a\left(e + \left(\frac{\psi}{a}\right)^n\right)\left(\ln\left(e + \left(\frac{\psi}{a}\right)^n\right)\right)^{m+1}}$
Kosugi (1994)	$S = \frac{1}{2} \operatorname{erfc}\left(\frac{\ln\left(\frac{\psi_{\text{aev}} - \psi}{\psi_{\text{aev}} - \psi_{\text{mode}}}\right) - s^2}{\sqrt{2\pi}s}\right)$	$\frac{1}{\sqrt{2\pi}s(\psi_{\text{aev}} - \psi)} \exp\left(\frac{\left(\ln\left(\frac{\psi_{\text{aev}} - \psi}{\psi_{\text{aev}} - \psi_{\text{mode}}}\right) - s^2\right)}{\sqrt{2\pi}s}\right)$

*All variables are defined in the text

Based on the results of mercury intrusion porosimeter tests and shrinkage tests, the relationship between the water content and pore size distribution of the soil can be estimated, and thereby, the soil-water characteristic curve can be computed Kong and Tan (2000). General formulae of the soil-water characteristic curve are described by Kong and Tan, (2000). Some pore size density functions and the corresponding models are listed in Table 1 and subsequently explained in more detail.

2.1. DERIVATION OF THE LINEAR MODEL

An example derivation is provided for the Linear model. The residual water content is assumed to be equal to 0. The equation takes the form of a simple linear function between the saturation water content and zero water content,

$$\theta = B - D\psi \quad (10)$$

The pore radius density function, $f(r)$, is assumed to be:

$$f(r) = \frac{A}{r^2} \quad (11)$$

where:

A = a constant of proportionality.

Substituting the capillary Equation (3), into Equation (11) gives,

$$f\left(\frac{C}{h}\right) = \frac{Ah^2}{C^2} \quad (12)$$

Substituting Equation (12) into the integral function of soil suction, Equation (9), gives

$$\theta(\psi) = \theta_s \int_{\psi}^{\psi_0} \frac{Ah^2}{C^2} \frac{C}{h^2} dh \quad (13)$$

Performing the integration on Equation (13) yields,

$$\theta(\psi) = \theta_s \frac{A}{C} \psi_0 - \theta_s \frac{A}{C} \psi \quad (14)$$

Equation (14) can be simplified to the following Linear Model form,

$$\theta = B - D\psi \quad (15)$$

where:

$$B = \theta_s \frac{A}{C} \psi_0$$

and

$$D = \theta_s \frac{A}{C}$$

The linear model has been shown not to provide a good estimate of the pore size distribution and as a result, cannot be considered as an adequate model for the soil–water characteristic curve (Fredlund and Xing, 1994)

2.2. DERIVATION OF THE KOSUGI (1994) MODEL

Another example derivation of a soil–water characteristic model is provided for the Kosugi (1994) model. The choice of a pore density function is shown in Equation (16). The complex pore size distribution gives the model greater flexibility to represent water contents in the wet and dry ranges for all soil types. However, the form of the model is complex and difficult to fit.

$$f(r) = \frac{(\theta_s - \theta_r)r_{\max}}{(2\pi)^{1/2}sr(r_{\max} - r)} \exp \left[\left(\ln \left\{ \frac{r}{r_{\max} - r} \right\} - \mu \right)^2 / 2s^2 \right] \quad 0 < r < r_{\max} \quad (16)$$

where:

- r_{\max} = the maximum pore size, and
- μ = dimensionless parameter related to the mean of the $(\ln r/(r_{\max} - r))$ distribution, and
- s = parameter related to the standard deviation.

Equation (16) is derived by applying a normal distribution form to the pore radii distribution (i.e. $(r/(r_{\max} - r))$), which is given by a transformation of the pore radius density function (Kosugi, 1994). Substituting the capillary pressure function, Equations (3) and (16), into Equation (6), and then simplifying gives,

$$f(\psi) = \frac{(\theta_s - \theta_r)}{(2\pi)^{1/2}s(\psi_{\text{aev}} - \psi)} \exp \left[\left(\ln \left\{ \frac{\psi_{\text{aev}}}{\psi - \psi_{\text{aev}}} \right\} - \mu \right)^2 / 2s^2 \right] \quad \psi < \psi_{\text{aev}} \quad f(\psi) = 0 \quad (17)$$

where:

- ψ_{aev} = air entry value related to the largest pore radius within the soil, r_{\max} , designated by the capillary pressure equation.

Differentiating Equation (17) with respect to soil suction and setting the first derivative to zero gives the capillary pressure at the peak of the pore size distribution, corresponding to the mode of the pore size distribution. The mode of the pore size distribution, can be written as a function of soil suction corresponding to the air entry value, as well as to the statistical properties, s and μ .

$$\psi_{\text{mode}} = \psi_{\text{aev}}[1 + \exp(-\mu - s^2)] \quad (18)$$

where:

- ψ_{mode} = the mode of the pore size distribution.

Solving Equation (18) for μ and substituting into Equation (17) gives,

$$f(\psi) = \frac{(\theta_s - \theta_r)}{(2\pi)^{1/2}s(\psi_{\text{aev}} - \psi)} \exp \left[\left(\ln \left\{ \frac{\psi_{\text{aev}} - \psi}{\psi_{\text{aev}} - \psi_{\text{mode}}} \right\} - s^2 \right)^2 / 2s^2 \right] \quad (19)$$

The pore size distribution is proportional to $d\theta/dh$. Substituting Equation (19) into Equation (9), (assuming the residual water content is zero), and integrating gives the final form of the Kosugi (1994) model,

$$\theta(\psi) = \theta_s \quad \psi_{\text{aev}} \geq \psi \quad (20)$$

$$\theta(\psi) = \theta_s \frac{1}{2} \operatorname{erfc} \left(\frac{\ln\{(\psi_{\text{aev}} - \psi)/(\psi_{\text{aev}} - \psi_{\text{mode}})\} - s^2}{2^{1/2}s} \right) \quad \psi > \psi_{\text{aev}} \quad (21)$$

where:

erfc = the complimentary error function.

Equation (21) shows the complex Kosugi (1994) model. The complementary error function could limit the usefulness of the Kosugi (1994) model because it becomes difficult to use. The Kosugi (1994) model is an example of a complex model but the derivation procedure is the same for both simple and complex models. The difference in the models depends on the assumption made regarding the pore size distribution.

2.3 DERIVATION OF THE FREDLUND AND XING (1994) MODEL

The Fredlund and Xing (1994) model is based on the following statistical pore size distribution.

$$f(r) = \frac{mn/r(rA)^{-n}}{\ln(e + (rA)^{-n})^{m+1} (e + (rA)^{-n})} \quad (22)$$

where:

A = constant related to the air entry value, and
 n and m = fitting parameters

Substituting Equations (7) and (22), into Equation (6) and assuming that A is equal to aC yields,

$$f(\psi) = \frac{nm \left(\frac{\psi}{C} \right) \left(\frac{\psi}{a} \right)^n}{\ln \left(e + \left(\frac{\psi}{a} \right)^n \right)^{m+1} \left(e + \left(\frac{\psi}{a} \right)^n \right)} \frac{C}{\psi^2} \quad (23)$$

where:

a = fitting parameter related to the air entry value.

Substituting Equation (23) into Equation (9), assuming that the residual water content is equal to 0 and that the saturated volumetric water content, θ_s , is known, integration gives the Fredlund and Xing (1994) model.

$$\theta(\psi) = \theta_s \left(1 / \ln \left[e + \left(\frac{\psi}{a} \right)^n \right]^m \right) \quad (24)$$

Equation (24), the Fredlund and Xing (1994) model, is a flexible model containing three fitting parameters that can readily be determined.

3. Description of Model Parameters

The model parameters are the variables used to define a model. For the three parameter models, the general parameters can be described as a , n and m . For the two parameter models, the parameters are a and n . The a parameter is a suction value corresponding to the inflection point on the soil–water characteristic curve, which has physical meaning in that it bears a relationship to the air entry value. The a parameter has units of soil suction or the inverse of soil suction. The n parameter is related to the rate of change of the desaturation zone of the soil–water characteristic curve. The m parameter is related to the asymmetry of the curve about the inflection point.

3.1. GARDNER (1956) MODEL

The Gardner (1956) equation is one of the first equations used to model the soil–water characteristic curve. It is a continuous function originally intended as a means of modelling the unsaturated coefficient of permeability of soil. However, the equation has been adapted to model the soil–water characteristic curve. The equation uses two fitting parameters, namely a and n . The parameter a is related to the inverse of the air entry value, and the n parameter is related to the pore size distribution.

$$S = \frac{1}{1 + a\psi^n} \quad (25)$$

where:

- S = degree of saturation,
- ψ = soil suction, and
- a and n = fitting parameters.

The normalized water content form of the Gardner (1956) model is as follows:

$$\theta = \theta_r + (\theta_s - \theta_r) \left(\frac{1}{1 + a\psi^n} \right) \quad (26)$$

where:

$$\begin{aligned} \theta &= \text{normalized water content,} \\ \theta_r &= \text{residual water content, and} \\ \theta_s &= \text{saturated water content.} \end{aligned}$$

3.2. BROOKS AND COREY (1964) MODEL

The Brooks and Corey (1964) equation is one of the first models proposed for the soil–water characteristic curve, and still remains a popular model. The model is assumed to be constant for suctions less than the air entry value. The soil–water characteristic curve is assumed to be an exponentially decreasing function at soil suctions greater than the air entry value. The equation uses two fitting parameters, namely, a and n . The parameter a is related to the air entry value of the soil. The n parameter is termed the pore size index and is related to the pore size distribution of the soil. The Brooks and Corey (1964) model is given by the following equations:

$$\begin{cases} S = 1 & \psi < a \\ S = \left(\frac{\psi}{a} \right)^{-n} & \psi > a \end{cases} \quad (27)$$

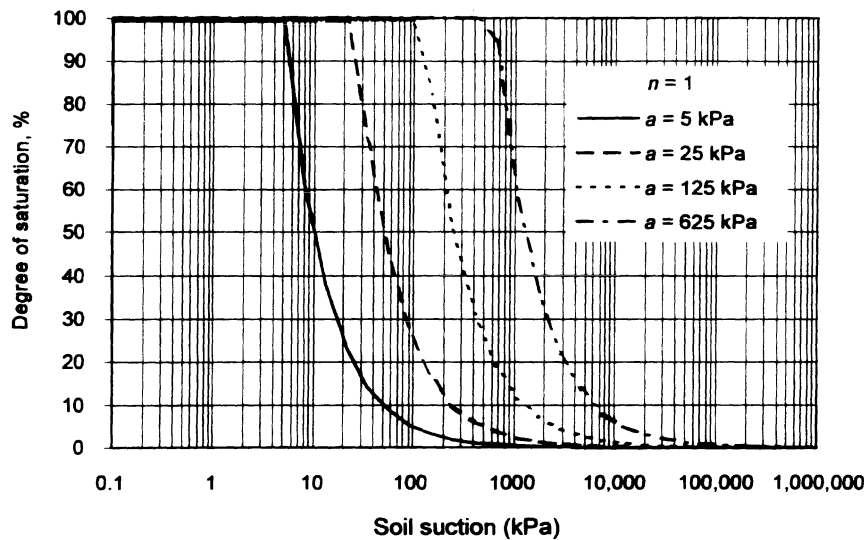
Figure 4(a) shows a plot of the Brooks and Corey (1964) model with n constant (i.e. 1) and a varying. The a parameter has units of suction and is commonly referred to as the bubbling pressure (Brooks and Corey, 1964). Each curve is simply translated horizontally on the plot as the a variable is increased.

Figure 4(b) shows the Brooks and Corey (1964) model with a constant (i.e. 25 kPa) and n varying. The n parameter is related to the pore size distribution. The more uniform the pore sizes in the soil, the larger the value of n . The larger the value of n , the steeper the soil–water characteristics curve within the desaturation zone.

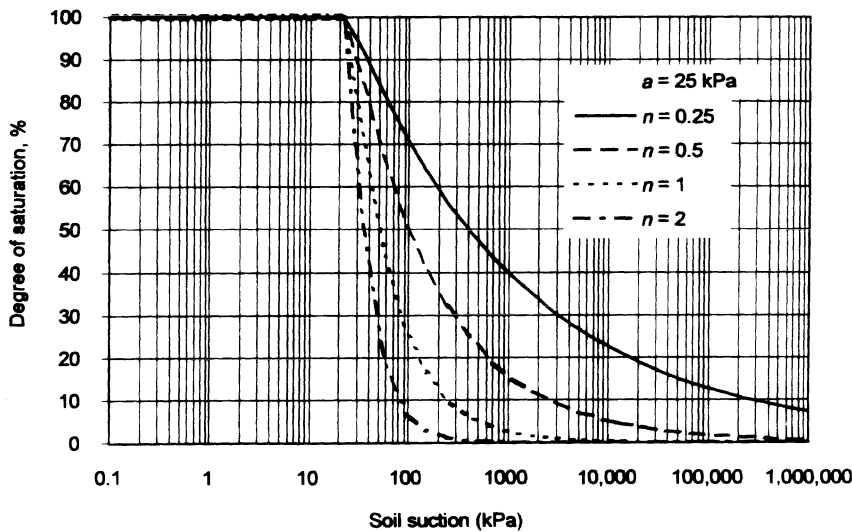
The normalized water content form of the Brooks and Corey (1964) model gives the volumetric water content at soil suctions higher than the air entry value and can be written as,

$$\theta = \theta_r + (\theta_s - \theta_r) \left(\frac{\psi}{a} \right)^{-n} \quad (28)$$

The Brooks and Corey (1964) model does not provide a continuous mathematical function for the entire soil–water characteristic curve. The abrupt change in the curve at the value of a can give rise to numerical instability when modeling unsatu-



(a) n constant and a varying.



(b) a constant and n varying.

Figure 4. Plot of Brooks and Corey (1964) model while varying one parameter when the other parameter is constant, (a) n constant and a varying; and (b) a constant and n varying.

rated soil behavior. However, both parameters have physical meaning and the effect of each parameter on the function, can readily be seen.

3.3. BRUTSAERT (1966) MODEL

Brutsaert (1966) proposed a model for the soil–water characteristic curve with meaningful parameters, with a form similar to that of the Gardner (1956) model. The Brutsaert (1966) model was one of the early continuous soil–water characteristic models. The model fits degree of saturation versus soil suction data over the entire range of soil suctions; however, a reduction in the a parameter or an increase in the n parameter forces the degree of saturation in the low suction range, below 100%, therefore, a restriction must be imposed on the relationship between the a and n parameters to ensure a reasonable function. The equation uses two fitting parameters; namely a and n . The parameter a is related to the air entry value in a general sense and the n parameter is related to the pore size distribution of the soil. The Brutsaert (1966) model can be mathematically described as follows:

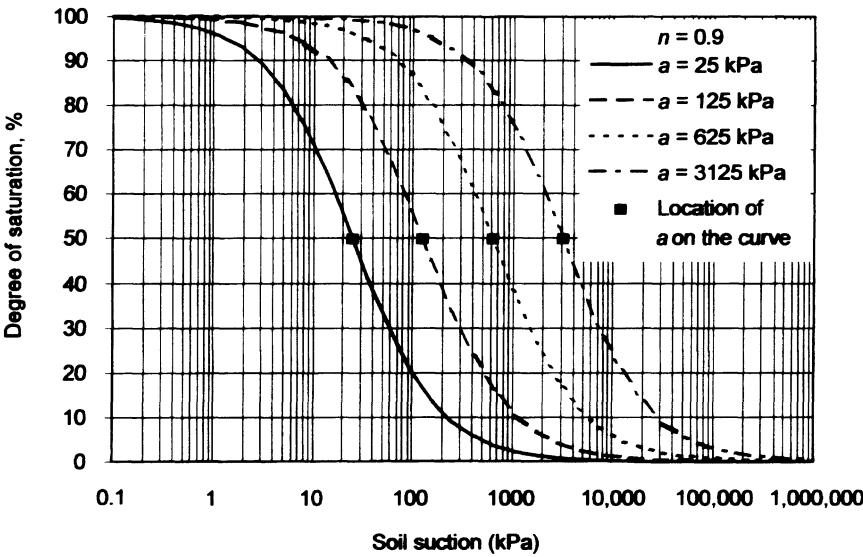
$$S = 1 / 1 + \left(\frac{\psi}{a} \right)^n \quad (29)$$

The normalized water content form of the Brutsaert (1966) model can be written as:

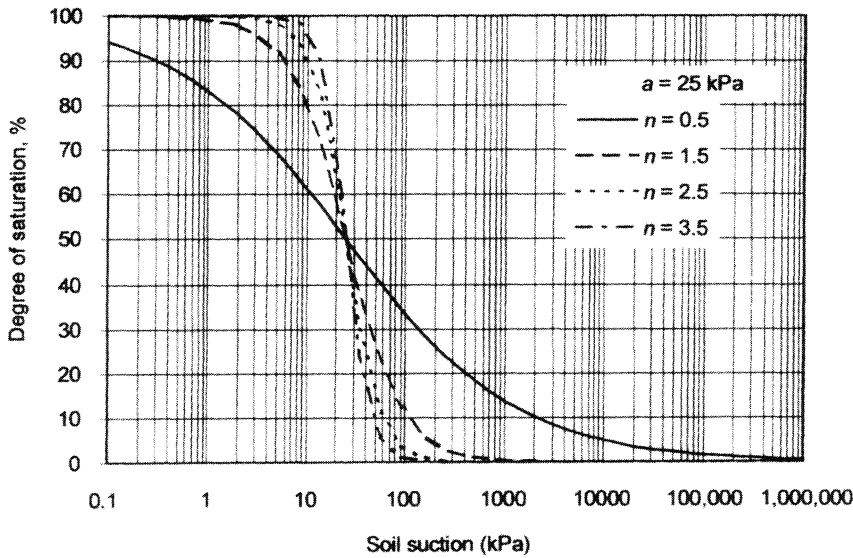
$$\theta = \theta_r + (\theta_s - \theta_r) \left(1 / 1 + \left(\frac{\psi}{a} \right)^n \right) \quad (30)$$

Figure 5(a) shows a plot of the Brutsaert (1966) model with n constant (i.e. 0.9) and a varying. The a parameter has units of suction and is equal to the soil suction where the effective degree of saturation is equal to 0.5. The a parameter appears at the inflection point on the log-normal scale. The Brutsaert (1966) equation is symmetrical on the log-normal scale. Each curve is translated toward the higher suction region as a is increased.

Figure 5(b) shows the Brutsaert (1966) model with a constant (i.e. 25 kPa) and n varying. The n parameter is related to the pore size distribution index. The more uniform the pore sizes in the soil, the larger the value of n . The larger the value of n , the steeper the curve in the desaturation zone. The primary advantages of the Brutsaert (1966) model are as follows: The soil parameters are meaningful; the effect of one parameter can be distinguished from the effect of the other parameter the equation has a simple form containing two parameters; the primary disadvantage is that the a and n parameters must conform to so as restrictions to ensure 100% saturation at low soil suction.



(a) n constant and a varying.



(b) a constant and n varying.

Figure 5. Plot of Brutsaert (1966) model while varying one parameter when the other parameter is constant, (a) n constant and a varying; and (b) a constant and n varying.

3.4. TANI (1982) MODEL

Tani (1982) suggested an exponential distribution for the relationship between degree of saturation and soil suction. The Tani (1982) model used in this paper has been modified by Kosugi (1994) to include the air entry value in order to maintain consistency with other models (Kosugi, 1994). The Tani (1982) equation is a continuous soil-water characteristic curve model. The equation uses two fitting parameters; namely, a and n . The parameter a has units of suction and is related to the air entry value; the n parameter is equal to the soil suction at the inflection point. The Tani (1982) model can be mathematically described as follows:

$$S = \left(1 + \frac{a - \psi}{a - n}\right) \exp\left(-\frac{a - \psi}{a - n}\right) \quad (31)$$

The normalized water content form of the Tani (1982) model is as follows:

$$\theta = \theta_r + (\theta_s - \theta_r) \left(1 + \frac{a - \psi}{a - n}\right) \exp\left(-\frac{a - \psi}{a - n}\right) \quad (32)$$

The Tani (1982) model gives a equal to the saturated water content for soil suctions below the value of the a parameter. Figure 6(a) shows a plot of the Tani (1982) model with n constant (i.e. $n = 0.25$ kPa) and a varying. Each curve is shifted toward the higher suction region and becomes steeper as a is increased.

Figure 6(b) shows the Tani (1982) model with a constant (i.e. $a = 25$ kPa) and n varying. The n parameter generally gets smaller as the pore size distribution becomes more uniform. The larger the value of n , the more rounded the curve becomes and the more gradual the transition between the capillary saturation zone and the desaturation zone, as well as between the desaturation zone and the zone of residual saturation.

The disadvantages of the Tani (1982) model are as follows. The equation is inflexible and both of the parameters affect the position and the shape of the curve. The overlap of one parameter with the other parameter may cause problems with curve fitting procedures. The Tani (1982) equation is difficult to mathematically fit to a unique set of parameters. Most sets of water content versus soil suction data required several trials to best-fit, with different initial guesses before the model can converge to reasonable values for the fitted parameters (i.e. residual sum of squares less than 0.5).

3.5. BOLTZMAN MODEL

McKee and Bumb (1984) suggested an exponential function called the Boltzman equation, to represent the relationship between degree of saturation and soil suction. The model is assumed to give a constant value for suctions less than the air entry value. The soil-water characteristic curve takes on an exponential function form at suctions greater than the air entry value.

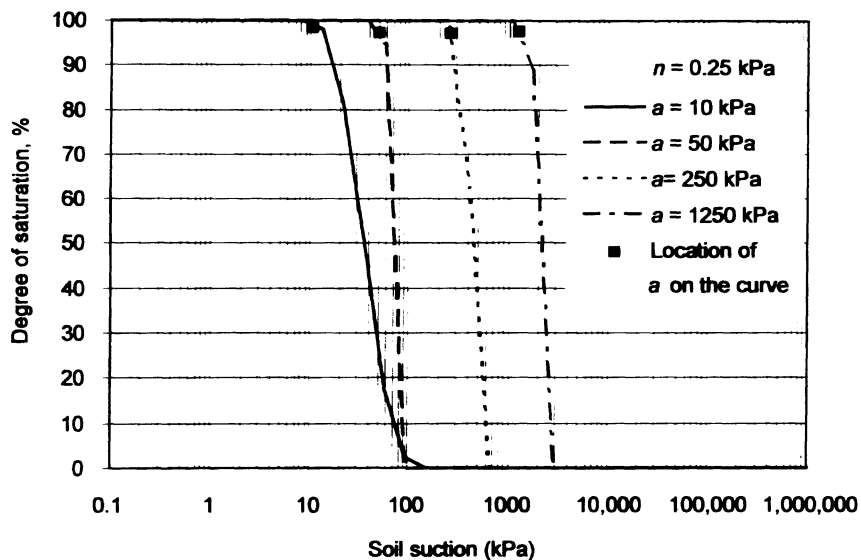
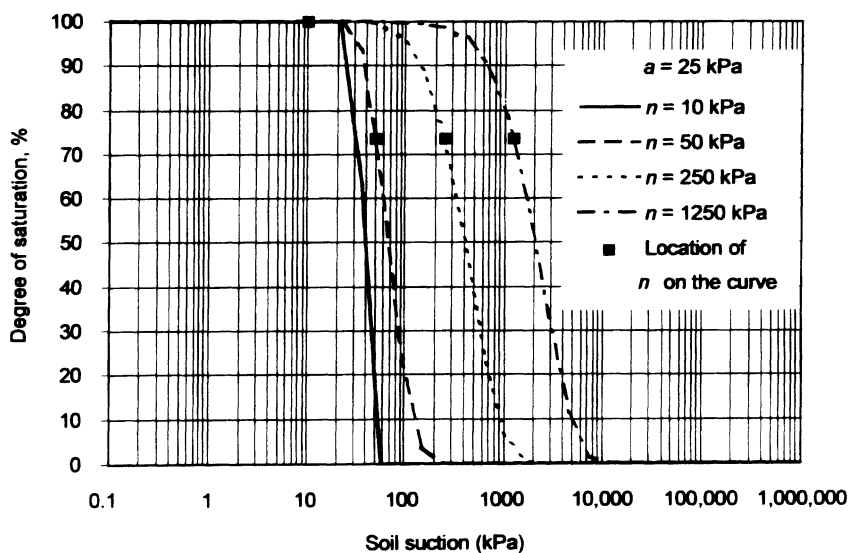
(a) n constant and a varying.(b) a constant and n varying.

Figure 6. Plot of Tani (1982) model while varying one parameter when the other parameter is constant, (a) n constant and a varying; and (b) a constant and n varying.

The equation uses two fitting parameters; namely, a and n . The a parameter is related to the air entry value and has units of suction; the n parameter is related to the pore size distribution of the soil. The value of the Boltzman model is equal to unity for soil suctions less than the air entry value. Therefore, the value of each derivative is zero for soil suctions lower than the air entry value. For suctions greater than the air entry value, the following equations can be written.

$$\begin{cases} S = 1 & \psi < a \\ S = \exp\left(\frac{a - \psi}{n}\right) & \psi > a \end{cases} \quad (33)$$

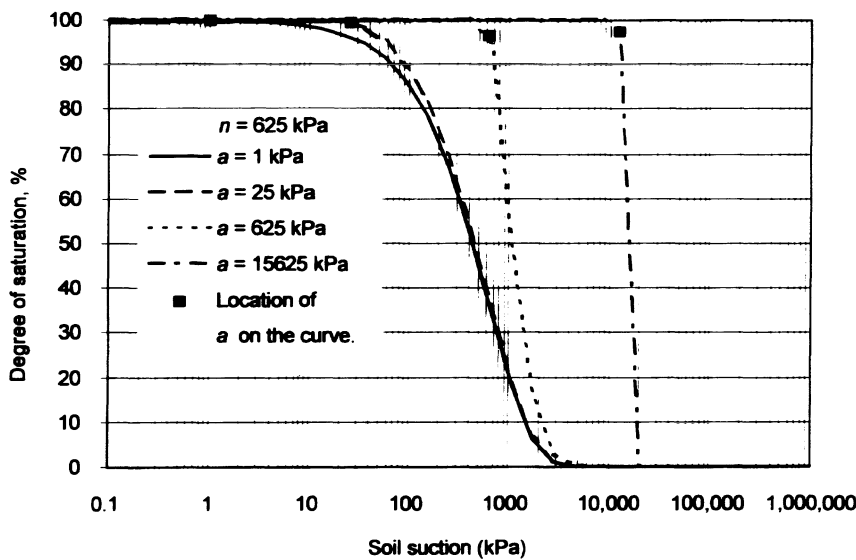
The normalized water content form of the Boltzman model at suctions less than the air entry value is equal to the saturated volumetric water content. For soil suctions greater than the air entry value, the normalized water content form of the Boltzman model can be written:

$$\theta = \theta_r + (\theta_s - \theta_r) \exp\left(\frac{a - \psi}{n}\right) \quad (34)$$

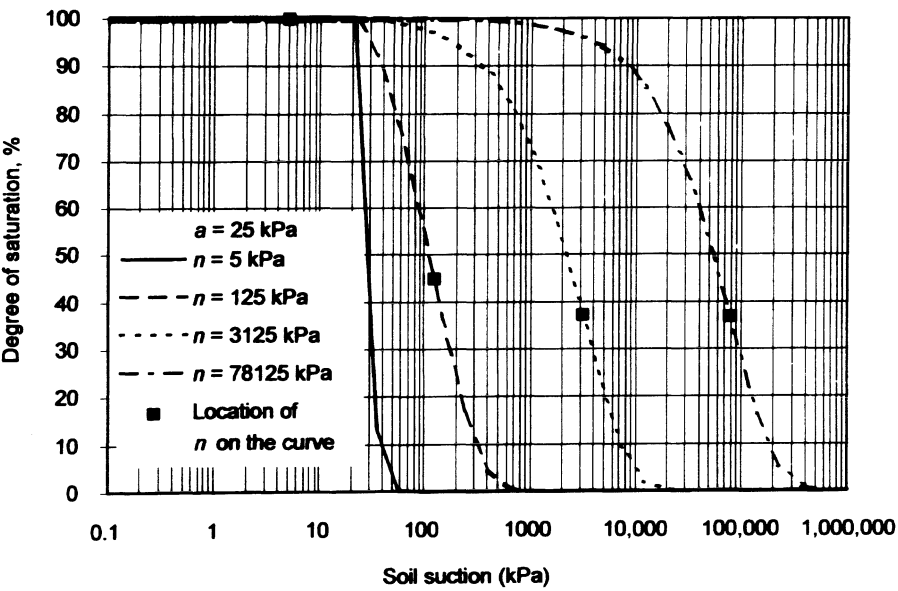
Figure 7(a) shows a plot of the Boltzman model with n constant (i.e. 625 kPa) and a varying. Each curve is shifted toward the higher suction region and becomes steeper as a is increased. Figure 7(b) shows the Boltzman model with a constant (i.e. 25 kPa) and n varying. The n parameter generally gets smaller when the pore size distribution becomes more uniform. The larger the value of n , the more rounded the curve becomes and the more gradual the transition is between the capillary saturation zone and the desaturation zone, as well as between the desaturation zone and the zone of residual saturation. The primary disadvantage of the Boltzman distribution is that both parameters affect the position and shape of the soil–water characteristic curve. The overlap in the effect of each parameter on the shape and position of the curve may increase the number of local minimums, resulting in difficulties associated with curve-fitting procedures. Like the Brooks and Corey (1964) model, the Boltzman distribution is not continuous. At soil suctions below the value of a , the Boltzman distribution is equal to the saturated water content. The main advantage of the Boltzman distribution is the simple form of the equation.

3.6. FERMI MODEL

McKee and Bumb (1987) suggested an alternate exponential function to represent the relationship between degree of saturation and soil suction, called the Fermi equation. This model is simply a variation of the Boltzman model. The Fermi equation is continuous, over the entire range of soil suction. The equation uses two fitting parameters; namely, a and n . The a parameter has units of suction and is related to the air entry value of the soil. The a parameter is equal to the soil suction when effective degree of saturation is equal to 0.5 (i.e. when the actual degree



(a) n constant and a varying.



(b) a constant and n varying.

Figure 7. Plot of McKee and Bumb (1984) (Boltzman) model while varying one parameter when the other parameter is constant, (a) n constant and a varying; and (b) a constant and n varying.

of saturation is equal to $((S_r + 1)/2)$. The n parameter is related to the pore size distribution of the soil. The Fermi model can be mathematically described as follows:

$$S = 1 / \left(1 + \exp\left(\frac{\psi - a}{n}\right) \right) \quad (35)$$

The normalized water content form of the Fermi model may be written as:

$$\theta = \theta_r + (\theta_s - \theta_r) \left(1 / \left(1 + \exp\left(\frac{\psi - a}{n}\right) \right) \right) \quad (36)$$

Figure 8(a) shows a plot of the Fermi model with n constant (i.e. 25) and a varying. Each curve is shifted toward the higher suction region and becomes steeper as a is increased.

Figure 8(b) shows the Fermi model with a constant (i.e. 25 kPa) and n varying. The n parameter generally gets smaller when the pore size distribution becomes more uniform (McKee and Bumb, 1987). The larger the value of n , the more rounded the curve becomes and the more gradual the transition between the capillary saturation zone and the desaturation zone, as well as between the desaturation zone and the zone of residual saturation. The disadvantages of the Fermi distribution are as follows: The equation is relatively inflexible and both of the soil parameters affect the position and the shape of the curve and as a result, the effect each parameter has on the curve is difficult to isolate; the overlap in the effect of each parameter on the shape and position of the curve may increase the number of local minimums resulting in difficulties when using curve-fitting procedures; there must be a restriction placed on the relationship between the a and n parameters in order to ensure that the initial degree of saturation is 100%.

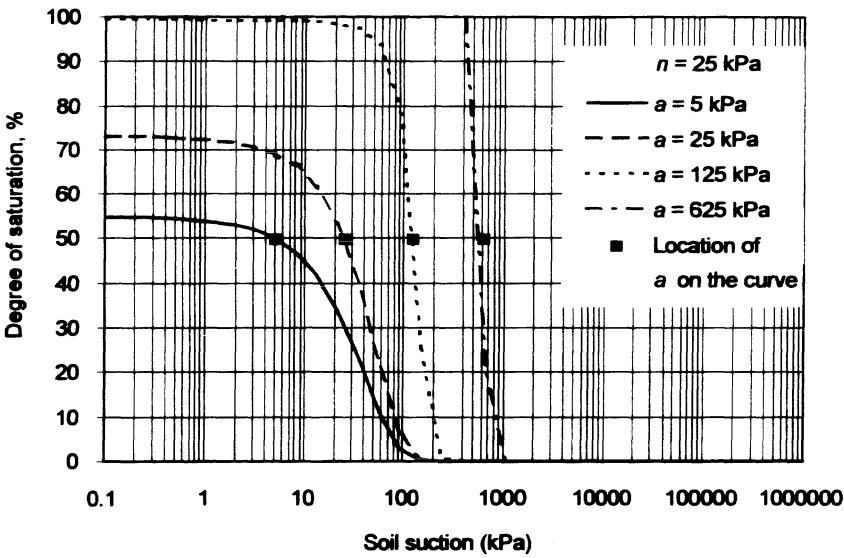
3.7. VAN GENUCHTEN (1980) MODEL

The van Genuchten (1980) model is a continuous soil–water characteristic curve model. The model fits degree of saturation versus soil suction data over the entire range of soil suctions. The equation uses three fitting parameters; namely, a , n and m . The parameter a is related to the inverse of the air entry value; the n parameter is related to the pore size distribution of the soil and the m parameter is related to the asymmetry of the model. The van Genuchten (1980) model can be described as follows:

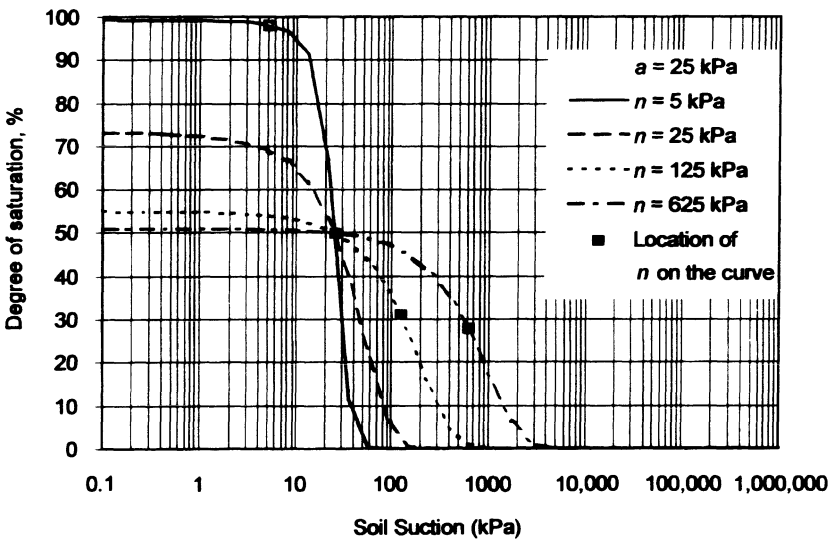
$$S = \frac{1}{[1 + (a\psi)^n]^m} \quad (37)$$

where:

a , n and m = fitting parameters.



(a) n constant and a varying.



(b) n constant and a varying.

Figure 8. Plot of McKee and Bumb (1987) (Fermi) equation while varying one parameter when the other parameter is constant, (a) n constant and a varying; and (b) a constant and n varying.

The van Genuchten (1980) equation bears some similarity in form to the Gardner (1956) model. When the m parameter is equal to 1.0, the van Genuchten (1980) model is equivalent to the Brutsaert (1966) model with the a parameter inverted. This is also true of the Gardner (1956) model.

Figure 9(a) shows a plot of the van Genuchten (1980) model with n and m parameters constant (i.e. n equal to 1.5, and m equal to 1.0) and a varying. The inverse of the a parameter is larger than soil suction at the air entry value and is equal to the inflection point on the curve. The a parameter does not affect the shape of the curve, but provides a shift in the curve toward the higher or lower suction regions of the plot.

Figure 9(b) shows the van Genuchten (1980) model with m and a constant (i.e. m equal to 1.0, and a equal to 0.001 kPa^{-1}) and n varying. The n parameter is related to the pore size distribution index, with the more uniform pore sizes in the soil corresponding to larger values of n . The larger the value of n , the steeper the curve in the desaturation zone.

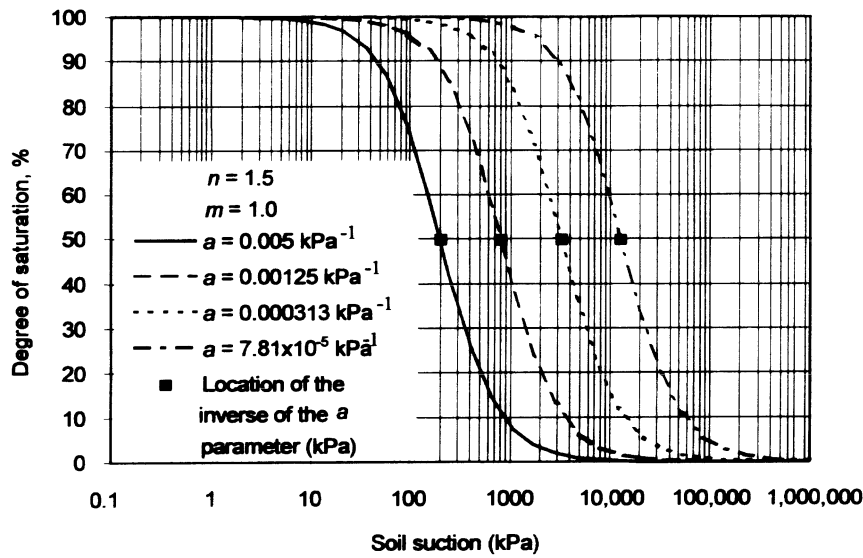
Figure 9(c) shows the van Genuchten (1980) model with n and a constant (i.e. n equal to 1.0, and a equal to 0.001 kPa^{-1}) and m varying. The m parameter is related to the asymmetry of the curve. Small values of m result in a moderate slope in the low suction range and a steeper slope in the high suction range. The advantages of the van Genuchten (1980) model are as follows: It provides a wide range of flexibility, allowing it to better fit data from a variety of soil types; the model parameters have physical meaning; the effect of one soil parameter can be distinguished from the effect of the other two parameters. However, the magnitude of the n and m best-fit values may vary somewhat depending on the convergence procedure. The van Genuchten (1980) model contains three fitting parameters and this limits the type of correction factors that may be added to the model.

3.7. BURDINE (1953) MODEL

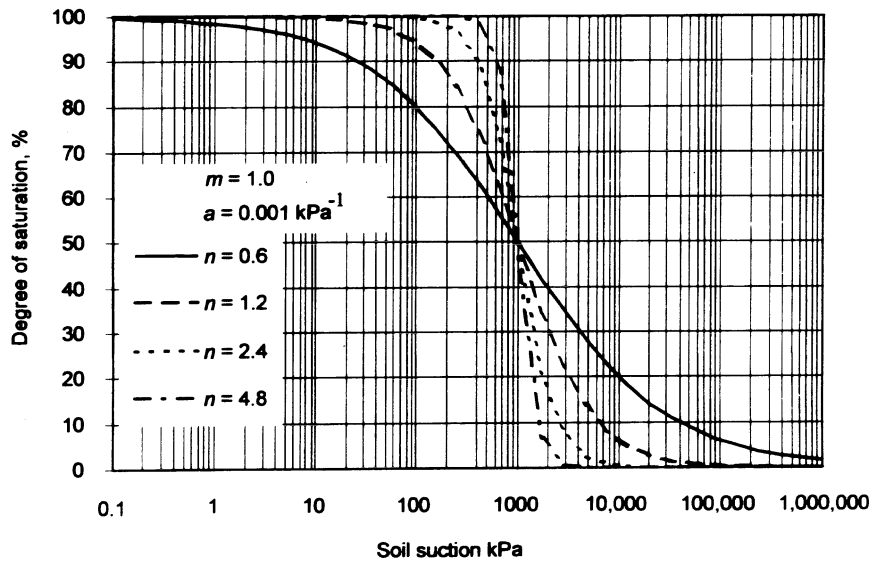
The Burdine (1953) model is a continuous soil–water characteristic curve model of similar character to the van Genuchten (1980) model. The Burdine (1953) model is a three parameter model with the relationship fixed between two of the parameters. The a parameter is related to the inverse of the air entry value; the n parameter is related to the pore size distribution of the soil. The m parameter is assumed to be a function of n , eliminating m as a fitting parameter. van Genuchten (1980) made reference to the assumptions defined by Burdine (1953).

$$m = 1 - \frac{2}{n} \quad (38)$$

The value of m cannot be negative and therefore n cannot be less than 2 for the

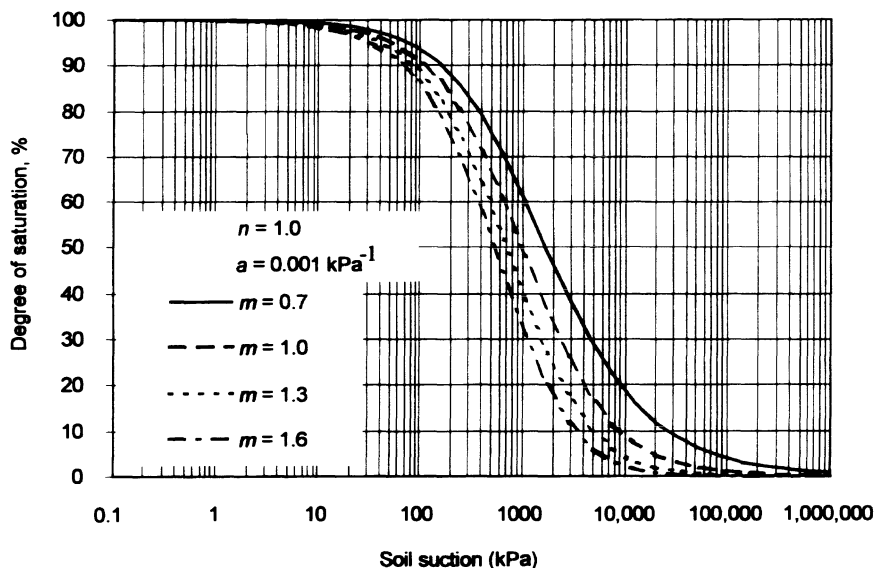


(a) m and n constant and a varying.



(b) m and a constant and n varying.

Figure 9.



(c) n and a constant and m varying.

Figure 9. Plot of van Genuchten (1980) model while varying one parameter when two other parameters are constant, (a) m and n constant and a varying; (b) m and a constant and n varying; and (c) n and a constant and m varying.

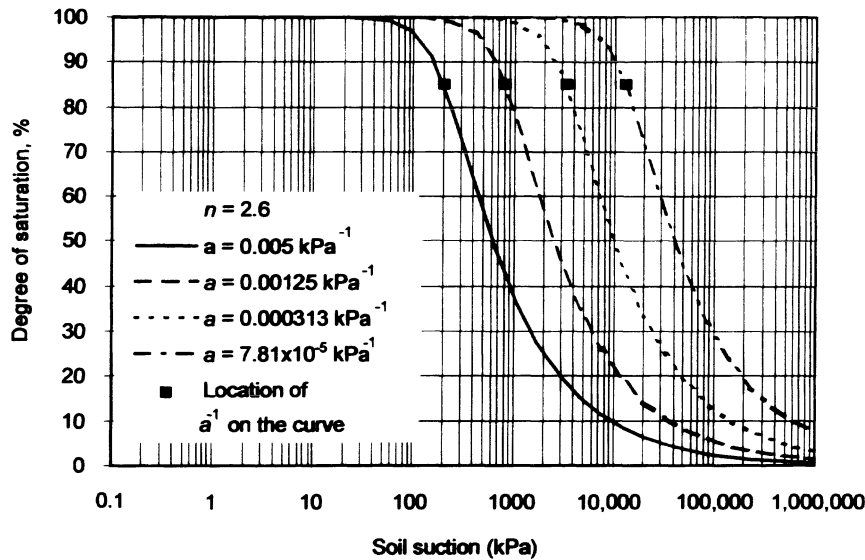
Burdine assumption. The Burdine (1953) model is described as follows:

$$S = \frac{1}{\left(1 + (a\psi)^n\right)^{(1-2/n)}} \quad (39)$$

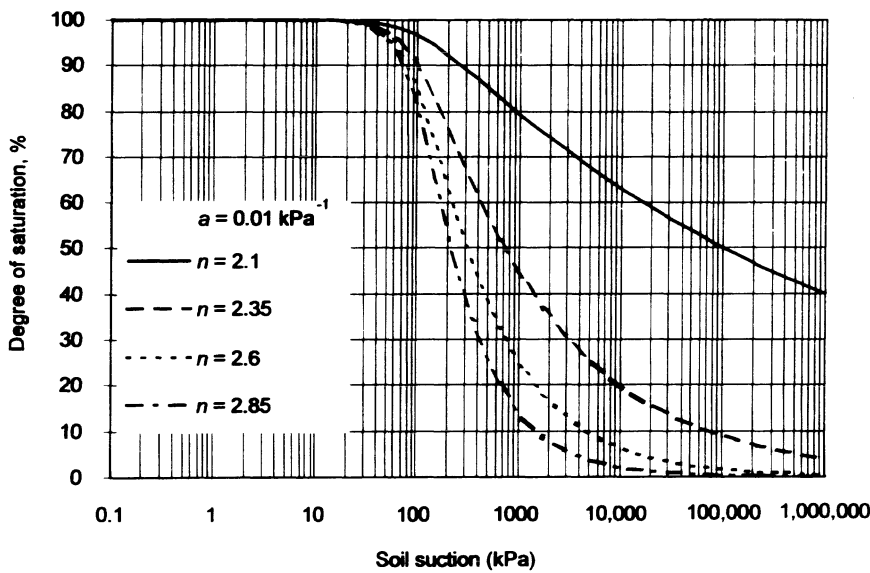
Figure 10(a) shows a plot of the Burdine (1953) model with the n parameter constant (i.e. n equal 2.6) and a varying. The a parameter has units of the inverse of soil suction. The inverse of the a parameter is larger than soil suction at the air entry value. The a parameter does not affect the shape of the curve but shifts the curve toward the higher or lower suction region of the plot.

Figure 10(b) shows the Burdine (1953) model with a constant (i.e. a equal to 0.01 kPa⁻¹) and n varying. The more uniform the pore sizes in the soil, the larger the value of n . The larger the value of n , the steeper the curve in the desaturation zone and the increased curvature in the high suction region.

The advantages of the Burdine (1953) model are as follows. The model provides a reasonably accurate representation of data for a variety of soils. The effect of one parameter can be distinguished from the effect of the other parameter, and the model contains only two parameters. One disadvantage is that the Burdine (1953) two par-



(a) n constant and a varying.



(b) a constant and n varying.

Figure 10. Plot of Burdine (1953) model while varying one parameter when the other parameter is constant, (a) n constant and a varying; and (b) a constant and n varying.

ameter model becomes less flexible than the van Genuchten (1980) three-parameter model.

The normalized water content form of the Burdine (1953) model is as follows:

$$\theta = \theta_r + (\theta_s - \theta_r) \left(1 / \left(1 + (a\psi)^n \right)^{(1-2/m)} \right) \quad (40)$$

3.9. MUALEM (1976) MODEL

Mualem (1976) proposed a model similar to the Burdine (1953) model and once again suggested that a fixed relationship be assumed between the n and m parameters (i.e. m equal to $1 - 1/n$). The value of m cannot be negative and therefore the value of n cannot be less than 1.0.

Figure 11(a) shows a plot of the Mualem (1976) model with the n parameter constant (i.e. n equal to 2.6) and a varying. The a parameter has units corresponding to the inverse of soil suction. The a parameter is related to the air entry value of the soil and the inverse of the a parameter is larger than the air entry value. The a parameter does not affect the shape of the curve but shifts the curve toward the higher or lower suction region of the plot.

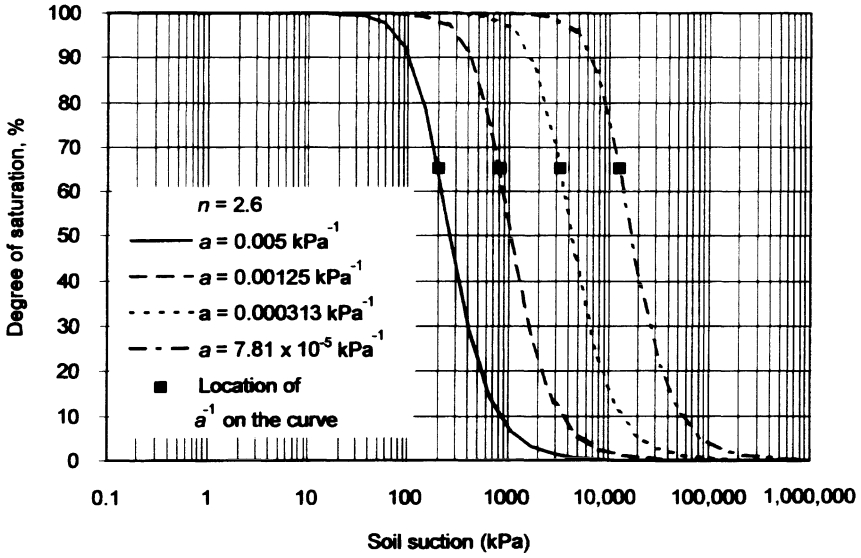
Figure 11(b) shows the Mualem (1976) model with a constant (i.e. a equal to 0.01 kPa^{-1}) and n varying. The n parameter is related to the pore size distribution index. The more uniform the pore size in the soil, the larger the value of n .

The advantages of the Mualem (1976) model are as follows: The model can provide a reasonable fit of data from a variety of soils; the effect of one parameter can be distinguished from the effect of the other parameter; the model contains only two parameters. The disadvantage is that the m assumption restricts flexibility, with respect to the shape of the curve. The Mualem (1976) model is commonly referred to in the geotechnical literature.

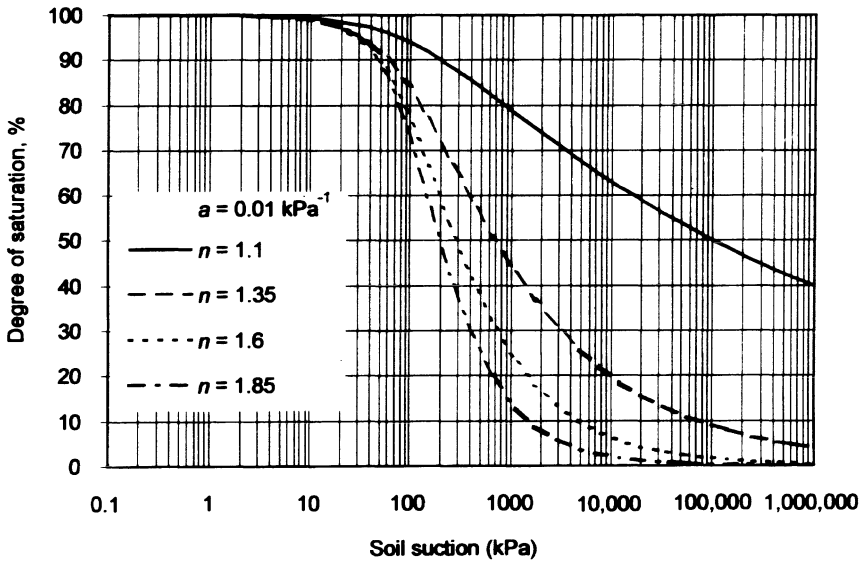
3.10. FREDLUND AND XING (1994) MODEL

Fredlund and Xing (1994) proposed a three parameter model for the soil–water characteristic curve and the form of the equations is somewhat similar to that of the van Genuchten (1980) equation. The Fredlund and Xing (1994) model provides a continuous soil–water characteristic curve model over the entire soil suction range. The equation uses three fitting parameters; namely, a , n and m . The parameter a is related to the air entry value; the n parameter is related to the pore size distribution of the soil and the m parameter is related to the asymmetry of the model. The Fredlund and Xing (1994) model is written as follows:

$$S = \frac{1}{\left[\ln \left[e + \left(\frac{\psi}{a} \right)^n \right] \right]^m} \quad (41)$$



(a) n constant and a varying.



(b) a constant and n varying.

Figure 11. Plot of Mualem (1976) model while varying one parameter when the other parameter is constant, (a) n constant and a varying; and (b) a constant and n varying.

Figure 12(a) shows a plot of the Fredlund and Xing (1994) model with n and m constant (i.e. n equal to 1.5 and m equal to 1.0) and a varying. The a parameter has units of suction and is related to, but greater than, the air entry value of the soil. The a value corresponds to the inflection point on the curve. The a parameter does not affect the overall shape of the curve but shifts the curve toward the higher soil suction region as a increases.

Figure 12(b) shows a plot of the Fredlund and Xing (1994) model with m and a constant (i.e. m equal to 1.0, and a equal to 25 kPa) and n varying. The n parameter is related to the pore size distribution index. The more uniform the pore sizes in the soil, the larger the value of n .

Figure 12(c) shows the Fredlund and Xing (1994) model with n and a constant (i.e. n equal to 1.5 and a equal to 25 kPa) and m varying. The m parameter is related to the asymmetry of the curve. Small values of m result in a moderate slope in the low suction range and a steeper slope in the high suction range.

The advantages of the Fredlund and Xing (1994) model are as follows: There is great flexibility for the model to fit a wide variety of datasets; the soil parameters are meaningful; the effect of one parameter can be distinguished from the effect of the other two parameters. It has been observed that the Fredlund and Xing (1994) model required fewer iterations to converge to the best-fit parameters than the van Genuchten (1980) three parameter model (Sillers, 1997). Fredlund and Xing (1994) also presented a correction factor for use with their model to ensure that the soil–water characteristic curve goes through 1,000,000 kPa at zero water content. The Fredlund and Xing (1994) correction is as follows:

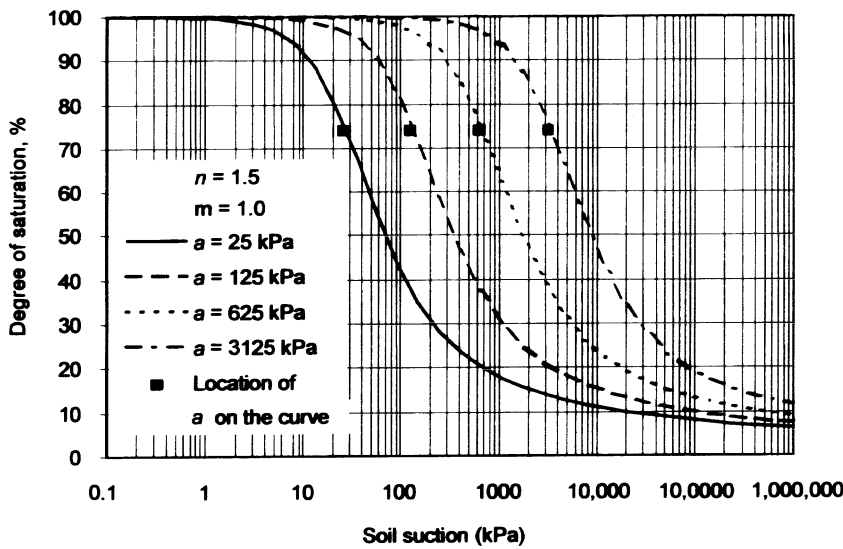
$$\theta = \theta_s \left(1 - \frac{\ln\left(1 + \frac{\psi}{\psi_r}\right)}{\ln\left(1 + \frac{10^6}{\psi_r}\right)} \right) \frac{1}{\left[\ln\left(e + \left(\frac{\psi}{a}\right)^n\right) \right]^m} \quad (42)$$

where:

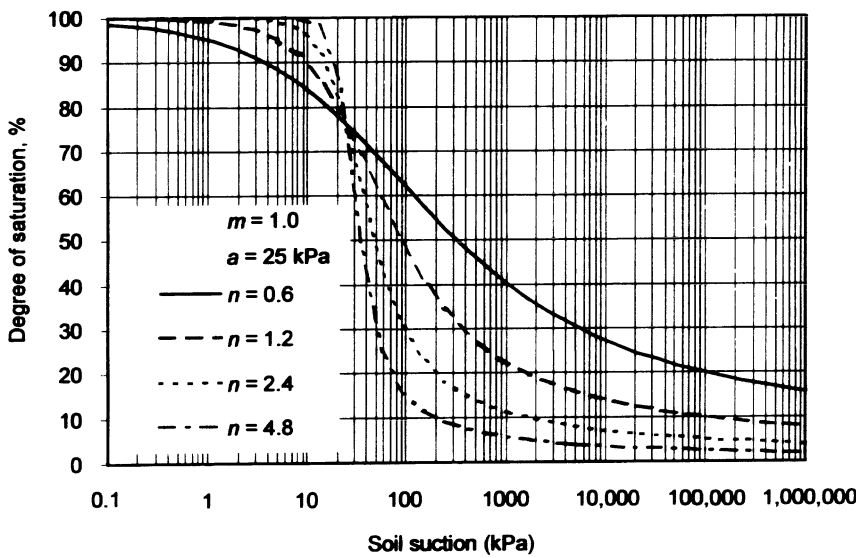
ψ_r = soil suction in residual condition that can be computed (Vanapalli et al., 1999) or assumed to be a value such as 1500 kPa or 3000 kPa.

4. Fitting the Soil–Water Characteristic Curve Models to Laboratory Data

The soil–water characteristic models are parametric equations derived from an assumed statistical pore size function. In order to fit the models using a Davidon–Fletcher–Powell optimization technique, the first derivatives of the equation with respect to each of the fitted parameters is required. The first derivative of the model with respect to soil suction provides an indication of the pore size distribution. It actually represents the water storage modulus (i.e. m_2^w) required when performing transient seepage modeling of analyses for unsaturated soils.

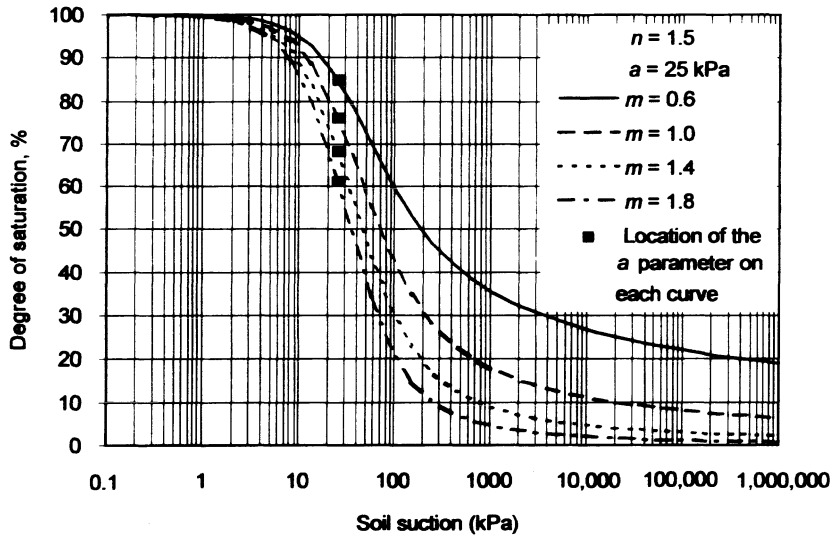


(a) m and n constant and a varying.



(b) m and a constant and n varying.

Figure 12.



(c) n and a constant and m varying.

Figure 12. Plot of Fredlund and Xing (1994) model while varying one parameter when two other parameters are constant, (a) m and n constant and a varying; (b) m and a constant and n varying; and (c) n and a constant and m varying.

4.1. DERIVATIVES OF THE VARIOUS MODELS

Table 2 shows the first derivatives for the various soil–water characteristic curve models. The Brooks and Corey (1964) model has a value of unity for soil suctions less than the air entry value. Therefore, the value of the derivatives is zero for soil suctions lower than the air entry value. For suctions that are greater than the air entry value, the first derivative of Brooks and Corey (1964) with respect to suction is given in Table 2.

Table 3 shows the second derivative for the various soil characteristic models. Table 4 shows the location of the inflection point along the curve for various models. Some models do not have an inflection point (e.g. the exponential functions, Brooks and Corey, 1964). Table 5 shows the equation for slope of the curve at the inflection point for various models and Table 6 shows the first derivatives of the normalized water content with respect to soil suction for the various models. Derivatives of normalized water content with respect to the correction factor, is shown for the Fredlund and Xing (1994) model in Table 6. Tables 7–9 show the derivative of the normalized water content with respect to n , a , or m parameters respectively. Derivatives of the normalized water content with respect to residual water content is shown for various models in Table 10.

Table 2. First derivatives of various soil–water characteristic curve models with respect to soil suction

Model	Formula
Gardner (1956)	$\frac{dS}{d\psi} = \frac{-1}{(1 + a\psi^n)^2} a\psi^n \frac{n}{\psi}$
Brooks and Corey (1964)	$\frac{dS}{d\psi} = -\left(\frac{\psi}{a}\right)^{-n} \frac{n}{\psi}$
Brutsaert (1966)	$\frac{dS}{d\psi} = \frac{-1}{\left(1 + \left(\frac{\psi}{a}\right)^n\right)^2} \left(\frac{\psi}{a}\right)^n \frac{n}{\psi}$
Tani (1982)	$\frac{dS}{d\psi} = \exp\left(-\frac{a - \psi}{a - n}\right) \frac{a - \psi}{(a - n)^2}$
Boltzman (1984)	$\frac{dS}{d\psi} = \frac{-1}{n} \exp\left(\frac{a - \psi}{n}\right)$
Fermi (1987)	$\frac{dS}{d\psi} = \frac{-1}{\left\{ \left[1 + \exp\left(\frac{\psi - a}{n}\right) \right]^2 n \right\}} \exp\left(\frac{\psi - a}{n}\right)$
van Genuchten	$\frac{dS}{d\psi} = \frac{-1}{[1 + (a\psi)^n]^m} \cdot \frac{nm(a\psi)^n}{\psi[1 + (a\psi)^n]}$
Burdine (1953)	$\frac{dS}{d\psi} = \frac{-1}{(1 + (a\psi)^n)^{(1-\frac{2}{n})}} \left(1 - \frac{2}{n}\right) (a\psi)^n \frac{n}{\psi(1 + (a\psi)^n)}$
Mualem (1976)	$\frac{dS}{d\psi} = \frac{-1}{[1 + (a\psi)^n]^{(1-1/n)}} \left(1 - \frac{1}{n}\right) (a\psi)^n \frac{n}{\psi[1 + (a\psi)^n]}$
Fredlund and Xing (1994)	$\frac{dS}{d\psi} = \frac{-1}{\left[\ln \left[e + \left(\frac{\psi}{a}\right)^n \right] \right]^m} m \left(\frac{\psi}{a}\right)^n \frac{n}{\psi \left\{ \left[\ln \left[e + \left(\frac{\psi}{a}\right)^n \right] \right]^m \left[e + \left(\frac{\psi}{a}\right)^n \right] \right\}}$

Table 3. Second derivative of soil–water characteristic curve models

Model	Formula
Gardner (1956)	$\frac{d^2S}{d\psi^2} = \frac{2}{(1+a\psi^n)^3} a^2 \psi^{2n} \frac{n^2}{\psi^2} - \frac{1}{(1+a\psi^n)^2} a \psi^n \frac{n^2}{\psi^2} + \frac{1}{(1+a\psi^n)^2} a \psi^n \frac{n}{\psi^2}$
Brooks and Corey (1964)	$\frac{d^2S}{d\psi^2} = + \left(\frac{\psi}{a}\right)^{-n} \frac{n^2}{\psi^2} + \left(\frac{\psi}{a}\right)^{-n} \frac{n}{\psi^2}$
Brutsaert (1966)	$\begin{aligned} \frac{d^2S}{d\psi^2} = & \frac{2}{\left(1 + \left(\frac{\psi}{a}\right)^n\right)^3} \left(\frac{\psi}{a}\right)^{2n} \frac{n^2}{\psi^2} - \frac{1}{\left(1 + \left(\frac{\psi}{a}\right)^n\right)^2} \left(\frac{\psi}{a}\right)^n \frac{n^2}{\psi^2} \\ & + \frac{1}{\left(1 + \left(\frac{\psi}{a}\right)^n\right)^2} \left(\frac{\psi}{a}\right)^n \frac{n}{\psi^2} \end{aligned}$
Tani (1982)	$\frac{d^2S}{d\psi^2} = \exp\left(-\frac{a-\psi}{a-n}\right) \frac{n-\psi}{(a-n)^3}$
Boltzman (1984)	$\frac{d^2S}{d\psi^2} = \frac{1}{n^2} \exp\left(\frac{a-\psi}{n}\right)$
Fermi (1987)	$\frac{d^2S}{d\psi^2} = \frac{\exp\left(2\frac{\psi-a}{n}\right) - \exp\left(\frac{\psi-a}{n}\right)}{\left\{\left[1 + \exp\left(\frac{\psi-a}{n}\right)\right]^3 n^2\right\}}$

Table 4. Equation for inflection point of the curve for various soil–water characteristic curve models

Model	Formula
Gardner (1956)	$\psi = \left[\frac{n-1}{an+a} \right]^{1/n}$
Brutsaert (1966)	$\psi = \left(\frac{n-1}{n+1} \right)^{(1/n)} a$
Tani (1982)	$\psi = n$
Fermi (1987)	$\psi = a$
van Genuchten (1980)	$\psi = \left[\frac{n-1}{nma^n+a^n} \right]^{(1/n)}$
Burdine (1953)	$\psi = \frac{1}{a}$
Mualem (1976)	$\psi = \frac{\left(\frac{n-1}{n} \right)^{1/n}}{a} \text{ that can be written as:}$ $\psi = m^{(1-m)}/a \text{ since } m = 1 - \frac{1}{n}$

Table 5. Equation for the slope of the curve at the inflection point of the soil–water characteristic curve model

Model	Equation
Gardner (1956)	$\frac{dS}{d\psi} = \frac{-1}{1 + a\left[\frac{n-1}{an+a}\right]} a\left[\frac{n-1}{an+a}\right] \frac{n}{\left[\frac{n-1}{an+a}\right]^{1/n}}$
Brutsaert (1966)	$\frac{dS}{d\psi} = \frac{-1}{(4n)} (n+1)^{[n+1/n]} \frac{(n-1)^{[n+1/n]}}{a}$
Tani (1982)	$\frac{dS}{d\psi} = \frac{\exp(-1)}{a-n}$
Fermi (1987)	$\frac{dS}{d\psi} = \frac{-1}{4n}$
van Genuchten (1980)	$\frac{dS}{d\psi} = -\frac{am(mn+1)^{(nm+1/n)}(n-1)^{(n-1/n)}}{n^m(m+1)^{m+1}}$
Burdine (1953)	$\frac{dS}{d\psi} = -a(n-2)4^{(1/n/n)}$
Mualem (1976)	$\frac{dS}{d\psi} = -na\left(\frac{n-1}{2n-1}\right)^{2n-1/n}$

Table 6. First derivative of the normalized water content with respect to soil suction

Model	Equation
Gardner (1956)	$\frac{d\theta}{d\psi} = \frac{(\theta_s - \theta_r)}{(1 + a\psi^n)^2} a\psi^n \frac{n}{\psi}$
Brooks and Corey (1964)	$\frac{d\theta}{d\psi} = (\theta_s - \theta_r) \left(\frac{\psi}{a}\right)^{-n} \frac{n}{\psi}$
Brutsaert (1966)	$\frac{d\theta}{d\psi} = \frac{-(\theta_s - \theta_r)}{\left(1 + \left(\frac{\psi}{a}\right)^n\right)^2} \left(\frac{\psi}{a}\right)^n \frac{n}{\psi}$
Tani (1982)	$\frac{d\theta}{d\psi} = \left(\frac{\theta_s - \theta_r}{a - n}\right) \left(\frac{a - \psi}{a - n}\right) \exp\left(-\frac{a - \psi}{a - n}\right)$
Boltzman (1984)	$\frac{d\theta}{d\psi} = -\frac{(\theta_s - \theta_r)}{n} \exp\left(\frac{a - \psi}{n}\right)$
Fermi (1987)	$\frac{d\theta}{d\psi} = \frac{-(\theta_s - \theta_r)}{\left(1 + \exp\left(\frac{\psi - a}{n}\right)\right)^2} \exp\left(\frac{\psi - a}{n}\right) \frac{1}{n}$
Burdine (1953)	$\frac{d\theta}{d\psi} = -\frac{(\theta_s - \theta_r)}{(1 + a\psi^n)^{(1-\frac{1}{n})}} \left(1 - \frac{2}{n}\right) (a\psi)^2 \frac{n}{\psi(1 + (a\psi)^n)}$
Mualem (1976)	$\frac{d\theta}{d\psi} = -\frac{(\theta_s - \theta_r)}{(1 + a\psi^n)^{(1-\frac{1}{n})}} \left(1 - \frac{1}{n}\right) (a\psi)^n \frac{n}{\psi(1 + (a\psi)^n)}$
Fredlund and Xing (1994), modified using correction factor	$\frac{d\theta}{d\psi} = \theta_s \frac{\frac{\psi}{\psi_r^2} \left[\left(1 + \frac{\psi}{\psi_r}\right) \ln\left(1 + \frac{10^6}{\psi_r}\right) \right] - \frac{10^6 \ln\left(1 + \frac{\psi}{\psi_r}\right)}{\ln\left(1 + \frac{10^6}{\psi_r}\right)^2 \psi^2 \left(1 + \frac{10^6}{\psi_r}\right)}}{\left[\ln\left(e + \left(\frac{\psi}{a}\right)^n\right) \right]^m}$

Table 7. Derivative of the normalized water content with respect to n parameter

Derivative of the model	Equation
Gardner (1956)	$\frac{d\theta}{dn} = -\frac{(\theta_s - \theta_r)}{(1 + a\psi^n)^2} a\psi^n \ln(\psi)$
Brooks and Corey (1964)	$\frac{d\theta}{dn} = -(\theta_s - \theta_r) \left(\frac{\psi}{a}\right)^{-n} \ln\left(\frac{\psi}{a}\right)$
Brutsaert (1966)	$\frac{d\theta}{dn} = \frac{-(\theta_s - \theta_r)}{\left(1 + \left(\frac{\psi}{a}\right)^n\right)^2} \left(\frac{\psi}{a}\right)^n \ln\left(\frac{\psi}{a}\right)$
Tani (1982)	$\frac{d\theta}{dn} = -(\theta_s - \theta_r) \left(\frac{1}{a-n} - \frac{a-\psi}{(a-n)^2}\right) \left(-\frac{a-\psi}{a-n}\right) \exp\left(-\frac{a-\psi}{a-n}\right)$
Boltzman (1984)	$\frac{d\theta}{dn} = -(\theta_s - \theta_r) \frac{a-\psi}{n^2} \exp\left(\frac{a-\psi}{n}\right)$
Fermi (1987)	$\frac{d\theta}{dn} = \frac{(\theta_s - \theta_r)}{\left(1 + \exp\left(\frac{\psi-a}{n}\right)\right)^2} \frac{\psi-a}{n^2} \exp\left(\frac{\psi-a}{n}\right)$
Burdine (1953)	$\begin{aligned} \frac{d\theta}{dn} = & -\frac{(\theta_s - \theta_r)}{(1 + a\psi^n)^{(1-2/n)}} \\ & \times \left[\frac{2}{n^2} \ln(1 + (a\psi)^n) + \left(1 - \frac{2}{n}\right) (a\psi)^2 \frac{n}{(1 + (a\psi)^n)} \right] \end{aligned}$
Mualem (1976)	$\begin{aligned} \frac{d\theta}{dn} = & -\frac{(\theta_s - \theta_r)}{(1 + a\psi^n)^{(1-1/n)}} \\ & \times \left[\frac{1}{n^2} \ln(1 + (a\psi)^n) + \left(1 - \frac{1}{n}\right) (a\psi)^2 \frac{n}{(1 + (a\psi)^n)} \right] \end{aligned}$
Fredlund and Xing (1994), modified using correction factor	$\frac{d\theta}{dn} = \frac{-\theta_s \left(1 - \frac{\ln\left(1 + \frac{\psi}{\psi_r}\right)}{\ln\left(1 + \frac{10^6}{\psi_r}\right)}\right)}{\left[\ln\left(e + \left(\frac{\psi}{a}\right)^n\right)\right]^m} m \left(\frac{\psi}{a}\right)^n \times \frac{\ln\left(\frac{\psi}{a}\right)}{\left(e + \left(\frac{\psi}{a}\right)^n\right) \left(\ln\left(e + \left(\frac{\psi}{a}\right)^n\right)\right)}$

Table 8. Derivative of the normalized water content with respect to a parameter

Derivative of the model	Equation
Gardner (1956)	$\frac{d\theta}{da} = -\frac{(\theta_s - \theta_r)}{(1 + a\psi^n)^2} \cdot \psi^n$
Brooks and Corey (1964)	$\frac{d\theta}{da} = (\theta_s - \theta_r) \left(\frac{\psi}{a}\right)^{-n} \frac{n}{a}$
Brutsaert (1966)	$\frac{d\theta}{da} = \frac{-(\theta_s - \theta_r)}{\left(1 + \left(\frac{\psi}{a}\right)^n\right)^2} \left(\frac{\psi}{a}\right)^n \frac{n}{a}$
Tani (1982)	$\frac{d\theta}{da} = (\theta_s - \theta_r) \frac{(\psi - n)^2}{(a - n)^4} \exp\left(-\frac{a - \psi}{a - n}\right)$
Boltzman (1984)	$\frac{d\theta}{da} = \frac{(\theta_s - \theta_r)}{n} \exp\left(\frac{a - \psi}{n}\right)$
Fermi (1987)	$\frac{d\theta}{da} = \frac{(\theta_s - \theta_r)}{\left(1 + \exp\left(\frac{\psi - a}{n}\right)\right)^2} \exp\left(\frac{\psi - a}{n}\right) \frac{1}{n}$
Burdine (1953)	$\frac{d\theta}{da} = -\frac{(\theta_s - \theta_r)}{(1 + (a\psi)^n)^{(1-2/n)}} \left(1 - \frac{2}{n}\right) (a\psi)^n \frac{n}{a(1 + (a\psi)^n)}$
Mualem (1976)	$\frac{d\theta}{dn} = -\frac{(\theta_s - \theta_r)}{(1 + (a\psi)^n)^{(1-1/n)}} \left(1 - \frac{1}{n}\right) (a\psi)^n \frac{n}{a(1 + (a\psi)^n)}$
Fredlund and Xing (1994), modified using correction factor	$\frac{d\theta}{da} = -\frac{-\theta_s \left(1 - \frac{\ln\left(1 + \frac{\psi}{\psi_r}\right)}{\ln\left(1 + \frac{10^6}{\psi_r}\right)}\right)}{\left[\ln\left(e + \left(\frac{\psi}{a}\right)^n\right)\right]^m} \ln\left(\ln\left(e + \left(\frac{\psi}{a}\right)^n\right)\right)$

Table 9. Derivative of the normalized water content with respect to *m* parameter

Derivative of the model	Equation
Fredlund and Xing (1994), modified using correction factor	$\frac{d\theta}{dm} = -\frac{-\theta_s \left(1 - \frac{\ln\left(1 + \frac{\psi}{\psi_r}\right)}{\ln\left(1 + \frac{\psi_r}{10^6}\right)} \right)}{\left[\ln\left(e + \left(\frac{\psi}{a}\right)^n\right) \right]^m} \ln\left[\ln\left(e + \left(\frac{\psi}{a}\right)^n\right) \right]$

Table 10. Derivative of the normalized water content with respect to residual water content

Derivative of the model	Equation
Gardner (1956)	$\frac{d\theta}{d\theta_r} = 1 - \frac{1}{(1 + a\psi^n)}$
Brooks and Corey	$\frac{d\theta}{d\theta_r} = 1 - \left(\frac{\psi}{a}\right)^{-n}$
Brutsaert (1966)	$\frac{d\theta}{d\theta_r} = 1 - \frac{1}{1 + \left(\frac{\psi}{a}\right)^n}$
Tani (1982)	$\frac{d\theta}{d\theta_r} = 1 - \left(1 + \frac{a - \psi}{a - n}\right) \exp\left(-\frac{a - \psi}{a - n}\right)$
Boltzman (1984)	$\frac{d\theta}{d\theta_r} = 1 - \exp\left(\frac{a - \psi}{n}\right)$
Fermi (1987)	$\frac{d\theta}{d\theta_r} = 1 - \frac{1}{\exp\left(\frac{\psi - a}{n}\right)}$
Burdine (1953)	$\frac{d\theta}{d\theta_r} = 1 - \frac{1}{(1 + (a\psi)^n)^{(1-2/n)}}$
Mualem (1976)	$\frac{d\theta}{d\theta_r} = 1 - \frac{1}{(1 + (a\psi)^n)^{(1-1/n)}}$

5. Summary of Mathematical Models for Soil–Water Characteristics Curves

Numerous mathematical models have been suggested to describe the soil–water characteristic curve. A number of proposed equations have been selected and their mathematical characteristics have been illustrated and described. The list of equations is not exhaustive but is illustrative of typical equations using two and three soil parameters.

The mathematical models presented can be categorized in a number of ways to illustrate the characteristics of the equations, as well as their advantages and disadvantages. First, the equations can be categorized on the basis of being either two or three parameter models. Three soil parameter equations are more flexible in terms of their ability to fit experimental data over a wide range of soil suctions. They are not necessarily more difficult to fit than two soil parameter equations. Second, the models can be categorized on the basis of whether the soil parameters are independent and have physical meaning. A model with independent and physically meaningful parameters is preferable from the standpoint of estimating and correlating their magnitude to classification soil properties. Third, the models can be categorized on the basis of whether or not the model produces one continuous mathematical function over the entire range of soil suction. It should be noted that there is also an advantage in having a correction factor that ensures that the soil suction goes to 1,000,000 kPa at zero water content.

When a limited range of soil suction versus water content data are being fitted, essentially any of the proposed models produce satisfactory results. However, some models are advantageous over other models when soil suctions need to be modelled up to 1,000,000 kPa, corresponding to zero water content.

References

- Brooks, R. and Corey, A. (1964) Hydraulic properties of porous media, *Hydrology Paper No. 3*. Colorado State University, Fort Collins, CO.
- Brutsaert, W. (1966) Probability laws for pore size distributions, *Soil Science* **101**, 85–92.
- Burdine, N.T. (1953) Relative permeability calculations from pore size distribution data, *Journal of Petroleum Technology* **5**, 71–78.
- Croney, D. and Coleman, J. (1961) Pore pressure and suction in soils. In *Proceedings of the Conference on Pore Pressure and Suction in Soils*. Butterworths, London, pp. 31–37.
- Fredlund, D.G. and Xing A. (1994) Equations for the soil–water characteristic curve. *Canadian Geotechnical Journal* **31**, 521–532.
- Fairbridge, R. and Finkl, C. (1979) *The Encyclopedia of Soil Science Part 1*, Dowden, Hutchinson and Ross, Inc. Stroudsburg, PA.
- Gardner, W. (1956) Mathematics of isothermal water conduction in unsaturated soils. *Highway Research Board Special Report 40 International Symposium on Physico-Chemical Phenomenon in Soils*. Washington D.C. pp. 78–87.
- Huang, S., Barbour, S.L. and Fredlund, D.G. (1994) A history of the coefficient of permeability function. *Sino-Canadian Symposium on Expansive Soils/Unsaturated Soils, Chinese Institution for Soil Mechanics and Foundation Engineering, CEES*. Wuhen, China. pp. 57–80.

- Kong, L.W. and Tan, L.R. (2000) A simple method of determining the soil–water characteristic curve indirectly. *Unsaturated Soils for Asia*. Editors: Rahardjo, H., Toll, D.G. and Leong, E.C. (eds), *Proceedings of the Asian Conference on Unsaturated Soils*, Singapore, 18–19 May 2000, 341–345.
- Kosugi, K. (1994) The parameter lognormal distribution model for soil water retention. *Water Resource Research* **30**, 891–901.
- McKee, C. and Bumb, A. (1984) The importance of unsaturated flow parameters in designing a hazardous waste site. *Hazardous Wastes and Environmental Emergencies (Hazardous Materials Control Research Institute National Conference)*. Houston, TX, March 1984, pp. 50–58.
- McKee, C. and Bumb, A. (1987) Flow-testing coalbed methane production wells in the presence of water and gas. *SPE Formation Evaluation*. pp. 599–608.
- Mitchell, J. (1976) *Fundamentals of Soil Behavior*, John Wiley and Sons, Inc. New York.
- Mualem, Y. (1976) A new model for predicting the hydraulic conductivity of unsaturated porous media. *Water Resources Research* **12**, 593–622.
- Olson, K.R. (1985) Characterization of pore size distribution within soils by mercury intrusion and water-release methods. *Soil Science* **139**(5), 400–404.
- Praparahan, S., Altschaeffl, A.G. and Dempsey, B.J. (1985) Moisture curve of compacted clay: mercury intrusion method. *Journal of Geotechnical Engineering* **111**(9), 1139–1143.
- Sillers, W. (1997) The mathematical representation of the soil–water characteristic curve. M.Sc. thesis, University of Saskatchewan, Saskatoon, Canada.
- Tani, M. (1982) The properties of a water-table rise produced by a one dimensional, vertical, unsaturated flow (in Japanese with an English summary). *Journal of Japan for Society* **64**, 409–418.
- Vanapalli, S.K., Pufahl, D.E. and Fredlund, D.G. (1998) The meaning and relevance of residual water content to unsaturated soils. *Proceedings of 51st Canadian Geotechnical Conference*, Edmonton, AB, October 4–7, pp. 101–108.
- van Genuchten, M. Th. (1980) A closed form equation predicting the hydraulic conductivity of unsaturated soils. *Soil Science Society of America Journal* **44**, 892–898.



Soil–water characteristic curves of Singapore residual soils

S. S. AGUS, E. C. LEONG and H. RAHARDJO

NTU-PWD Geotechnical Research Centre, Nanyang Technological University, School of Civil & Structural Engineering, Nanyang Avenue, Singapore 639798 (E-mail: cecleong@ntu.edu.sg)

(Received 17 August 2000; revised 29 December 2000; accepted 6 April 2001)

Abstract. Soil–water characteristic curves were obtained for a number of Singapore residual soil samples. Soil samples were obtained from the two main residual soil formations, the Jurong sedimentary formation and the Bukit Timah granitic formation, at various depths. The effect of weathering on the shape of the soil–water characteristic curve is examined. As the test procedure in obtaining the soil–water characteristic curve is tedious and time-consuming, empirical relationships based on multivariate analysis relating the parameters of the Fredlund and Xing (1994) soil–water characteristic curve equation to basic soil properties are suggested for the Singapore residual soils. The multivariate equations were found to be suitable for providing a quick preliminary estimate of the soil–water characteristic curve of Singapore residual soils.

Key words: multivariate, residual soil, soil–water characteristic curve, statistical analyses, suction.

1. Introduction

Singapore, located between latitude $1^{\circ}09' \text{ N}$ and $1^{\circ}29' \text{ N}$ and longitude $103^{\circ}38' \text{ E}$ and $104^{\circ}06' \text{ E}$, is a tropical country with a hot and humid climate. Singapore has an average daily temperature of 26.6°C , an average relative humidity of 85% and a high annual rainfall of about 2400 mm. The tropical climate is conducive to the erosion and weathering process in the formation of residual soils. Residual soils occupy approximately two thirds of the land area of Singapore (Figure 1). The residual soils derived from the Jurong sedimentary formation and the Bukit Timah granitic formation are found in the western and central regions of Singapore, respectively. The depth of weathering is highly variable. In the Jurong sedimentary formation, the weathering depth extends to a depth of 45 m and is generally deeper in the faulted areas and in the mudstone region whereas the thickness of the weathered zone for the Bukit Timah granitic formation varies between 10 m and 40 m (Tan *et al.*, 1987).

The Jurong sedimentary formation which covers about one third of the Singapore land area, consists of grey to black interbedded mudstone and sandstone, or reddish sandstone and mudstone conglomerates. Sediments in the forms of shale and con-

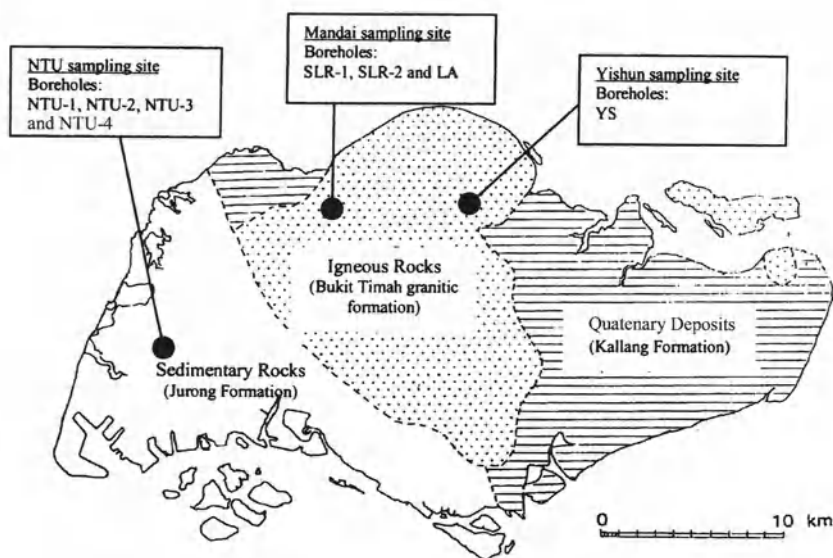


Figure 1. The geological map of Singapore and undisturbed sampling locations.

glomerates are also found in this area (Public Works Department, 1976). The soils are classified as clayey silt, sandy clay of medium plasticity and clayey to silty sand.

The Bukit Timah granitic formation residual soils range from silty sand to silty clay depending on the degree of weathering. Their colours vary from cream to reddish brown. The primary weathering stage produces sandy clayey silt whereas the secondary weathering yields laterite which is present within the silty clay layer as indicated by its reddish colour. Poh *et al.* (1985) have grouped the Bukit Timah granitic residual soils into two main groups based on their grain-size distribution curves. Group I is coarse-grained soils with a silt content varying from 7% to 50% and having a liquid limit below 50. Group II is categorized as fine-grained soils with a clay content as high as 40% and having a liquid limit above 40.

As products of weathering, the Singapore residual soils are commonly constituted above the groundwater table and therefore, they are usually unsaturated. Indeed, the characterization of Singapore residual soils must include both their saturated and unsaturated properties. The soil-water characteristic curve (SWCC) is one of the fundamental relationships for unsaturated soil. The SWCC can be used to estimate other unsaturated soil properties such as shear strength and permeability (Fredlund and Rahardjo, 1993).

Very limited research has been conducted on the properties of Singapore residual soils, particularly their unsaturated properties. In this paper, SWCCs of Singapore residual soils are presented. The effect of depth of weathering on the SWCCs of the residual soils is also examined. As the procedure for obtaining SWCC is very

tedious and time-consuming, empirical relationships based on a multivariate regression approach for obtaining SWCCs are suggested. These empirical relationships enable a quick preliminary estimate of the SWCC of Singapore residual soils to be obtained from the basic soil properties.

2. Soil–Water Characteristic Curve

The soil–water characteristic curve (SWCC) expresses the relationship between water content and suction. The water content can be either gravimetric water content, volumetric water content or degree of saturation. An analogous curve to the SWCC in saturated soils is the consolidation curve that relates void ratio to effective stress (Fredlund and Rahardjo, 1993). Two paths are obtained in the SWCC, analogous to the compression and swelling lines of the consolidation curve, namely drying (desorption) and wetting (adsorption) paths. The water content of a soil decreases as its suction increases following a drying path and the reverse process occurs in the wetting path. In this paper, the SWCCs were obtained following the drying path.

3. Matric Suction and Total Suction

Total suction is defined as free energy of the soil water or the relative humidity of the pore-water vapour in the soil (Aitchison, 1965). It encompasses both matric and osmotic suctions. Matric suction is the capillary component of free energy. It is defined as the negative pore-water pressure in the soil due to capillary and adsorption forces. Therefore, matric suction is always present in the case of soils above the groundwater table. In suction terms, it is the equivalent suction derived from the measurement of the partial pressure of the water vapour in equilibrium with the soil water, relative to the partial pressure of the water vapour in equilibrium with a solution identical in composition with the soil water.

Osmotic suction is the solute component of free energy. It is related to the amount of dissolved salt in the pore-water. It is equivalent to suction derived from the measurement of the partial pressure of the water vapour in equilibrium with a solution, which has identical composition to the soil water, relative to the partial pressure of water vapour in equilibrium with free pure water.

In terms of relative humidity in the soil–water system, the total suction is given by (Lang, 1967):

$$\psi_t = \frac{1000RT}{W_a} \ln\left(\frac{p}{p_0}\right) \quad (1)$$

where ψ_t is total suction [$\text{ML}^{-1} \text{T}^{-2}$], R is gas constant (8.31432 J/mol K), T is absolute temperature (K), W_a is molecular weight of water (mol/m^3), p is partial pressure of pore-water vapour [$\text{ML}^{-1} \text{T}^{-2}$] and p_0 is saturation pressure of water

vapour over a flat surface of pure water at temperature T [$\text{ML}^{-1} \text{T}^{-2}$]. The ratio p/p_0 is relative humidity.

Lang (1967) also suggested that suction could be created in the soil by establishing a relative vapour pressure. The relative vapour pressure is related to the osmotic coefficient of the solution which depends on the number of moles of solute in the solution (e.g. for aqueous solutions of sodium chloride). Thus, a specific total suction can be generated in the vapour by adding a corresponding amount of solute into the solvent.

4. Equation for SWCC

Numerous equations have been suggested to describe the SWCC. Leong and Rahardjo (1997) showed that most of these equations could be obtained from the following generic equation:

$$a_1 \Theta^{b_1} + a_2 \exp(a_3 \Theta^{b_1}) = a_4 \psi^{b_2} + a_5 \exp(a_6 \psi^{b_2}) + a_7 \quad (2)$$

where $a_1, a_2, a_3, a_4, a_5, a_6, a_7, b_1$, and b_2 are constants, ψ is matric suction, Θ is normalised volumetric water content [i.e., $(\theta_w - \theta_r)/(\theta_s - \theta_r)$], θ_w is volumetric water content, θ_s is saturated volumetric water content and θ_r is residual volumetric water content.

In soil science, Brooks and Corey (1964) and van Genuchten (1980) equations are popular. Brooks and Corey's (1964) SWCC equation is given by:

$$\begin{aligned} \theta_w &= \theta_s & \text{for } \psi &\leq \psi_b \\ \theta_w &= \theta_s \left(\frac{\psi_b}{\psi} \right)^\lambda & \text{for } \psi &> \psi_b \end{aligned} \quad (3)$$

where ψ is matric suction [$\text{ML}^{-1} \text{T}^{-2}$], ψ_b is air entry value of soil [$\text{ML}^{-1} \text{T}^{-2}$] and λ is a constant.

Van Genuchten's (1980) SWCC equation is given by the following formula:

$$\theta_w = \theta_s \left[\frac{1}{1 + (\alpha \psi)^p} \right]^q \quad (4)$$

where α, p and q are constants.

In geotechnical engineering, Fredlund and Xing (1994) suggested the following SWCC equation:

$$\theta_w = \frac{\theta_s}{\left\{ \ln \left[e + \left(\frac{\psi}{a} \right)^n \right] \right\}^m} \quad (5)$$

where a, n and m are constants.

Leong and Rahardjo (1997) assessed the above three SWCC equations together with other popular SWCC equations and concluded that the Fredlund and Xing (1994) equation gave the best fit to experimental data.

5. Soil Properties

Undisturbed residual soil samples from both the Jurong sedimentary and the Bukit Timah granitic formations were obtained from different sites using a Mazier sampler (Mazier, 1974; Brenner and Phillipson, 1979). Residual soil samples from Jurong sedimentary formation were obtained from four boreholes within the Nanyang Technological University (NTU) campus denoted as NTU-1 to NTU-4. Residual soil samples from the Bukit Timah granitic formation were also obtained from four boreholes at two different sites. Three boreholes are in Mandai denoted by SLR-1, SLR-2 and LA and the fourth borehole is in Yishun, denoted by YS. The locations of the sites are shown in Figure 1. Soil samples were collected from various depths. Index soil properties of the residual soils from the Jurong sedimentary and Bukit Timah granitic formations are listed in Tables 1 and 2, respectively.

6. Test Procedures for Obtaining SWCC

Two methods have been used to obtain the SWCCs of Singapore residual soils. Pressure plate (PP) test was used for low matric suctions (i.e. less than 1500 kPa) while salt solution (SS) method was adopted for higher suctions (greater than 1500 kPa). Leong and Rahardjo (1997) had recommended that the SWCC should include points in the high suction range (after the residual volumetric water content, θ_r), especially if it is utilised to estimate unsaturated soil properties.

6.1. PRESSURE PLATE (PP) TEST

The SWCCs for low suctions (less than 1500 kPa) were determined using the PP test in accordance with ASTM D2325-68 (ASTM, 1998). The apparatus consists of a chamber with a pressure plate cell (a high-air entry disk and a water compartment) and a burette supported by a stand (Figure 2).

The test procedure commences with placing the soil specimen on the high-air entry disk that has been previously saturated. Good contact between the soil specimen and the high-air entry disk is required. The water compartment is usually opened to the atmosphere (i.e. pore-water pressure, $u_w = 0$). Since, matric suction is the difference between pore-air pressure, u_a , and pore-water pressure, u_w , the applied air pressure (u_a) gives the matric suction. During testing the soil specimen was periodically removed from the pressure plate and its weight and volume were determined. The air pressure was increased to impose the next desired matric suction in the soil specimen when change in the weight of the soil specimen was considered negligible. The procedure was repeated to the final matric suction.

Table 1. Basic properties of Jurong sedimentary residual soils used in study

Location	Depth (m)	Colour	Code	Saturated unit weight (kN/m ³)	Specific gravity	Liquid limit	Plastic limit	Grain size distribution				
								Plasticity index	Clay (%)	Silt (%)	Sand (5)	
NTU campus (1)	3.00–3.45	Yellow	NTU-1-a	20.51	2.77	39	29	10	33	53	14	CL
	6.00–6.20	Red	NTU-1-b	19.72	2.63	32	5	7	26	49	25	CL
	9.00–9.20	Dark reddish grey	NTU-1-c	20.00	2.73	28	18	10	12	25	63	SM
NTU campus (2)	0.30–0.80	Yellowish brown	NTU-2-a	20.58	2.63	39	23	16	17	55	28	CL
	2.00–3.00	Orange	NTU-2-b	21.40	2.67	47	26	21	37	40	23	CL
	4.00–4.20	Purple	NTU-2-c	23.00	2.72	34	21	13	26	58	16	CL
NTU campus (3)	3.00–3.45	Red	NTU-3-a	20.11	2.52	55	33	22	31	42	27	MH
	6.00–6.45	Brownish white	NTU-3-b	19.94	2.56	36	26	10	15	35	50	ML
	9.00–9.45	Grey	NTU-3-c	20.33	2.72	44	30	14	32	60	8	CL
NTU campus (4)	4.50–5.00	Brown	NTU-4-a	20.92	2.67	42	27	15	1	55	44	ML
	8.00–9.00	Reddish brown	NTU-4-b	21.22	2.76	43	28	15	2	54	44	ML
	12.00–13.00	Darkish reddish brown	NTU-4-c	20.70	2.63	35	26	9	1	20	79	ML

Table 2. Basic properties of Bukit Timah granitic residual soils used in study

Location	Depth (m)	Colour	Code	Saturated unit weight (kN/m ³)	Specific gravity	Liquid limit	Plastic limit	Plasticity index	Grain size distribution			USCS
									Clay (%)	Silt (%)	Sand (%)	
Stephen Lee Rd (1)	1.60–2.15	Yellow	SLR-1-a	18.34	2.60	108	47	61	1	38	61	SM
	3.50–4.15	Reddish brown	SLR-1-b	18.50	2.61	64	34	30	0	28	72	SM
	14.50–15.15	Reddish brown	SLR-1-c	18.15	2.55	60	35	25	7	18	75	SM
Stephen Lee Rd (2)	1.80–2.80	Light brown	SLR-2-a	18.26	2.60	105	47	58	41	21	38	MH
	5.60–6.60	Light brown	SLR-2-b	18.27	2.61	116	48	68	37	25	38	MH
	17.50–18.00	Pink	SLR-2-c	18.12	2.55	61	36	25	12	45	43	CH
Lorong Asrama	1.50–2.10	Reddish brown	LA-a	19.01	2.53	48	37	11	24	10	66	SC
	3.50–4.10	Light brown	LA-b	18.75	2.60	97	38	59	1	27	72	SM
	11.50–12.10	Red	LA-c	18.12	2.54	61	4	20	10	27	62	SM
	17.50–18.00	Red	LA-d	18.70	2.60	97	38	59	1	24	75	SM
Yishun	1.50–2.00	Pink	YS-a	18.90	2.61	54	33	21	12	44	44	MH
	6.00–6.70	Yellow	YS-b	17.08	2.53	68	49	19	12	56	32	MH

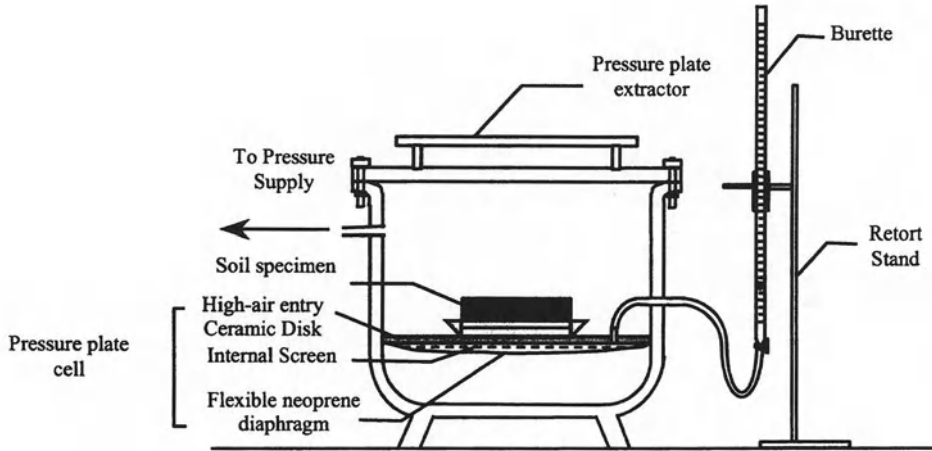


Figure 2. Schematic drawing of pressure plate (PP) test.

Once the test was completed, the final mass, volume and water content of the soil specimen were determined. The water contents of the soil specimen at all other matric suctions were back-calculated from the final mass of the soil and the mass change at each matric suction. The volumetric water content of the soil specimen was computed using the following equation:

$$\theta_w = \frac{wG_s}{1 + e} \quad (6)$$

where e is void ratio, w is gravimetric water content and G_s is specific gravity of soil specimen.

It is important to note that during the test, the total volume of the soil specimen may change. In the case of deformable soils, the change in total volume of the soil specimen is significant and thus Equation (6) applies only when void ratio at each matric suction value is known. The change in total volume of the residual soil specimen during the test was found to be negligible and therefore e was assumed to be constant.

6.2. SALT SOLUTION (SS) METHOD

At high suction values (i.e. higher than 1500 kPa), the salt solution (SS) method was used instead of the PP test. The method is based on the theoretical standpoint that a water potential (i.e. suction) is related to a particular relative vapour pressure of the water in the soil–water system. The relative vapour pressure of water in equilibrium with the system is characterised by its relative humidity. Therefore, suction can be established by creating the relative humidity, which is related to the concentration of a solution identical with the composition of the soil water (Lang, 1967).

The concentration of salt in water creates a vapour pressure corresponding to a relative humidity at a certain temperature of the air above the surface of the salt solution. It should be noted that the SS method generates a total suction in the soil–water system. However, at high suctions (greater than 1500 kPa), matric suction is equal to total suction (Fredlund and Xing, 1994). Thus, results from SS tests can be utilised together with PP test results to obtain a complete SWCC from θ_s to θ_r .

In the SS method, the undisturbed soil specimen (about 5–10 g) is placed in a ceramic crucible (Vanapalli, 1994, Vanapalli *et al.*, 1996). A solution of sodium chloride with a certain concentration was prepared and placed in a vacuum desiccator to generate a vapour pressure (total suction) in the desiccator (Figure 3). The soil specimens in the ceramic crucibles were then put into the desiccator (one desiccator can accommodate up to four ceramic crucibles). The desiccator was subsequently placed on a magnetic stirrer, which was operated for 5–10 min. to accelerate the equilibrium of the vapour pressure in the desiccator. The soil specimen together with the ceramic crucible was weighed periodically every week until there was negligible change in mass of the soil specimen.

It should be noted that the total suction (i.e. vapour pressure) generated in the desiccator may not have reached equilibrium during the test. A piece of filter paper (Whatman No. 42) was placed in each desiccator to ascertain the total suction generated in the desiccator. The total suction in the desiccator was determined by relating the water content of the filter paper with total suction. ASTM D5298-94 (ASTM, 1998) provides a calibration curve to correlate the water content of the filter paper with total suction for Whatman No. 42 and Schleicher and Schnell No. 589 filter papers. He (1999) had noted that the calibration curves from different researchers for the same filter paper types are different. He recommended that calibration should be performed for the filter paper batch before use and in the same suction measurement mode (i.e. for matric suction or total suction). He (1999) pro-

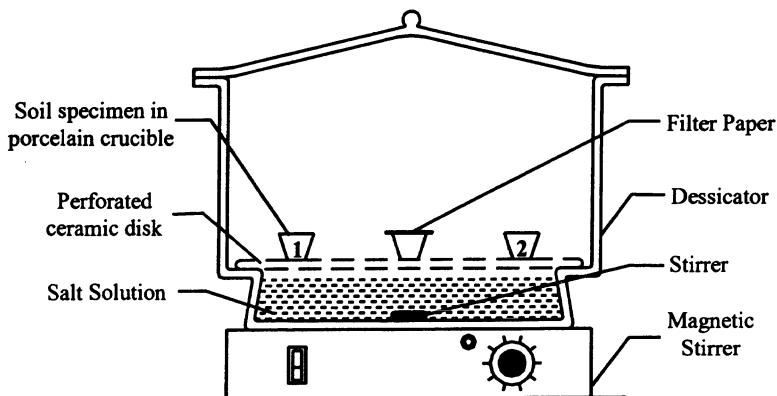


Figure 3. Schematic drawing of salt solution (SS) test set-up.

vided the calibration curves for matric and total suctions for Whatman 42 filter paper, the same batch as those used in this study. Hence, the calibration curve by He (1999) is used in this study.

Since the filter paper was placed in the desiccator to equilibrate with the vapour pressure, the water content of the filter paper corresponds to total suction. Thus, the calibration curve for total suction is used. The total suction is calculated using the following equations (He, 1999):

$$\begin{aligned} \log \psi &= 8.778 - 0.222w_f & \text{for } w_f \geq 26\% \\ \log \psi &= 5.31 - 0.301w_f & \text{for } w_f < 26\% \end{aligned} \quad (7)$$

where w_f is the water content of the filter paper.

The targeted suctions in each desiccator and the measured suctions using the filter paper method are listed in Table 3. The maximum deviations from the targeted suctions is less than 13%. The measured suctions were used in the SWCC plots.

The gravimetric water content and degree of saturation at each matric suction were obtained from the PP and SS tests. The soil–water characteristic curve was then established by plotting the volumetric water content or the degree of saturation versus matric suction.

7. Results, Analyses and Discussion

7.1. EFFECT OF DEPTH OF WEATHERING ON SWCC

Two major factors that play an important role in the development of residual soils are parent rock and degree of weathering. Soils nearer the ground surface are more weathered compared with those from deeper depths. Therefore, the characteristics of two soils from one borehole may be different if they are from different depths. Soils near the ground surface are expected to have less water retention capacity as they are commonly looser than those from deeper layers, regardless of their parent rock type.

Figures 4 and 5 show SWCCs for residual soils from the Jurong sedimentary and the Bukit Timah granitic formations, respectively. SWCCs for soils at different depths from the same borehole are plotted together and compared. The lines on the plots represent the fitted Fredlund and Xing SWCC equations. The plots indicate that no significant trends can be drawn from the relationship between the shape of

Table 3. Targeted and measured suctions in SS tests

Target suction (kPa)	Measured suction (kPa)
3000	3375
5000	5586
8000	7604
10000	9696
20000	17447

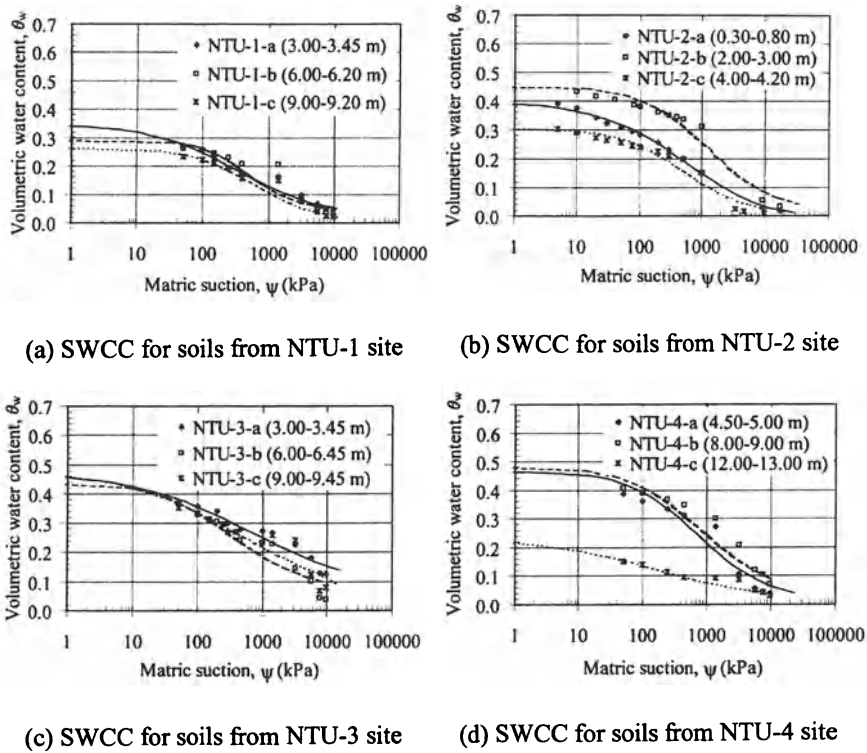


Figure 4. Soil–water characteristic curves for Jurong sedimentary residual soils.

SWCCs and the depth of weathering for soils from both Jurong sedimentary and Bukit Timah granitic formations. It is perhaps more surprising that no discernible trend for the SWCCs of the Bukit Timah granitic residual soils considering that the parent rock is only of one type, granite. This illustrates the complex engineering behaviour of residual soils.

7.2. ENVELOPE FOR SWCC OF SINGAPORE RESIDUAL SOILS

The SWCCs of Singapore residual soils are plotted in terms of normalised volumetric water content, Θ ($= \theta_w / \theta_s$), versus matric suction, ψ , for the Jurong sedimentary formation and the Bukit Timah granitic formation residual soils in Figures 6 and 7, respectively. The upper and lower bounds are drawn on the plots. An average SWCC for each formation is also obtained. It can be seen that the envelope of the SWCCs for Bukit Timah granitic formation residual soils is wider than the envelope of the SWCCs for Jurong sedimentary formation residual soils. Since the shape of SWCC is related to pore size, the Bukit Timah granitic formation residual soils seem to have a wider range of pore size distributions compared with the Jurong sedimentary formation residual soils. By applying the following capillary law to the SWCC

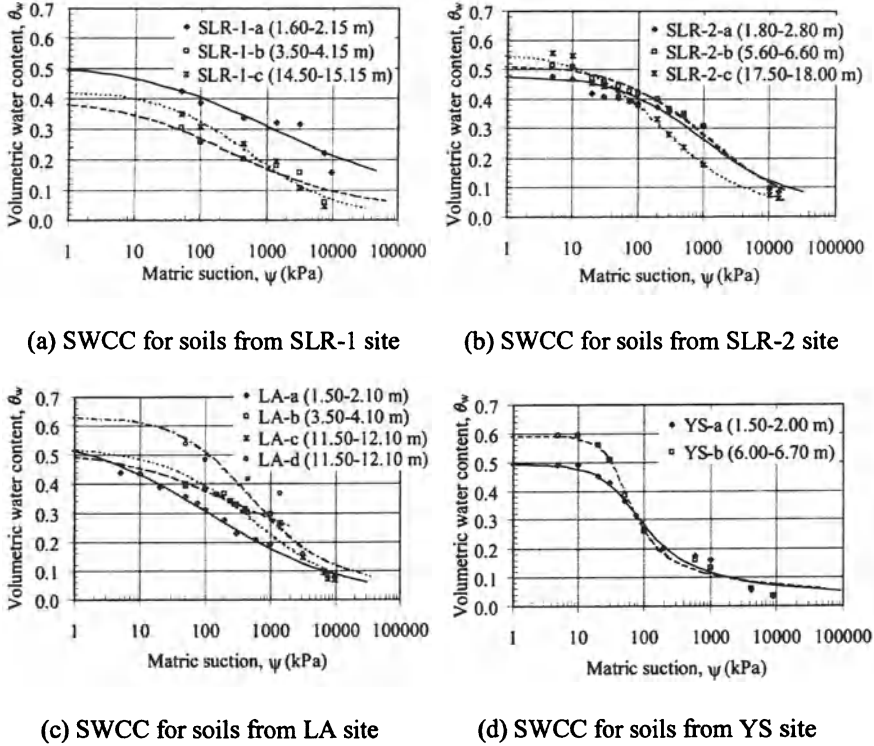


Figure 5. Soil–water characteristic curves for Bukit Timah granitic residual soils.

envelopes, the pore-size distribution curves are generated (Figures 8 and 9):

$$D_p = \frac{4T_s}{\psi} \quad (8)$$

where D_p is the pore diameter of the soil, T_s is the surface tension of water (72.75 mN/m at 20°C).

The cumulative pore volume, V_p , in Figures 8 and 9 is calculated as follows:

$$V_p = \frac{\theta_w}{n_s} \quad (9)$$

where n_s is the porosity of soil.

Figures 8 and 9 depict clear evidence that the pore size distributions of the Bukit Timah granitic residual soils are wider ranging compared with those for the Jurong sedimentary formation residual soils.

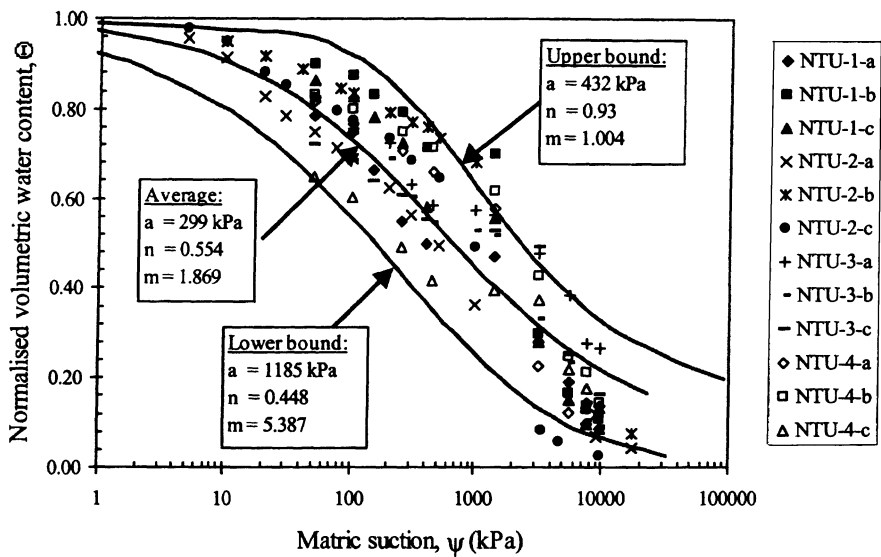


Figure 6. Soil-water characteristic curves envelope for Jurong sedimentary formation residual soils.

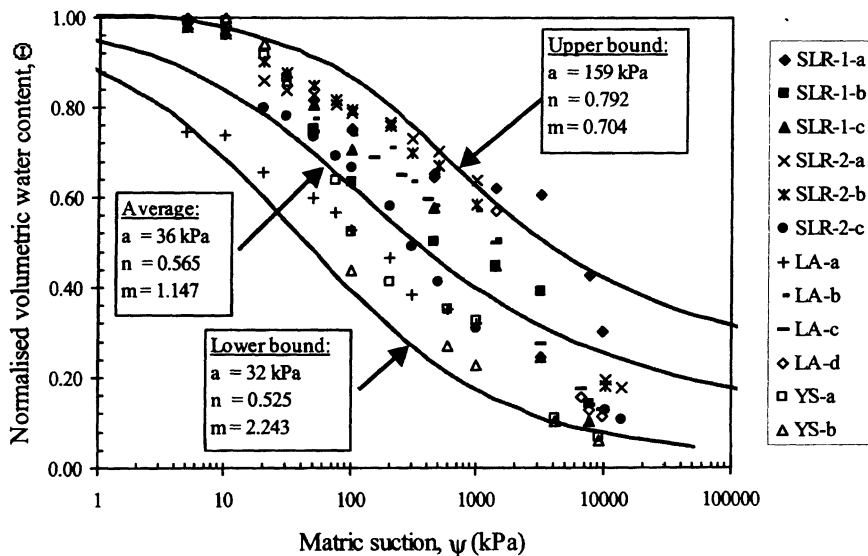


Figure 7. Soil-water characteristic curves envelope for Bukit Timah granitic residual soils.

7.3. RELATIONSHIP BETWEEN SWCC AND BASIC SOIL PROPERTIES

There have been a number of attempts to correlate SWCC with basic soil properties. Most of the correlations that have been established so far are with grain size dis-

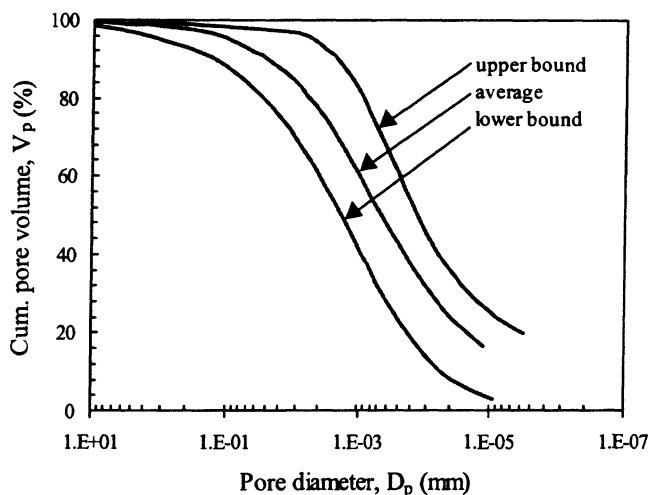


Figure 8. Pore-size distribution envelope for Jurong sedimentary formation residual soils.

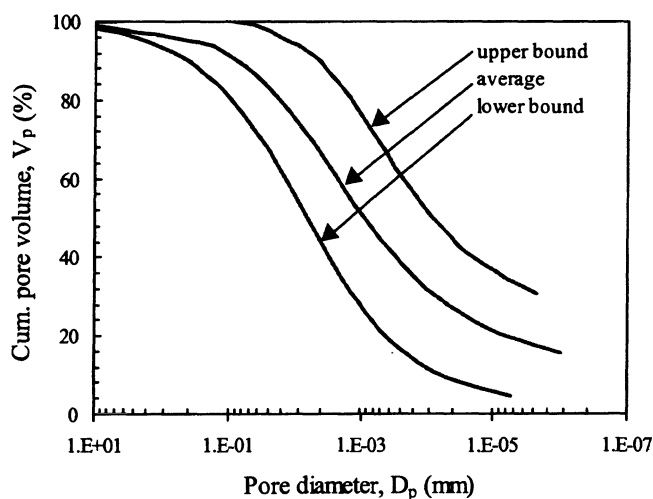


Figure 9. Pore-size distribution envelope for Bukit Timah granitic residual soils.

tribution curves (e.g. Arya and Paris, 1981; Ahuja *et al.*, 1985; Saxton *et al.*, 1986; Fredlund *et al.*, 1997 and Arya *et al.*, 1999). Among the methods for indirect determination of the SWCC, the Saxton *et al.* (1986) method is simplest and gives good agreement with experimental data used in its derivation. Saxton *et al.* (1986) established a relationship between SWCC and soil textures using a multivariate regression approach for a large database (2541 soils). The parameters in Brooks and Corey's SWCC equation were correlated with clay and sand contents based on United States Department of Agriculture (USDA) classification system. It was suggested that the

SWCC be divided into three suction ranges. In each suction range, one equation is valid where the coefficients of each equation are obtained from soil textures using best-fit equations. Details of the method can be found in Saxton *et al.* (1986). Briefly, the equations are:

$$\theta_w = \theta_s \quad \text{for } \psi \leq \psi_b \quad (10a)$$

$$\theta_w = \frac{(10 - \psi)(\theta_s - \theta_{w(10)}) + \theta_{w(10)}(10 - \psi_b)}{(10 - \psi_b)} \quad \text{for } \psi_b < \psi < 10 \text{ kPa} \quad (10b)$$

$$\theta_w = \left(\frac{\psi}{A'} \right)^{1/B'} \quad \text{for } \psi \geq 10 \text{ kPa} \quad (10c)$$

where $\theta_{w(10)}$ is volumetric water content at ψ of 10 kPa, A' (kPa) and B' are constants obtained from grain size distribution through statistical analyses.

The results presented by Saxton *et al.* showed good agreement with the experimental data. However, it should be noted that the method might not work for soils that are not within the database due to the influence of some other parameters that were not taken into account in the analyses. For instance, in the case of fine-grained soils, SWCC may not only be related to grain-size distribution parameters but it is probably also related to their mineralogy and density.

7.3.1. Single and multivariate statistical analyses

A slightly different approach is adopted in this study. The Fredlund and Xing SWCC equation is used to describe the SWCCs of the residual soils. Parameters a , n and m in the Fredlund and Xing SWCC equation are obtained through curve fitting the experimental SWCC data. Fredlund (1997) suggested that parameters a , n and m in the SWCC equation can be related to the grain size distribution. Parameter a is thought to be related to the large particle sizes in the grain size distribution, parameter n is related to the coefficient of uniformity, C_u , of the soil while parameter m is believed to be related to the residual particle sizes.

A statistical analysis was performed to assess the correlation between parameters a , n , and m and basic soil properties. For parameter a , the natural logarithm value (i.e. $\ln a$) is used in the analysis as a can vary over several orders of magnitude. However, the main concern regarding basic soil parameters that should be considered in empirical approaches to predicting of the SWCC remains a challenge. Arya *et al.* (1999) noted that the most popular basic soil parameters to be used were texture or grain size distribution, mineralogy, density and organic content. In this study, nine basic soil parameters representing texture and grain size distribution, mineralogy, and density have been chosen. Organic content is not taken into consideration since local residual soils are classified as inorganic soils (Public Works Department, 1976). The nine basic soil parameters used in this study are D_{10} , D_{30} , D_{60} , coefficient of uniformity (C_u), coefficient of curvature (C_c) representing

texture or grain size distribution, liquid limit (LL), plastic limit (PL), activity (A) representing mineralogy, and dry density (γ_{dry}).

The assessment was carried out by evaluating the coefficient of correlation, r , defined by the following formula:

$$r = \frac{\sum_{i=1}^n (X_i - \bar{X})(Y_i - \bar{Y})}{\sqrt{\sum_{i=1}^n (X_i - \bar{X})^2 \sum_{i=1}^n (Y_i - \bar{Y})^2}} \quad (11)$$

where X and Y are independent random variables.

X is the basic soil parameter whereas Y denotes the parameter in the Fredlund and Xing SWCC equation. The value of r ranges between -1 and 1 . The greater the absolute value of r , the stronger will be the correlation between the two parameters.

A matrix of correlation between parameters a , n and m with the nine basic soil parameters is shown in Table 4. The results indicate that parameter a and n are strongly correlated to C_u whereas m is strongly correlated to γ_{dry} . However, the r -values determined for a , n and m , are low. This may be attributed to the fact that the use of a single parameter to predict the SWCC for the Singapore residual soils is insufficient.

A multivariate analysis was also conducted to study the possibility of relating parameters a , n and m with more than one basic soil parameters. Multivariate coefficients for a , n and m are generated using the following equations:

$$\ln a = C_{0(a)} + C_{1(a)}X_1 + C_{2(a)}X_2 + \cdots + C_{k(a)}X_k \quad (12)$$

$$n = C_{0(n)} + C_{1(n)}X_1 + C_{2(n)}X_2 + \cdots + C_{k(n)}X_k \quad (13)$$

$$m = C_{0(m)} + C_{1(m)}X_1 + C_{2(m)}X_2 + \cdots + C_{k(m)}X_k \quad (14)$$

where $C_{0(a)}$, $C_{1(a)}$, \dots , $C_{k(a)}$, $C_{0(n)}$, $C_{1(n)}$, \dots , $C_{k(n)}$, $C_{0(m)}$, $C_{1(m)}$, \dots , $C_{k(m)}$ are coefficients determined via regression analysis and k is the number of descriptors (i.e. basic soil parameters used).

Table 4. Coefficient of correlation between parameters a , n and m and basic soil parameters

	D_{10}	D_{30}	D_{60}	C_u	C_c	LL	PL	A	γ_{dry}
$\ln a$	-0.010	-0.055	-0.146	-0.308	-0.046	0.068	-0.137	-0.139	0.250
n	-0.241	-0.229	-0.283	-0.298	0.157	-0.016	0.232	-0.110	-0.227
m	-0.224	-0.005	-0.090	-0.020	-0.107	-0.272	-0.222	-0.071	0.260

The regression analysis was performed by minimising the sum of square of normalised error (SSE_{norm}) as computed by:

$$SSE_{\text{norm}} = \sum_{i=1}^{\ell} \left(\frac{Y_i - Y_{i(\text{est})}}{Y_i} \right)^2 \quad (15)$$

where $Y_{i(\text{est})}$ is the estimated value of Y_i and ℓ is the number of data.

It should be noted that there might be correlation among the basic soil parameters used in the multivariate analysis. The use of more basic soil parameters in the development of empirical relationships for a , n and m , becomes ineffective when two or more basic soil parameters used are strongly related each other. Table 5 shows the correlation matrix between basic soil parameters used in the study. Six combinations of four basic soil parameters can be accordingly extracted from nine basic soil parameters used in the analysis. The resulting coefficients of correlation for a , n and m determined from multivariate analyses using nine and four descriptors are listed in Table 6. Among the six four-descriptor combinations, the first combination, of D_{60} , LL, A and γ_{dry} as descriptors of the empirical equation, gives the highest average r -value. It is also shown in Table 6 that r -value for a , n and m decrease by approximately 10%, 2% and 8% as the number of descriptors is reduced from nine to four, respectively.

Table 5. Coefficient of correlation between basic soil parameters used in the study

	D_{10}	D_{30}	D_{60}	C_u	C_c	LL	PL	A	γ_{dry}
D_{10}	1	0.701	0.657	−0.082	0.337	0.214	0.071	0.475	−0.039
D_{30}		1	0.927	0.024	0.673	0.038	−0.012	0.119	0.150
D_{60}			1	0.315	0.498	0.119	0.110	0.120	0.039
C_u				1	−0.102	−0.044	0.137	−0.048	−0.220
C_c					1	−0.149	−0.031	−0.064	0.120
LL						1	0.856	0.046	−0.761
PL							1	0.028	−0.884
A								1	0.014
γ_{dry}									1

Table 6. Coefficient of correlation determined from multivariate analysis

No.	Parameters Used	$\ln a$	n	m	Average
1	D_{60} , LL, A, γ_{dry}	0.633	0.756	0.767	0.719
2	D_{60} , PL, A, γ_{dry}	0.555	0.755	0.766	0.692
3	C_u , C_c , LL, A	0.468	0.753	0.770	0.664
4	C_u , C_c , PL, A	0.506	0.753	0.777	0.679
5	C_c , LL, A, γ_{dry}	0.627	0.743	0.773	0.714
6	C_c , PL, A, γ_{dry}	0.540	0.745	0.779	0.688
7	All parameters	0.702	0.773	0.830	0.768

Table 7. Regression coefficients for parameters a , n and m

(a) Using nine descriptors									
Coefficients	C_0	C_1	C_2	C_3	C_4	C_5	C_6	C_7	C_9
	constant	$D_{10}/0.002^*$	$D_{30}/0.002^*$	$D_{60}/0.002^*$	C_u	C_c	LL	PL	A
$\ln(a/P_{\text{atm}})^{**}$	-7.5880	0.2837	-0.0207	0.0005	0.0002	0.3666	0.0562	-0.0383	-0.0356
n	1.5043	0.008	-0.0061	0.0005	-0.0003	0.0604	0.0014	-0.0135	-0.0053
m	-0.7104	0.1634	0.0268	-0.0029	0.0012	-0.0745	0.0065	0.0100	0.0049
									$\gamma_{\text{dry}}/\gamma_w$
									4.0668
									-0.0343
									0.6500
(b) Using four descriptors									
Coefficients	C_0	C_1	C_2	C_3	C_4	C_5	C_6	C_7	C_9
	constant	$D_{10}/0.002^*$	$D_{30}/0.002^*$	$D_{60}/0.002^*$	C_u	C_c	LL	PL	A
$\ln(a/P_{\text{atm}})^{**}$	-6.5955	—	—	-0.0002	—	—	0.0341	—	-0.0040
n	0.6542	—	—	0.0000	—	—	-0.0003	—	-0.0021
m	0.4231	—	—	0.0004	—	—	0.0031	—	0.0071
									0.2868

*Clay size according to USCS.
** P_{atm} is atmospheric pressure (101.3 kPa).

7.3.2. Regression coefficients

The regression coefficients obtained via the regression analyses are listed in Table 7. The regression coefficients are normalised such that the resulting formulae become dimensionless. The parameters D_{10} , D_{30} and D_{60} are normalised by clay size (i.e. 0.002 mm according to USCS), whereas γ_{dry} is normalised by density of water, γ_w . The parameter a , which has unit kPa, is normalised by atmospheric pressure (i.e. 101.3 kPa). Since there are no units for C_u , C_c , LL, PL and A, normalisation was not required.

7.4. EVALUATION OF EQUATIONS FOR DETERMINING SWCC FROM BASIC SOIL PROPERTIES

The validity of estimating the SWCC for Singapore residual soils using the proposed method is evaluated using five independent data sets found in the literature. Three residual soils denoted as soil A, soil B, and soil C, from the Jurong sedimentary formation, were reported by Teong and Kong (1994), Lim (1995) and Raj and Tan (1996), respectively. The other two residual soils denoted as soil D and soil E from the Bukit Timah granitic formation, were reported by Aung *et al.* (2000).

Soils A and D are classified as silty soil (USCS: MH) whereas soils B, C and E are classified as sandy soils (USCS: SM). Index properties of soil A, soil B, soil C, soil D and soil E and the resulting a , n and m values computed from the empirical equations are listed in Tables 8 and 9, respectively.

Table 8. Index properties of residual soils used for verification

Properties	Soil A	Soil B	Soil C	Soil D	Soil E
Reference	Teong and Kong (1994)	Lim (1995)	Raj and Tan (1996)	Aung <i>et al.</i> (2000)	Aung <i>et al.</i> (2000)
Saturated unit weight (kN/m ³)	20.1	20	20.5	19.0	22.0
Specific gravity	2.61	2.68	2.65	2.70	2.70
Liquid limit	65	45	31	60	35
Plastic limit	35	25	18	32	30
Plasticity index	30	20	13	28	5
USCS:					
Clay (%)	42	5	6	10	7
Silt (%)	28	15	24	52	15
Sand (%)	30	80	70	38	78
USDA:					
Clay (%)	42	5	6	10	7
Silt (%)	25	13	19	50	11
Sand (%)	33	82	75	40	82
D_{10} (mm)	0.0005	0.015	0.01	0.002	0.006
D_{30} (mm)	0.0009	0.17	0.075	0.01	0.21
D_{60} (mm)	0.009	0.3	0.35	0.05	0.77
Porosity, n_s	0.51	0.34	0.37	0.64	0.43
USCS	MH	SM	SM	MH	SM

Table 9. Parameters a , n and m of residual soils used for verification

(a) Using nine basic soil parameters

Parameter	Soil A	Soil B	Soil C	Soil D	Soil E
a	194 kPa	2374 kPa	259 kPa	529 kPa	1206 kPa
n	0.604	0.632	0.731	0.591	0.659
m	1.039	3.510	1.918	1.250	2.561

(b) Using four basic soil parameters

Parameter	Soil A	Soil B	Soil C	Soil D	Soil E
a	233 kPa	209 kPa	101 kPa	403 kPa	199 kPa
n	0.622	0.608	0.614	0.616	0.599
m	1.043	1.107	1.039	1.107	1.164

Table 10. Saxton *et al.* parameters of residual soils used for verification

Parameter	Soil A	Soil B	Soil C	Soil D	Soil E
A' (kPa)	0.0051	0.0077	0.0121	0.1391	0.0037
B'	-8.6496	-4.3668	-4.3958	-3.9194	-4.8886
$\theta_{w(10)}$	0.4160	0.1935	0.2172	0.3360	0.1990
θ_s	0.5152	0.3617	0.3769	0.4306	0.3804
ψ_b (kPa)	6.8	1.5	2.1	3.88	2.17

Figures 10–14 show the SWCCs for soils A to E as predicted from the empirical equations. The experimental data are represented by markers while the solid and dashed lines represent the predicted SWCCs from basic soil parameters using 9 descriptors and 4 descriptors, respectively. The bestfit curve using Equation (5) is also shown, as a thick solid line, together with the SWCC envelopes obtained earlier.

The results indicate that the proposed equations give a reasonably good estimate of the SWCC for Singapore residual soils. It is also shown that the use of four descriptors in predicting the SWCCs tends to give higher values of θ_w at high matric suctions compared with those predicted using nine descriptors, except in the case of soil A. However, the proposed equations using four and nine basic soil properties as descriptors tend to give close results for low matric suction values (i.e. less than 100 kPa). It is not possible to determine if the nine-descriptor or four-descriptor equations, gives better fit to the experimental data as data is not available in the very high suction range. However, the shape of the SWCC predicted using the nine-descriptor equations tend to be closer in trend to the experimental data.

For comparison, the predicted SWCC using Saxton *et al.* (1986) equations are also shown on the plots as dashed lines. The plots show that the predictions using Saxton *et al.* equations are not applicable for the Singapore residual soils. It may be due to

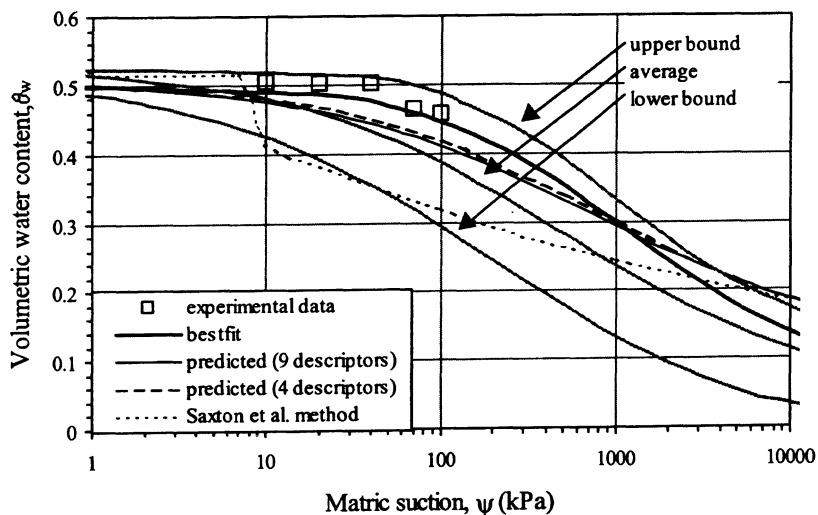


Figure 10. Soil–water characteristic curves for soil A.

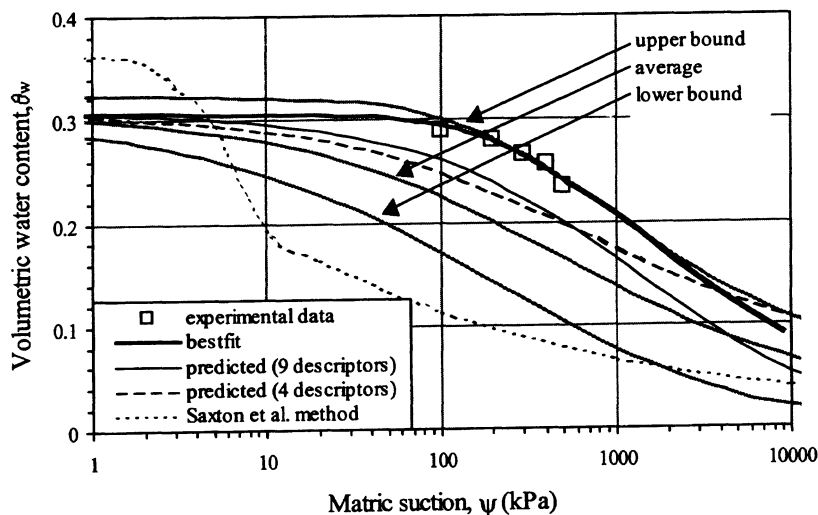


Figure 11. Soil–water characteristic curves for soil B.

the assumptions adopted by Saxton *et al.* (1986). In the Saxton *et al.* method, the air entry value of the soils, ψ_b , is assumed to be less than 10 kPa. The other assumption is that the SWCC follows linear and power equations for matric suctions ranging from ψ_b to 10 kPa and for matric suctions greater than 10 kPa, respectively. However, for Singapore residual soils where ψ_b is likely to be much greater than 10 kPa, the Saxton *et al.* method underpredicts θ_w significantly in the high suction range.

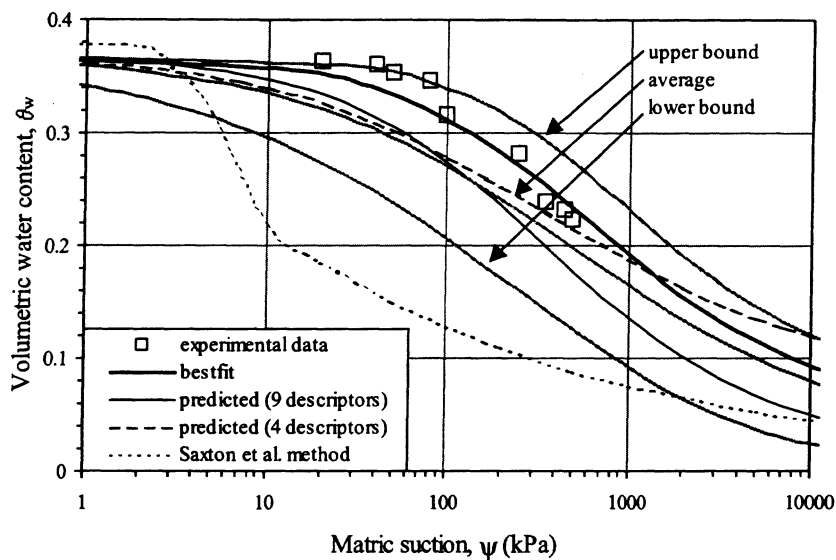


Figure 12. Soil–water characteristic curves for soil C.

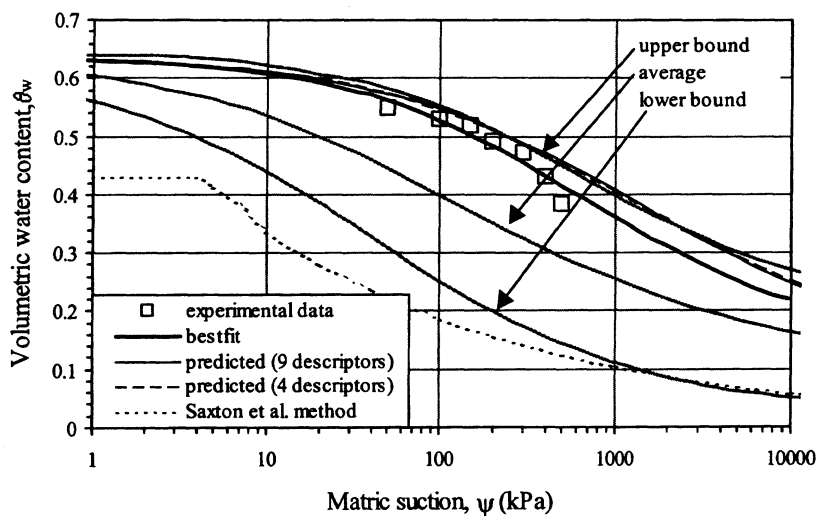


Figure 13. Soil–water characteristic curves for soil D.

The proposed method is promising even with the limited database. With an expanded database, better correlation coefficients can be obtained. Nevertheless, the proposed empirical equations can be utilised to provide a quick preliminary estimate of the soil–water characteristic curve for Singapore residual soils.

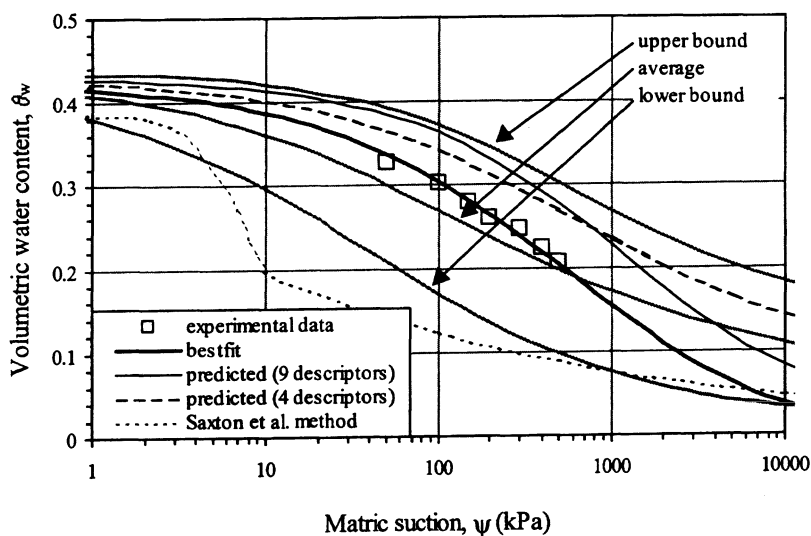


Figure 14. Soil–water characteristic curves for soil E.

8. Conclusions

Soil–water characteristic curves (SWCCs) of Singapore residual soils have been presented in this paper. For both Jurong sedimentary and Bukit Timah granitic formation residual soils, the depth of weathering does not seem to have a consistent effect on the SWCCs. It is more likely that the parent rock type has a more significant influence on the SWCCs. From the SWCC envelopes of the residual soils, the residual soils from Bukit Timah granitic formation seem to have a wider range of pore size distribution compared with those from the Jurong sedimentary formation.

Multivariate empirical equations using nine and four basic soil parameters have been proposed to estimate the SWCCs of Singapore residual soils. Both sets of equations were tested with five independent sets of data and found to provide a good estimate of SWCCs for the Singapore residual soils.

Acknowledgements

This research is funded by grants from National Science and Technology Board, grant no. NSTB 17/6/16, and the Ministry of Education, grant no. ARC 12/96. The first author acknowledges the research scholarship provided by Nanyang Technological University.

References

- Ahuja, L. R., Naney, J. W. and Williams, R. D. (1985) Estimating soil–water characteristics from simpler properties or limited data, *Soil Science Society of America Journal* **49**, 1100–1130.
- Aitchinson, G. D. (1965) Engineering concepts of moisture equilibria and moisture changes in soils, In *Moisture Equilibria and Moisture Changes in Soils Beneath Covered Areas*, Statement of Review Panel, Butterworths, Australia. pp. 7–21.
- Arya, L. M. and Paris, J. F. (1981) A psychoempirical model to predict soil moisture characteristics from particle-size distribution and bulk density data. *Soil Science Society of America Journal* **45**, 1023–1030.
- Arya, L. M., Leij, F. J., van Genuchten, M. T. and Shouse, P. (1999) Scaling parameter to predict the soil water characteristic from particle-size distribution data. *Soil Science Society of America Journal* **63**, 510–519.
- Aung, K. K., Rahardjo, H., Toll, D. G. and Leong, E. C. (2000) Mineralogy and microfabric of unsaturated residual soils. In *Proceeding of the Asian Conference on Unsaturated Soils. Unsat-ASIA 2000*, Singapore, Balkema, Rotterdam, pp. 317–321.
- ASTM (1998) Soil and rock: dimension stone, geosynthetics. *Annual Book of Standards*, 04.08. Philadelphia.
- Brenner, R. P. and Phillipson, H. B. (1979) Sampling of residual soils in Hong Kong, State of the Art on Current Practice of Soil Sampling. In *Proceeding of the International Symposium of Soil Sampling*, Singapore, **1**, 109–120.
- Brooks, R. H. and Corey, A. T. (1964) *Hydraulic Properties of Porous Medium*, *Hydrology Papers*, Fort Collins, Colorado.
- Fredlund, D. G. (1997) From theory to the practice of unsaturated soil mechanics. Keynote speech, In *Proceedings of 3rd Brazilian Symposium on Unsaturated Soils NSAT'97*, Brazil.
- Fredlund, M. D., Fredlund, D. G. and Wilson, G. W. (1997) Prediction of the soil–water characteristic curve from grain size distribution and volume-mass properties, In *Proceedings of 3rd Brazilian Symposium on Unsaturated Soils NSAT'97*, Brazil.
- Fredlund, D. G. and Rahardjo, H. (1993) *Soil Mechanics for Unsaturated Soils*, John Wiley & Sons, Canada.
- Fredlund, D. G. and Xing, A. (1994) Equation for the soil–water characteristic curve, *Canadian Geotechnical Journal* **31**, 521–532.
- He, L. C. (1999) *Evaluation of Instrument for Measurement of Suction in Unsaturated Soils*, MEng Thesis, School of Civil and Structural Engineering, Nanyang Technological University, Singapore.
- Lang, A. R. G (1967) Osmotic coefficient and water potentials of sodium chloride solutions from 0°C to 40°C, *Australian Journal of Chemistry* **20**, 2017–2023.
- Leong, E. C. and Rahardjo, H. (1997) Review of soil–water characteristic curve equations, *Journal of Geotechnical and Geoenvironmental Engineering* **123**(12), 1106–1117.
- Lim, T. T. (1995) *Shear Strength Characteristics and Rainfall-induced Matric Suction Changes in a Residual Soil Slope*, MEng Thesis, School of Civil and Structural Engineering, Nanyang Technological University, Singapore.
- Mazier, G. (1974) Méthodes de prélèvement des sols meubles. *Annales de l'Institut Technique du Bâtiment et des Travaux Publics* **319**, 75–85.
- Poh, K. B., Chuah, H. L. and Tan, S. B. (1985) Residual granite of Singapore, In *Proceedings of 8th Southeast Asian Geotechnical Conference*. Kuala Lumpur, pp. 3-1–3-9.
- Public Works Department of Singapore (1976) *The geology of the Republic of Singapore*.
- Raj, K. N. and Tan, H. G. (1996) *Permeability Functions of Unsaturated Soils*, Final Year Project Report, School of Civil and Structural Engineering, Nanyang Technological University, Singapore.

- Saxton, K. E., Rawls, W. J., Romberger, J. S. and Papendick, R. I. (1986) Estimating generalized soil–water characteristics from texture, *Soil Science Society of America Journal* **50**(4), 1031–1036.
- Tan, S. B., Tan, S. L., Lim, T. L. and Yang, K. S. (1987) Landslide problems and their control in Singapore, In *Proceedings of 9th Southeast Asian Geotechnical Conference*. Bangkok, pp. 1-25–1-36.
- Teong, L. T. and Kong, M. T. (1994) *A Study of Permeability of Typical Residual Soils in Singapore*, Final Year Project report, School of Civil and Structural Engineering, Nanyang Technological University, Singapore.
- Van Genuchten, M.T. (1980) A closed-form equation for predicting the hydraulic conductivity of unsaturated soils. *Soil Science Society of America Journal* **44**, 892–898.
- Vanapalli, S. K. (1994) *Simple Test Procedures and Their Interpretation in Evaluating the Shear Strength of Unsaturated Soils*. Ph.D. thesis, University of Saskatchewan, Saskatoon.
- Vanapalli, S. K., Fredlund, D. G., Pufahl, D. E. and Clifton, A. W. (1996) Model for the prediction of shear strength with respect to soil suction. *Canadian Geotechnical Journal* **33**, 379–392.



Temperature effects on the hydraulic behaviour of an unsaturated clay

E. ROMERO,* A. GENS and A. LLORET

Geotechnical Engineering Laboratory, Department of Geotechnical Engineering and Geosciences, Technical University of Catalonia, Barcelona, Spain

(Received 23 August 2000; revised and accepted 29 May 2001)

Abstract. The influence of temperature on the hydraulic properties of unsaturated clays is of major concern in the design of engineered barriers in underground repositories for high-level radioactive waste disposal. This paper presents an experimental study centred on the investigation of the influence of temperature on soil hydraulic properties related to water retention and permeability. Laboratory tests were conducted on artificially prepared unsaturated fabrics obtained from a natural kaolinitic-illitic clay. Special attention is given to the testing procedures involving controlled suction and temperature oedometer cells and the application of the vapour equilibrium technique at high temperatures. Retention curves at different temperatures show that total suction tends to reduce with increasing temperatures at constant water content. Temperature influence on water permeability is more relevant at low matric suctions corresponding to bulk water preponderance (inter-aggregate zone). Below a degree of saturation of 75% no clear effect is detected. Experimental data show that temperature dependence on permeability at constant degree of saturation and constant void ratio is smaller than what could be expected from the thermal change in water viscosity. This behaviour suggests that phenomena such as porosity redistribution and thermo-chemical interactions, which alter clay fabric and pore fluid, can be relevant.

Key words: permeability, retention curve, suction, temperature, unsaturated clay

1. Introduction

The range of geotechnical engineering applications is becoming increasingly wider in recent years, mainly in the geoenvironmental area. The need to successfully tackle these new geoenvironmental problems requires the extension of current understanding of soil behaviour with the description of new phenomena and the incorporation of relevant stress and environmental state variables. Two of such variables, suction (as a stress state variable) and temperature (as an environmental state variable), are discussed in this paper regarding their effects on hydraulic features, namely the water retention capacity and the water permeability of an unsaturated clay.

The influence of temperature on the hydraulic properties of clays is of major concern in the design of engineered barriers in underground repositories for high-level radioactive waste disposal (Gens *et al.*, 1998; Kanno *et al.*, 1999). These

* Corresponding author. Campus Nord, Jordi Girona 1–3, Building D-2, 08034 Barcelona, Spain. Fax: +34-93 401725 1; E-mail: enrique.romero-morales@upc.es

initially unsaturated barriers experience a transient wetting phase governed by the rate of absorption of natural water from the host geological medium and a transient temperature regime controlled by the decaying heat power input induced by the waste.

The distribution and transfer of humidity and their consequences on the mechanical behaviour of pavement–base–subgrade systems represent another example where seasonal and daily cyclic changes of temperature and suction regimes play an important role (Alonso, 1998).

There are a number of laboratory results concerning thermal effects on saturated water permeability (Towhata *et al.*, 1993; Khemissa, 1998; Cho *et al.*, 1999; Delage *et al.*, 2000), but on the contrary, experimental information concerning unsaturated states is very limited and restricted to sandy and silty soils (Hopmans and Dane, 1986). In addition, results related to temperature effects on water retention curves have been usually limited to low suctions or low temperatures (Nimmo and Miller, 1986; Constantz, 1991; Wan, 1996; She and Sleep, 1998). To gain insight into these aspects of behaviour, a systematic research program has been carried out on artificially prepared clayey samples to investigate changes in hydraulic properties induced by heating. In this study, maximum temperature is limited to 80°C so that no appreciable phase change can occur.

These new applications, related mainly to the effects of partial saturation and the consequences of temperature changes, require new experimental equipment and the adaptation of conventional controlled suction techniques. Two well-posed techniques have been used in the experimental program: vapour equilibrium and axis translation techniques. Special attention is also given in the paper to the development of a new oedometer cell and testing procedures consisting of axis translation application with simultaneous control of temperature. Experimental aspects and problems concerning the use of the vapour equilibrium technique at high temperatures are also described.

The paper presents water retention results of gravimetric water content – temperature relationships at constant suction, and retention curves at constant void ratios under different temperatures. Water permeability and relative water permeability dependence on degree of saturation, void ratio and temperature obtained from inflow/outflow test data are also presented. Finally, a phenomenological interpretation of temperature and suction effects on hydraulic properties is described.

2. Material, testing procedures and equipment

2.1. ARTIFICIALLY PREPARED MATERIAL

Laboratory tests were conducted on an artificially prepared powder (statically compacted on the dry side of optimum water content) obtained from natural Boom clay (Mol, Belgium). This moderately swelling clay (20%–30% kaolinite, 20%–30%

illite and 10%–20% smectite) has a liquid limit of $w_L = 56\%$, a plastic limit of $w_P = 29\%$, a specific gravity of $G_s = 2.70$ and 50% of particles less than $2\ \mu\text{m}$.

Two types of procedures were followed to prepare samples at low and high water contents. Specimens used for the study of water retention at four different temperatures using vapour equilibrium control were prepared at low water content. In preparing these samples, powder was left in equilibrium with laboratory atmosphere at an average relative humidity of 47% (total suction $\psi \approx 100\ \text{MPa}$) to achieve a hygroscopic water content of $2.5 \pm 0.3\%$. Soil samples (15 mm in diameter and 12 mm high) were one-dimensionally compacted under constant water content at seven different initial dry unit weights ranging from 14.7 to 20.6 kN/m^3 .

Specimens for the study of water retention and permeability at two different temperatures using the axis translation technique were prepared at high water content. In these samples, the required quantity of demineralised water to achieve a predetermined water content of $15.0 \pm 0.3\%$ was added to the powder, previously cured at a relative humidity of 90%. After equalisation, an initial total suction of $\psi \approx 2.3\ \text{MPa}$ was attained at 22°C . Afterwards, a one-dimensional and isothermal static compaction was followed at two different temperatures (22 and 80°C) until a specified final volume was achieved under constant water content. The compaction was performed in a hermetic mould (constant mass system) surrounded by a thermostatically controlled heater. Further details of sample preparation techniques are described in Romero (1999). The experimental program was performed with two soil fabrics: a high-porosity fabric at a dry unit weight of $13.7\ \text{kN/m}^3$ with a collapsible structure upon wetting and a low-porosity fabric with a swelling tendency upon wetting at $16.7\ \text{kN/m}^3$.

The compacted samples display an aggregated fabric, as detected from freeze-dried samples observed using scanning electron microscopy (Romero, 1999). Experimental data are interpreted on the basis of the existence of two main pore size regions, as observed from the analysis of mercury intrusion/extrusion porosimetry results (Romero *et al.*, 1999). Firstly, an intra-aggregate porosity, containing quasi-immobile water, exists at water contents lower than 13–15% and pore sizes smaller than 150 nm. Secondly, an inter-aggregate and interconnected porosity containing bulk water occurs at water contents greater than 13–15%. Experimental results presented by Romero *et al.* (1999) show that intra-aggregate water represents 54–59% of the total volume of water in a low-porosity packing compacted at $16.7\ \text{kN/m}^3$, whereas it corresponds to a maximum of 38% for a packing compacted at $13.7\ \text{kN/m}^3$.

2.2. WATER RETENTION TESTS USING THE VAPOUR EQUILIBRIUM TECHNIQUE

2.2.1. General aspects of the vapour equilibrium technique at different temperatures

The vapour equilibrium technique is appropriate for prescribing high suction values by imposing a known total suction. This technique was used for the study of water retention at low water contents and at four different temperatures (22, 40, 60 and 80°C). It was

implemented by controlling the relative humidity of a constant mass system with respect to vapour. Soil water potential was applied by means of water molecule transfer through the vapour phase from the reference system to the soil pores. This technique is associated with the control of total suction, since the gaseous phase acts like a membrane that is permeable to water but not to dissolved salts.

Partially saturated solutions with varying solute quantities were used in order to achieve the predetermined relative humidity. Sodium chloride, a non-volatile solute at the applied temperature, was chosen to prepare the aqueous solutions. Since testing was carried out at four different temperatures (22, 40, 60, 80°C) the concentrations to achieve the desired suctions had to be calculated for different temperatures. The relationship between the relative vapour pressure or activity a_l of the NaCl aqueous solution and the molality of the solute m (mol of NaCl/kg of pure water), as a function of temperature T (°C), is given by the following empirical expression (Horvath, 1985; Romero, 1999):

$$a_l = 1 - 0.035m - m(m - 3)f(T) \quad (1)$$

$$f(T) = 1.977 \times 10^{-3} - 1.193 \times 10^{-5}T \quad \text{for } m \geq 3 \text{ mol/kg} \quad (2)$$

$$f(T) = 1.142 \times 10^{-3} \quad \text{for } m < 3 \text{ mol/kg} \quad (3)$$

The energy status or total suction that is imposed on the soil water can be related to the activity of the solution through the psychrometric law (Fredlund and Rahardjo, 1993). Figure 1 represents the total suction ψ as a function of the molality of the NaCl solution at different temperatures, according to Equations (1) to (3). Theoretical values reported by Lang (1967) obtained from osmotic coefficients at different concentrations and temperatures of the electrolyte solution are also indicated in Figure 1. A value of 3 MPa was selected as the total suction lower limit. This is due to the difficulty of controlling, with accuracy, high relative humidity values that require small quantities of solute. As indicated in Figure 1, the slope of the curve is steeper at low values, hindering total suction control. In addition, small variations of temperature of the order of $80.0 \pm 0.2^\circ\text{C}$ at constant vapour pressure, can induce total suction changes of around 3.0 ± 1.3 MPa due to temperature effects on saturated vapour pressure and the proximity to the dew point temperature. The total suction upper limit is controlled by the salt solubility ($m = 6.1$ mol/kg at 22°C) that restricts the relative humidity to a minimum of 0.75 at 22°C .

2.2.2. Water retention tests at low water contents

Water retention results were obtained from isothermal wetting paths performed with the vapour equilibrium technique at four different temperatures and under free swelling conditions with zero boundary stresses. Compacted soil samples, according to the initial conditions indicated in Section 2.1, were equilibrated in hermetic jars (partially filled with 4×10^5 mm³ of NaCl solution) at specified temperatures (22,

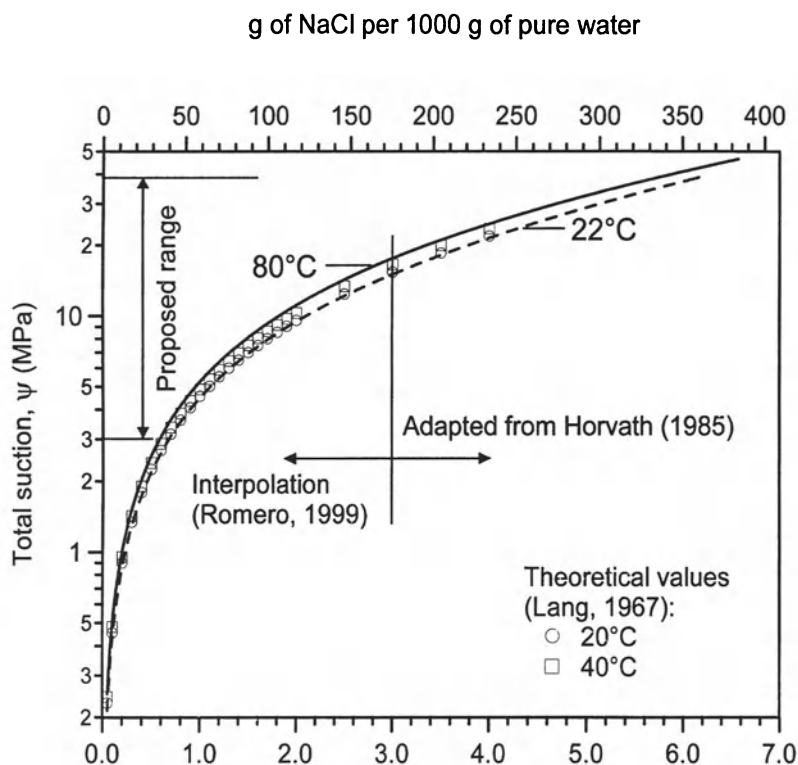


Figure 1. Total suction application using vapour equilibrium technique with partially saturated NaCl solutions at different temperatures

40, 60 and 80°C). Samples were allowed to equilibrate for a constant period of two weeks at different relative humidity values, corresponding to the following total suctions: 32, 10, 8, 6 and 3 MPa. At the end of each single-stage equilibrium test the different samples were carefully and quickly weighed (water content resolution of 0.02% associated with the moisture content loss during the weighing operation) and measured (volumetric resolution less than 0.2%). In addition, the water content of the specimens was determined. More details concerning the experimental procedure are described in Romero (1999).

2.3. WATER RETENTION AND WATER PERMEABILITY TESTS USING THE AXIS TRANSLATION TECHNIQUE

2.3.1. Controlled suction equipment with axis translation technique

The axis translation technique was used for the study of water retention and permeability at high water contents and at two contrasting temperatures of 22 and 80°C. This method is associated with the matric suction component

$s = (u_a - u_w)$, in which soil water potential is predominantly controlled by liquid phase transfer through an interface that is permeable to dissolved salts. The procedure involves the translation of the reference air pressure by an artificial increase of the atmospheric pressure in which the soil is immersed. The air overpressure methodology was applied in the experiments with a constant air pressure of $u_a = 0.5$ MPa. The water pressure u_w is translated into the positive range. However, a limitation of axis translation at high temperatures is that the system of air pressure regulation is open to vapour (non-constant mass), which induces soil water to evaporate.

Figure 2 shows the layout of the temperature and controlled suction system and a number of auxiliary devices necessary to perform the tests. A controlled suction oedometer cell surrounded by a thermostatically controlled heater (silicone oil bath and heater indicated by number 1 in Figure 2) was employed for the study of the soil in the low suction range ($s \leq 0.45$ MPa). Soil temperature was measured with thermocouples located close to the sample, used as feedback signals acting on a programmable thermostat. A water volume change indicator connected to the high air-entry value (HAEV) ceramic disc (number 3 in Figure 2) and maintained at a reference laboratory temperature was used to obtain the values of inflow and

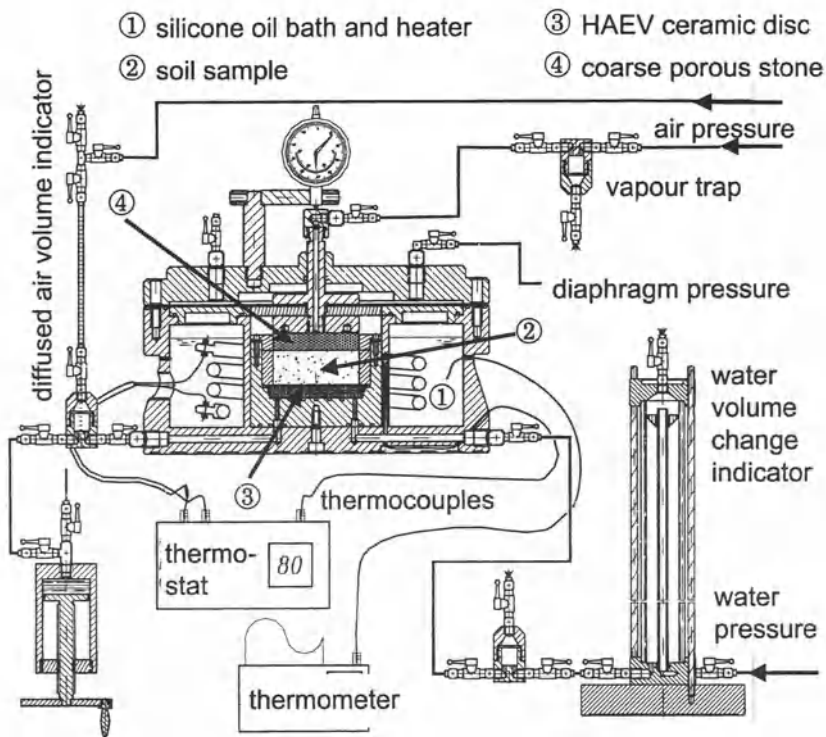


Figure 2. Experimental layout of the temperature and controlled suction system (Romero *et al.*, 1995)

outflow of water, as well as the water retention for each suction and temperature condition.

Once the hot sample was compacted as described in Section 2.1 and removed from the hermetic mould, it was quickly installed in the oedometer cell to minimise water content losses due to evaporation (number 2 in Figure 2). The different pieces of the oedometer cell were previously heated to the target temperature. Spurious expansions of the different elements were hence minimised while thermal equilibrium was reached. Transferring the specimen from the compaction mould to the cell induced a maximum temperature change of around -5°C and water content changes between -0.6 and -0.9% . The estimated initial total suction of the heated sample is between 2.6 and 3.0 MPa. Further experimental details are described in Romero (1999).

In order to accurately determine water volume changes it is necessary to account for water volume losses due to evaporation in the air pressure system (open system to vapour). Evaporative fluxes originate due to the difference in vapour pressure between soil voids and the air pressure system (coarse porous stone, number 4 in Figure 2). Volumetric evaporative fluxes are detected in the water volume change device under steady-state conditions. Evaporative fluxes reduce with increasing applied matric suction, with increasing relative humidity in the air pressure system and with lower soil porosity (Romero, 1999).

A series of 1-D coupled thermo-hydraulic analysis were carried out by Romero (1999) to simulate evaporative fluxes at 80°C . Measured volumetric evaporative fluxes are compared to the predictions of the simulation in Figure 3, in which different relative humidity values h_{rf} at the soil surface in contact with the coarse porous stone have been prescribed (95.0, 98.0, 99.0, 99.5 and 99.9%). A matric suction of $s = 0.20$ MPa was fixed at the bottom boundary of the soil in contact with the HAEV ceramic disc. An initial relative humidity of $h_{ro} = 95\%$ was imposed at the top boundary in contact with the coarse porous stone, which progressively tended to the different target values h_{rf} previously indicated. The objective of the simulation was to determine the feasibility of matric suction equalisation throughout the sample height of 10 mm at 80°C . Two different water fluxes are involved in the process. Firstly, an evaporative flux that tries to dry the clay, dependent on soil properties (mainly porosity and degree of saturation affecting vapour diffusivity) and top boundary conditions (relative humidity of the air above the evaporating surface). Secondly, a liquid water transfer through the HAEV ceramic disc that is dependent on soil and ceramic disc permeability. As observed in Figure 3, if volumetric evaporative fluxes measured at a reference temperature of 22°C are kept under a value of $1 \times 10^{-6} (\text{mm}^3/\text{s})/\text{mm}^2$, a relative humidity higher than 98.5% is ensured in the air pressure system. This relative humidity restricts water vapour transfer at high temperatures and permits the attainment of matric suction equalisation over the entire sample height. Under these conditions, maximum matric suction at the top boundary is expected to increase up to 0.22 MPa, as indicated in Figure 3. Therefore, a vapour trap was installed in the air pressure system to maintain a relative humidity higher than 98.5% (Figure 2).

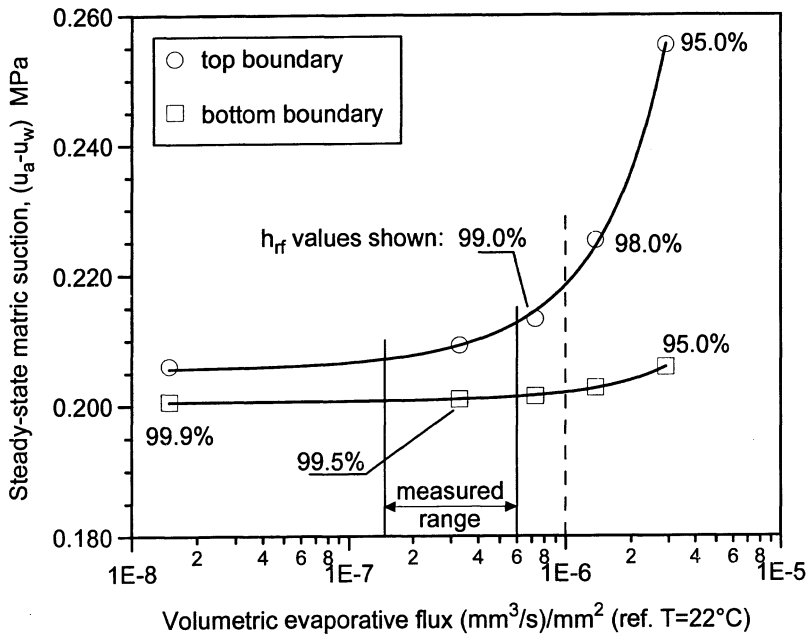


Figure 3. Matrix suctions reported by the thermo-hydraulic analysis for different relative humidity values in the air pressure system. Measured range of evaporative fluxes

It is also important to flush air bubbles periodically from below the HAEV ceramic disc. This accumulation can induce the progressive loss of continuity between the pore water and the water in the measuring system, especially at high temperatures and high-applied matrix suctions. An increase of the air diffusion coefficient through HAEV ceramic discs at high temperatures has been measured by Romero (1999): between 6×10^{-11} and 1×10^{-10} m²/s at 22°C and between 2×10^{-10} and 3×10^{-10} m²/s at 80°C. A diffused air volume indicator was therefore incorporated in the water pressure system to allow periodic flushings and measurements, as observed in Figure 2.

2.3.2. Water retention and water permeability tests at high water contents

Isothermal wetting and drying cycles were performed on both compacted fabrics at constant net vertical stresses (varying between 26 kPa and 1.2 MPa) or constant volume (isochoric) conditions. In this way, a wide void ratio range – from 0.60 to 0.95 – was covered. The same matrix suction steps were followed in the wetting and drying paths: 0.45, 0.20, 0.06 and 0.01 MPa. Water permeability was determined under transient conditions by analysing the inflow data (wetting paths) or outflow data (drying paths). On the other hand, water retention values were measured only in wetting paths after matrix suction equalisation under isochoric conditions.

The water permeability values were obtained from inflow and outflow data using the expressions that are presented below and the correction proposed by Kunze and Kirham (1962), which takes into account ceramic disc impedance. The inflow/outflow approach is an unsteady-state method based on the use of the pressure plate apparatus and initially developed by Gardner (1956) only for outflow. A step matric suction decrease/increase was applied to the soil and the transient inflow/outflow of water was carefully measured with time and interpreted with a simplified resolution of Richards's equation. Experimental methods for determining water permeability are described in Vicol (1990), Fredlund and Rahardjo (1993) and Jucá and Frydman (1996). The volume $Q(t)$ of intruded/extracted water at time t is given by the following expression (Kunze and Kirham, 1962):

$$\frac{Q(t)}{Q_o} = 1 - \sum_{n=1}^{\infty} \frac{2 \exp(-\alpha_n^2 D_w t / L^2)}{\alpha_n^2 (a + \csc^2 \alpha_n)} \quad (4)$$

where Q_o is the total volume of inflow/outflow for a water pressure increment/decrement, L the soil height, D_w the capillary diffusivity that is dependent on the water permeability, a the ratio of impedance of the ceramic disc to the impedance of the soil $a = k_w e / (L k_d)$ (e is the ceramic disc thickness and k_d its water permeability), and α_n , the n th solution of the equation $a \alpha_n = \cot \alpha_n$ (for $n = 1, 2, \dots$). Equation (4) is subject to a number of simplifications and assumptions: the soil matrix is rigid, the water flow is isothermal and one-dimensional, the fluid is homogeneous and incompressible and the flow of air in the porous medium is neglected or considered to be instantaneous. A non-linear, least-squares optimisation procedure was used according to Equation (4) to approximate test readings (time evolution of inflow/outflow data $Q(t)/Q_o$) to the predictions of the model, in order to obtain the D_w parameter. Test data were evaluated using inflow/outflow results that did not exceed 30% of the total change ($0.20 \leq Q(t)/Q_o \leq 0.30$). Under this short period, D_w and the soil volume are not constant, but their variation can be neglected as a first approximation. Water permeability k_w was calculated from the following expression:

$$k_w = \frac{D_w \gamma_w Q_o}{V \delta u_w} \quad (5)$$

where δu_w is the water pressure increment/decrement, V the volume of the sample and γ_w the water unit weight.

3. Test results and interpretations

3.1. WATER RETENTION RESULTS

3.1.1. *Water retention results at low water contents*

Figure 4 summarises the water retention data obtained through the application of the vapour equilibrium technique. Temperature derivatives at constant total suction

$(\partial w/\partial T)_\psi$ are also indicated. It can be seen that moisture retention capacity of the clay at low water contents (corresponding to the adsorbed water contained in the intra-aggregate porosity) is influenced by temperature. At a given total suction, water content reduces with increasing temperatures, as clearly detected for 8, 10 and 32 MPa. However, the reduction at $\psi = 6$ MPa is hardly noticeable. In addition, it appears that temperature derivatives $(\partial w/\partial T)_\psi$ tend to increase at higher total suctions, showing less evident temperature effects. Water retention data reported by Romero (1999) of the same soil and ranging from $\psi = 55$ to 240 MPa showed no noticeable temperature effects.

Lower values of moisture retention under constant total suction and higher temperatures are in agreement with experimental results reported by Wan (1996) testing Boom clay up to 50°C and using vapour equilibrium technique. In addition, lower water contents for the same matric suction and higher temperatures are also consistent with data reported in the low suction range (sandy and silty material) by Saha and Tripathi (1979), by Nimmo and Miller (1986), by Hopmans and Dane (1986), by Constantz (1991) and by She and Sleep (1998).

Total suction – temperature plots at constant water content varying between 6% and 11% are indicated in Figure 5. Temperature derivatives at constant water content $(\partial \psi/\partial T)_w$, are also reported. Deviations at 80°C may be associated with some water evaporation affecting water content determinations. As clearly detected

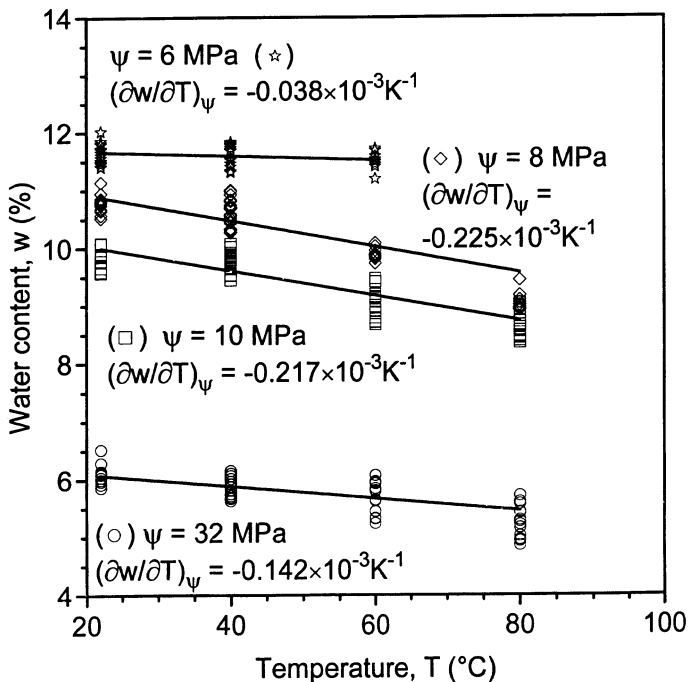


Figure 4. Water content – temperature plots at constant total suction

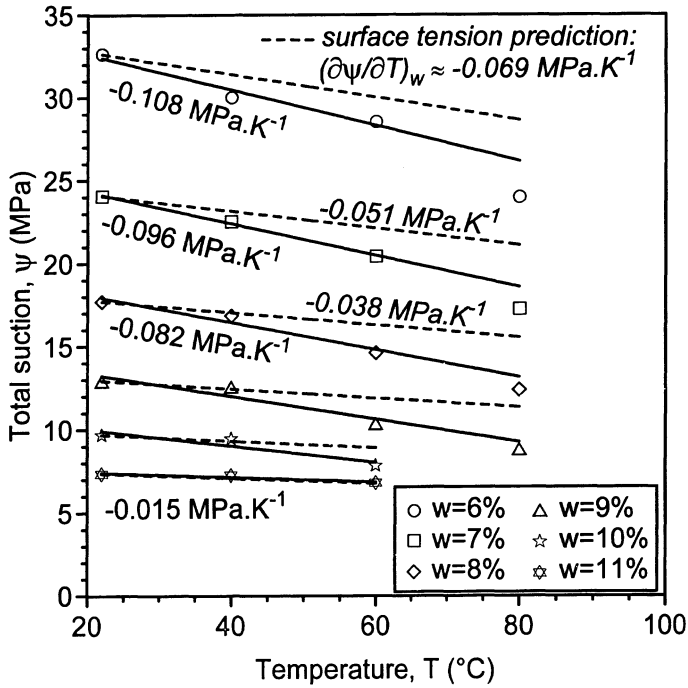


Figure 5. Total suction – temperature plots at constant water content

in the figure, for a specified water content contained in the intra-aggregate porosity, total suction tends to decrease with increasing temperatures.

Following the suggestion of Philip and de Vries (1957), numerous experimental results of temperature effects on matric suction s at constant water content w and for monotonic paths have been interpreted on the basis of temperature dependence on surface tension of water $\sigma(T)$:

$$\left(\frac{\partial s(w, T)}{\partial T} \right)_w = \frac{s(w, T)}{\sigma(T)} \frac{d\sigma(T)}{dT} = \frac{b}{a + bT} s(w, T) \quad (6)$$

The simplest empirical relationship between σ and T is a linear fit as indicated in Equation (6), which describes temperature effects in the experimental range: $\sigma(T) = a + bT$, with $a = 0.118 \text{ Nm}^{-1}$ and $b = -1.54 \times 10^{-4} \text{ Nm}^{-1} \text{ K}^{-1}$. A theory to allow the incorporation of temperature induced changes in wetting coefficients in Equation (6) has been proposed by Grant and Salehzadeh (1996) derived from thermodynamics of interfacial phenomena. Integrating Equation (6) between a reference temperature T_r and an observational temperature T , temperature effects

on energy status of soil water can be derived from the following coefficients affecting a reference matric suction $s(w, T_r)$ (Grant and Salehzadeh, 1996):

$$\frac{s(w, T)}{s(w, T_r)} = \left(\frac{a_1 + b_1 T}{a_1 + b_1 T_r} \right)^{b_1} \quad (7)$$

where a_1 and b_1 are empirical coefficients reflecting the actual behaviour compared to the surface tension mechanism. If values estimated from the analysis of experimental data tend to $b_1 = 1$ and $a_1 = a/b = -766$ K, then temperature induced changes may be described by temperature effects on surface tension.

Comparisons between total suction – temperature plots at constant water content and predicted in terms of surface tension mechanism of pure water are also shown in Figure 5. At higher temperatures, the theory under-predicts the influence of temperature on total suction. Therefore, the capillary model cannot solely explain the effect of temperature at high suctions, as expected for adsorbed water in relatively active clays. Additional thermal disturbances altering clay fabric and intra-aggregate fluid chemistry are to be postulated. Test results showing greater temperature dependence have been reported by Hopmans and Dane (1986), Nimmo and Miller (1986) and Constantz (1991) in the low suction range for sandy and silty soils.

3.1.2. Overall picture of water retention results: low and high water contents

The overall picture of water retention results is depicted in Figure 6, in which the relationship between suction and water content under isochoric conditions and two different temperatures (22 and 80°C) is plotted. Data at high total suctions ($3 \text{ MPa} \leq \psi \leq 32 \text{ MPa}$), corresponding to the intra-aggregate water, were interpolated at constant dry unit weight from free swelling data, following the procedure detailed in Section 2.2.2. Wetting data at low matric suctions ($s \leq 0.45 \text{ MPa}$) were obtained from isochoric tests, according to the procedure indicated in Section 2.3.1. The end point of the wetting curves at 80°C is somewhat lower in terms of water content compared to the end point of the wetting curves at ambient temperature. This fact is due to the lower gravimetric water storage capacity at higher temperatures, mainly caused by water dilatation and possibly due to thermal expansion of entrapped air.

Test results shown in Figure 6 have been fitted to a modified form of the van Genuchten (1980) expression for water content w as a function of matric suction s at the observational temperature T (Romero, 1999):

$$\frac{w}{w_{sat}} = S_r = C(s) \left[\frac{1}{1 + (\alpha_T s)^n} \right]^m; \quad C(s) = 1 - \frac{\ln \left[1 + \frac{s}{a_r} \right]}{\ln \left[1 + \frac{a}{a_r} \right]} \quad \text{with } 0.1a < a_r \leq a \quad (8)$$

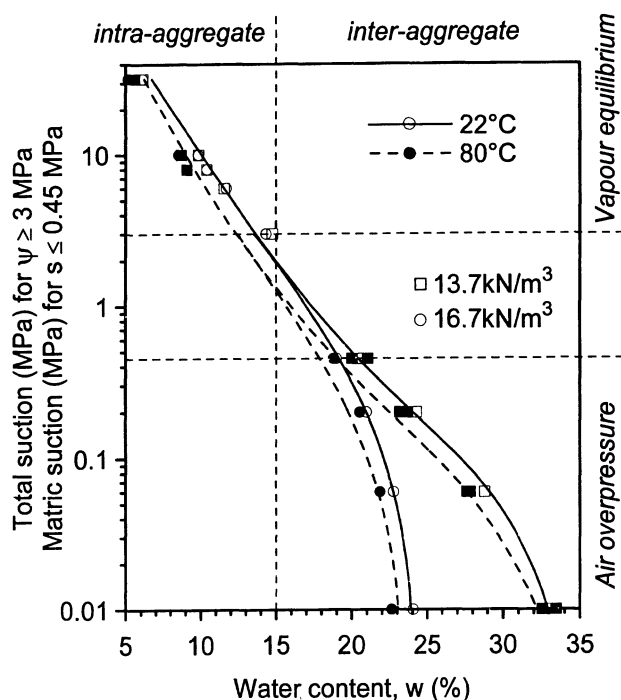


Figure 6. Water retention curves for different temperatures at fixed dry unit weights

$$\alpha_T = \alpha_r \left(\frac{a_1 + b_1 T_r}{a_1 + b_1 T} \right)^{b_1} \quad (9)$$

Parameters n and m are the same as used in van Genuchten's (1980) expression. The parameter α_T in Equation (8) is like van Genuchten's α , and is mainly associated (inversely) with the air-entry value of the soil. However, α_T allows for a temperature effect as it is associated with the observational temperature T . α_T is related to α_r (the value determined at the reference temperature T_r (the ambient temperature)) through Equation (9).

Equation (8), like van Genuchten's expression, is not adequate to fit retention curve data for high activity clayey soils. For this reason, the equation is modified using an expression that is similar to the proposal of Fredlund and Xing (1994). The objective of this correction is to make the curve tend to a linear relationship between the logarithm of suction and water content in the high suction zone (the intra-aggregate zone). However, the physical meaning of the parameters involved in this correction are different from the proposal of Fredlund and Xing (1994). Material parameter a represents the intersection with the y-axis of this linear part

of the semi-log plot. This parameter depends mainly on the specific surface (or alternatively on the liquid limit) of the clay, as suggested by Romero and Vaunat (2000). On the other hand, a_r , is a fitting parameter that controls the shape and slope of the retention curve in the high suction zone (some low-activity soils and artificially aggregated double-porosity fabrics deviate from a linear relationship). In clays it is realistic to assume $a = a_r$, so that the correction function is $C(s) = 1 - \ln(1 + s/a)/\ln(2)$.

For simplicity in the curve-fitting process, it was assumed that temperature effects only affect the α_T parameter and the water storage capacity w_{sat} . Parameters $C(s)$, n and m are considered temperature independent.

A non-linear curve-fitting algorithm using least-squares method was used to determine parameters n , m , α_r and α_T for the two soil fabrics and temperatures. A number of assumptions were made to simplify the fitting procedure. Total suctions ψ above 3 MPa were considered equivalent to matric suctions s , assuming that the osmotic suction π does not substantially alter the values: $\psi = s + \pi$. It should be noted that an osmotic component of $\pi \approx 0.4$ MPa at 22°C was measured by Romero (1999) using the squeezing technique. Therefore, this assumption is reasonable. For simplicity, $a = a_r = 300$ MPa, according to test results reported by the same author. In addition, as it is expected that $b_1 \rightarrow 1$, it is accurate enough to consider $b_1 = 1$ in Equation (9). It can be seen in Figure 6 that water storage capacity at the reference temperature $T_r = 295$ K (22°C) is $w_{sat} = 32.9\%$ for the low-density fabric and $w_{sat} = 23.9\%$ for the high-density packing. At $T = 353$ K (80°C), $w_{sat} = 32.2\%$ for the low-density fabric and $w_{sat} = 23.1\%$ for the high-density packing.

Fitting parameters were found to be $n = 1.14$, $m = 0.20$ and $\alpha_r = 21.3 \pm 0.8$ MPa⁻¹ for the low-density packing, and $n = 0.75$, $m = 0.35$ and $\alpha_r = 1.55 \pm 0.43$ MPa⁻¹ for the high-density fabric. Fitted values of α_T were 25.0 ± 0.7 MPa⁻¹ for the low-density packing and 1.98 ± 0.75 MPa⁻¹ for the high-density fabric. The value of a_1 was -608 ± 89 K, which was somewhat higher than the surface-tension prediction. Therefore, the temperature parameter α_T should be considered as an empirical fitting parameter. It is clear that the surface tension model cannot explain the temperature dependence.

In spite of the assumptions involved in the fitting process, it can be seen that Equations (8) and (9) are adequate to fit water retention data at different temperatures over a wide suction range (Figure 6). It is suggested that two regions can be defined in the retention curves shown in Figure 6, an intra-aggregate porosity region and an inter-aggregate region, the latter with a water content high enough to partially fill the inter-aggregation voids. The inter-aggregate region presents a dominant capillary storage mechanism containing bulk water, dependent on void ratio. In this region, temperature induced changes can be mainly associated with temperature dependence on interfacial tension and wetting coefficient, thermal expansion of entrapped air, dissolved air release upon heating or interfacial tension change caused by dilatation of water (Hopmans and Dane, 1986; Nimmo and Miller, 1986; Mohamed *et al.*, 1992; Grant and Salehzadeh, 1996; Wan, 1996; She and Sleep,

1998). At low water contents, moisture is contained in the intra-aggregate porosity, and the influence of equilibrated dry unit weights is found to be negligible. The suction – water content relationship is therefore mainly dependent on clay microstructure and pore fluid chemistry. The intra-aggregate domain, which presents an adsorption storage mechanism and contains quasi-immobile water, will be water-saturated in a wetting path before water fills the macropores. Inside the aggregates, predominant temperature effects are expected to be induced by thermo-chemical disturbances altering clay fabric and quasi-immobile water, as well as temperature influence on chemical induced water adsorption potential (Zhang *et al.*, 1993; Almanza *et al.*, 1995). However, little theoretical development of such mechanisms has been accomplished because of the difficulty in contrasting experimental data on active clays under a wide range of suctions and temperatures.

3.2. WATER PERMEABILITY RESULTS

3.2.1. *Temperature effects on water permeability. Interpretation of results*

Measured water permeability values are represented in Figure 7 for different degrees of saturation, void ratios and at two different temperatures (the upper plot represents data at 22°C and the lower graph shows data at 80°C). Data have been fitted with curves representing two different void ratios: 0.60 and 0.93. An important dependence of water permeability on void ratio and degree of saturation is observed. The effect of temperature, though not so remarkable, appears to be more significant at higher degrees of saturation.

In Figure 8, water permeability values have been grouped into different degree of saturation ranges and plotted versus void ratios for both temperatures (the upper plot represents data at 22°C and the lower graph shows data at 80°C). Temperature effect is more important under near-saturated conditions with a preponderance of bulk water, as indicated in the lower graph which has the data for 22°C superimposed as dotted lines. The ratio of $k_w(80^\circ\text{C})/k_w(22^\circ\text{C}) \approx 1.3$ for comparable void ratio and water contents. On the other hand, below a degree of saturation of 75%, corresponding to the upper limit of the intra-aggregate porosity, no clear difference in k_w is detected. The ratio $k_w(80^\circ\text{C})/k_w(22^\circ\text{C}) \approx 1.0$.

At $S_r \approx 75 \pm 5\%$, the coefficient of permeability presents a variation of one order of magnitude when changing the void ratio from $e = 0.90$ to 0.60. This variation is just as important as the change of the degree of saturation from $S_r = 72\%$ to 50% for a fixed $e = 0.93$, according to Figure 7.

Temperature effects on water permeability at saturation are usually derived from viscosity changes under free water considerations. This interpretation can be extrapolated to unsaturated states at constant void ratio e and water content w , according to the following expression:

$$\left. \frac{k_w(e, w, T)}{k_w(e, w, T_r)} \right|_{e, w} = \frac{\rho_w(T)\mu_w(T_r)}{\rho_w(T_r)\mu_w(T)} \approx 1 + \beta_T(T - T_r) \quad (10)$$

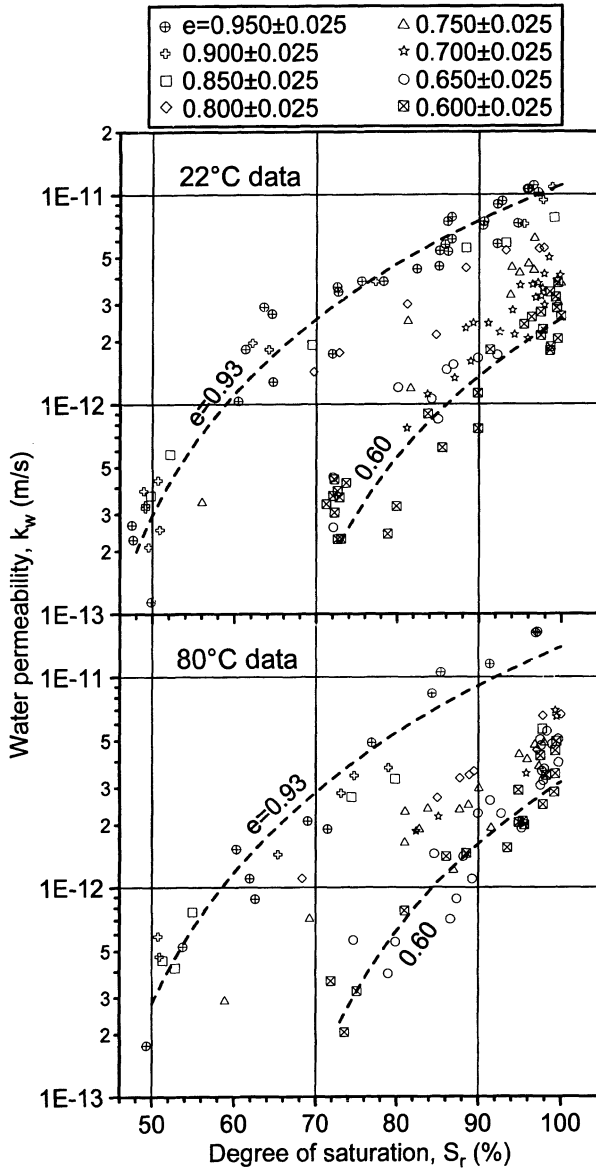


Figure 7. Water permeability vs. degree of saturation at 22°C (upper graph) and 80°C (lower graph)

where ρ_w , is the density of water, μ_w , the absolute viscosity and $\beta_T = 0.030 \text{ K}^{-1}$ (for a reference temperature $T_r = 22^\circ\text{C}$) an empirical coefficient that fits relative viscosity data over a temperature range of $22^\circ\text{C} \leq T \leq 80^\circ\text{C}$. The slight increase of permeability with temperature at $S_r = 95 \pm 5\%$ of $k_w(80^\circ\text{C})/k_w(22^\circ\text{C}) = 1.3$ cannot be explained in terms of a reduction of free water viscosity in the same interval of temperature (solid lines at 80°C and dashed lines at 22°C in the lower graph of

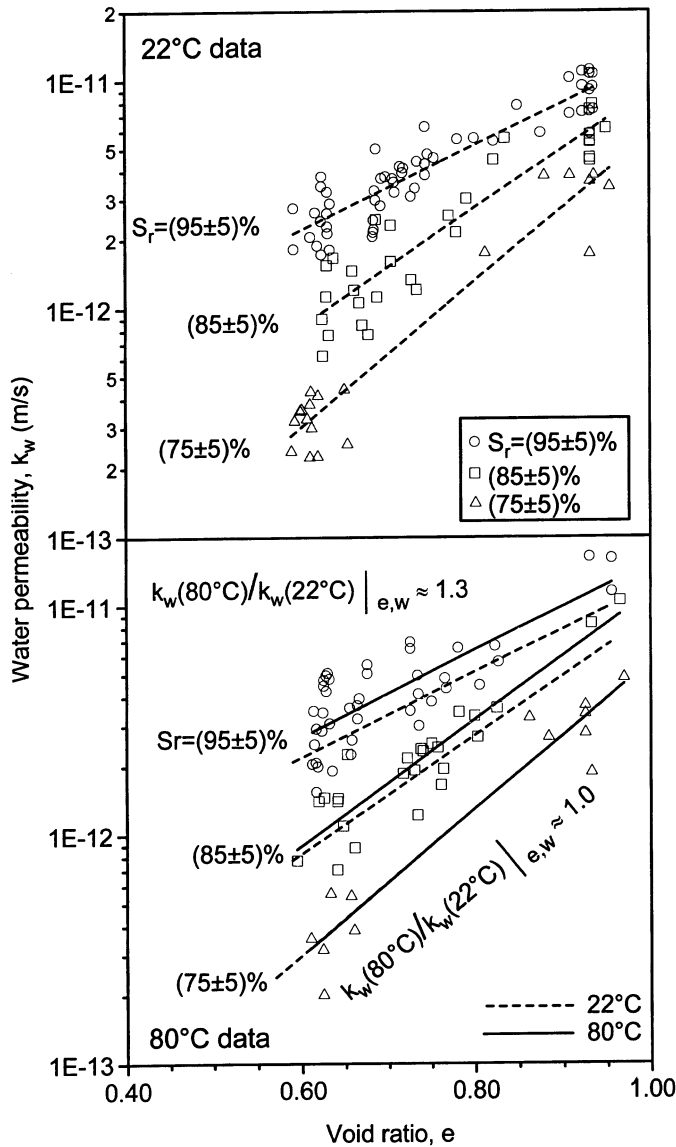


Figure 8. Water permeability vs. void ratio for constant degrees of saturation at 22°C (upper graph) and 80°C (lower graph). Data at 22°C is also superimposed on the lower graph as dotted lines

Figure 8). Experimental data are associated with $\beta_T = 0.005 \text{ K}^{-1}$ at nearly saturated conditions $S_r = 95 \pm 5\%$. At lower bulk water contents, in the proximity of the intra-aggregate zone at $S_r = 75 \pm 5\%$, experimental results show $\beta_T \rightarrow 0$.

As far as saturated states are concerned, Towhata *et al.* (1993) studied the effects of temperature on a kaolinite-clay up to 90°C using indirect methods. An additional temperature effect, over that predicted on the basis of free water considerations, was

observed (an estimated value of $\beta_T = 0.042 \text{ K}^{-1}$ was obtained from experimental data). Permeability measurements up to 120°C have also been reported on a saturated montmorillonite by VoIckaert *et al.* (1996). A value of $\beta_T = 0.014 \text{ K}^{-1}$ can be deduced from experimental data analysed up to 120°C . Khemissa (1998) reported direct measurements of permeability for a saturated kaolinite-clay up to 130°C . An estimated $\beta_T = 0.010 \text{ K}^{-1}$ was obtained from experimental data up to 80°C . Recently, Cho *et al.* (1999) studied water permeability changes of saturated bentonites over a temperature range of 20 to 80°C . A slightly higher value of around $\beta_T = 0.022 \text{ K}^{-1}$ was obtained.

The scarce experimental data available about temperature effects on water permeability in unsaturated soils have always been limited to low suctions and temperatures. Experimental results have been reported by Haridasan and Jensen (1972) on a silty soil up to 35°C using the pressure plate outflow method. Somewhat greater temperature dependence seems to have been observed at higher volumetric water contents (although this fact has not been stressed by the authors). Hopmans and Dane (1986) tested a sandy soil using tensiometers up to 45°C . Lower values of permeability at high temperatures than those predicted from viscosity changes can be interpreted, at constant porosity, if the amount of bulk water and the cross-sectional area, available for water to flow, decreases. This effect is associated with aggregate expansion upon heating, which gives rise to smaller inter-aggregate voids affecting bulk water flow. Apart from porosity redistribution, thermo-chemical interactions on soil fabric and pore fluid properties could also be relevant. Flocculation/dispersion phenomena have been observed when temperature increases in clays (Almanza *et al.*, 1995). In addition, it seems possible that the sensitivity of viscosity to temperature is different for intra-aggregate and bulk water.

3.2.2. Relative water permeability

Relative water permeability values k_w/k_{ws} (unsaturated water permeability to permeability at saturation) are shown in Figure 9 as a function of the effective saturation ratio S_e and for different constant void ratios e and temperatures T , following the expression:

$$\left. \frac{k_w(e, w, T)}{k_{ws}(e, T)} \right|_{e, T} = S_e^\lambda; \quad S_e = \frac{w - w_{ref}}{\frac{e}{G_s} - w_{ref}} = \frac{S_r - \frac{G_s \cdot w_{ref}}{e}}{1 - \frac{G_s \cdot w_{ref}}{e}} \quad (11)$$

where λ is an empirical constant usually related to pore size distribution. S_e can be evaluated on the basis of water content w or degree of saturation S_r . Subscript *ref* refers to a reference water content. In order to avoid a high dependence of λ on void ratio, Romero *et al.* (1999) normalised S_e with respect to the water contained inside the intra-aggregate porosity. Below a threshold water content of $w_{ref} = 13\%$, the relative water permeability is maintained $k_w/k_{ws} < 0.01$ (Romero, 1999). This

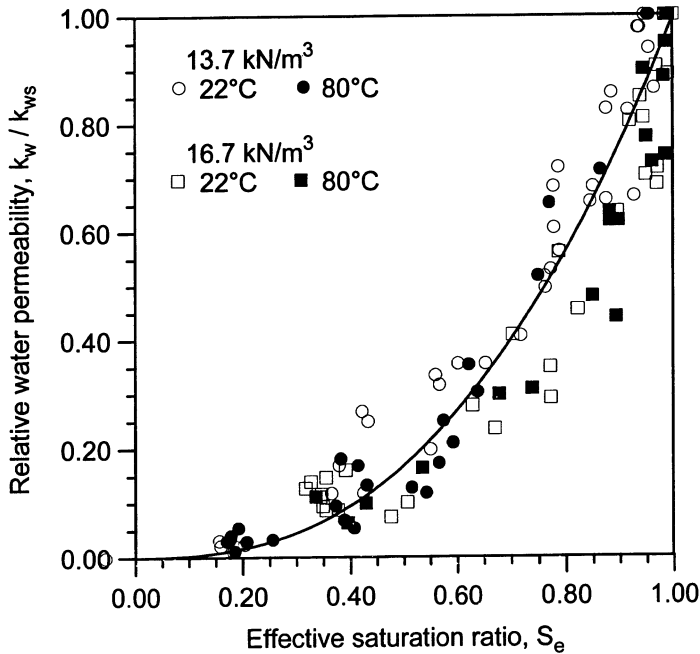


Figure 9. Relative water permeability values vs. effective saturation ratios for different void ratios and temperatures (Romero *et al.*, 1999)

quasi-immobile water content is consistent with the intra-aggregate water content determined from retention curves presented in Figure 6.

Relative permeability values have been fitted to Equation (11). A parameter $\lambda = 2.6$ adequately fits experimental data corresponding to the different void ratios and temperatures. As observed in Figure 9, no important temperature dependence has been detected for the relative permeability function.

4. Conclusions

As a summary of the experimental technique and equipment used, the tests performed and the results obtained, the following conclusions may be drawn. Vapour equilibrium using partially saturated NaCl solutions and axis translation techniques have demonstrated their applicability for studying the combined effects of temperature and partial saturation. However, a careful control with auxiliary devices (vapour traps and diffused air volume indicators) is required to use axis translation technique at high temperatures. Important problems concerning this technique refer to the accumulation of diffused air under the HAEV ceramic disc and uncontrolled evaporative fluxes, which affect the measurement of transient and steady-state inflow and outflow of water.

Experimental results, which are presented for different artificially prepared unsaturated clay fabrics, offer a consistent pattern of temperature effects on water retention and water permeability over a wide range of suction and temperature. In the studied range of the intra-aggregate porosity zone, water retention of the clay is influenced by temperature. Total suction tends to reduce with increasing temperatures at constant water content. However, the influence that temperature has over water retention cannot only be attributed to temperature dependence on surface tension. Additional thermal disturbances altering clay fabric and intra-aggregate fluid chemistry are possible. Wetting retention curves, covering a wide suction range (from 0.01 to 32 MPa), have been presented for different void ratios and temperatures. The results indicate a clear delimiting zone separating a region of intra-aggregate porosity from an inter-aggregate adjoining area. In both regions, different temperature induced phenomena affecting water retention are expected.

Temperature influence on water permeability is more relevant at low suctions corresponding to bulk water preponderance (inter-aggregate zone). Below a degree of saturation of 75% (in the proximity of the intra-aggregate zone) no clear effect is detected. Experimental data show that temperature dependence at constant degree of saturation and void ratio is smaller than what could be expected from the thermal change in water viscosity. Thermo-chemical effects altering clay fabric (flocculation or dispersion), porosity redistribution (creating preferential pathways or blocking macropores) and pore fluid chemistry (affecting viscosity) could be relevant. Relative water permeability values at constant void ratio showed no temperature dependence.

Finally, on the basis of phenomenological evidence, expressions and material parameters for retention curves and water permeability functions at different temperatures have been presented.

Acknowledgements

The first author acknowledges the financial support provided by TDOC grant from the Comissionat per a Universitats i Recerca de la Generalitat de Catalunya. The support of DGICYT through research grant PB95-0771 is also acknowledged. The first author thanks Dr. A. Di Marianno for her help during the preparation of the paper. The comments made by the reviewers of the paper were greatly appreciated.

References

- Almanza, R., Castañeda, R. and Silva, G. (1995) *Temperature-electrolyte effects on clay soil liners*, in *Proceedings of the 1st International Conference on Unsaturated Soils*. Vol. 1 Paris, 1995 (edited by E. E. Alonso and P. Delage). Balkema/Presses des Ponts et Chaussées. pp. 343–348.

- Alonso, E. E. (1998) *Succión y humedad en bases y explanadas de carreteras*, in *Proceedings of the Simposio Internacional sobre Drenaje Interno de Firmes y Explanadas*. Granada, November 1998. pp. 3–55.
- Cho, W. J., Lee, J. O. and Chun, K. S. (1999) The temperature effects on hydraulic conductivity of compacted bentonite, *Applied Clay Science*, **14**, 47–58.
- Constantz, J. (1991) Comparison of isothermal and isobaric water retention paths in nonswelling porous materials, *Water Resour. Res.* **12**(12), 3165–3170.
- Delage, P., Sultan, N. and Cui, Y. J. (2000) On the thermal consolidation of Boom clay, *Can. Geotech. J.*, **37**, 343–354.
- Fredlund, D. G. and Rahardjo, H. (1993) *Soil mechanics for unsaturated soils*, John Wiley and Sons, Inc. New York.
- Fredlund, D. G. and Xing, A. (1994) Equations for the soil-water characteristic curve, *Can. Geotech. J.*, **31**, 521–532.
- Gardner, W. R. (1956) Calculation of capillary conductivity from pressure plate outflow data, *Soil Sci. Soc. Am. Proc.*, **20**, 317–320.
- Gens, A., García-Molina, A. J., Olivella, S., Alonso, E. E. and Huertas, F. (1998) Analysis of a full scale in situ test simulating repository conditions, *Int. J. Numer. Anal. Meth. Geomech.*, **22**, 515–548.
- Grant, S. and Salehzadeh, A. (1996) Calculation of temperature effects on wetting coefficients of porous solids and their capillary pressure functions, *Water Resour. Res.*, **32**(2), 261–270.
- Haridasan, M. and Jensen, R. D. (1972) Effect of temperature on pressure head – water content relationship and conductivity of two soils, *Soil Sci. Soc. Am. Proc.*, **36**, 703–708.
- Hopmans, J. W. and Dane, J. H. (1986) Temperature dependence of soil hydraulic properties, *Soil Sci. Soc. Am. J.*, **50**, 4–9.
- Horvath, A. L. (1985) *Handbook of aqueous electrolyte solutions: physical properties, estimation and correlation methods*, Ellis Horwood Limit, New York.
- Jucá, J. F. T. and Frydman, S. (1996) *Experimental techniques. State of the art report*, in *Proceedings of the 1st International Conference on Unsaturated Soils*. Vol. 3 Paris, 1995 (edited by E. E. Alonso and P. Delage). Balkema/Presses des Ponts et Chaussées. pp. 1257–1292.
- Kanno, T., Fujita, T., Takeuchi, S., Ishikawa, H., Hara, K. and Nakano, M. (1999). Coupled thermo-hydro-mechanical modelling of bentonite buffer material, *Int. J. Numer. Anal. Meth. Geomech.*, **23**, 1281–1307.
- Khemissa, M. (1998) Mesure de la perméabilité des argiles sous contrainte et température, *Rev. Franç. Géotech.*, **82**, 11–22.
- Kunze, R. J. and Kirkham, D. (1962) Simplified accounting for membrane impedance in capillary conductivity determinations, *Soil Sci. Soc. Am. Proc.*, **26**, 421–426.
- Lang, A. R. G. (1967) Osmotic coefficients and water potentials of sodium chloride solutions from 0°C to 40°C, *Australian J. Chem.*, **20**, 2017–2023.
- Mohamed, A. M., Yong, R. N. and Cheung, S. C. H. (1992) Temperature dependence of soil water potential, *Geot. Testing J.*, **15**(4), 330–339.
- Nimmo, J. R. and Miller, E. E. (1986) The temperature dependence of isothermal moisture vs. potential characteristics of soils, *Soil Sci. Soc. Am. J.*, **50**, 1105–1113.
- Philip, J. R. and de Vries, D. A. (1957) Moisture movement in porous materials under temperature gradients, *Trans. American Geophysical Union*, **38**(2), 222–232.
- Romero, E., Lloret, A. and Gens, A. (1995) *Development of a new suction and temperature controlled oedometer cell*, in *Proceedings of the 1st International Conference on Unsaturated Soils*. Vol. 2 Paris, 1995 (edited by E. E. Alonso and P. Delage). Balkema/Presses des Ponts et Chaussées. pp. 553–559.

- Romero, E. (1999) *Characterisation and thermo-hydro-mechanical behaviour of unsaturated Boom clay: an experimental study*. PhD Thesis, Universidad Polit cnica de Catalu a.
- Romero, E. and Vaunat, J. (2000) *Retention curves of deformable clays*, in *Experimental Evidence and Theoretical Approaches in Unsaturated Soils* (eds. A. Tarantino and C. Mancuso) Rotterdam: Balkema, pp. 91–106.
- Romero, E., Gens, A. and Lloret, A. (1999) Water permeability, water retention and microstructure of unsaturated Boom clay, *Engineering Geology*, **54**, 117–127.
- Saha, R. S. and Tripathi, R. P. (1979) Effect of temperature on the soil water content suction relationship, *J. Indian Soc. Soil Sci.*, **27**, 222–224.
- She, H. Y. and Sleep, B. E. (1998) The effect of temperature on capillary pressure-saturation relationships for air-water and perchloroethylene-water systems, *Water Resour. Res.*, **34**(10), 2587–2597.
- Towhata, I., Kuntiwattanukul, P., Seko, I. and Ohishi, K. (1993) Volume change of clays induced by heating as observed in consolidation tests, *Soils and Foundations*, **33**(4), 170–183.
- van Genuchten, M.Th. (1980) A closed-form equation for predicting the hydraulic conductivity of unsaturated soils, *Soil Sci. Soc. Am. J.*, **44**, 892–898.
- Vicol, T. (1990) *Comportement hydraulique et m canique d'un sol fin non satur . Application   la mod lisation*. PhD Thesis, Ecole Nationale des Ponts et Chauss es, Paris.
- Volckaert, G., Bernier, F., Alonso, E. E., Gens, A., Samper, J., Villar, M. V., Martin-Martin, P. L., Cuevas, J., Campos, R., Thomas, H., Imbert, C. and Zingarelli, V. (1996) *Thermal-hydraulic-mechanical and geochemical behaviour of the clay barrier in radioactive waste repositories (model development and validation)*. Publications of the European Communities, EUR 16744 EN, Luxembourg.
- Wan, A. W. L. (1996) *The use of thermocouple psychrometers to measure in situ suctions and water contents in compacted clays*. PhD Thesis, University of Manitoba.
- Zhang, F., Zhang, Z. Z., Low, P. F. and Roth, C. B. (1993) The effect of temperature on the swelling of montmorillonite, *Clay Minerals*, **28**, 25–31.



Geotechnical engineering practice for collapsible soils

SANDRA L. HOUSTON, WILLIAM N. HOUSTON, CLAUDIA E. ZAPATA and
CHRIS LAWRENCE

*Department of Civil and Environmental Engineering, Arizona State University, Tempe,
Arizona, 85287-5306, USA*

(Received 3 August 2000; revised 12 April 2001; accepted 23 May 2001)

Abstract. Conditions in arid and semi-arid climates favor the formation of the most problematic collapsible soils. The mechanisms that account for almost all naturally occurring collapsible soil deposits are debris flows, rapid alluvial depositions, and wind-blown deposits (loess). Collapsible soils are moisture sensitive in that increase in moisture content is the primary triggering mechanism for the volume reduction of these soils. One result of urbanization in arid regions is an increase in soil moisture content. Therefore, the impact of development-induced changes in surface and groundwater regimes on the engineering performance of moisture sensitive arid soils, including collapsible soils, becomes a critical issue for continued sustainable population expansion into arid regions.

In practicing collapsible soils engineering, geotechnical engineers are faced with (1) identification and characterization of collapsible soil sites, (2) estimation of the extent and degree of wetting, (3) estimation of collapse strains and collapse settlements, and (4) selection of design/mitigation alternatives. Estimation of the extent and degree of wetting is the most difficult of these tasks, followed by selection of the best mitigation alternative.

Key words. arid soils, collapsible soils, identification, mitigation, wetting,

Introduction

Moisture-sensitive soils earn their name by swelling, collapsing, or losing strength when wetted. Wetting may arise from a variety of sources, most of which are a result of urbanization. Thus, the aspect of urbanization that is the most relevant to engineering performance is the change in surface and groundwater regimes resulting in wetting to water contents well above the natural water content. The effects of wetting include loss of apparent cementation, volume change, and loss of shear strength. Volume change upon wetting is either swell (if the material is plastic, initially dry, and lightly confined) or collapse (if the material is non-plastic or slightly plastic, initially dry, and heavily confined). In this paper emphasis will be placed on moisture-sensitive soils exhibiting collapse upon wetting.

For natural arid region conditions in undeveloped areas, rainfall either runs off surface soils or infiltrates a relatively shallow depth into the soil and then evaporates to the surface. However, there are numerous potential sources of water that arise from urbanization/development processes. These sources of added soil water include landscape irrigation, broken water or sewer lines, roof runoff, poor surface

drainage, intentional and unintentional groundwater recharge, damming due to cut/fill construction, groundwater rise, and moisture increase due to capillary rise and soil surface protection from the sun by paved surfaces. In several cases the groundwater table has risen after building occupation due to cessation of pumping in a near-by region or due to localized groundwater table mounding resulting from recharge or irrigation. Perched water can easily develop in irrigated regions where clay lenses are extensive. Thus, one effect of urbanization is a general increase in soil water contents. Localized areas may experience a minor increase in water content, a decrease in water content (e.g. from drawdown due to pumping), or thorough wetting from groundwater table rise. It is this change from the natural moisture state that results in most of the negative impacts of urbanization on arid soil performance.

Collapsible soils are not confined to arid regions and have been encountered in most parts of the world. The conditions in arid environments, however, tend to favor the formation of collapsible soils. Almost all naturally occurring collapsible soil deposits are either debris flows deposits or wind deposits (loess). Debris flows are at low density, but are relatively stiff and strong in their natural dry state. Cementation consists of dried clay and other chemical precipitates that may have been added after deposition. Wetting under load weakens the cementation, reduces the soil suction, and causes densification or collapse.

Loessial deposits comprise a relatively narrow size range of particles, usually silt to fine sand, with coatings of small amounts of clay being common (Fookes and Parry, 1994). Cementing materials are often added after deposition or dissolved and re-precipitated at particle contacts. Loess exhibits low density, moderately high shear strength and stiffness when dry, and is subject to densification and collapse upon wetting under load.

In addition to naturally deposited collapsible soils, engineered compacted fills may exhibit volume moisture sensitivity if compaction specifications and quality control are not appropriate. Compaction to low density and dry of optimum produces the greatest susceptibility to densification upon wetting, but almost any compacted soil can exhibit collapse if the confining pressure is sufficiently high. For clayey soils with significant plasticity the response to wetting may be swelling if the confining pressure is low.

An overview of collapsible soil behavior and methods for identification, testing, analysis, and mitigation for collapsible soil sites are presented herein. The detrimental volume change for these soils is almost always triggered by increased soil water content, and increased soil water content is expected in developed and urban regions.

Characterization of collapsible soil sites

The greatest problems with collapsible soils arise when the existence and extent of the collapse potential are not recognized prior to construction. Therefore, the identifi-

cation of collapsible soils and estimation of the collapse potential are major components in appropriate engineering for these moisture-sensitive soil sites.

GEOLOGICAL RECONNAISSANCE

Geologic and geomorphologic information can be helpful in anticipating collapsible soil deposits. Geotechnical and geological engineers know from experience that alluvial and colluvial deposits in arid regions are likely to exhibit some collapse potential. Beckwith (1995) recommends that alluvial fans in southwestern regions of the U.S.A. should be assumed to be collapsible unless a comprehensive testing program demonstrates otherwise. Chinese researchers have found that geographical and geomorphologic information can be strongly correlated with collapsibility (Lin, 1995).

INDIRECT CORRELATIONS

Qualitative and semi-quantitative correlations between collapse potential and various index properties have been developed and reported. Low initial density is, of course, a fair indicator of collapse potential, but some soils with moderately high density have also exhibited significant collapse. Another index property, which relates closely to density, is the water content at saturation. When the water content corresponding to full saturation significantly exceeds the liquid limit, substantial collapse potential is indicated. Correlations with seismic velocity, SPT N-values, and CPT tip resistance have also been attempted with low to moderate success. A disadvantage of all these correlations with index properties is that the correlations are typically weak, with considerable scatter, and in most cases the quality of the collapse potential prediction is not high enough to be reasonably used for subsequent settlement analyses. Therefore, the most effective use of available site characterization funds is to perform actual collapse tests, either laboratory or in-situ. The advantage of these tests over other indirect correlations is that they provide not only identification data but also quantitative data for later assessment of settlements.

LABORATORY TESTING

The one-dimensional response-to-wetting test, performed using conventional consolidation equipment, represents the most used laboratory collapse test. A specimen, at *in-situ* moisture content, is first subjected to a total stress corresponding to that anticipated for the field conditions. Then, with the total load in place, the specimen is given free access to water, and the collapse settlement is observed. The advantage of this simple laboratory test is that the test interpretation is simplified due to the relatively uniform stress state within the specimen, so that reasonable stress-strain relationships can be developed for estimating collapse settlements.

Compacted soils may be susceptible to compression upon wetting. The response to wetting of a compacted fill depends on the soil type, compactive effort, compaction water content, and stress level at the time of wetting (Houston and Houston, 1997). Identification of collapsible fills is best accomplished by testing specimens compacted at various water contents and dry densities over a range of stress levels expected for the field conditions. The best engineering approach is to identify the conditions leading to collapse of a compacted fill through laboratory testing before fill construction. Appropriate compaction specifications and construction control can then be used to avoid or minimize the collapse problem.

If wetting were expected to a very high degree of saturation (for example, wetting from rising groundwater table) then the full-wetting laboratory collapse data would be used directly in making estimates of collapse settlement. At a number of points within the anticipated wetted region, the total stress resulting from the overburden soil stress and the structural loads would be evaluated. An appropriate wetted stress-strain curve, such as that depicted in Figure 1, is assigned to each point, and the fully-wetted collapse strain is read from the curve as the ordinate from the origin to the wetted curve, for naturally-occurring collapsible soils. The curve AB in Figure 1 represents the dry compression curve for a truly undisturbed specimen. It can be assumed to be flat for initially dry arid region soils without significant error. Curves AC, AD, and AE represent successively greater amounts of sample disturbance. Curve H'FG represents the wetted curve. The band of data

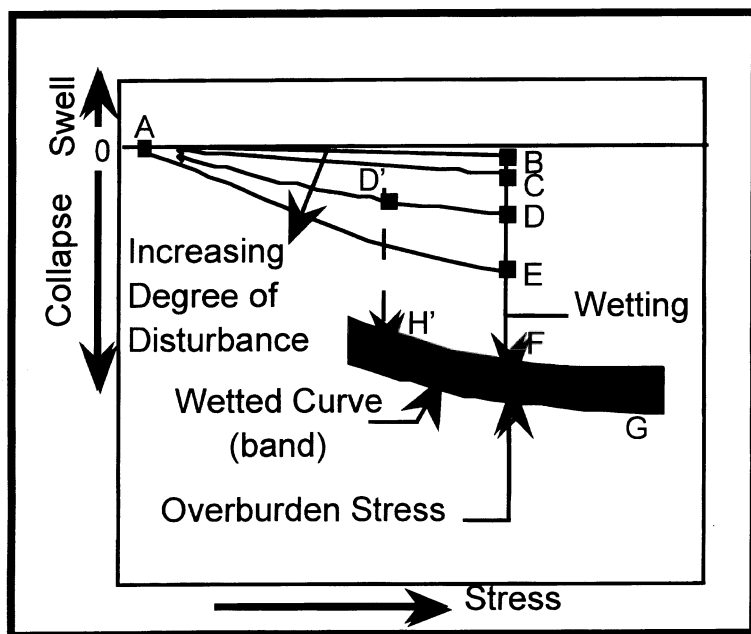


Figure 1 Response to wetting for a collapsible soil

representing a series of tests will usually exhibit significant width, due to site heterogeneity. It is reasonable to select a design curve approximately halfway between the average for the band and the lower limit of the band. The collapse settlement is computed by integrating the strain profile over the extent of the zone of wetting. The path D'H' in Figure 1 represents wetting at a lower stress for a laboratory test specimen. For the field, however, the strain would be taken from the origin to point H', because this assumption simplifies the analysis and is conservative, but only slightly conservative.

The justification for this procedure is as follows. Medium- to large-scale footings on dry collapsible soils in the field show almost no measurable settlement upon dry loading. The compression curve is typically similar to AB in Figure 1, or flatter. Thus the dry strain for a laboratory test specimen, such as a specimen following path AD, is almost entirely due to sample disturbance. The strain induced by disturbance is strain that would have occurred due to wetting. Therefore, whether the sample is disturbed or not, it ends up more or less within the shaded band labeled as the wetted curve in Figure 1. It is these findings that have prompted the authors to recommend use of the full strain from the origin to the wetted curve as an estimate of the strain that would occur for a corresponding element of soil in the field, at a particular stress. If the laboratory-wetted curve corresponds to full saturation, then the strain from the origin to the curve (band) is the full saturation strain.

Estimated collapse settlements based on full-wetting collapse potential may not be realized for many field conditions. In fact, it is extremely uncommon that complete saturation to the full depth of the collapsible silty or sandy soil deposit occurs, unless wetting is by slowly rising ground water. This fact must be taken into consideration when estimating collapse settlements and in assessing the magnitude of the "calculated risk". When significant soil suction remains after wetting, as for field situations for which only partial wetting occurs, the soil will not fully collapse. This can be observed in the laboratory by conducting response to wetting tests over a range of soil suction (degree of saturation) values. Partial wetting considerations are particularly useful for forensic studies and for assessment of prewetting and controlled wetting mitigation alternatives.

FIELD TESTING

Field tests are frequently used to help identify and characterize collapsible soil deposits. Field tests normally consist of some type of plate load test, wherein water is introduced to the loaded soil. The disadvantages of conventional field collapse tests include non-uniform stress state within the region of soil contributing to settlement, and the corresponding difficulty in obtaining stress-strain relationships. It is typically only the load and displacement relationship that is obtained for the field collapse test. Advantages of field collapse tests include minimization of sample disturbance, typically larger volume of soil tested, and attainment of a degree of wetting that is likely to be similar to the prototype.

Mahmoud et al. (1995), and Houston et al. (1995) have devised plate load test methodologies and data analysis procedures, which allow the determination of the wetted stress-strain curve from the test data. These techniques allow extrapolation of test data to slightly higher or lower stress levels, for improved interpretation of test data, and for comparison to laboratory collapse test results.

A slight variation on the plate load test described by Mahmoud et al. (1995) is as follows. A shallow pit is excavated to the desired testing depth, as indicated in Figure 2. A cavity is then excavated in the floor of the pit for a moderate-sized ($1.3 \text{ m} \times 1.3 \text{ m}$) unreinforced concrete slab. After the concrete is set, Box 1 is placed on the slab and the initial elevation of the box is recorded. Box 1 is then filled, by backhoe, with soil of known density, and then Box 2 is added, and so on until all boxes are added. Although dry compression is usually negligible for very dry, slightly cemented soils, settlement readings should be taken as each successive box is filled. After the last box is filled, water is added to the pit to wet the soil under the model footing. After an estimated time to achieve wetting to a depth equal to about two thirds of the footing width has elapsed, continuous sampling with a drive tube is used to obtain the degree of wetting behind the wetting front and the position of the wetting front. Alternatively, water contents can be inferred from capacitance, TDR, or neutron probe readings. If desired, an additional loaded box may be placed to obtain a modest extrapolation of the wetted curve.

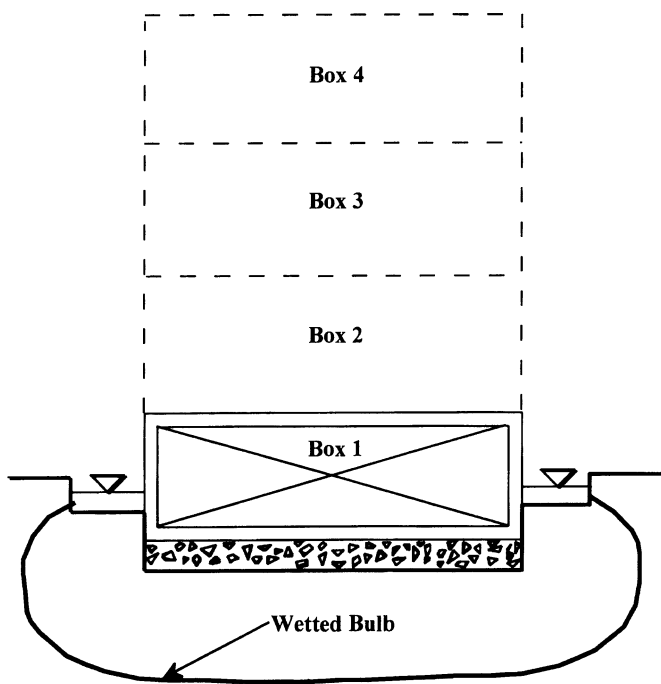


Figure 2 Schematic of *in-situ* collapse test set-up, using soil boxes on a concrete pad

The disadvantage of this type of test is that an overburden of only 2 to 3 m of soil can be applied. In addition, this test and the plate load test described by Mahmoud et al. (1995) are limited to fairly shallow depths, due to excavation costs and safety issues. Advantages of these plate load tests include the relatively large volume of material tested, with the result that the tests are statistically representative for the site. The 1.3 m square concrete pad can be used to test soils with large aggregate, even cobbles, and other difficult-to-sample materials of low cohesion and cementation. Particularly in the case of the concrete pad, an intimate contact with the underlying soil is obtained, thus eliminating seating problems. Also, the results of the in-situ tests are available instantly, while the equipment is still on site and the testing program can be modified at minimum cost. Figure 3 shows two example plots of data from plate load tests such as those described above.

In addition to the shallow to moderately shallow plate load tests described above, Mahmoud et al. (1995) describe a down-hole test, which can be performed at considerable depth. Because this test is performed at the bottom of a borehole, the plates are typically much smaller. To date plates in the range of 6 to 7 cm in diameter have been used, but plates up to 20 to 30 cm could be used. The unit cost of the down-hole collapse test is somewhat higher than the laboratory collapse test, particularly if a drill rig and crew assist the testing operation.

The data obtained from these plate load tests include applied load, plate settlement, and the depth of wetting. The applied load and plate dimensions yield the average contact stress. The average vertical normal stress within the wetted zone is obtained as the product of the contact stress and an influence factor, I_F or I_S , from Figure 4. For the first load increment, the load stays constant and the wetting front

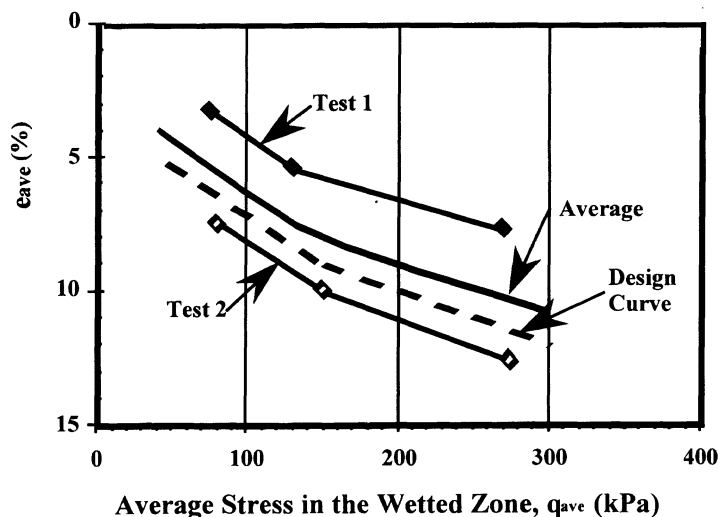


Figure 3 Example plots of average vertical stress vs average strain in the wetted zone from an *in-situ* collapse test

advances. For the subsequent load increments, the wetting front advances very slowly at an exponentially decaying rate and is in a more nearly constant position. The load, on the other hand, is increased substantially, perhaps doubled or tripled. The differences in these two sets of boundary conditions lead to two different influence value curves, I_F (for the first load increment) and I_S (for the subsequent load increment). Houston et al. (1995) give further explanations of these differences. The average strain within the wetted zone is simply the observed plate settlement divided by the thickness of the wetted zone.

The greatest difficulty in performing the down-hole *in-situ* collapse test is to obtain a clean hole for the test. The technique that appears to work best is as follows. After the driller cleans the hole as well as possible using the usual tools and techniques, a PVC casing that is just smaller than the diameter of the hole is lowered to the bottom of the hole. A clean out tube having an outside diameter just less than the casing is then driven into virgin soil about 0.7 to one tube diameter. Withdrawal of this tube of soil leaves a clean tension break at the bottom of the hole, on which the loading plate can be placed. Although this tension break is relatively clean, it is not necessarily planar and flat. When the loading plate is placed on the soil under the weight of the string of tools, some of the pinnacles are crushed and some leveling of the plate occurs. However, a recent series of tests with the *in-situ* device suggest that remaining pinnacles and small voids under the plate have lead to values of collapse that are slightly too high (by about 1 to 2% strain). This effect is under study, and the following modifications to the plate seating method proposed by Mahmoud et al. (1995) are proposed.

- (a) Use a loading plate with small holes in it and clean the holes in the plate before use.

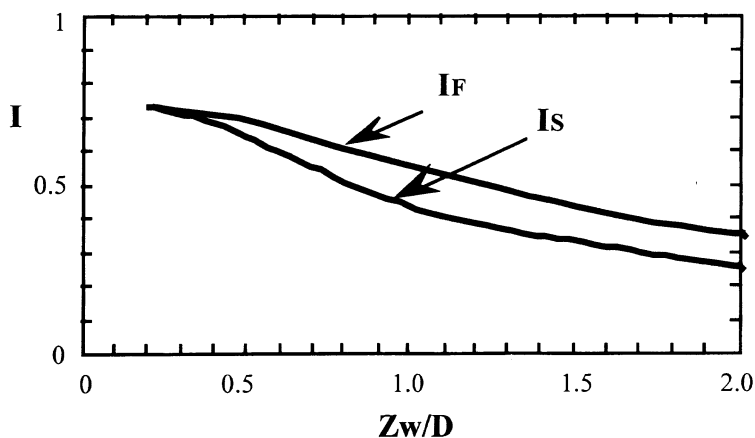


Figure 4 Average influence factors for the wetted zone for the first and subsequent loading for an *in-situ* collapse test (Houston et al., 1995)

- (b) Clean the borehole bottom as described above and load the plate up to the overburden pressure plus structural load.
- (c) With the load in place, rotate the string of tools and the loading plate two to three revolutions to shave off pinnacles under the plate and improve its seating.
- (d) Reduce the load back to about one-half to two-thirds of that used in step (b).
- (e) Install the displacement measurement devices and zero them.
- (f) Add water and proceed with the test.

The test data obtained is of the same form as that shown in Figure 3, which is also of the same form as that obtained from the one dimensional laboratory response to wetting test, Figure 1. Figure 5 shows a comparison between lab and field collapse data at a site in Benson, Arizona.

Minimum number of collapse tests needed for site characterization

The minimum number of collapse tests needed to satisfactorily characterize a site or a layer of collapsible soil at a site depends on (a) the degree of heterogeneity with respect to collapse potential, (b) the required accuracy of the collapse potential estimate. Houston et al. (1999) have statistically characterized seven sites in Arizona and California and found that variability over very small distances horizontally and vertically of a meter or less is typically about the same as over much larger distances of several meters or more. For each of these seven sites the mean value of collapse, \bar{x} , the standard deviation, S , and coefficient of variation, COV, were evaluated. The COV was the most stable parameter, averaging about 0.3 for all sites combined.

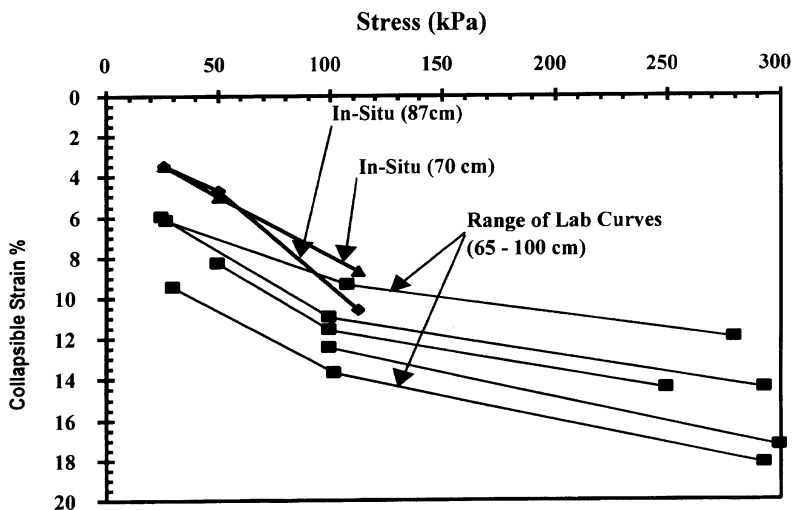


Figure 5 Comparison between lab and field collapse data at Benson, Arizona

Based on the results of this study, the decision about how many tests to perform to characterize a site or an identifiable layer at a site can be made as follows. First, the engineer in charge decides what level of accuracy is required. For example, if some number of tests, n_t , is performed for the site, \bar{x} and S will be obtained. If the accuracy of the estimate is given by $\bar{x} \pm 20\%$, then this means that the probability is very high that the true mean (collapse strain) lies within the range of $\bar{x} - 20\%$ to $\bar{x} + 20\%$. Therefore, the required accuracy could logically be chosen as the largest error band within which the engineering design, or other major engineering decisions, would be unchanged. Having chosen the acceptable error band, Figure 6 is then entered with an a priori estimate of $COV = 0.3$, based on the statistical studies cited above. Figure 6 was developed by assuming that the collapse strains fit a normal distribution. The magnitude of the acceptable error determines the number of tests, n_t . After the collapse tests have been performed the actual \bar{x} and S will be known for these tests. The site-specific COV , obtained from S/\bar{x} for the n_t tests performed, represents an improved estimate of the COV for the site, which may differ somewhat from the 0.3 value initially assumed. By moving across Figure 6 at the fixed value of n_t to the improved estimate of the COV for the site, a new improved estimate of the magnitude for the error band can be obtained. In other words, Figure 6 is a three-parameter plot and fixing any two values determines the third.

Mechanisms of wetting from activities of urbanization

Wetting from downward infiltration is more likely to result in a shallow depth of wetting than wetting to great depth. The probability of relatively shallow partial wetting from sources such as landscape irrigation and broken pipelines is very high.

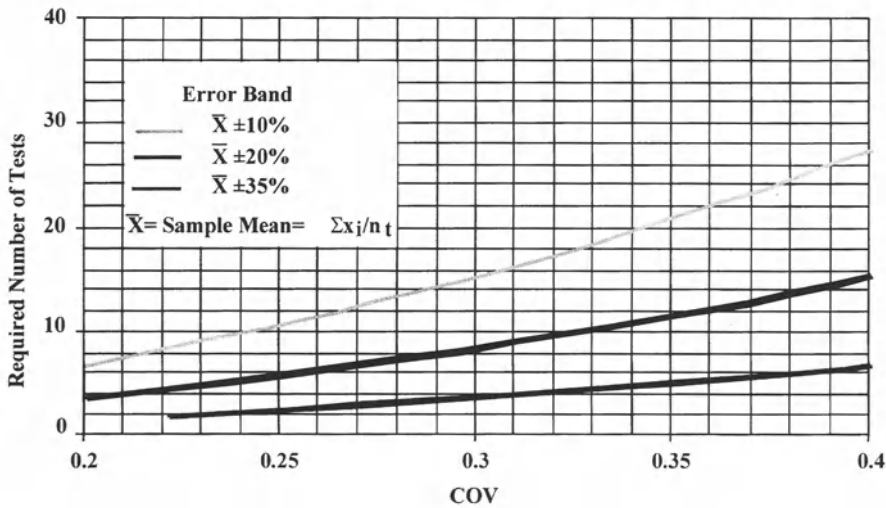


Figure 6 Number of samples required for probability of 95% that true site mean lies within error band shown

The likelihood of wetting to great depth or to a relatively high degree of saturation is less probable, but can occur for certain topography and sustained surface wetting situations. Several processes can lead to rising groundwater and the most obvious of these are as follows.

Increased infiltration due to urbanization can effectively change an arid or semi-arid climate to a humid climate. For example, in connection with a forensic investigation in San Diego, California, it was reported to the authors that the annual precipitation was about 30 cm before a residential subdivision was built and about 170 cm (counting landscape irrigation) after it was built. This change in the effective precipitation level resulted in substantial settlements of the underlying compacted fill. Although this subdivision was set in a generally semi-arid region, the lawns were spongy to walk on and the street side curbs had moss growing on them as a result of heavy landscape watering. In another example in semi-arid New Mexico, a commercial building won an award from the city for the year's most beautiful lawn and landscaping. However, they also suffered about \$0.5 million dollars in foundation damage due to differential settlement, having wetted the collapsible foundation soils to a depth of 15 m in some locations.

For a given amount of infiltration from the surface, the rate of groundwater rise depends on several factors including the depth to groundwater, slope of the groundwater table, and vertical and horizontal hydraulic conductivities. The problem of groundwater rise may be exasperated by an increased surface flux resulting from urban activities, together with low permeability geologic formations. As an example, the city of Riyadh, Saudi Arabia has shallow bedrock, which is either clayey or weathered to clay, and in this city the residential plots are typically large enough to accommodate septic tanks and leaching fields, which add further to infiltration rates. The result is that there are rising groundwater table problems and associated soil collapse.

Intentional groundwater recharge differs only slightly from the examples cited above in that the preceding water sources associated with landscape irrigation are typically more or less unintentional. By contrast, reinjection of water with wells, trenches and surficial ponds is typically intentional. The state of Arizona and several other states in the arid and semi-arid southwestern United States are currently engaged in various water reuse projects. One of these, soil-aquifer-treatment (SAT), involves the percolation of secondary and tertiary effluent from water treatment plants through the vadose zone. Although the primary objective of this project may be the disposal of the effluent, a strong secondary objective is the recharge of the groundwater. Depending on the rates of groundwater extraction by pumping in adjacent areas, the effect of this recharges maybe a rise in groundwater table. For example, the city of Mesa, Arizona, utilizes four recharge ponds at its reclamation plant near the Salt River. The net effect of this recharge has been a local rise in groundwater table from about 16m below the surface to about 5 m below the surface.

The damming of laterally moving groundwater by construction of fills in valleys could perhaps fall under the heading of urbanization. However, this mechanism deserves some special attention because of its large impact in southern California. Urban developments in rough, mountainous terrain give rise to filled-in-valleys and leveled-off adjacent mountaintops. The materials used for these fills are typically somewhat homogenized and thus a small to moderate amount of clay renders them a low permeability barrier to groundwater moving generally down the valleys. Under these circumstances, rising groundwater may present a problem, both for potentially collapsible alluvium under the fill and for the heavily stressed lower portions of the fill. Parts of San Diego and Los Angeles, California, represent examples of this type of problem.

Irrigation of agricultural lands can result in groundwater table rise, if the irrigation is sufficiently heavy. The consequences of the groundwater rise are of course not likely to be great for agricultural lands where infrastructure is sparse, but if the raised groundwater table extends laterally to an urban area, the consequences could be significant.

Cessation of pumping on a wide scale can, of course, result in a rise of groundwater table. If the pumping were initially the cause of lowering the groundwater table, then cessation would be expected to result in recovery of the water table.

The various mechanisms for rising groundwater cited above are not all equally problematic. Probably the most problematic case is that of increased infiltration due to urbanization. Urbanization implies new infrastructure which, when combined with overburden, produces higher stress than has previously acted on the soil. Wetting under this higher stress, particularly the thorough wetting due to rising groundwater, is quite likely to cause collapse problems. Rising groundwater due to damming effects of cut/fill operations is also very likely to produce significant collapse problems, for the same reasons cited above.

General effects of wetting

Arid soils are relatively dry and unsaturated in their natural state. Construction in and on these soils is typically performed without changing the natural water content. Even compacted fills and embankments are constructed at water contents well below saturation. In their natural, unsaturated condition these soils tend to exhibit low compressibility and relatively high shear strength. The addition of water reduces the soil shear strength and increases compressibility. In some cases the loss of strength and the amount of volume change can be quite significant. Forensic studies show that failures such as excessive building settlement and differential heave rarely occur for unsaturated soils in the absence of wetting.

Shear strength and volume change of unsaturated soils is controlled by the following stress state variables: net normal stress ($\sigma - u_a$) and matric suction ($u_a - u_w$). The soil matric suction is greatly reduced by wetting, as indicated in the soil water characteristic curves (SWCCs) of Figure 7. When the matric suction

is reduced, under load, compression occurs in collapsible soils. When the matric suction is reduced the soil shear strength is reduced. Because of the great importance of matric suction to engineering performance of unsaturated soils and the difficulties which arise when trying to directly measure this important stress state variable, a great deal of emphasis has been placed on development of typical SWCCs such as those shown in Figure 7. The predicted SWCCs shown in Figure 7 were developed by the authors using correlations between the fitting parameters of the Fredlund and Xing (1994) SWCC equation with well-known soil properties such as the Diameter D_{60} for non-plastic soils. For plastic soils, the soil index properties used were the Plasticity Index, PI, and the Percentage Passing #200 (75 μ m) sieve, P_{200} (Zapata, 1999). Knowledge-based systems comprised of a large database from various laboratories and literature sources have been developed, which are of great help for estimating soil water characteristic curves (Fredlund et al., 1998).

Table 1 tabulates some collapsible soils encountered in the western USA, China, Italy, and Brazil. The soil index properties needed to predict their moisture-suction characteristics are also shown in this table. Except perhaps for the Recife soil in Brazil, the collapsible soils collected have similar characteristics in terms of plasticity, ranging from being non-plastic to moderately low plasticity. The shaded area in Figure 7 shows the range of SWCCs for the soils presented in Table 1, and is believed to be representative of most naturally occurring collapsible soils encountered in the field.

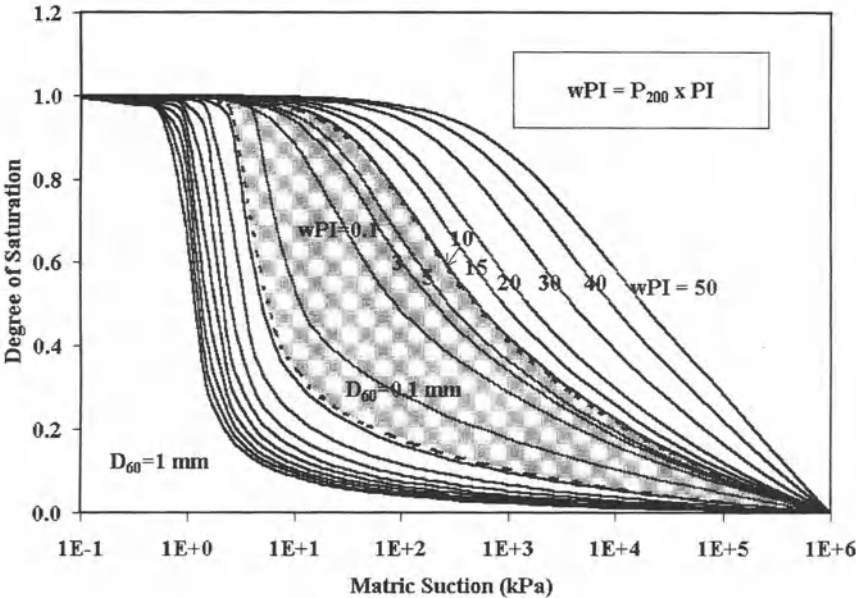


Figure 7 Typical soil-water characteristic curves

Volume change: Full wetting versus partial wetting

The usual method of investigating the potential collapsibility (or expansion) of a given unsaturated soil deposit is to perform one-dimensional laboratory response to wetting tests on undisturbed specimens of the material, as discussed previously. The usual test method is to provide the soil with free access to water, resulting in essentially full wetting. For an ideal undisturbed specimen of naturally occurring collapsible soil the dry strain corresponding to overburden load alone would be expected to be very small (essentially negligible). An undisturbed specimen collected from an existing compacted fill would also be expected to exhibit negligible dry strain upon loading to overburden stress alone because the dry strains should have already occurred in the field. Likewise, typical structural loads do not normally result in significant dry-loading strain of collapsible soils in their dry natural state if they are undisturbed. Thus the full collapse for a truly undisturbed field specimen would be approximately equal to the strain that would occur upon full saturation under load, as depicted in Figure 8. For the following discussion of volume change, the full wetting collapse strain will be assumed to be that strain which occurs under load when the specimen is given free access to water.

Full wetting of a collapsible soil would be expected only when rising groundwater table or perched water conditions developed. Where rising groundwater table is

Table 1 Naturally occurring collapsible soils

Name	D ₆₀ (mm)	P ₂₀₀ [†] (decimal)	PI (%)	wPI [‡]	Source
Site A: Weak cemented gray silt, AZ	0.05	0.74	0	0	1
Site B: Cemented silt with sand, AZ	0.063	0.62	0	0	1
Site C: Gray sandy silt, AZ	0.18	0.20	0	0	1
Northern Scottsdale, AZ soil (I)	–	0.65	1	0.7	2
Northern Scottsdale, AZ soil (II)	–	0.67	3	2	2
Price Club silt, Arizona	0.085	0.54	4	2.2	3
Loess from Missouri Basin*	0.06	0.93	9	8.4	4
Lanzhou Province Loess, China*	0.02	0.78	12	9.4	4
Loess from Shaansi Province, China	–	0.80	10	8	4
Malan loess – Gansu Province, China	–	0.92	7.1	6.5	5
Lishih loess – Gansu Province, China	–	0.92	7	6.4	5
Wucheng loess – Gansu Province, China	–	0.96	7.4	7.1	5
Petronila – Pernambuco, Brazil	–	0.59	10	5.9	6
Sta Maria da Boa Vista – Brazil	–	0.29	9	2.6	6
Carnaiba – Pernambuco, Brazil	–	0.36	22	7.9	6
Recife – Pernambuco, Brazil	–	0.80	36	28.8	6
CL from Parecis – Western Brazil	–	0.91	11	10	7
Metramo dam soil – Italy	–	0.38	13.3	5.1	8

Sources:

¹Houston and El-Ehwany (1991); ²Houston et al. (1988); ³Zapata (1999); ⁴Bell (1992); ⁵Fookes and Parry (1994); ⁶Ferreira and Lacerda (1998); ⁷Conciani et al. (1998); ⁸Rampino et al (1998)

*Average values; [†]Percent passing #200 (75 µm) sieve; [‡]wPI = P₂₀₀ × PI

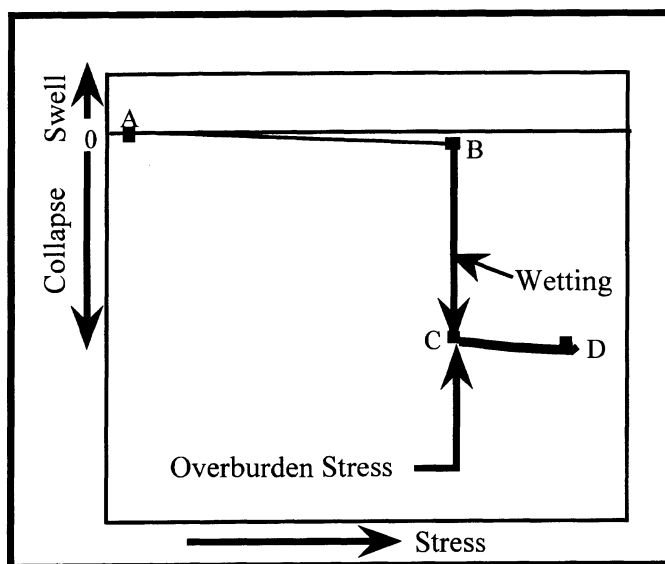


Figure 8 Schematic of response to wetting for a collapsible soil

anticipated the full wetting collapse strains from a response to wetting test should be used to make collapse settlement predictions. In contrast, full collapse potential would not be expected in zones that are wetted by downward infiltration only and which are not submerged by groundwater. The effects of partial wetting on actual collapse strain are shown for a typical silty collapsible soil in Figure 9. Because landscape irrigation has been found to result in relatively low degrees of saturation of only about 35 to 60% for typical silty/sandy collapsible soils, it is clear that the greatest settlements of collapsible soil deposits result when substantial groundwater table rise occurs.

To make an accurate estimate of collapse settlement potential it is necessary to have a good estimate of the degree and extent of wetting that may occur. The regions that experience complete submergence would experience full collapse potential, but the zones of wetting by downward infiltration alone would exhibit collapse consistent with the partial collapse relationship for that particular soil (e.g. Figure 9). It is the estimation of the degree and extent of wetting that is the most difficult part of the collapse settlement prediction.

Dynamic settlement and liquefaction considerations

Soils that exhibit significant collapse potential when dry may be more susceptible, when wetted by groundwater table rise, to dynamic settlement, lateral spreading, and liquefaction than other soils. This is because they are highly contractive under

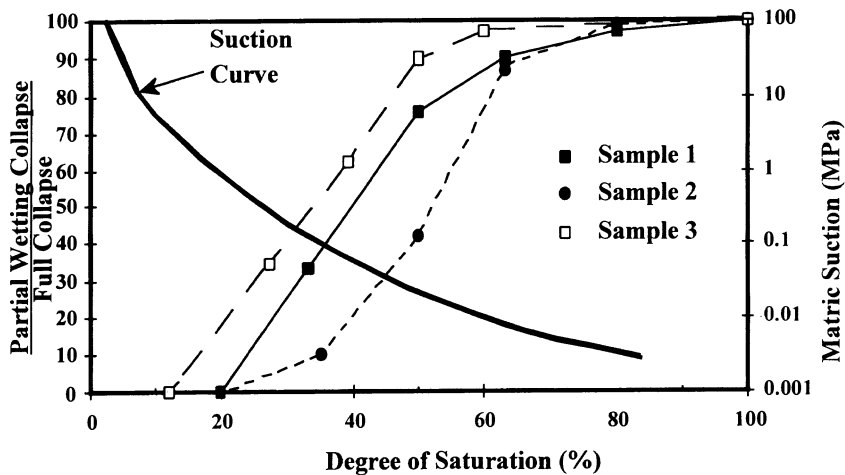


Figure 9 Partial collapse due to partial wetting curves for three ML soils

shear loading. The detection of the liquefaction and dynamic settlement potential of these soils may be masked during site investigation due to the high dry strength resulting from cementation and negative pore water pressures, which usually result in high SPT N-values.

Although any soil may compress upon wetting (depending on the density, water content, and applied stress), soils that exhibit significant compression (collapse) upon wetting are often non-plastic silts and silty sands. In general, it cannot be assumed that there will be sufficient fines in collapsible soils (either natural or compacted) to render these soils non-liquefiable if saturated. In addition, metastable soils have been shown to collapse under dynamic loading if the bond strength is sufficiently low. A collapsible silt in northern Scottsdale, Arizona, has been shown to exhibit collapse of about 12% when wetted under confining pressure of 100 kPa, then subjected to static CU testing and liquefaction testing. Even after the collapse induced by saturating under 100 kPa, the test specimens were so contractive that the CU tests showed S_u/p of 0.25 and \bar{A}_f of 1.7 (Govil, 1992). These values of S_u/p and \bar{A}_f are commensurate with highly metastable Scandinavian quick clays (Mitchell and Houston, 1969).

Southern California is a highly earthquake-prone region, and is well known for the creation of housing and commercial building sites by filling in alluvial canyons with compacted fill soils. When dry, these naturally occurring or engineered collapsible soils often possess cementation adequate to prevent significant deformations upon dynamic/earthquake loading. However, collapsible alluvium and compacted fills often become wetted when facilities become occupied and landscape water, leaks from pipes, and other wetting processes commence. In several cases, the groundwater table has risen after building occupation (due possibly to damming effects

of the fills), creating submerged, saturated soil deposits. This subsequent wetting of medium to loose soils results in significant reduction in bond strength.

The collapse settlements that occur due to rising groundwater table may cause damage, but this damage would be realized more or less immediately upon wetting of the soils. Some of our recent investigations indicate that the compression that occurs upon wetting-induced collapse may be inadequate to mitigate liquefaction and corresponding dynamic settlement potential of these soils. An investigation was carried out of a collapsible soil site in Southern California on alluvium that had become saturated, and collapsed significantly in response to rising groundwater table. The groundwater table had risen primarily due to irrigation associated with a nearby golf course. The average (corrected) SPT values of the saturated alluvium were only about 8 to 12. This is after collapse settlements large enough to cause major ground cracking and structural damage were already realized. In this same alluvium the prewetting SPT values were substantially higher than the post-wetting values because the soils in their natural dry state exhibit relatively high shear strength due to soil suction and other cementation.

Mitigation and site improvement

Mitigation measures may be broadly defined as any actions or designs that lessen or solve collapsing soil problems. In this context, soil improvement techniques are a subset of mitigation measures generally, although soil improvement is needed and used for many problems other than collapsing soils.

The best technique or combination of mitigation methods for a collapsible soil site depends on several factors, including (a) the timing of the discovery of soil collapsibility – whether during investigation, during construction, or after structures are in place (b) the primary source of the driving stress – overburden or structural load (c) the depth range of the collapsibility problem – usually deposits are simply classified as shallow or deep (d) the probable source(s) of wetting, and (e) mitigation costs – including, particularly in the USA, the cost of risk/liability.

Mitigation measures have been summarized and described by several authors (Beckwith, 1995, Clemence and Finbarr, 1981, Evstatiev, 1995, Houston and Houston, 1989, Pengelly, et al., 1997, Rollins and Rogers, 1994, and Turnbull, 1968). The following list shows the categories into which these techniques may be placed.

- Removal of volume moisture-sensitive soil
- Removal and replacement or compaction
- Avoidance of wetting
- Chemical stabilization or grouting
- Prewetting
- Controlled wetting
- Dynamic compaction
- Pile or pier foundations

- Differential settlement resistant foundations

In classifying deposits of collapsible soil as shallow or deep, several factors come into play. If collapsible soils exist to only a shallow depth, then of course the deposit must be called shallow. If the design engineer is convinced that the probability of wetting beyond a shallow depth is acceptably small, then it may be appropriate to classify the deposit, or the “problem,” as shallow. In a case where the collapse potential under overburden stress alone is small to negligible, the loads applied by the structure become paramount. If these structural stresses dissipate to small values at shallow depth, then this problem can likewise be classed as shallow.

When the collapsible soils are identified prior to construction, removal and/or recompaction is commonly chosen and can be very effective. Unless the depth of soil removal is shallow to moderately shallow, this option is not likely to incur the least initial cost. However, collapsible soil deposits up to 6 to 10 m deep are frequently removed and recompacted in southern California. Care must be taken to ensure that the recompacted soil has negligible collapse potential. Before compaction specifications are finally selected, a test program should be undertaken wherein representative samples of the fill material are initially compacted to a range of densities and water contents and a range in confining pressures and then subjected to wetting. The response-to-wetting results are then used to select compaction specifications. For thicker, deeper fills more than one set of specifications may prove desirable, with higher minimum density being used for the deeper zones of the fill.

Deep dynamic compaction is rather widely used in certain parts of the USA. The adjective “deep” is appropriate because the depth of soil improved is considerably greater than when only compactive rollers at the surface are used. However, the compaction process is expected to be effective only to about 5 m depth, with the greatest improvement in the upper 3 m (Rollins and Rogers, 1994). If sufficiently large weights are dropped from sufficiently great heights, then the effectiveness can extend somewhat deeper (Pengelly, et al, 1997). It should be noted that when effectiveness to 6 m is projected, for example, the soil improvement at 6 m would generally be minimal and would transition to being very substantial at about 2 m.

Grouting for soil improvement is also used frequently in certain parts of the USA and in other countries (Pengelly et al., 1997). Grouting purports to provide soil improvement by one or more of three mechanisms. First, if the grout viscosity is low enough and the soil permeability is high enough, the grout simply permeates into the soil and greatly strengthens and stiffens it. Second, for higher viscosity grout and lower permeability soil, the grout bulb compresses and densifies the surrounding soil. For this case the process is called compaction grouting. The third mechanism can be called soil reinforcement. Whether permeation or compaction occurs, if enough grout is put into the ground at enough locations and depths, then the stiff,

grouted zones will tend to carry the overburden and structural loads and the remaining loose, moisture-sensitive zones between the grout bulbs will be unloaded to some extent. A notable advantage of grouting is that it can be used after a structure is already in place. Mudjacking can even be used in some cases to re-level or partially re-level a tilted slab or footing. A primary disadvantage of grouting is the typically high initial cost, which is usually significantly higher than other alternatives.

The use of piles, piers, stone columns, or soil piles can provide mitigation, provided that the load is transferred below the collapsible soil or the depth of wetting. The cost of deep foundations is usually on the high side of average for mitigation alternatives.

Prewetting has been used as a mitigation alternative in cases where the collapse problem is recognized prior to construction. Its use was quite frequent during the period three to five decades ago, but during the last decade or so it has been selected much less frequently in the U.S.A. Water is introduced through some combination of ponds or trenches at the surface and boreholes. If the collapsible soil deposit is deep and the collapsible soils extend to the surface, a combination of methods may be indicated. For example, the deeper layers could be densified by prewetting through boreholes, using overburden pressure to drive the collapse. For the shallow layers where overburden provides insufficient stress, a temporary surcharge fill may be used, or another method such as deep dynamic compaction or removal and recompaction may be used to ensure densification of the shallower layers. When prewetting has been used, it has been found to be a moderately low cost alternative.

In addition to employing the best mitigation technique available, it is good practice to design differential settlement resistant foundations and to take measures to minimize wetting of the collapsible soils. The best precautions against wetting (Houston, 1996) can be expected to reduce the probability of deep wetting, but not to zero.

If the structure is already in place before the severity of the collapsing soil problem is recognized and some tilting or damage has occurred, the following measures can be considered for mitigation: (1) controlled wetting, wherein water is introduced in a carefully-monitored manner so as to correct the tilt (Bally and Oltulesen, 1980), (2) chemical stabilization, including grouting and/or mudjacking, and (3) underpinning. All three methods involve some risk of additional damage during the remediation process. Therefore, considerable skill and care must be utilized in each case. An advantage of underpinning is that precedent dates back perhaps centuries. A disadvantage of underpinning is its high cost, typically comparable to that of grouting.

Controlled wetting has very few precedents; however, available data indicate that the cost of implementing this method can be quite low. As a part of a large research project the authors and colleagues have supervised the performance of a controlled wetting experiment of about two years duration, which can be briefly described as follows. A reinforced concrete slab, $6\text{ m} \times 6\text{ m} \times 0.22\text{ m}$, was constructed in

collapsible soil in Benson, Arizona. A wooden box on the slab was filled with soil to a height of about 2.5 m. Differential wetting under the north half of the slab was imposed and a tilt to the north of about 15 cm was intentionally achieved. Then differential wetting through eight separately-controllable trenches around the slab was commenced, in an effort to correct the tilt. It was possible to correct the tilt to less than 3 cm in the next two weeks. Thereafter, wetting was continued, adjusting the flow to the various trenches so as to maintain the slab as level as possible. The maximum tilt of the slab never exceeded 5 cm during subsequent wetting settlement. The total final settlement was about 50 cm. There were two aspects of this result that were encouraging. First, it was possible to re-level the slab and maintain it fairly level during subsequent, substantial settlement – thereby eliminating the future collapse potential of the soil. Second, it was possible to train the property owner of the test site to take readings and adjust the flow rates to the trenches. This minimized the number and frequency of required visits to the site by the research personnel during the controlled wetting phase. Overall, this exercise in controlled wetting was regarded a success.

It is impossible to evaluate all of the relative merits of the various alternatives for collapsible soil site mitigation without considering risk. Particularly in the U.S.A., concern about possible future litigation/liability has become a driving force in the decision making process. This condition is not limited to collapsible soil problem mitigation, but is pervasive throughout geotechnical practice. In other countries with different legal systems and different laws, concern over litigation may not be such a major issue. A case in point is as follows:

A recently completed survey of arid soil engineering practice in the southwestern U.S.A. revealed that, although many alternatives for collapsible soil problem mitigation are available, practitioners in southern California have gradually migrated to the use of essentially one method: removal and recompaction. There could be two explanations for this trend – (1) It has become the general consensus of geotechnical engineers in this region that removal and recompaction is the best method, all factors considered, for practically every project, or (2) Even though an alternative method may appear less expensive and generally viable, it may have few relatively recent precedents, particularly in the local and nearby regions. With very few precedents, an engineer may be reluctant to use the method out of concern over possible litigation, if problems develop with time. With a scarcity of precedents there may be legitimate concern about whether or not the method in question would be construed to fall within the “standard of practice.” Which of these two explanations more accurately describes the situation is not immediately apparent. Thus the decision to use the same procedure that everyone else uses may or may not represent good engineering, although it may well represent good business. Whatever the advantages of this approach, it has the drawback of doing very little to advance the state of the practice.

The most easily defensible approach to this decision-making process is as follows: The engineer should choose mitigation methods designed to minimize the owners

expected total life cycle project costs. These total costs would include geotechnical investigations, testing, analysis and design costs plus construction costs, estimated maintenance costs, and expected costs that can be assigned to risk/liability. Although this approach is simple in concept and difficult to debate, the methodology for performing the minimization is not well established. In particular, the required statistical methods, including the assessment of the probability of failure for each alternative, need some work.

As a final comment on the liability issue, it can be said that geotechnical engineers in the U.S.A. feel that they have little or no control over the extent to which litigation concerns have dominated their practice. However, it should be noted that geotechnical professionals do exert some influence over how narrow or how broad the standard of practice is construed to be through their publications and testimony as expert witnesses.

Summary and conclusions

Geologic and geomorphologic information can be very helpful in anticipating the location of collapsible soil deposits. However, collapsibility should be confirmed by direct response to wetting tests, either laboratory or *in-situ*. The advantage of these tests over indirect correlations is that they provide not only identification data but also quantitative data for later assessment of settlements.

The most challenging task of collapsible soil engineering is that of predicting the extent and degree of future wetting. Field data indicate that typical silty and sandy arid soils rarely become thoroughly wetted to 100% saturation by downward infiltration of water. However, rising groundwater typically does wet soil thoroughly.

Whether response to wetting tests are performed in the laboratory or *in-situ*, it is possible to express the results in terms of stress versus strain for the wetted condition. For a given site or an identifiable layer of soil at a site, this stress-strain curve will usually exhibit significant width, due primarily to soil heterogeneity. It is recommended that a design curve be chosen about halfway between the average and the lower limit of the band. This design curve can then be used to estimate strains for a given combined structural and overburden stress. An integration of expected strains for a vertical profile yields an estimate of collapse settlement.

By assuming that collapse strain can be adequately represented with a normal distribution, selecting an acceptable level of accuracy, and adopting an average value of $COV = 0.3$ from previous research, it is possible to select the number of collapse tests needed to assure the level of accuracy chosen.

When the predicted settlement is intolerably large, one or more methods from a long list of alternatives for mitigation may be chosen. The best mitigation method depends on numerous factors including the timing of mitigation, source of loading, source of wetting, and cost.

Acknowledgements

This material is based upon work supported by the National Science Foundation under Grant No. BCS-9307787 and Grant No. CMS-9612073. Any opinions, findings, and conclusions or recommendations expressed in this material are those of the authors and do not necessarily reflect the views of the National Science Foundation.

References

- Bally, R. and Oltulescu, D. (1980) Settlement of Deep Collapsible Loessial Strata Under Structures Using Controlled Infiltration. In *Proceedings of the 6th Danube-European Conference*, SMFE, Varna.
- Beckwith, G. (1995) Foundation Design Practices for Collapsing Soils in the Western United States in Unsaturated Soils. In *Proceedings of the First International Conference on Unsaturated Soils*, E.E. Alonso and P. Delage (eds), Vol. 2, Paris, September 6–8. Balkema, Rotterdam.
- Bell, F.G. (1992) Engineering Properties of Soils and Rocks, 3rd edition. Butterworth-Heinemann Ltd., Oxford.
- Clemence, S. and Finbarr, A. (1981) Design Considerations for Collapsible Soils, *J. Geotech. Engr., ASCE*, **107**(3).
- Conciani, W., Futai, M.M. and Soares, M.M. (1998) Plate Load Tests with Suction Measurements, in Problematic Soils, *Proceedings of the International Symposium on Problematic Soils*, E. Yanagisawa, N. Moroto, and T. Mitachi (eds), Vol. 1., Is-Tohoku, Japan, 28–30 October, A. A. Balkema, Rotterdam, pp. 301–304.
- Evstatiev, D. (1995) Design and Treatment of Loess Bases in Bulgaria.. *Genesis and properties of collapsible soils. NATO ASI Series C: Mathematical and Physical Sciences*. Vol. 468, Kluwer Academic Publishers, The Netherlands.
- Ferreira, S.R.M. and Lacerda, W.A. (1998) Volume Change Measurements in Collapsible Soils in Pernambuco Using Laboratory and Field Tests, in Problematic Soils. In *Proceedings of the International Symposium on Problematic Soils*, E. Yanagisawa, N. Moroto, and T. Mitachi (eds), Vol. 1., Is-Tohoku, Japan, 28–30, October. A. A. Balkema, Rotterdam, pp. 289–292.
- Fookes, P.G. and Parry, R.H.G., eds. (1994) Engineering Characteristics of Arid Soils, In *Proceedings of the First International Symposium on Engineering Characteristics of Arid Soils*, London, U.K., July 6–7, 1993, A. A. Balkema, Brookfield, VT.
- Fredlund, D.G. and Xing, A. (1994) Equations for the soil-water characteristic curve, *Canadian Geotechnical Journal*, **31**, 521–532.
- Fredlund, M., Wilson, G.W. and Fredlund, D.G. (1998) Estimation of Hydraulic Properties of an Unsaturated Soil Using a Knowledge-Based System, In *Proceedings of the Second International Conference on Unsaturated Soils*, Vol. 1, Beijing, International Academic Publisher, Beijing.
- Govil, S. (1992) Characterization of Dynamic Shear Strength of Soils. *PhD Dissertation*, Arizona State University, Department of Civil and Environmental Engineering, Tempe, AZ.
- Houston, S., Houston, W. and Spadola, D. (1988) Prediction of Field Collapse of Soils due to Wetting, *J. of Geot. Engineering Division, ASCE*, **1**, pp. 40–58.
- Houston, S. and El-Ehwany, M. (1991) Sample Disturbance of Cemented Collapsible Soils. *J. of Geot. Division, ASCE*, **117**(5), 731–752.

- Houston, S.L. (1996) State of the Art Report on Foundations on Unsaturated Soils. Part One: Collapsible Soils, in Unsaturated Soils, *Proceedings of the First International Conference on Unsaturated Soils*, E.E. Alonso and P. Delage (eds), Vol. 3, Paris, Sept. 6–8, Balkema Press.
- Houston, S.L. and Houston, W.N. (1989) State-of-the-practice Mitigation measures for Collapsible Soil sites. In *Proceedings of the Foundation Engineering Congress, ASCE*, Evanston, Ill., June 25–29.
- Houston, S.L. and Houston, W.N. (1997) Collapsible Soil Engineering. *Unsaturated Soil Engineering Practice, Geotechnical Special Publication No. 68, ASCE*, (edited by Houston and Fredlund).
- Houston, S.L., Houston, W.N., Febres, E. and Chen, Chunlin (1999) Site Variability for Collapsible Soil Deposits. *J. of Geotech. and Geoenvironmental Engr., ASCE*, submitted.
- Houston, S.L., Mahmoud, H. and Houston, W.N. (1995) Down-hole Collapse Test System. *J. of Geotech. Engr., ASCE*, **121**(4).
- Lin, Z. (1995) Variation in Collapsibility and Strength of Loess with Age. *Genesis and properties of collapsible soils. NATO ASI Series C: Mathematical and Physical Sciences*, Vol. 468, Kluwer Academic Publishers, The Netherlands.
- Mahmoud, H., Houston, W. and Houston, S.L. (1995) Apparatus and Procedure for an In-situ Collapse Test. *ASTM Geot. Testing J.*, **121**(4).
- Mitchell, J.K. and W. Houston (1969) Properties and Interrelationships in Sensitive Clays, *Journal Soil Mechanics and Foundations Div., ASCE*, **95**(SM4), July.
- Pengelly, A., Boehm, D., Rector, E. and Welsh, J. (1997) Engineering Experience with in Situ Modification of Collapsible and Expansive Soils. *Unsaturated Soil Engineering, ASCE, Special Geotechnical Publication*.
- Rampino, C., Mancuso, C. and Vinale, F. (1998) Swelling/Collapse Behaviour of a Dynamically Compacted Silty Sand, in Problematic Soils. In *Proceedings of the International Symposium on Problematic Soils*, E. Yanagisawa, N. Moroto and T. Mitachi (eds), Vol. 1., Is-Tohoku, Japan, 28–30 October, A. A. Balkema, Rotterdam, pp. 321–324.
- Rollins, K. and Rogers, G.W. (1994) Mitigation Measures for Small Structures on Collapsible Alluvial Soils, *J. Geot. Engr., ASCE*, **120**(9).
- Turnbull, W. (1968) Construction Problem Experiences With Loess Soils, *Hwy. Research Record*, No. 212.
- Zapata, C.E. (1999) *Uncertainty in Soil-Water Characteristic Curve and Impacts on Unsaturated Shear Strength Predictions*. Ph.D. Dissertation, Arizona State University, Tempe, United States.



The extent of soil desiccation near trees in a semi-arid environment

D. A. CAMERON

*Discipline of Civil Engineering, University of South Australia, Mawson Lakes Campus,
Mawson Lakes Boulevard, Mawson Lakes SA 5095, Australia*

(Received 17 August 2000; revised 27 December 2000; accepted 1 May 2001)

Abstract. Australian standards provide guidance on classification of sites for ground movement and the subsequent design of shallow footings for residential buildings on expansive soils. It does not however provide any guidance on how the drying effects of vegetation might be incorporated in the footing design. Despite there not being a prescriptive Standard for designing for the effects of trees, engineers have been pressed by the community to allow for the extra soil drying. Some rules of thumb have been promoted and empirical design suction changes have been adopted. The design suction changes depend on the relative proximity of the tree to the building, as well as the site classification level and whether or not a single tree or group of trees is to be considered. Although it is understood that different species develop different root systems and so affect the soil differently, tree species is not a parameter that is required in the models.

The primary purpose of this paper is to present measured suction profiles pertaining to urban sites in a semi-arid climate (Adelaide, South Australia). All sites contained Australian native eucalypts or 'gum' trees. Generally the data were gathered as part of site investigation for footing failures—excessive movement and cracking, rather than structural failure. At least two suction profiles were determined for each site, close to and well away from the vegetation. A preliminary model is proposed to account for the drying settlement caused by trees.

Key words: design, expansive soil, soil drying, suction, trees

1. Current Knowledge

1.1. GENERAL EFFECT OF TREES ON CLAYS

It is generally accepted that vegetation is unable to draw moisture from the soil at high levels of soil desiccation or suction. The limit at which this occurs for a particular species is termed the wilting point and has been reported to reach values of total suction of 1.55–3.1 MPa (McKeen 1992).

The way that roots respond to soil water depletion depends on the hardiness of the plant. The roots may extend into new areas where there is greater water availability, or the vegetation may die, or the plant become dormant until water becomes available. All these possibilities are dependent on the species of vegetation.

Much of what civil engineers know about trees is based on indirect evidence. For example, the aggressiveness of different root systems of trees near water pipes was revealed in studies of root chokes by the Engineering and Water Supply Depart-

ment (South Australia) in Adelaide. CSIRO (Australia) published information sheets on potential damage to houses by trees, which was based on this information. It was assumed that roots, which travelled long distances to get moisture from pipes, would potentially be the most treacherous plants to have on a suburban allotment. Most people would find little argument with the species that were revealed as potential threats to house footings. It was also assumed that climate differences around Australia would make little difference, although it is well known that the extent of a tree root system is greatly affected by water availability. For example, if water is plentiful (but not excessive), the tree root system is contained within a relatively small volume (Yeagher 1935).

Soil moisture data have been collected about trees in quite different environments, which generate different patterns of root development. It is contended that the most useful data for footing design will come from studies of desiccation in the urban environment. Investigations of damaged buildings can be fruitful, but require careful engineering judgement. The adequacy of the footings for the site classification and the structure must be incorporated into the assessment, as well as the possibility of other contributing factors such as plumbing leaks, over-watering of gardens, or previous use of the site. A number of researchers have simply equated a measure of building distress (crack width, differential movement) to the proximity of the vegetation to the building (Tucker and Poor 1978; Cutler and Richardson 1981; Wesseldine 1982; Cameron and Walsh 1981).

1.2. SPECIES, PROXIMITY AND SOIL DESICCATION

Many authors have used the concept of proximity of the vegetation in their work. Proximity can be expressed by the ratio of the minimum horizontal distance, D , between the base of the tree and the building perimeter, to the height of the tree, H . The ratio, $D:H$, may be expressed as a range for a group of trees. Alternatively the proximity of the trees can be based on the average tree height within the group and the distance of a measuring point from the nearest tree trunk, $D:H_{av}$.

Bozozuk (1962) in Canada monitored shrinkage settlement with depth and distance away from a row of elm trees, 17 m high. He was able to demonstrate that the overall ground movement and the depth of the movement decreased with increasing $D:H_{av}$ ratio. The elm trees were seen to have most effect close to the trees, at ratios less than 0.5 or so.

Biddle (1983) conducted studies of soil moisture deficits around specimens of certain tree species in open grassland in the UK. The species included poplar, horse chestnut, silver birch, lime and a cypress. Five different clay soil profiles were investigated at locations in Cambridge, Milton Keynes and London. Soil moisture was monitored with a down-hole neutron moisture meter to a maximum depth of 4 m. Generally it was seen that the lateral extent of drying was contained within a radius equal to the height of the tree. However the extent of drying, both horizontally and vertically, appeared to be species dependent. Poplars caused drying

to a radius of over 1.5 times the tree height and caused the deepest drying close to the trees, probably to a depth in excess of 4 m. Other species dried the soil to a maximum depth of 2 m. The cypress produced the smallest zone of drying within the soil.

Richards et al. (1983) studied total soil suction regimes near groups of three different species of trees in parkland in Adelaide, South Australia. The tree groups were described as eucalypts, casuarinas and pines, with average heights of 17, 13 and 10 m and consisting of 13, 5 and 25 trees in each group, respectively. Boreholes for soil sampling were made progressively away from the tree groups. It can be deduced from this work that the eucalypts had the greatest drying effect while the pines had little effect on the surrounding clay soil. For the eucalypt site, the total soil suction reached 3.5 MPa at depth below the group, and was not lower than 2 MPa throughout the exploration depth of 8 m. The radial extent of near-surface drying appeared to be $1.3 H_{av}$. The depth of drying decreased with distance away from the group.

The differences in total suction across a site are more important than the absolute values of suction. As pointed out by Richards et al. (1983), soil salinity affects the suction values from one site to another. Where water tables are quite deep and significant vegetation is absent, it is generally accepted that soil suctions become relatively constant at depth. This equilibrium suction value, u_{eq} , relates to the suction expected under the centre of a large paved area in the same environment (Richards and Chan 1971). Where practical, this value should be used to define suction differences across a site due to trees. As a soil's response to suction change (soil reactivity) is defined in terms of the change of the logarithm of suction, the suction change due to trees, Δu_{tree} , should be similarly expressed. For the eucalypt site the deep suction value (or u_{eq}) away from the trees ($D:H_{av} > 1.5$) averaged approximately 1.7 MPa. Consequently the logarithm of the difference in total suction, Δu_{tree} , was equal to 0.31.

1.3. SPECIES AND PROXIMITY AND BUILDING DAMAGE

Probably the most substantial research into species was conducted by Cutler and Richardson (1981). They reported on the investigations of 2600 cases of building damage in the UK. Trees implicated as a cause of the damage were recorded and their proximity to the building noted. A database of species was subsequently established and was reviewed to find the maximum distance for a tree to 'cause' damage in 75% of the cases recorded for that species. The greater the distance relative to the height of the tree ($D:H_{75\%}$), the more dangerous the tree.

Unfortunately the information has had little impact on Australian practices owing to differences in climate, differences in range of tree species and different sensitivities to damage between homeowners in the UK and Australia. In fact, the degree of damage was not considered in Cutler and Richardson's report and may have often been insignificant in the Australian context. Furthermore, the usual construction in the UK is cavity brick walls on strip footings, which is much less tolerant to

movement than masonry veneer walls on a stiffened raft, the dominant construction style in Australia.

In the USA in Texas, Tucker and Poor (1978) studied a housing estate, which was in the process of being demolished because of the extent of damage to the houses (masonry veneer walls on slabs). Tree species were mulberry, elm, cottonwood and willows. Differential movements were measured and compared with D:H ratios. The results of the study revealed an average background movement of approximately 50 mm due to site reactivity, which was apparent at D:H ratios above two. The data strongly indicated that tree effects were significant at D:H values greater than one. Differential movements in excess of 120 mm were observed where trees were close to the building.

In New Zealand, Wesseldine (1982) demonstrated the influence of the silver dollar gum (*e. Cinerea*) on houses. A plot of the ratio D against H for damaged houses indicated a threshold value of 0.75 for single trees to cause damage and between 1 and 1.5 for groups of these trees. The extent of damage was not included in the correlation.

In Melbourne, Victoria, studies of damaged masonry veneer houses on strip footings (Holland 1979; Cameron and Walsh 1981) drew the conclusion that significant damage (cracking in walls greater than 3 mm) was only likely if the proximity of a single tree was less than or equal to 0.5 H.

From Adelaide in South Australia, Pile (1984) reported building distortions and suction profiles to a maximum depth of 4 m for eight sites, which were affected at least in part by trees. The approach taken by Pile is similar to the approach taken in this paper, however some deeper suction profiles are provided.

Silvestri et al. (1992) studied movements over three years of two damaged buildings in Montreal, Canada, and the associated patterns of soil movements, particularly around rows of maple trees adjacent to the buildings. The more severely damaged building was influenced also by two catalpa trees. This work was unique in that investigations of building distress were allowed to continue over a significant period of time, allowing the installation of three or four neutron moisture meter access holes at each site and the subsequent monitoring of soil moisture. The access holes were taken to a depth of almost three metres.

Volumetric moisture contents were inferred from measured moisture count ratios and the authors, with some judgement, were able to correlate the movements of the buildings with the measured variations of volumetric moisture content. Soil suctions were not determined.

2. Total Suction Changes in the Built Environment

2.1. SUCTION MEASUREMENTS

Suction profiles for four sites are given in Figures 1–5 and a summary of all the data is presented in Table 1. Generally these data have been obtained during investi-

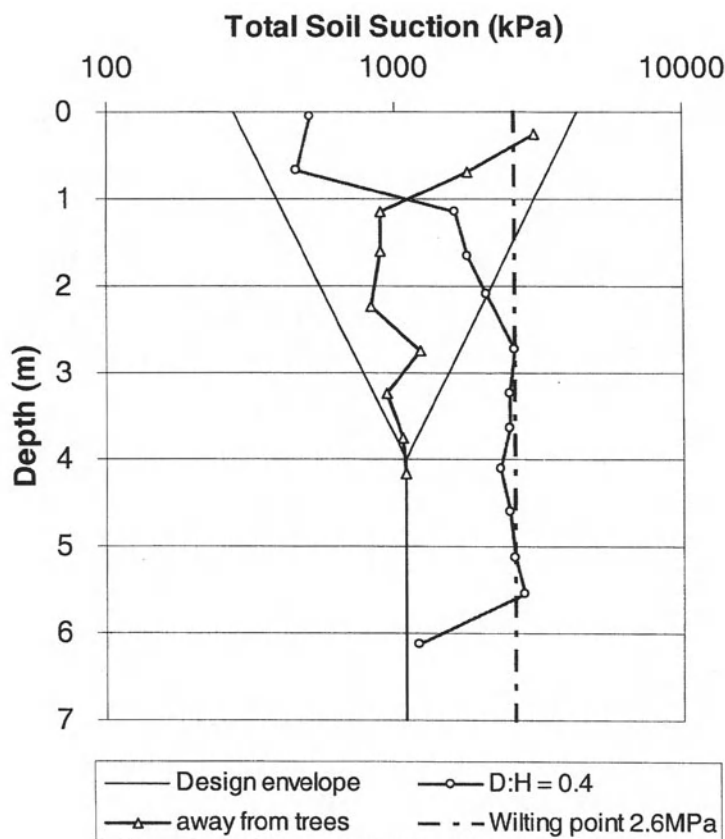


Figure 1. Total suction profiles near a row of trees of mixed species (Ingle Farm, Adelaide, South Australia).

gations into building damage in Adelaide; one case study originates from Melbourne in the State of Victoria. All suctions reported in this paper are total suctions, determined by measurement of relative humidity in a small air space above the soil in a controlled laboratory environment to Australian Standard AS1289 2.2.1 (1995). In all cases investigated by the author, the relative humidity established by interaction with the soil, was measured with a Wescor C52 chamber and hygrometer. The hygrometer enables measurement of the dew point temperature, which is directly related to the relative humidity and hence the total soil suction.

Total suction profiles are provided at a location between the tree/s and the structure, and for a location remote from the tree/s. The trees were usually native Australian species, often eucalypts, but details on species of eucalypt were generally not available. Most of the information is for groups of trees.

The suction profiles provide a snapshot of relative differences in soil moisture condition about a site at the time of taking the soil samples. In some instances,

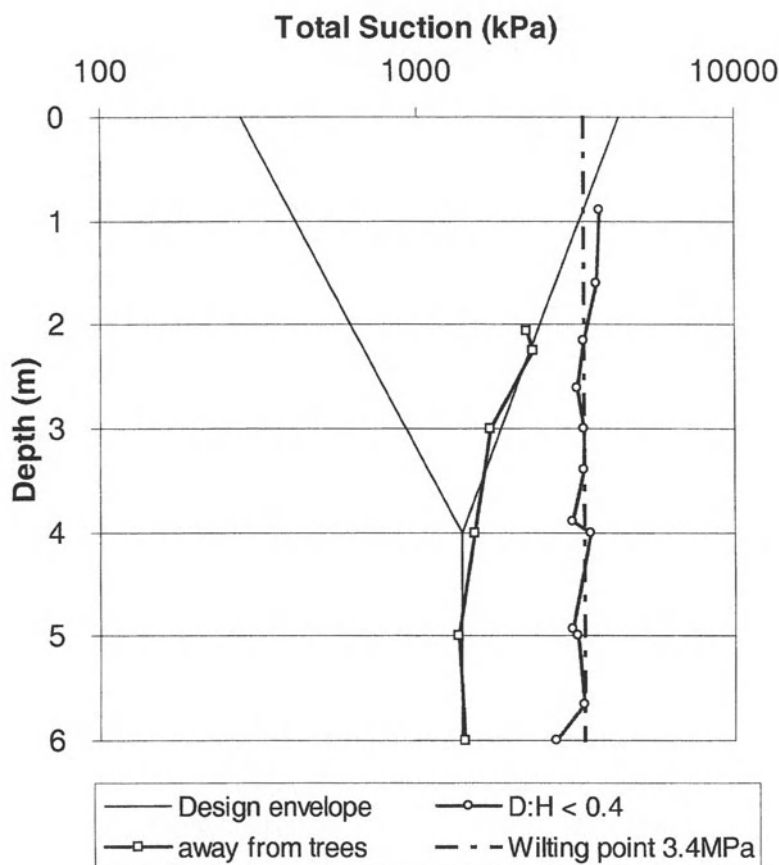


Figure 2. Total suction profiles near a row of large eucalypts (Klemzig, Adelaide, South Australia).

it was clear that other factors contributed to the distortion of the building. As it was the practice to try to get soil suction data near the relative high and low spots on the building, suctions near the high spot were on occasions seen to be unusually low. Often these locations coincided with heavily watered gardens or ponds.

As the suction data were tied to the time of the investigation, which may not have coincided with the peak of the building distortion, some seasonal climatic influences may have affected the first one metre or so of the soil moisture profile.

For the purpose of design of footings in Adelaide, ground movements in the absence of vegetation are estimated on the basis of design suction changes representative of the range of wet to dry profiles expected for the site. The suction change is defined as a change of the logarithm of suction. Regional climate dictates the design suction change profile and for Adelaide, which enjoys a semi-arid climate, the design surface suction change, Δu_o , is 1.2, decreasing linearly to zero at a design

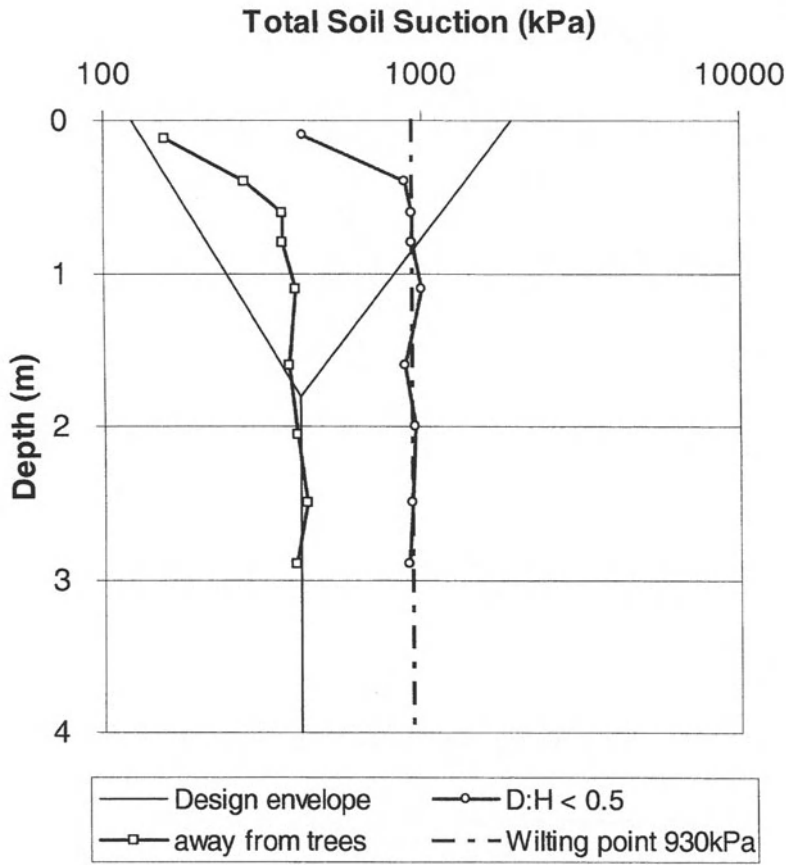


Figure 3. Total suction profiles near a row of large eucalypts (Williamstown, Victoria).

depth of suction change, H_s , of 4 m (Standards Australia 1996). The linearity is a convenient design simplification.

It should be noted that seasonal suction changes in Adelaide below grassed open land have been shown to occur to depths of between 1.5 and 2 m (Mitchell and Avalle 1984), far less than the design depth of suction change of 4 m in the same metropolitan area, in an urban environment. Deeper suction changes occur as a consequence of the environmental change arising from the imposition of buildings, pavements and drains.

The figures of suction profiles presented in this paper have a design suction envelope superimposed. The deep suction value was judged from the data to locate the base of the envelope and the surface suctions were postulated to give the wet and dry extreme suction profiles. Linearity of the extreme suction profiles was assumed.

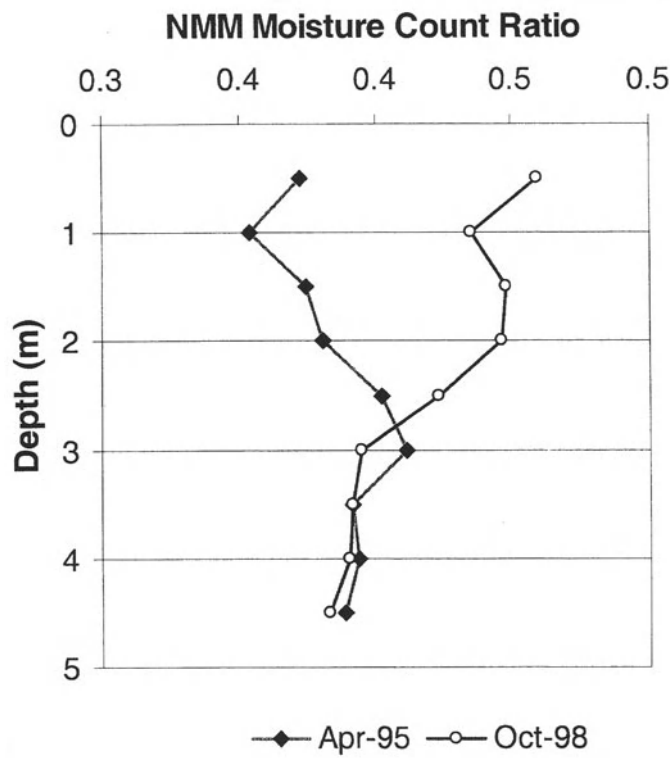


Figure 4. Neutron moisture meter count ratios near a roadside plantation of native trees (Hallett Cove, South Australia).

In Figure 1, the suction profiles relate to a row of trees consisting mainly of eucalypts. The profile close to the tree, referred hereafter as the ‘dry suction profile’, was wetter in the top one metre than the ‘wet suction profile’. Presumably attempts had been made by the homeowners to water the ground in the vicinity of the trees. The dry suction profile at D:H of 0.4 lay outside the design envelope, below a depth of 2 m. At greater depths, suction remained relatively constant at a value of 2.6 MPa down to 5.7 m. At a depth of 6.1 m, the suction approximated u_{eq} , which was judged to be 1.1 MPa. The logarithm of the suction difference, Δu_{tree} , is therefore 0.37.

It is contended that the almost constant value of suction at depth near vegetation represents the wilting point for the tree species, u_{wp} . A wilting point line has been superimposed on each of the figures. When compared with the design envelope for the site, it can be seen that tree root systems are unlikely to be active close to the soil surface in dry periods. Moreover it indicates that trees cause problems by generating shrinkage of clay soils at depth in the soil profile, greater than the assumed depth of normal suction changes for a site.

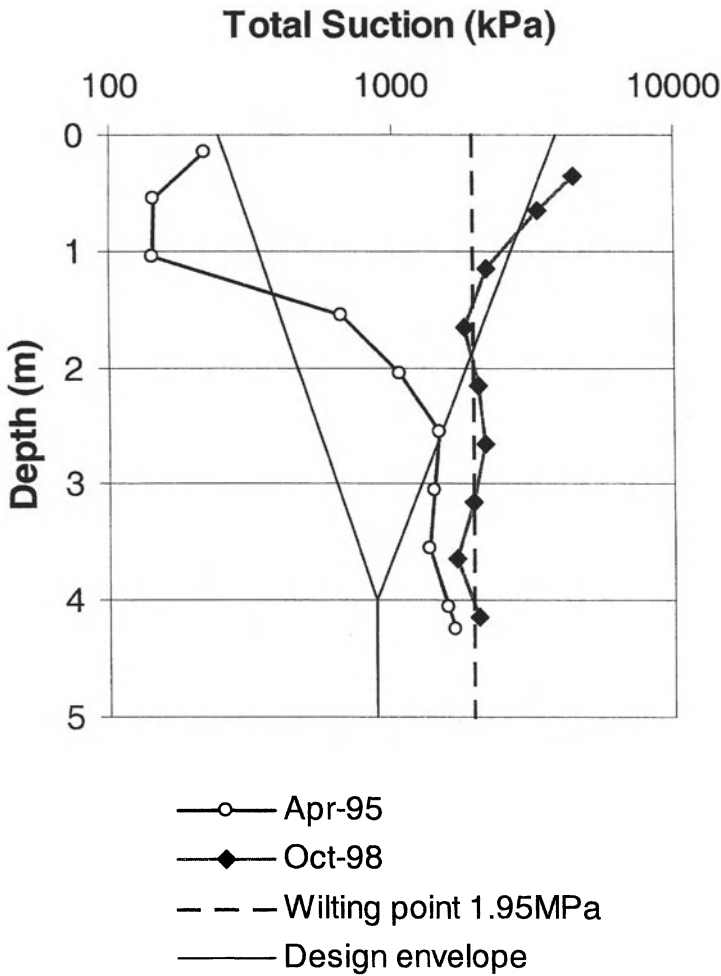


Figure 5. Total suction profiles near a roadside plantation of native trees (Hallett Cove, South Australia).

Figure 2 provides another example for a row of eucalypts. The dry profile was located at a D:H of less than 0.4. The values for u_{eq} , u_{wp} and Δu_{tree} are $1.4 \log_{10}$ MPa, $3.4 \log_{10}$ MPa and $0.4 \log_{10}$ MPa, respectively. Below 0.9 m, the suction values for the dry profile remained relatively constant down to a depth of 5.7 m and seemed to be heading towards u_{eq} by the exploration depth of 6 m.

Figure 3 provides the data for another row of eucalypts, but in another climatic region, Melbourne in Victoria. Although the design envelope is quite different, being only 1.8 m deep, the principles discovered at sites in Adelaide are evident at this site. The wilting point and equilibrium suction values are obvious. The values for u_{eq} , u_{wp} and Δu_{tree} are $0.42 \log_{10}$ MPa, $0.93 \log_{10}$ MPa and $0.35 \log_{10}$ MPa, respectively.

Table 1. Summary of suction data

Site	Trees (H)	D:H	u_{eq} (MPa)	u_{wp} (MPa)	Δu_{tree}^\dagger (log ₁₀ MPa)
Broadview, SA	Gum (9 m)	< 0.5	0.98	2.2	0.35
Greenacres, SA*	<i>e. Torquata</i> (8.3 m)	0.4–0.7	1.15	1.95	0.23
Greenacres, SA*	<i>e. Mannifera</i> (19.3 m) and 2 smaller gums	0.6	1.15	1.95	0.23
Ingle Farm, SA	Row of eucalypts (8 m)	1.5	1.1	1.95	0.25
Ingle Farm, SA	Row of eucalypts (10 m)	0.4	1.1	2.6	0.37
Klemzig, SA	Row of mature eucalypts	< 0.5	1.38	3.4	0.39
Hallett Cove, SA	Native plantation	0.1	0.87	1.95	0.35
The Levels, SA	Native plantation	< 0.5	0.98	2.45	0.35
Williamstown, Vic.	Row of gums	< 0.5	0.42	0.93	0.35

*Data from Jaksa (1998).

$$^\dagger \Delta u_{tree} = \log_{10} \left(\frac{u_{wp}}{u_{eq}} \right)$$

Drying is deeper than the depth of exploration of 3 m, which was limited by the equipment available on a tight residential site.

A different type of site is represented by Figures 4 and 5. The site was located at Hallett Cove (SA) and was part of a road roughness monitoring project, undertaken with Transport SA. A down-hole neutron moisture meter was used to evaluate moisture changes in the soil with time. Figure 4 provides moisture count ratios taken in the one access borehole in April 1995 and in October 1998. Count ratios varied strongly between the two observation dates to a depth of three metres. Count ratios were high (wet soil) in the spring of 1998, while low counts (dry soil) were taken at the beginning of the monitoring program in the autumn of 1995. To verify these trends, samples were taken nearby to evaluate suction profiles (Figure 5).

The two suction profiles supported the neutron moisture meter data. It would appear that seasonal wetting was influenced by the local site drainage patterns below the road embankment. Run-off could pond below the embankment. The dry suction profile was interpreted to provide a value of u_{wp} of 1.95 MPa. The wet suction profile was slightly wetter than this value below 2.5 m, indicating some deep wetting could occur near the vegetation, seasonally. The equilibrium suction value for this site could not be evaluated directly from these data as all the moisture data was influenced by the trees. Instead it was evaluated from data on nearby sites. A value of 0.87 MPa was estimated giving rise to the suction difference, Δu_{tree} of 0.35.

Table 1 includes data for a further five sites, two being provided by Jaksa (1998). The D:H value applies to the close or dry suction profile.

2.2. OBSERVATIONS

The value of u_{eq} was not always as evident as in the figures, often because of limited depth of exploration. The Williamstown (Melbourne) site was investigated to 3 m or 160% of the normal design depth for the region. All the Adelaide sites were explored to the minimum depth of the design suction change envelope, with depths ranging between 4 m and 6.1 m. The Adelaide sites in Figures 1 and 2 represent the deepest investigations. Only at these two sites was there any indication of a lessening of the drying effect of the vegetation at depth. Future investigations should be taken to a minimum depth of 150% of the normal depth of suction change for the area.

For the Adelaide sites, the equilibrium suction, u_{eq} , varied between 0.87 and 1.4 MPa (average 1.1 MPa). The wilting point suction ranged between 1.95 and 3.4 MPa, similar to the range suggested by McKeen (1992), with the upper limit close to the 3.5 MPa reported by Richards et al. (1983).

Although the Melbourne site had remarkably lower values of both these suction signposts, the suction difference of 0.35 fell within the range of all the data, namely 0.23 to 0.40. The lower end of the range contained data for a single tree and a high D:H ratio (distant vegetation). Ignoring these two sites would tighten the range of Δu_{eq} to 0.35 to 0.4.

3. Design Implications

3.1. DESIGN PHILOSOPHY

Trees increase the dry side of the suction profile at depth and have little influence near the surface in a semi-arid environment. The drying effect extends past the normal design depth of soil movement. The dry suction profile will depend upon the ability of the trees to extract moisture from the soil in line with the wilting point of the vegetation. It has been demonstrated in this paper that the wilting point of trees may be deduced from soil suction data gathered close to the trees. Wilting point may be expressed in terms of total suction, u_{wp} , which forms a dry side boundary to the potential soil suction range in a soil profile, at depth within the soil.

The value of u_{wp} will vary with species, but may also vary with soil salinity, as will the value of u_{eq} . Therefore estimates of the extra shrinkage settlement due to trees should be based on the suction difference, Δu_{tree} . The suction difference is moderate, being approximately a third of the current surface design suction change for Adelaide. However the suction changes persist to greater depths than are currently designed for. Therefore, to estimate movement reliably, site investigations need to be conducted to greater depths than is currently practised to evaluate the soil profile.

3.2. DESIGN GUIDELINES

In the absence of further data, for the purpose of estimating the extra settlement on semi-arid sites similar to Adelaide, containing groups or rows of eucalypts within D:H of 0.6, a design suction change of $0.4 \log_{10}$ MPa, may be adopted to a depth of 6 m. This recommendation is embodied in Figure 6. The diagram pre-supposes that equal wetting and drying can happen across the site to the depth of suction change, H_s , in the absence of vegetation.

Applying this proposal to a uniform soil profile and ignoring lateral confinement effects, a group of trees would potentially generate approximately 50% more movement than the same site without trees. So a reactive site with an estimated design movement of 100 mm would have to cope with 150 mm if landscaping created a garden of Australian native trees.

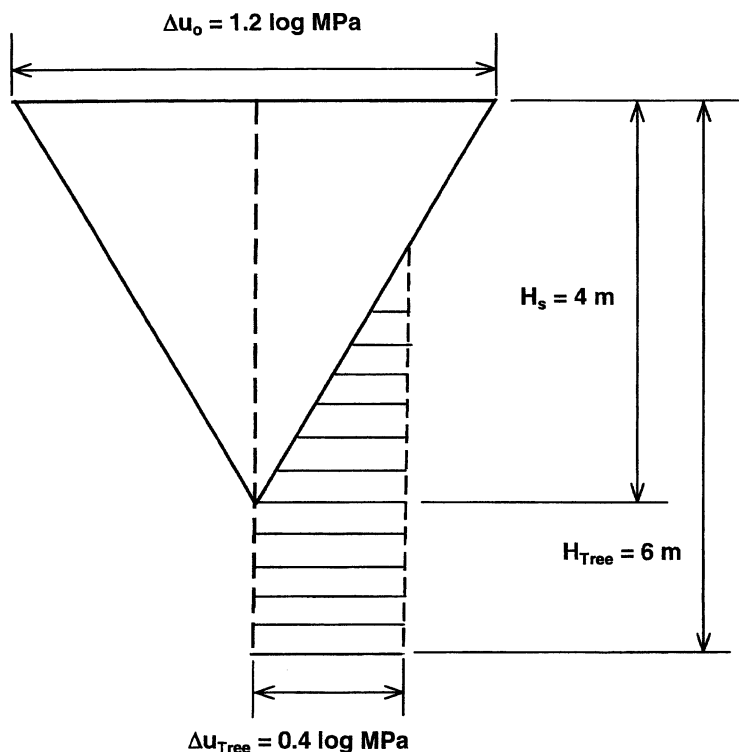


Figure 6. Recommended total suction change profiles for semi-arid sites with groups of trees (D:H < 0.6)

4. Concluding Comments

The cases within this paper generally represent extreme conditions. Much more data are needed over a variety of conditions, which will enable some comprehension of the influences of species, climate and solute suction. Ideally more monitoring of sites should be undertaken, particularly in the urban environment.

Australian eucalypts have often been blamed for shrinkage problems, however some eucalypts like *e. Torquata* are known to be relatively benign. Likewise conifers are believed to pose little threat to the serviceability of buildings. Continued studies should lead to a valuable listing of preferred species in certain environments, including street trees.

The dissipation of movement with distance from vegetation is not well understood and comparative drying potential of single trees to tree groups needs to be better appreciated. Further research along the lines of the work conducted by both Biddle (1983) and Silvestri et al. (1992), extended to other species and climates and including some suction data, would be most welcome. However, research funding has been limited by the complexity of the problem and the length of time over which monitoring of a site is required. If remedies for a damaged building are being sought, building owners are unlikely to tolerate a lengthy monitoring period before their buildings can be rectified.

This paper has suggested an alternative and supplementary approach, based on engineering assessment of damaged structures, which requires the accumulation of soil suction data at the time of the investigation and at greater depths than previously recommended.

References

- Biddle, P.G. (1983) Patterns of soil drying and moisture deficit in the vicinity of trees on clay soils. *Geotechnique*, **33**(2), 107–126.
- Bozozuk, M. (1962) Soil shrinking damages shallow foundations at Ottawa, Canada. *Division of Building Research, NRCC, Canada*. Research paper 163.
- Cameron, D.A. and Walsh, P.F. (1981) Inspection and treatment of residential foundation failures. *Proceedings 1st National Local Government Eng. Conference*, Adelaide, pp. 186–190.
- Cutler, D.F. and Richardson, I.B.K. (1981) *Trees and Buildings*. Construction Press: London.
- Holland, J.E. (1979) Trees—how they can affect footings. *Public Officers Assoc. of Victoria Journal*, pp. 11–14.
- Jaksa, M.B. (1998) The influence of trees on expansive soils. Presentation to Footings Group, SA, IEAust. Adelaide.
- McKeen, R.G. (1992) A model for predicting expansive soil behavior. *Proceedings 7th Int. Conference on Expansive Soils*, Dallas, VI, pp. 1–6.
- Mitchell, P.W. and Avasle, D.L. (1984) A technique to predict expansive soil movements. *Proceedings 5th Int. Conference on Expansive Soils*, Adelaide, pp. 124–130.
- Pile, K.C. (1984) The deformation of structures on reactive clay soils. *Proceedings 5th Int. Conference on Expansive Soils*, Adelaide, pp. 292–299.

- Richards, B.G. and Chan, C.Y. (1971) Theoretical analyses of subgrade moisture under environmental conditions and their practical implications. *Aust. Road Research* **4**(6), 32–49.
- Richards, B.G., Peter, P. and Emerson, W.W. (1983) The effects of vegetation on the swelling and shrinking of soils in Australia. *Geotechnique* **33**(2), 127–139.
- Sivestri, V., Soulié, M., Lafleur, J., Sarkis, G. and Bekkouche, N. (1992) Foundation problems in Champlain clays during droughts. II. Case histories. *Canadian Geotechnical Journal* **29**, 169–187.
- Standards Australia (1996) Residential slabs and footings—construction. AS2870-1996.
- Tucker, R.L. and Poor, A.R. (1978) Field study of moisture effects on slab movements. *ASCE, Journal of Geotechnical Engineering*, **104**(4), 403–415.
- Wesseldine, M.A. (1982) House foundation failures due to clay shrinkage caused by gum trees. *Transactions, Institution of Professional Engineers, N.Z.* March, CE9(1).
- Yeagher, A.F. (1935) Root systems of certain trees and shrubs grown on prairie soils. *Journal of Agricultural Research* **51**(12), 1085–1092.



The effect of antecedent rainfall on slope stability

H. RAHARDJO, X. W. LI, D. G. TOLL and E. C. LEONG

School of Civil & Structural Engineering, Nanyang Technological University, Singapore

(Received 30 January 2001; revised 1 May 2001; accepted 23 May 2001)

Abstract. A case study is presented in order to identify the effect of antecedent rainfall on slope stability for Singapore. A storm in February 1995 (during which 95 mm of rain fell in $2\frac{1}{2}$ h) caused more than twenty shallow landslides on the Nanyang Technological University Campus. Details of the location, size and morphology of the landslides are presented. The antecedent rainfall during the five days preceding the event was significant in causing these landslides since other rainfall events of similar magnitude (but with less antecedent rainfall) did not cause landslides. To further understand the effect of antecedent rainfall, numerical modelling of one of the slope failures is presented. The changes in pore-water pressure due to different rainfall patterns were simulated and these were used to calculate the changes in factor of safety of the slope. The results demonstrate that antecedent rainfall does play an important role in slope stability.

Key words: antecedent rainfall, landslide, numerical modelling, residual soil, seepage, slope stability, unsaturated

1. Introduction

Minor landslides are a common occurrence in many parts of Singapore (Toll *et al.*, 1999). The landslides are mainly shallow slips in residual soils and take place during periods of heavy rainstorms. Such slope failures cause economic loss, although the damage is not as significant as that which occurs in other Southeast Asian countries.

Although the correlation between rainfall and landslides is widely recognised, there has been some debate as to the relative roles of antecedent rainfall (i.e. rain that falls in the days immediately preceding a landslide event) and the triggering rainfall (i.e. rain that falls at the time that the landslide occurs). Experiences from different regions of the world have resulted in different conclusions as to the significance of antecedent rainfall for slope instability (Morgenstern, 1992).

A case study is presented in order to investigate the effect of antecedent rainfall for Singapore. On 26 February 1995 a storm caused heavy rainfall at the Nanyang Technological University (NTU) campus in Jurong, Western Singapore. The rain storm lasted about $2\frac{1}{2}$ h and 94.6 mm of rain fell during this period. An investigation on the following morning showed that more than twenty landslides had occurred on the NTU campus. The locations and morphological features of these landslides were recorded.

However, other heavy storms with a daily rainfall larger than 80 mm had occurred on 15 November 1993, 12 November 1994 and 4 February 1995. On these occasions

no landslides were observed, even though the daily rainfall was of the same order as the storm on 26 February 1995. A study of the antecedent rainfall prior to each of these events allowed the effect of antecedent rainfall to be studied.

To further understand the role of antecedent rainfall, numerical modelling was used to investigate one of the failed slopes on the NTU Campus. The pore-water pressure response to different rainfall patterns was simulated using a finite element seepage program. The effects on the stability of the slope was then investigated using a limit equilibrium slope stability program with the simulated pore-water pressure profiles. In this manner the effect of the antecedent rainfall conditions on the factor of safety of the slope was investigated.

2. Background

This investigation continues a long-term study of landslides at the NTU campus. Pitts (1983, 1985) mapped the occurrence of landslides up to March 1984. He observed spates of landslides associated with periods of heavy rain in November 1982 and January–March 1984. A total of 70 minor landslide events were observed up to this time, with another 9 additional landslides due to reactivation of earlier slips. Chatterjea (1989) mapped the campus again after another heavy rainfall period in January 1987 and observed a further 9 landslides. These studies, together with other major landslides in Singapore, have been reviewed by Toll *et al.* (1999). It is clear from these studies that rainfall has been the dominant triggering event for landslides in Singapore. The periods of December 1978, March 1984, January 1987 and December 1989 (when a significant number of major slips occurred) were periods of very heavy rainfall (>100 mm/day).

Brand (1984) identified some noteworthy studies in which the incidence of landslides has been correlated with the pattern of rainfall. Simple direct correlations have been made for Brazil (Barata, 1969) and Japan (Fukuoka, 1980). More sophisticated correlation attempts are available for New Zealand (Eyles, 1979; Crozier and Eyles, 1980) and Hong Kong (Lumb, 1975; 1979; Brand *et al.*, 1984; Au, 1993; Kay and Chen, 1995).

Brand *et al.* (1984) suggested that the majority of landslides in Hong Kong were induced by localised and short duration rainfall of high intensity. A rainfall intensity of about 70 mm/h appeared to be the critical rainfall intensity above which landslides would occur in Hong Kong. Alternatively, a significant number of failures could be expected in Hong Kong if the rainfall exceeded about 100 mm/day. Murray and Olsen (1988) suggest that a rainfall intensity of 70 mm/h also appeared to have some validity as a criterion for landslides in Papua New Guinea.

Au (1993) suggested that slope failures in Hong Kong typically occurred when the 24 h rainfall is more than 70 mm, and could sometimes occur when the daily rainfall was as low as 50 mm. Major incidents would not be expected to occur until the 24 h rainfall exceeded 110 mm. Murray and Olsen (1988) noted that major slides in Papua New Guinea occurred after 24 h rainfall of 125 mm.

Experiences from different regions of the world have resulted in different conclusions as to whether or not antecedent rainfall has a significant effect on slope instability (Morgenstern, 1992). Brand (1984) suggested that antecedent rainfall was not a significant factor for landslides in Hong Kong. This limited influence of the antecedent rainfall can be attributed to the high permeability of the local soils (Brand, 1992). Pitts (1985) similarly concluded that antecedent rainfall was not thought to be significant for Singapore. However, Tan *et al.* (1987) re-examined Pitts' conclusion and suggested that antecedent rainfall could be significant in affecting slope stability. Chatterjea (1989) came to a similar conclusion. It was clearly the case for the Bukit Batok landslide in Singapore (Wei *et al.*, 1991) since the failure occurred after a period of heavy rain and there was no rainfall at the time of the failure. Wei *et al.* (1991) how that the rainfall in the preceding months resulted in raised ground water levels.

Lumb (1975) used a 15-day period to quantify antecedent rainfall for Hong Kong, and this was adopted by Tan *et al.* (1987) for Singapore. However, Chatterjea (1989) suggested that such a long period was inappropriate for the rainfall pattern in Singapore and adopted a period of 5 days.

3. Landslide events

The Nanyang Technological University (NTU) campus is located in the south-western part of Singapore. The campus covers an area of 200 hectares. Compared with many other parts of the country, there is a relatively high relief around the campus. The topography comprises a series of hills and valleys ranging in height from about 21 m to 56 m above sea level and is classified as Ridge and Valley (steep, high relief). Many of the slopes were terraced during the landscaping of the campus in the 1950s. The angles of slope used during terracing were divided into two groups, 30–40° and 50–70° (Pitts, 1985).

The geological formation at the NTU campus is very complicated since it has been subjected to intrusions, isoclinal overfolds and faults in the past (Moh and Associates, 1994). According to the study by Pitts (1985), the ridges consist of a series of folded silty mudrocks, sandstone and conglomerates of the Tengah and Queenstown facies of the sedimentary Jurong formation. These are covered by variable thickness of residual soil or in some cases, slope wash or colluvium. The valleys are deeply infilled with sandy and clayey soils representing the alluvial member of the Kallang formation. Limited observations have indicated that the groundwater tables on the NTU campus are generally at a low level between 6 and 9 m below the ground surface (Pitts, 1985).

On the day of 26 February 1995, a heavy storm occurred on the NTU campus. The rain started at 17:02 and lasted about $2\frac{1}{2}$ h. According to rainfall readings recorded by the School of Civil and Structural Engineering, NTU, the daily rainfall on that day was 94.6 mm. Since all the rainfall on that day took place during a $2\frac{1}{2}$ h period, the average hourly rainfall was 37.8 mm/h.

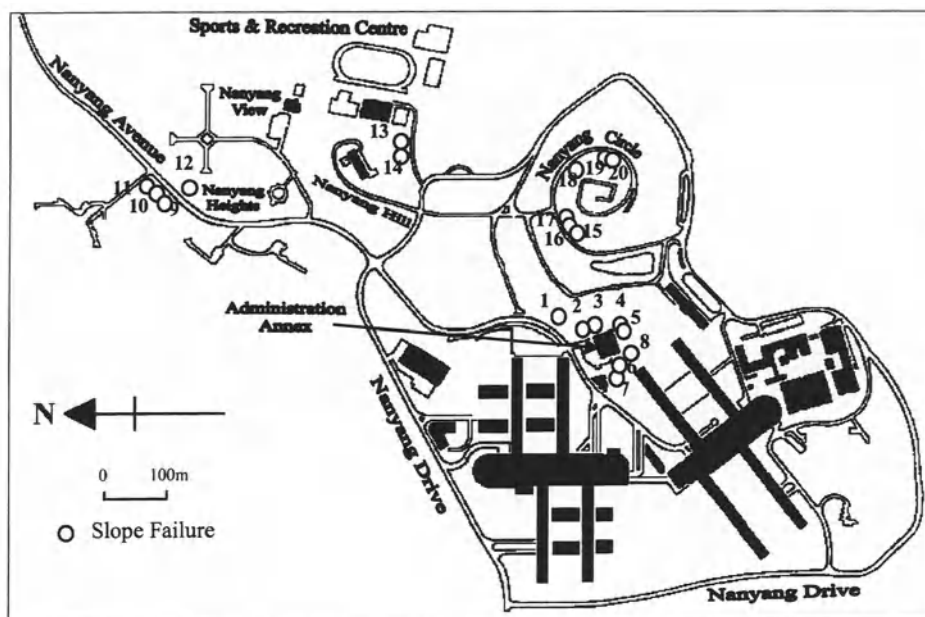


Figure 1. Locations of landslides on the NTU campus due to the storm of 26 February 1995

More than 20 landslides were found on the NTU campus the following day. A field study was carried out in the morning of 27 February 1995 when the geometries of the failed slopes were measured. The morphological features of landslides were also recorded. Figure 1 show the locations of landslides that occurred on the day of 26 February 1995. The details of landslides are listed in Table 1.

The landslides were mainly distributed in four areas of the campus, namely, Nanyang Heights, Nanyang Green, Nanyang Circle and the hill on which the Administration Annex building sits (Figure 1). The slopes at Nanyang Circle and around the Administration Annex were cut and backfilled during construction on the campus in the early 1980s. Therefore, the slopes around these two areas had been formed for about ten years. However, the slopes at Nanyang Heights and Nanyang Green were built in the early 1990s. Most of the failed slopes are located alongside roads except for those around the Administration Annex. None of these landslides could be attributed to changes in geometry or additional loading applied to the slopes.

It should be noted that the slope angles shown in Table 1 refer to the part of a slope where the failure occurred. Pitts (1985) pointed out that most slopes at the NTU campus resulted from regrading during the development of the University. Consequently, a slope with a comparatively large height may have several slope angles. The upper part of the slope was typically flattened to a smaller angle (about 30°) and the lower part was trimmed to a larger angle (about 50°).

Table 1. Details of landslides on the NTU campus due to the storm of 26 February 1995

Slip No.	Location	Slope Angle (degree)	Volume (m ³)	Length (m)	Width (m)	Thickness (m)	Landslide Classification	Position of slip surface	Morphological features
1	Admin. Annex	33	1.6	4	2	0.2	Rotational	Within Grade 6 material	Disintegration and spread at the toe
2	Admin. Annex	31	298	7.6	2.8	1.4	Rotational	Within Grade 6 material	Disintegrated accumulation zone at the toe
3	Admin. Annex	29	45	5*	6	1.5*	Rotational	Within Grade 6 material	Deep backscar, convex, and intact accumulation zone
4	Admin. Annex	44	54.6	7	7.8	1	Translational	At interface between Grade 5 and Grade 6	Intact accumulation zone at the toe
5	Admin. Annex	28	53.6	7.5	6.5	1.1	Rotational	Within Grade 6 material	Deep backscar, convex, and intact accumulation zone at the toe
6	Admin. Annex	34	52.3	11.5	3.5	1.3	Rotational	Within Grade 6 material	Disintegrated accumulation in the midslope and at the toe
7	Admin. Annex	36	30.9	9.5	2.5	1.3	Rotational	Within Grade 6 material	Disintegrated accumulation in the midslope and at the toe
8	Admin. Annex	46	0.93	1.5	3.1	0.2	Rotational	Within Grade 6 material	Disintegrated accumulation zone
9	Nanyang Heights	31	21.9	7.6	4.8	0.6	Rotational	Within Grade 6 material	Disintegration and accumulation at the toe
10	Nanyang Heights	31	17.6	5.0*	8.8	0.4*	Rotational	Within Grade 6 material	Short backscar, convex, and intact accumulation zone
11	Nanyang Heights	31	21.5	5.0*	14.3	0.3*	Rotational	Within Grade 6 material	Short backscar, convex, and intact accumulation zone
12	Nanyang Heights	24	15	5.7	3.3	0.8	Rotational	Within Grade 6 material	Disintegrated accumulation zone
13	Nanyang Green	30	143.8	14	7.9	1.3	Translational	At interface between Grade 5 and Grade 6	Disintegration and spread at the toe
14	Nanyang Green	49	5.9	3.3	4.5	0.4	Translational	At interface between Grade 5 and Grade 6	Intact accumulation zone

Table 1. (continued)

Slip No.	Location	Slope Angle (degree)	Volume (m ³)	Length (m)	Width (m)	Thickness (m)	Landslide Classification	Position of slip surface	Morphological features
15	Nanyang Circle	44	93.6	11.3	4.6	0.8	Rotational	Within Grade 6 material	Intact accumulation in the midslope and at the toe
16	Nanyang Circle	33	230.2	15.5	9.9	1.5	Rotational	Within Grade 6 material	Disintegration and accumulation in the midslope and the toe
17	Nanyang Circle	39	4.5	4.7	4.8	0.2	Translational	At interface between Grade 5 and Grade 6	Disintegration and spread at the toe
18	Nanyang Circle	52	3.7	2.7	3.4	0.4	Rotational	Within Grade 6 material	Disintegration and spread at the toe
19	Nanyang Circle	50	5.5	3.8	3.6	0.4*	Rotational	Within Grade 6 material	Short backscar, convex, and intact accumulation zone
20	Nanyang Circle	50	5.8	3.6	4	0.4*	Rotational	Within Grade 6 material	Short backscar, convex, and intact accumulation zone

*Indicates estimated values

Table 2. Basic properties of the residual soils

	Total unit weight (kN/m ³)	Natural water content (%)	Specific gravity	Liquid Limit (%)	Plasticity Index	Grain Size (%)			
						Gravel	Sand	Silt	Clay
Sandy silty CLAY (Grade 6)	19.2	19.5	2.64	48	24	0	22	39	39
Hard sandy SILT (Grade 5)	21.2	13.5	2.66	35	17	3	45	30	22

The depths of the landslides were found to be between 0.2 m and 1.8 m (Table 1). Two broad groups could be used to distinguish the landslides. The deeper landslides occurred at an average depth of 1.3 m to 1.5 m while the shallower landslides took place at an average depth of around 0.4 m. The shallower slides usually took place in the lower part of a slope.

The volumes involved in the landslides varied from 1.6 to 230.2 m³ and were relatively small (Table 1). The volume was not found to have a clear relationship with the angle of slope but it appeared to be associated with the depth of slip surface.

The field observations showed that there were two main types of residual soils involved in the landslides. These soils were identified as sandy silty clay and a hard sandy silt. Disturbed samples were taken from the locations of Slip No. 5 and No. 13 and Table 2 lists some basic properties of the two soil types. Some data were also obtained from a report by Moh and Associates (1994). According to Little's (1969) weathering grades, the silty clay can be categorized as a Grade 6 residual soil and the sandy silt as a Grade 5 soil. The Grade 6 silty clay has totally lost the structure of its parent rock. However, the Grade 5 sandy silt is completely weathered but the structure of its parent rock has been partly kept. Some cementation and bonding between the soil particles are still present.

A distinct interface exists between the Grade 5 and 6 soils. The depth of the interface as a great influence on slope stability. When the interface between Grade 5 and Grade 6 residual soils lies near the slope surface, the depth of failure is governed by the interface; the top Grade 6 residual soils slide along the interface.

Two types of landslide were observed in the investigation, i.e., rotational and translational types (following the landslide classification proposed by Varnes, 1978). Rotational failures were the most common type found on the soil slopes. They occurred in the soil slopes without structural controls i.e. where the depth of the interface between Grade 6 and Grade 5 was sufficiently deep not to affect the slide. Translational failures occurred when the interface between Grade 6 and Grade 5 residual soils was close to the slope surface.

4. Observations of antecedent rainfall

The rainfall records from November 1993 through February 1995 were studied to identify major storm events. All the rainfall data were collected from the automatic rain recording station which was set up by the School of Civil and Structural Engineering, Nanyang Technological University. The maximum monthly rainfall during these 16 months was 481.8 mm in February 1995 and the minimum was 26.8 mm in September 1994.

During this period there were four days in which the daily rainfall exceeded 80 mm; these were 94 mm on 15 November 1993, 83.2 mm on 12 November 1994, 86 mm on 4 February 1995 and 94.6 mm on 26 February 1995. The daily rainfall records for November 1993, November 1994 and February 1995 are shown in Figure 2.

The rainfall on 26 February 1995 (94.6 mm/day) was sufficient to cause a spate of landslides but a storm of almost identical intensity on 15 November 1993 (94 mm/day) produced no landslides. Therefore the difference must be due to the antecedent rainfall. Figure 3 shows cumulative antecedent rainfall plotted against the number of days prior to a heavy-storm day. The curves show the accumulated rainfall for a certain period (up to five days in this study) prior to a heavy-storm day. It can be clearly seen from Figure 3 that 26 February 1995 has the highest cumulative antecedent rainfall compared to the other three heavy-storm days. The cumulative rainfall for 26 February 1995 is at least twice those of the other days.

These limited observations for the slope failures on the NTU Jurong campus suggest that, although the daily rainfall is a very important triggering factor for landslides (in this case, a rainfall of 90 mm/day appears to be the threshold magnitude), the rainfall amount alone is not sufficient to cause slope failures. The antecedent rainfall has a significant influence on the initiation of landslides. A 5-day antecedent rainfall exceeding 60 mm combined with a daily rainfall greater than 90 mm (i.e. a total rainfall exceeding 150 mm over 6 days) appears to have been sufficient to cause landslides in this case.

It should be noted that the above conclusions are not the same as those obtained from the experience in Hong Kong. Brand *et al.* (1984) quoted the threshold value of 24-hour rainfall for major landslides in Hong Kong as 100 mm. This is not unlike the value of 90 mm observed in this study. However, Brand *et al.* (1984) suggested that the antecedent rainfall was not a major factor for landslides in Hong Kong. The different conclusions could be due to the different properties of soils in these two cities which lead to the different responses to rainfalls. The residual soils in Hong Kong are sandier in nature and would therefore have a higher permeability than the silty clay residual soils that are typical of Singapore. In more permeable soils there is greater possibility for drainage of water and hence a gradual build up in pore-water pressure over time would be less likely.

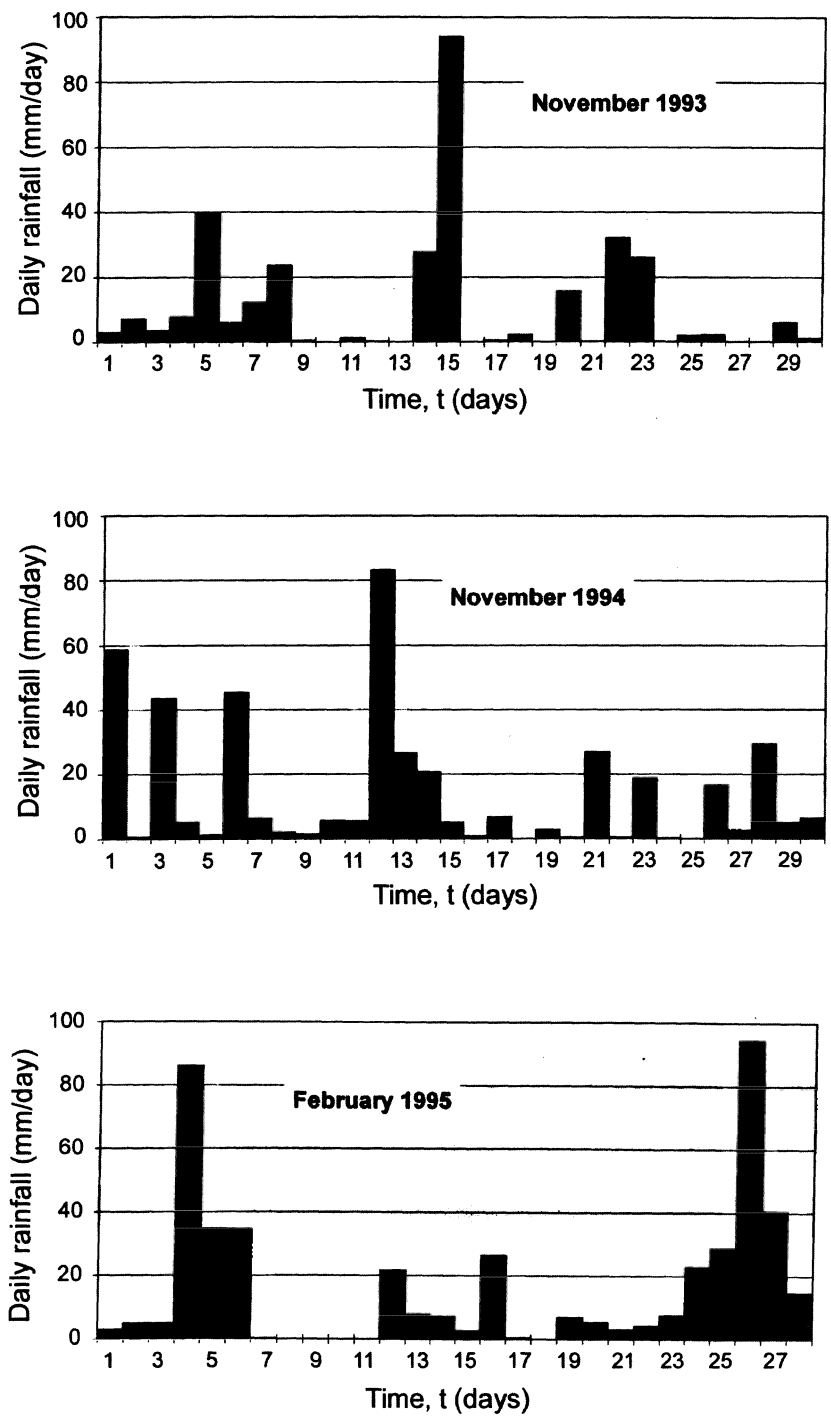


Figure 2. Daily rainfall for the months of (a) November 1993 (b) November 1994 (c) February 1995

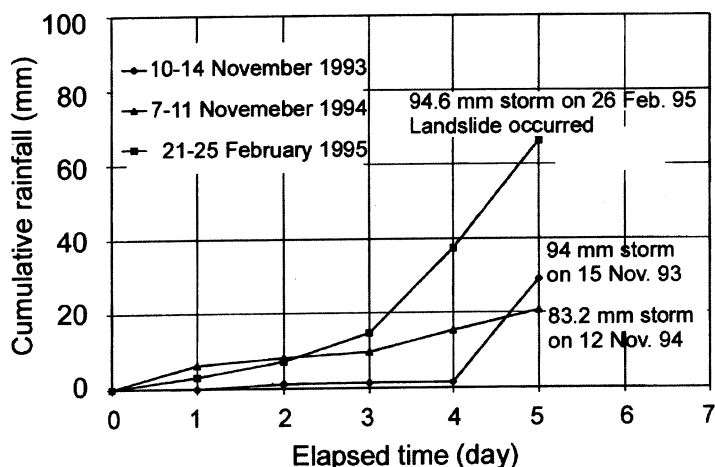


Figure 3. Relationship between antecedent rainfall and the occurrence of landslides

5. Case study

In order to further investigate the effect of antecedent rainfall, one of the slopes that failed was examined in more detail. The slope under investigation is located at the eastern side of the Administration Annex building on the NTU campus (shown as Slip No. 3 in Figure 1). The profile of the slope is plotted in Figure 4. The slope was formed by fill placement in the upper part and was a natural slope with minor cuts in the lower part at the time of the construction of the Administration Annex building. The slope had been trimmed into three terraces. The angle of the upper slope was about 29° while that of the lower slope was around 25° . The slope was covered with grass. According to the site investigation report by Moh and Associates (1994), four soil layers were identified (as shown in Figure 4):

- (1) Soft to medium sandy silty clay with building debris (fill)
- (2) Medium to stiff silty clay/clayey silt with sand
- (3) Stiff to hard silty clay/clayey silt with sand
- (4) Hard sandy silt to very dense silty sand.

Since the first three layers of soil had similar characteristics in terms of physical properties and shear strengths, these three soils were simply considered as one layer of soil in the following analyses.

The slope failed due to the heavy rain on the day of 26 February 1995. There were no measurements of piezometric level at this location. According to Pitts (1985) and Moh and Associates (1994) the groundwater tables at the ridges of the NTU campus are typically low. In this study, the groundwater table in the area of interest was assumed to be 6 m below the ground surface.

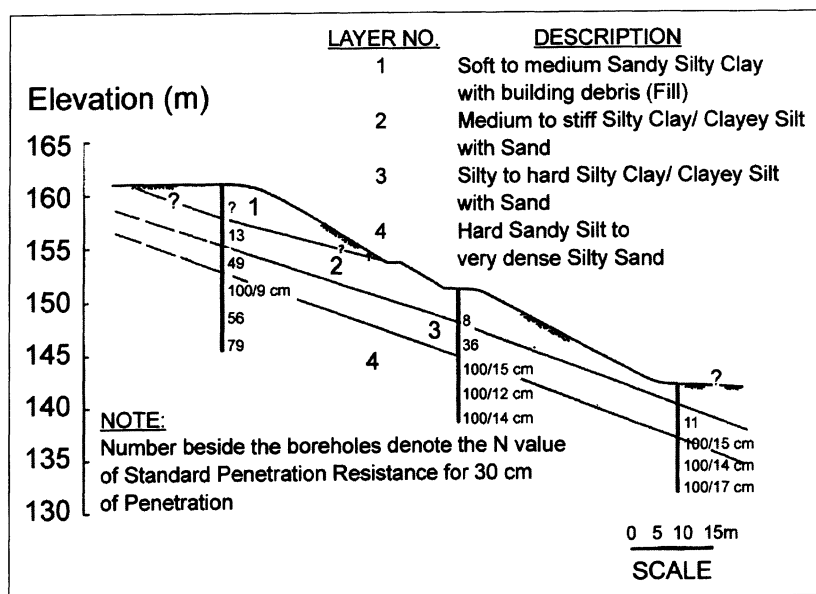


Figure 4. Slope profile for Slip No. 3 (from Moh and Associates, 1994)

5.1. SOIL PROPERTIES

In the following analyses, two soil properties are required. i.e. permeability and shear strength. The coefficient of permeability is used for the seepage analysis and the shear strength is needed in the slope stability analysis.

5.1.1. Permeability

In an unsaturated soil, the coefficient of water permeability (hydraulic conductivity) varies considerably with respect to matric suction. Accordingly, a function of permeability with respect to matric suction must be determined prior to analyses. Due to the difficulties associated with direct measurement of the permeability function (Fredlund and Rahardjo, 1993) an indirect method was adopted in this study. The procedures for the indirect method were as follows:

- (1) A soil-water characteristic curve was determined by performing pressure plate tests;
- (2) The saturated coefficient of permeability was obtained from a triaxial permeameter test;
- (3) The non-linear relationship between the unsaturated coefficient of permeability and matric suction was established using the soil-water characteristic curve and the saturated coefficient of permeability as explained by Fredlund and Rahardjo (1993).

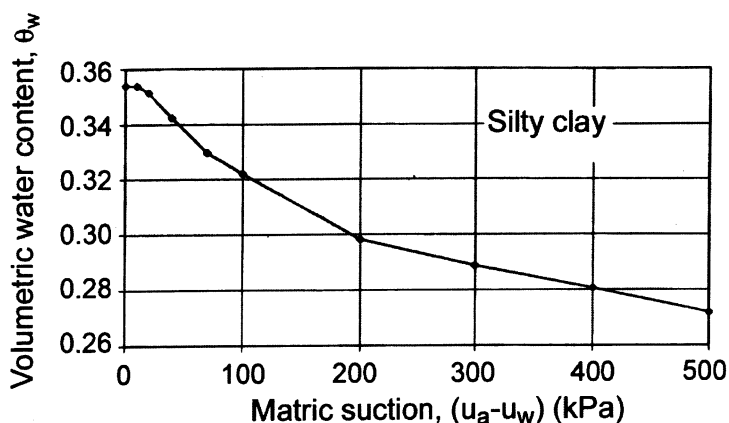


Figure 5. Soil-water characteristic curve for a residual soil from the Jurong Sedimentary Formation

Four soil-water characteristic curves were obtained for soil samples taken from the investigated slope. The specimens were taken from a depth of 0.5 m. They were saturated before starting the tests. A Tempe pressure cell manufactured by Soilmoisture Equipment Corporation, USA was used to apply matric suctions up to 100 kPa and a 5-bar pressure plate was used for suctions above 100 kPa (up to 500 kPa). Figure 5 shows a typical soil-water characteristic curve from one of the soil specimens.

A triaxial permeameter apparatus was used to measure the saturated coefficient of permeability, k_s . The soil specimen used in the test was 55 mm, in diameter and 50 mm in height. The specimen was saturated by back pressure prior to carrying out the permeability measurement. The flow rates under three different pressure gradients were quite consistent and gave a permeability value of $k_s = 1.193 \times 10^{-9}$ m/s.

The function relating the unsaturated coefficient of permeability with respect to matric suction was generated using the ACUPIM (Automated Computation of Unsaturated Permeability from Indirect Measurements) computer program (Leong, 1993). This uses the indirect method outlined by Fredlund and Rahardjo (1993). The permeability function calculated in this way is plotted in Figure 6 (for the soil-water characteristic curve shown in Fig. 5). It can be seen that the estimated coefficient of permeability decreases by almost four orders of magnitude over the matric suction range of 500 kPa.

5.1.2. Shear strength

As discussed earlier, two types of residual soils were involved in the landslide, namely the Grade 6 silty clay (layers 1 to 3) and the Grade 5 sandy silt (layer 4). The results of shear strength tests conducted at NTU (Lim, 1995, Rahardjo *et al.*, 1995) and by Moh and Associates (1994) were used to characterise the soils for slope stability

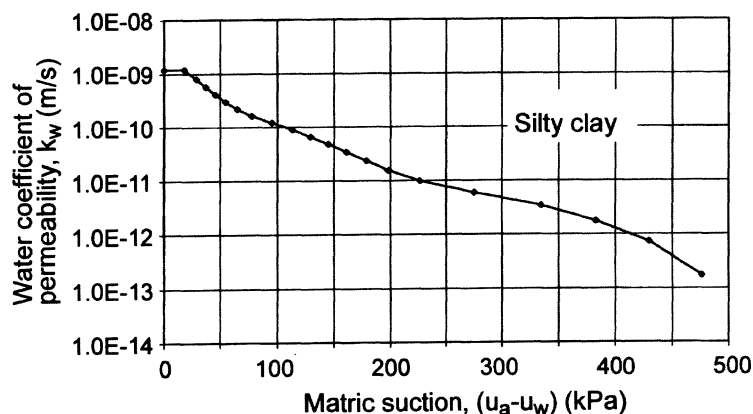


Figure 6. Permeability function for a residual soil from the Jurong Sedimentary Formation

analyses. The following values of the shear strength parameters and total unit weight were used for these two soil types:

- | | | |
|---------------|-----------------------|--|
| Layers 1 to 3 | Silty clay (Grade 6): | $\gamma = 19.6 \text{ kN/m}^3$
$c' = 2 \text{ kPa}$, $\phi' = 26^\circ$ and $\phi^b = 13^\circ$ |
| Layer 4 | Sandy silt (Grade 5): | $\gamma = 21.5 \text{ kN/m}^3$
$c' = 20 \text{ kPa}$, $\phi' = 35^\circ$ and $\phi^b = 17^\circ$ |

5.2. RAINFALL CHARACTERISTICS

Three different rainfall patterns were identified in order to examine the effects of antecedent rainfall on slope stability. The purpose was to examine the different pore-water pressure conditions that would result in each case. The three cases were based on actual rainfall patterns for major storm events on 15 November 1993 (Case 1), 12 November 1994 (Case 2) and 26 February 1995 (Case 3) (Figure 3). The daily rainfalls during the storms were greater than 80 mm for the three cases (Figure 2). The cumulative antecedent rainfall for Cases 1 and 2 were similar (i.e., around 20 to 30 mm in Figure 3) whereas that for Case 3 was higher (over 60 mm). The rainfall patterns for the 5 days (120 h) preceding each of the major events were expressed as equivalent hourly rainfall intensities and these are plotted in Figure 7. The equivalent hourly rainfalls during the storms in Cases 2 and 3 were similar (i.e., around 33 to 38 mm/h in Figure 7) whereas that for Case 1 was lower (19 mm/h).

5.3. NUMERICAL ANALYSIS

The finite element computer program SEEP/W (GeoSlope International Ltd, 1992) was used to compute the changes in pore-water pressure when the slope was

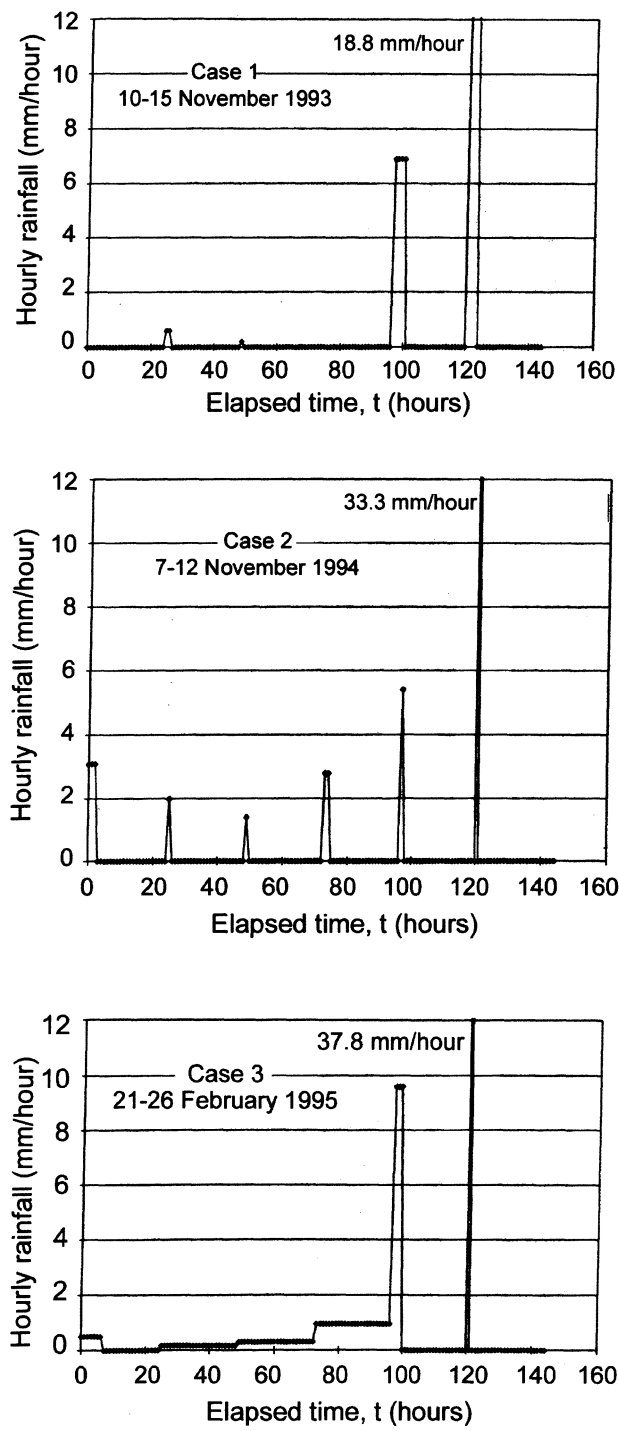


Figure 7. Rainfall intensities with elapsed time used in simulations for (a) Case 1 (b) Case 2 (c) Case 3

subjected to different rainfall patterns. SEEP/W can model various material types and boundary conditions such as unsaturated soils and infiltration flux boundaries. The nonlinear relationship between the coefficient of permeability and matric suction is incorporated into the program.

The mesh used in the analysis comprised 418 nodes and 424 triangular or quadrilateral elements. The bottom boundary was set to zero flux. The left and right boundaries were specified as constant total head boundaries below the groundwater table and as zero total flux boundaries above the groundwater table. The total head applied corresponds to a hydrostatic condition. The slope surface was treated as a flux boundary condition. It was assumed that there would be no ponding on the surface of the slope. Therefore, a pore-water pressure greater than zero was not allowed on the slope surface.

Prior to carrying out a transient seepage analysis for the storm event it was necessary to establish some initial conditions. Firstly a steady state analysis was used to produce a hydrostatic condition. Then a transient analysis was used to establish an initial pore-water pressure (suction) profile. The initial insitu condition of pore-water pressure before a storm is governed by seasonal infiltration and evaporation. In this analysis, the pre-storm initial condition was achieved by performing a transient analysis using a low unit flux applied to the slope surface for a long duration. This low unit flux corresponds to the net influx of water into the slope over the year. The value of the applied net flux on the slope surface was adjusted by trial and error until the required initial pore-water pressure condition was achieved.

According to Lim *et al.* (1996) the average matric suction in the residual soils on the NTU campus is around 20 kPa. In this case, the initial matric suction profile in the slope was adjusted to be close to this magnitude.

For the seepage analysis, the same soil water characteristic curve and permeability function were used for both soil types. Only the shear strength parameters were taken to be different for the slope stability analysis.

The computer program SLOPE/W (GeoSlope International LTD, 1991) was used to perform a limit equilibrium analysis on the landslide investigated in this study. Bishop's simplified method was used in this study. The pore-water pressure distribution computed in the program SEEP/W was imported into SLOPE/W for the slope stability analysis. The time-dependent pore-water pressure distribution could therefore be used directly to compute the factor of safety with time.

5.3.1. Results for Case 1

The simulated pore-water pressure distributions within the slope for Case 1 are shown in Figure 8 for four different elapsed times. The results illustrate the rapid rise of the water table and the reduction in matric suction above the water table during rainfall. The pore-water pressure profiles with depth near the crest of the slope are given in Figure 9 for different elapsed times. The worst pore-water pressure condition is that developed at the end of the storm (i.e., at 125 h). The factor of safety

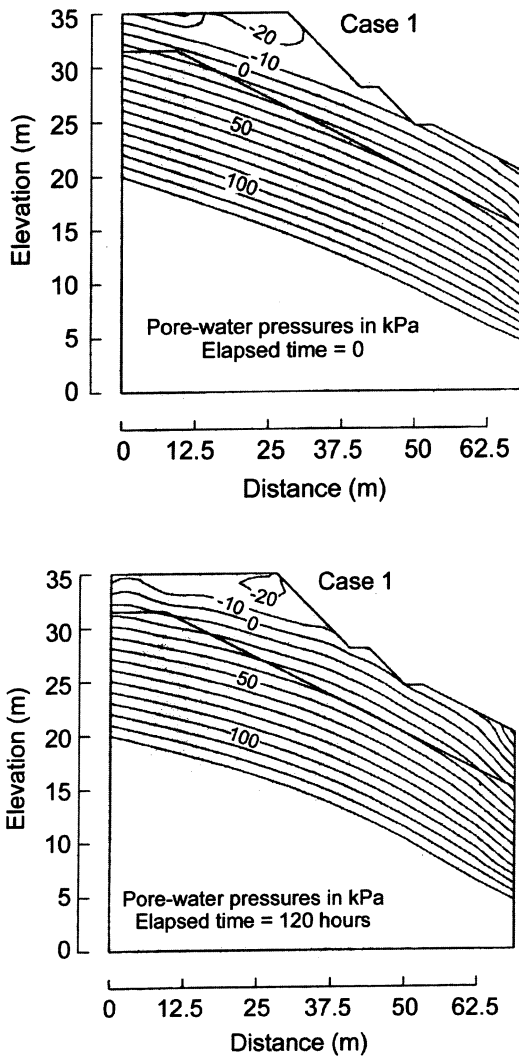


Figure 8. Simulated pore-water pressure contours for Case 1 at elapsed times of (a) 0 h (b) 120 h

of the slope decreased from a value greater than 1.6 at 5 days before the storm to the lowest factor of safety of 1.25 at the end of the storm (Figure 10). The critical slip surface corresponding to the lowest factor of safety is shown in Figure 11.

5.3.2. Results for Case 2

The simulated pore-water pressure distributions within the slope for Case 2 are shown in Figure 12 for four different elapsed times. The results also illustrate a rise in the water table that reached a maximum elevation at the end of the storm (i.e., 122.5 h). The pore-water pressure profiles with depth near the crest of the slope

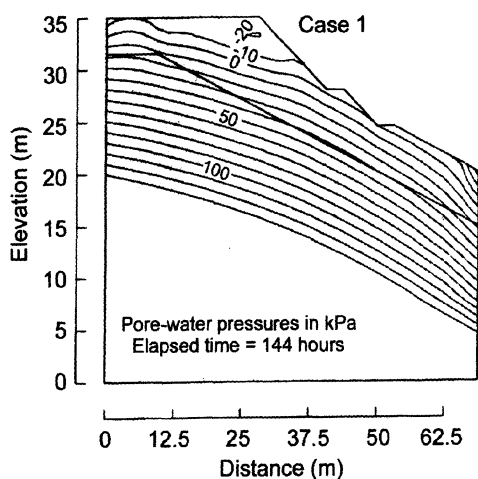
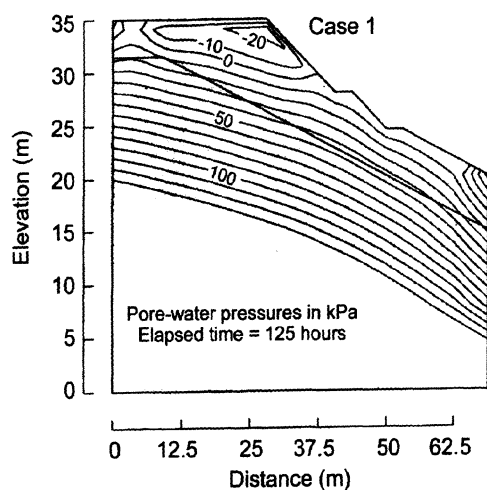


Figure 8. Simulated pore-water pressure contours for Case 1 at elapsed times of (c) 125 h (d) 144 h

are given in Figure 13 for different elapsed times. The factor of safety of the slope decreased from a value greater than 1.6 at 5 days before the storm to the lowest factor of safety of 1.23 at the end of the storm (Figure 14). The critical slip surface corresponding to the lowest factor of safety is shown in Figure 15.

5.3.1. Results for Case 3

The simulated pore-water pressure distributions within the slope for Case 3 are shown in Figure 16 for four different elapsed times. The results show a rise in the water table that reached a maximum elevation at the end of the storm (i.e.,

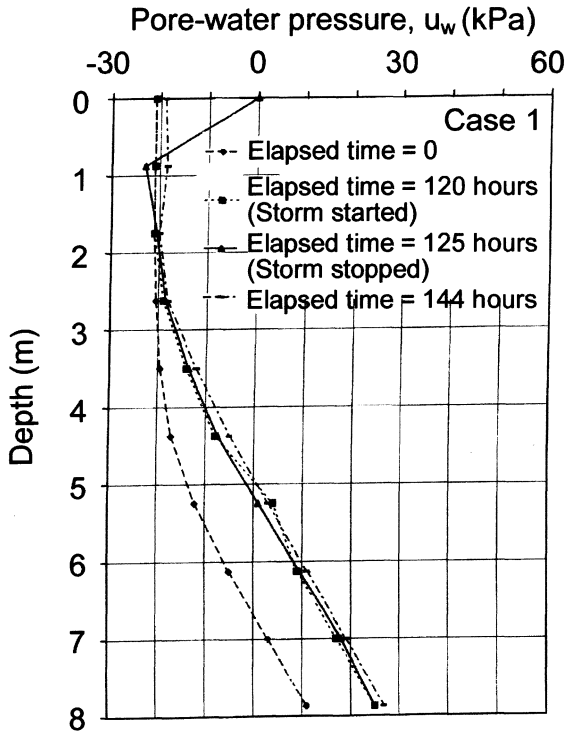


Figure 9. Simulated pore-water pressure profiles with depth for Case 1

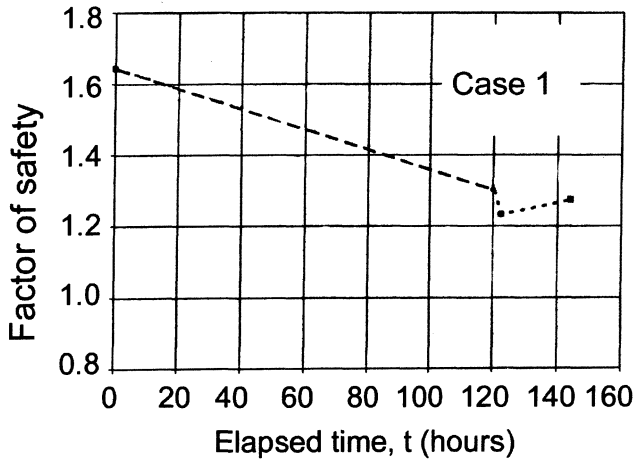


Figure 10. Factor of safety variations with elapsed time for Case 1

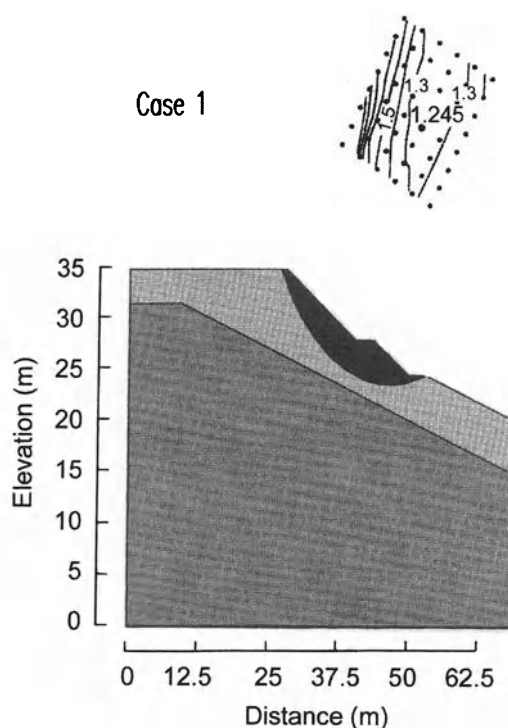


Figure 11. The critical slip surface for Case 1 (elapsed time = 125 h)

122.5 h). The pore-water pressure profiles with depth near the crest of the slope are given in Figure 17 for different elapsed times. The factor of safety of the slope decreased from a value greater than 1.6 at 5 days before the storm to the lowest factor of safety of 1.05 at the end of the storm (Figure 18). The lowest factor of safety of 1.05 was very close to unity indicating that limiting equilibrium was reached and slope failure would be expected to occur at the end of the storm for the conditions represented by Case 3. The critical slip surface corresponding to the lowest factor of safety is shown in Figure 19. The infiltration rate across the slope surface is plotted in Figure 20 together with the rainfall rate. Figure 20 shows that the infiltration rate was large in the beginning when the slope was still unsaturated and the infiltration rate decreased when the slope was near saturation.

Therefore, Case 3 shows the role of antecedent rainfall in slope stability. The factor of safety (FoS) calculated for Case 3 after the storm ($\text{FoS} = 1.05$) was considerably lower than that calculated for Case 2 ($\text{FoS} = 1.23$), even though the rainfall intensity for the main storm events was similar (33 and 38 mm/h). This difference was due to the amount of antecedent rainfall (around 30 mm for Case 2 and over 60 mm for Case 3) as illustrated in Figure 3.

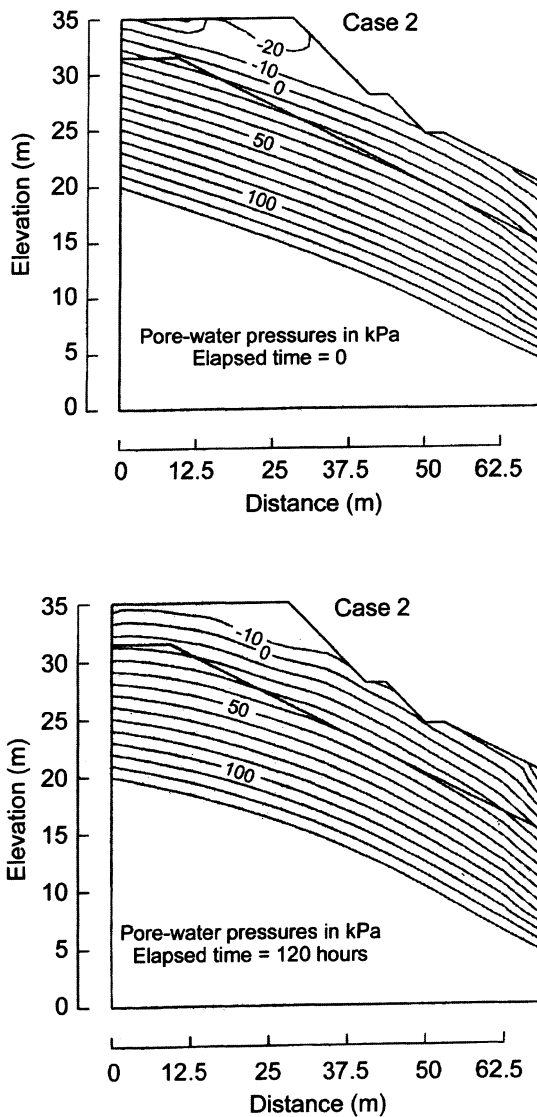


Figure 12. Simulated pore-water pressure contours for Case 2 at elapsed times of (a) 0 h (b) 120 h

6. Discussion

In general it can be observed that the water table (as indicated by the zero pore-water pressure contour) rises rapidly during rainfall causing the pore-water pressures to increase or the matric suction to decrease. The antecedent rainfall prior to the storm event has decreased the matric suction in the slope causing the coefficient of permeability of the soil to increase, making the soil more permeable to infiltration. As a result, the shear strength decreases and consequently, the factor of safety

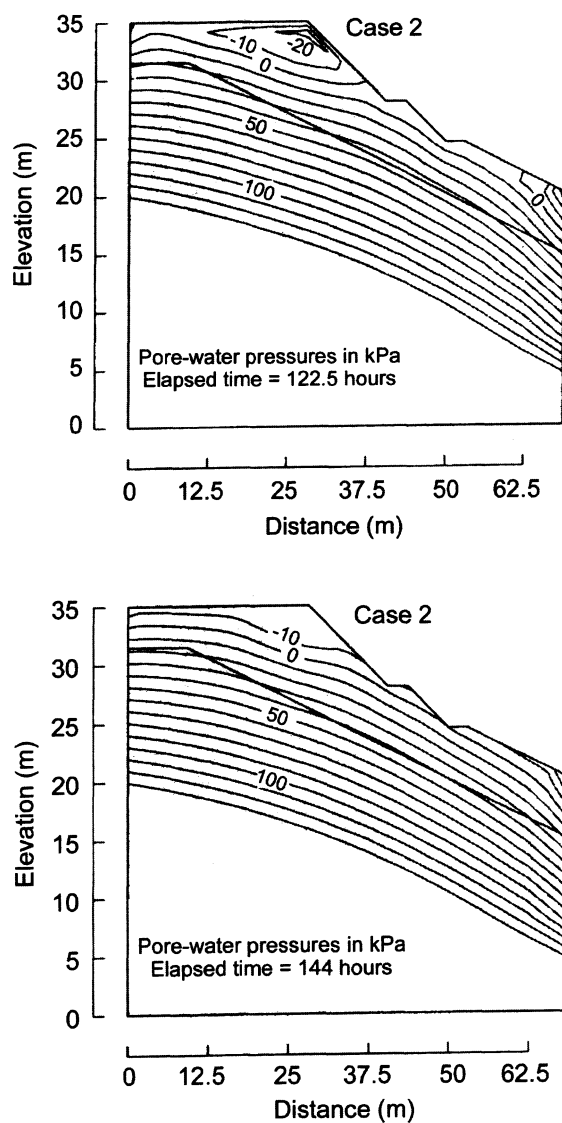


Figure 12. Simulated pore-water pressure contours for Case 2 at elapsed times of (c) 122.5 h (d) 144 h

of the slope decreases during rainfall. The lowest factor of safety occurs at the end of the storm and recovers after the storm has stopped. It is interesting to note that the water table continues to rise after the rain has stopped as shown in all the three cases (Figures 9, 13 and 17) indicating that infiltrated water continues to percolate downward even when the rain has stopped. However, the pore-water pressures that have built up near the ground surface (within 1 m of the surface) decrease significantly after the storm has stopped.

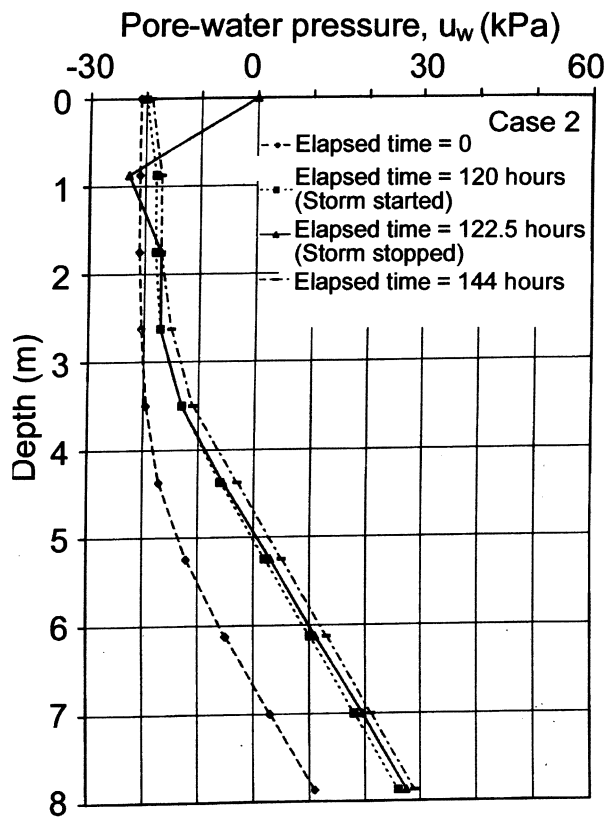


Figure 13. Simulated pore-water pressure profiles with depth for Case 2

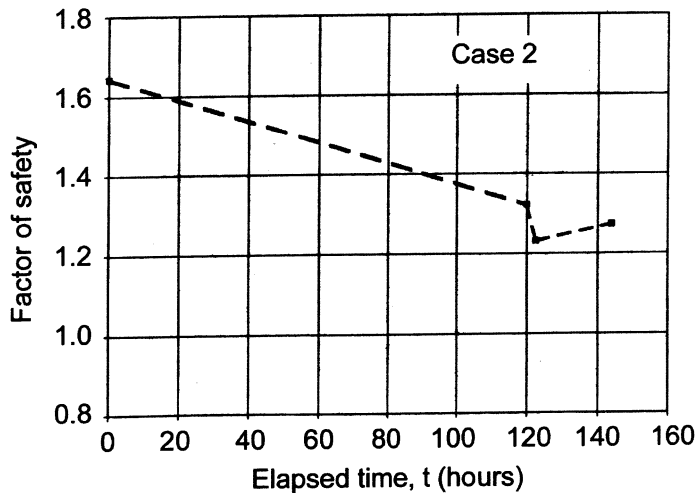


Figure 14. Factor of safety variations with elapsed time for Case 2

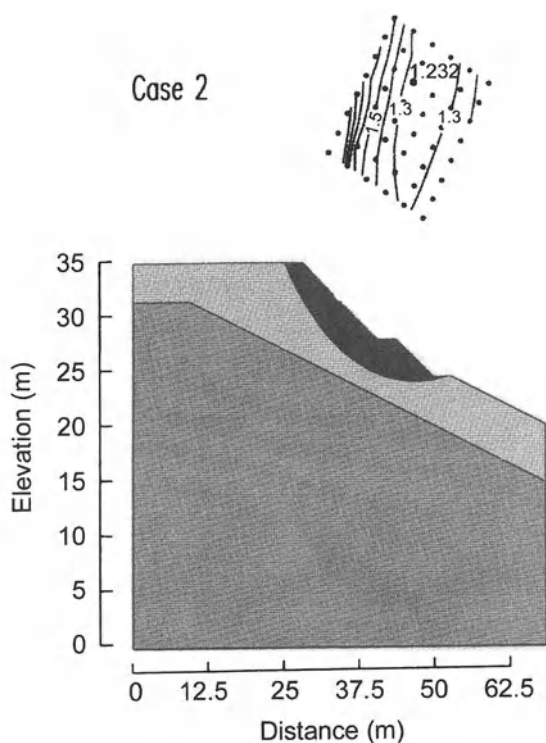


Figure 15. The critical slip surface for Case 2 (elapsed time = 122.5 h)

7. Conclusions

An examination of the landslides that occurred on the Nanyang Technological University campus in February 1995 indicates that the landslides were initiated by rainwater infiltration. There had been no changes in geometry or additional loading applied to the slopes that could have initiated failure. All the landslides were shallow and the displaced soil volumes were small. The main mode of landsliding in relatively uniform soil layers was rotational. When the interface between Grade 6 residual soil and Grade 5 soil was located near the slope surface, failures occurred along the interface.

Both the daily rainfall and the antecedent rainfall are important triggering factors for the occurrence of the landslides. The daily or the threshold rainfall alone cannot be used as the determinant for landslide as antecedent rainfall increases permeability of soil and subsequent storm events may trigger a landslide. A 5-day antecedent rainfall exceeding 60 mm combined with a daily rainfall greater than 90 mm (i.e. a total rainfall exceeding 150 mm over 6 days) appears to have been sufficient to cause landslides in this case.

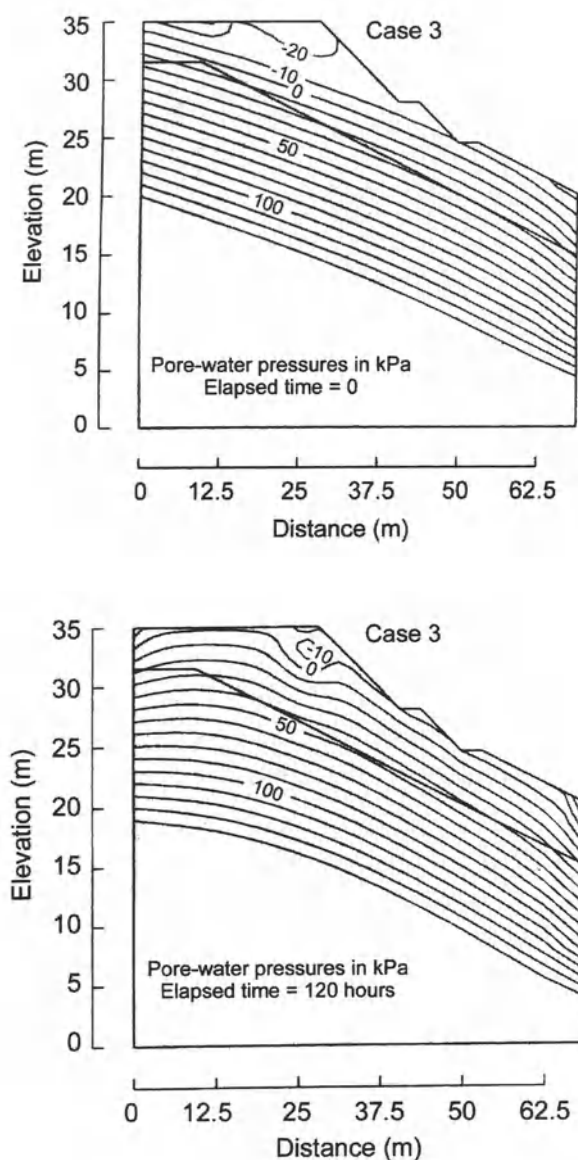


Figure 16. Simulated pore-water pressure contours for Case 3 at elapsed times for (a) 0 h (b) 120 h

Numerical modelling confirmed the role of antecedent rainfall in slope stability. Different factors of safety were calculated for two cases where the rainfall intensity for the main storm events was similar (33 and 38 mm/h) but the amount of antecedent rainfall was different (around 30 mm and over 60 mm for a 5-day period). However, it should be noted that the role of antecedent rainfall in slope stability will

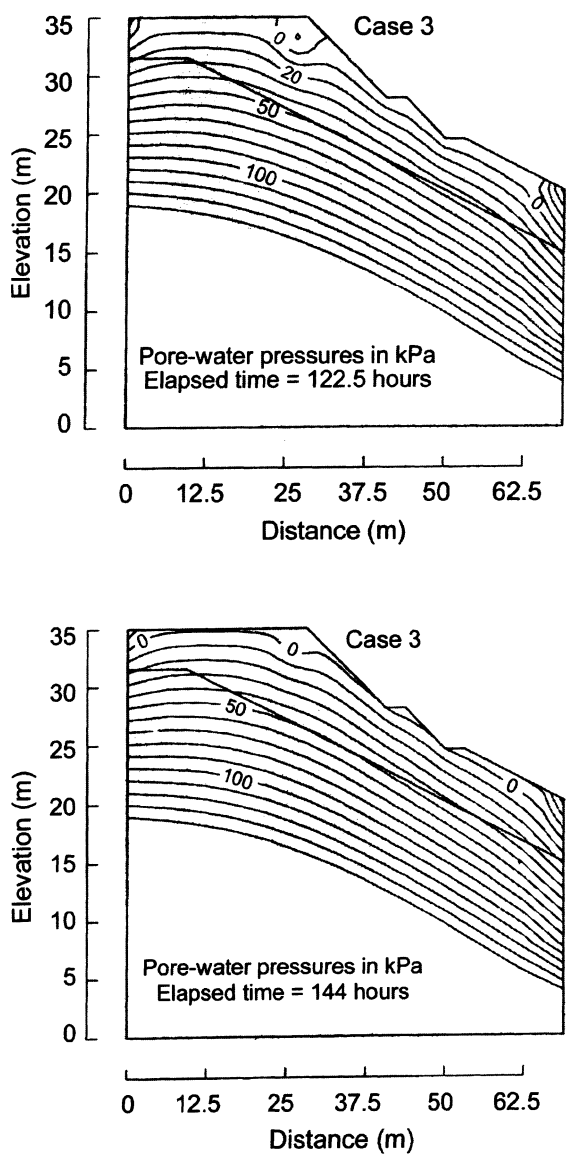


Figure 16. Simulated pore-water pressure contours for Case 3 at elapsed times for (c) 122.5 h (d) 144 h

not be the same for slopes at different locations that have different soil properties, different surface conditions of the slopes, highly variable tropical rainfalls or different microclimatic conditions.

The factor of safety calculated for the case with the higher antecedent rainfall (over 60 mm) was 1.05. This indicates a state close to limiting equilibrium and

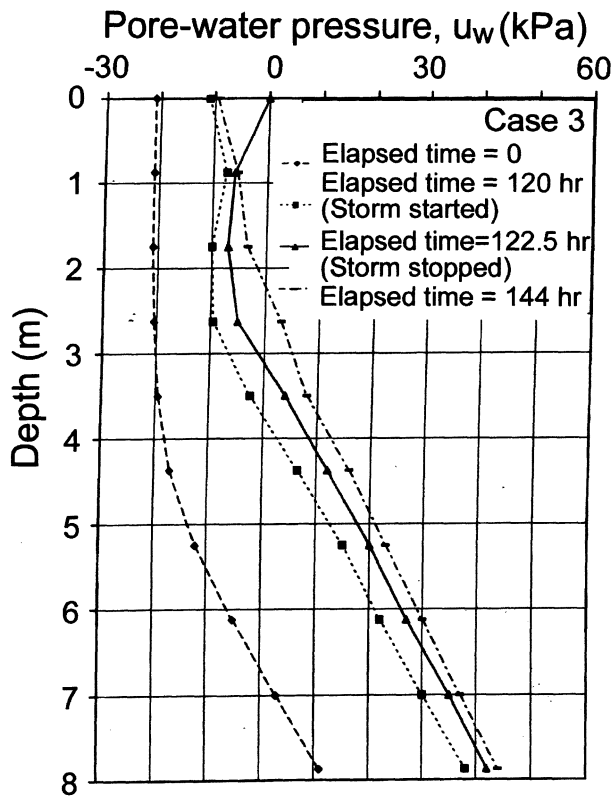


Figure 17. Simulated pore-water pressure profiles with depth for Case 3

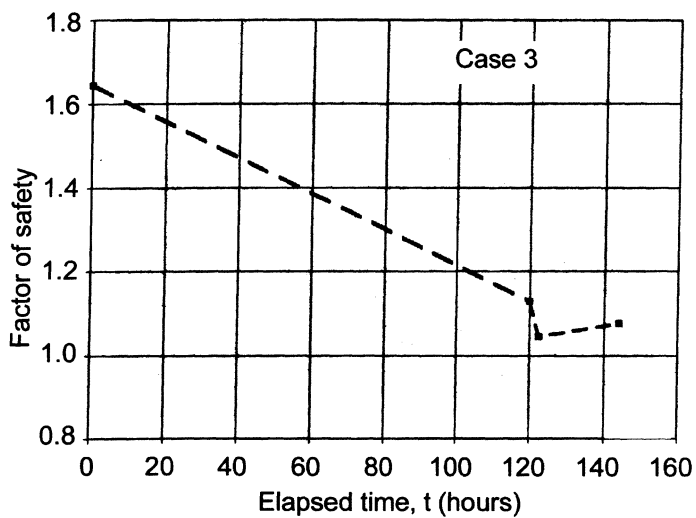


Figure 18. Factor of safety variations with elapsed time for Case 3

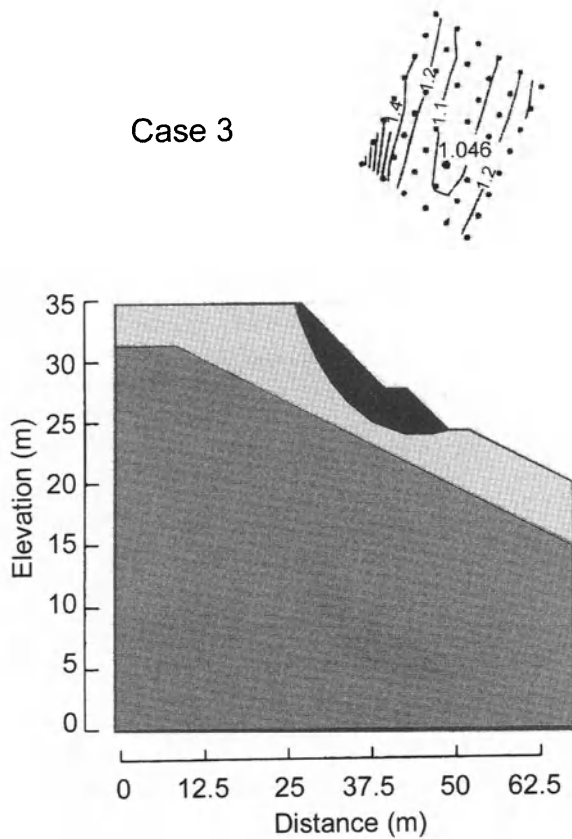


Figure 19. The critical slip surface for Case 3 (elapsed time = 122.5 h)

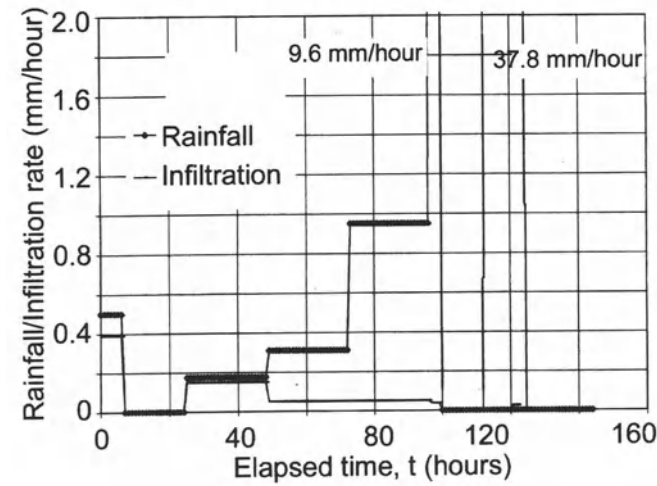


Figure 20. Comparison of infiltration to rainfall rates for Case 3

suggests that a slope failure could be expected for these conditions. For the case with an antecedent rainfall of around 30 mm, the factor of safety did not fall below 1.23 indicating that failure was unlikely. The modelling indicated that the water table continued to rise after rainfall had stopped because of the downward percolation of the infiltrated water.

Acknowledgements

This study is part of the research project on “Rainfall-induced slope failures” (NSTB 17/6/16) funded by the National Science and Technology Board, Singapore. The assistance of Dr Rezaur Rahman Bhuiyan in revising the figures of the paper is acknowledged.

References

- Au, S. W. C. (1993) Rainfall and Slope Failure in Hong Kong, *Engineering Geology*, **36**, 141–147.
- Barata, F. E. (1969) Landslides in the Tropical Region of Rio de Janeiro, *Proc. 7th International Conference on Soil Mechanics and Foundation Engineering*, Mexico City, Vol. 2, pp. 507–516.
- Brand, E. W. (1984) Landslides in Southeast Asia: a State-of-the-art Report. *Proc. 4th Int. Symp. on Landslides*, Toronto, Vol. 1, pp. 17–59.
- Brand, E. W. (1992) Slope Instability in Tropical Areas. *Proc. 6th Int. Symp. on Landslides*, Christchurch, New Zealand, Vol. 3, pp. 2031–2051.
- Brand, E. W., Premchitt, J. and Phillipson, H. B. (1984) Relationship Between Rainfall and Landslides in Hong Kong, *Proc. 4th Int. Symp. on Landslides*, Toronto, Vol. 1, pp. 377–384.
- Chatterjea, K. (1989) Observations on the Fluvial and Slope Processes in Singapore and their Impact on the Urban Environment, PhD Thesis, National University of Singapore.
- Crozier, M. J. and Eyles, R. J. (1980) Assessing the Probability of Rapid Mass Movement, *Proc. 3rd Australia–New Zealand Conf. on Geomechanics*, Wellington, Vol. 2, pp. 47–51.
- Eyles, R. J. (1979) Slip-triggering Rainfalls in Wellington City, New Zealand, *New Zealand Journal of Science*, **22**, 117–121.
- Fredlund, D. G. and Rahardjo, H. (1993) *Soil Mechanics for Unsaturated Soils*, John Wiley & Sons, New York, 517 pp.
- Fukuoka, M. (1980) Landslides Associated with Rainfall, *Geotechnical Engineering, Journal of Southeast Asian Geotechnical Society*, **11**, 1–29.
- GeoSlope International Ltd (1991) *Slope/W User's Guide for Slope Stability Analysis*, GeoSlope International Ltd., Calgary, Alberta, Canada.
- GeoSlope International Ltd (1992) *Seep/W User's Guide for Finite Element Analysis, Version 2*, GeoSlope International Ltd., Calgary, Alberta, Canada.
- Kay, J. N. and Chen, T. (1995) Rainfall Landslide Relationship for Hong-Kong, *Proc. Institution of Civil Engineers – Geotechnical Engineering*, Vol. 113, No. 2, pp. 117–118.
- Leong, E. C. (1993) *ACUPIM 1.0. Automated Computation of Permeability from Indirect Measurements*, Nanyang Technological University, Singapore.
- Lim, T. T. (1995) Shear Strength Characteristics and Rainfall-Induced Matric Suction Changes in a Residual Soil Slope, MEng Thesis, School of Civil & Structural Engineering, Nanyang Technological University, Singapore.

- Lim, T. T., Rahardjo, H., Chang, M. F. and Fredlund, D. G. (1996) Effect of Rainfall on Matric Suctions in a Residual Soil Slope, *Canadian Geotechnical Journal*, **33**, 618–628.
- Little, A. L. (1969) The Engineering Classification of Residual Tropical Soils, *Proc. 7th Int. Conf. on Soil Mechanics and Foundation Engineering*, Mexico, Vol. 1, pp. 1–10.
- Lumb, P. (1975) Slope Failures in Hong Kong, *Quarterly Journal of Engineering Geology*, **8**, 31–65.
- Lumb, P. (1979) Statistics of Natural Disasters in Hong Kong, *Proc. 3rd Conf. on Application of Statistics and Probability to Soils and Structural Engineering*, Vol. 1, pp. 9–22.
- Moh and Associates (1994) Report on Geotechnical Study and Conceptual Design of Slope Stabilization Works at Administration Annex and Block 15, Hall of Residence 1, Nanyang Technological University, Jurong, Singapore, Unpublished Report, 58 pp.
- Morgenstern, N. R. (1992) The Evaluation of Slope Stability – A 25 Year Perspective, *Proc. Stability and Performance of Slopes and Embankments – II*, Berkeley, California, Vol. 1, pp. 1–26.
- Murray, L. M. and Olsen, M. T. (1988) Colluvial Slopes – A Geotechnical and Climatic Study, *Proc. 2nd Int. Conf. on Geomechanics in Tropical Soils*, Singapore, Vol. 2, pp. 573–579.
- Pitts, J. (1983) The Form and Causes of Slope Failures in an Area of West Singapore Island, *Singapore Journal of Tropical Geography*, **4**(2), 162–168.
- Pitts, J. (1985) *An Investigation of Slope Stability on the NTI Campus*, Singapore, Applied Research Project RPI/83, Nanyang Technological Institute, Singapore, 54 pp.
- Rahardjo, H., Lim, T. T., Chang, M. F. and Fredlund, D. G. (1995) Shear Strength Characteristics of a Residual Soil, *Canadian Geotechnical Journal*, **32**, 60–77.
- Tan, S. B., Tan, S. L., Lim, T. L. and Yang, K. S. (1987) Landslides Problems and their Control in Singapore, *Proc. 9th Southeast Asian Geotechnical Conf.*, Bangkok, pp. 1:25–1:36.
- Toll, D. G., Rahardjo, H. and Leong, E. C. (1999) Landslides in Singapore, *Proc. 2nd International Conference on Landslides, Slope Stability and the Safety of Infra-Structures*, Singapore, pp. 269–276.
- Varnes, D. J. (1978) Slope Movement Types and Process, in *Landslides—Analysis and Control*, Special Report 176, Transportation Research Board, National Academy of Sciences, USA, pp. 11–33.
- Wei, J., Heng, Y. S., Chow, W. C. and Chong, M. K. (1991) Landslide at Bukit Batok Sports Complex, *Proc. 9th Asian Conf. on Soil Mechanics and Foundation Engineering*, Bangkok, Thailand, Rotterdam: Balkema, Vol. 1, pp. 445–448.



TECHNICAL NOTE

Relationship between porosimetry measurement and soil–water characteristic curve for an unsaturated residual soil

K. K. AUNG, H. RAHARDJO,¹ E. C. LEONG and D. G. TOLL

¹*Corresponding Author Dr H. Rahardjo at NTU-PWD Geotechnical Research Centre, Nanyang Technological University, School of Civil & Structural Engineering, Nanyang Avenue, Singapore 639798*

(Received 30 August 2000; revised 22 February 2001; accepted 22 May 2001)

Abstract. Soil–water characteristic curve (SWCC) is an important tool for determining the engineering properties of unsaturated soil. This depends on the size and distribution of pore structures which control the permeability and amount of volume change. Mercury Intrusion Porosimetry tests can be used to determine the size, amount and distribution of pore spaces of the soil in a shorter time period compared to the pressure plate test. A soil–air characteristic curve (SACC) can be determined using the volumetric air content as measured in the Mercury Intrusion Porosimetry test. In this paper, SACC parameters are introduced. There appears to be a relationship between the soil–air characteristic curve and the soil–water characteristic curve of a soil. Relations between the SACC and the SWCC parameters are analysed in the light of unsaturated soil mechanics. The results indicate that the pore size distribution of a residual soil varies with depth due to differing degrees of weathering.

Introduction

The relationship between gravimetric water content or volumetric water content with matric suction is the soil–water characteristic curve (SWCC). A typical SWCC is shown in Figure 1. Pressure plate tests are commonly used to determine the SWCC. A fully saturated soil specimen having a volumetric water content of θ_s , starts to lose water rapidly when matric suction is increased beyond the air-entry value of the soil. The slope of the SWCC describes the rate of water lost and is termed m_2^w (Figure 1). At high matric suctions, the rate of water loss is negligible and volumetric water content tends to a residual value θ_r . A drying curve can be drawn during water desorption when matric pressure is applied from low to high pressure. When the matric suction in the soil specimen is reduced from high to low pressure, water will be absorbed into the soil specimen and volumetric water content will increase as represented by the wetting curve. Due to hysteresis effects of the soil, the drying and wetting curves do not coincide.

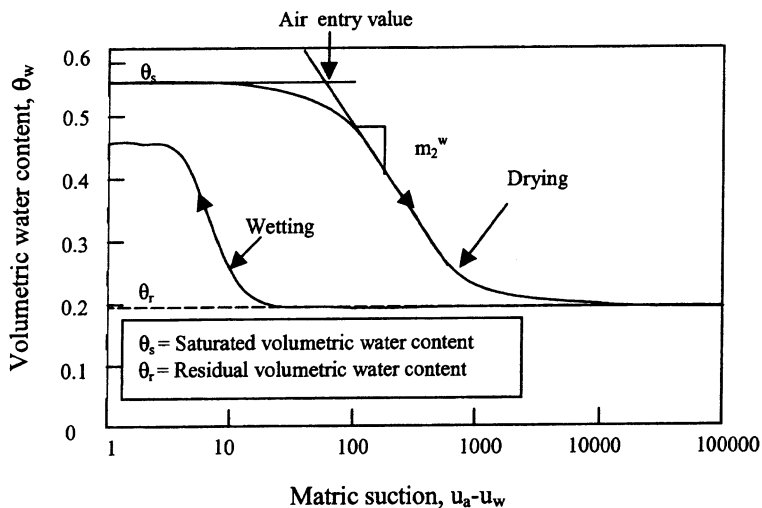


Figure 1. Typical soil-water characteristic curve of a soil.

The SWCC is an important tool in unsaturated soil mechanics. Permeability of unsaturated soil can be calculated using the SWCC and the saturated permeability of the soil (Fredlund and Rahardjo, 1993). Fredlund et al. (1995) and Vanapalli et al. (1996) described a model for the prediction of shear strength with respect to matric suction using SWCC. However, determination of a SWCC is time consuming. The higher the matric suction the longer the time required for the water content of the soil specimen to reach equilibrium. Moreover, total volume change due to swelling and shrinkage of a soil specimen during drying and wetting processes in a pressure plate apparatus cannot be avoided when determining the volumetric water content for the SWCC.

The volume, size, configuration and distribution of pores control the engineering characteristics of the soil. These properties are more prominent in unsaturated soil where effects of air and water phases depend on the amount and distribution of pores in the soil. Various methods such as the tensiometer method, the direct suction method, the pressure plate method and the centrifuge method can be used to determine the soil-water characteristic curve (Croney et al. 1951).

Danielson and Sutherland (1986) identified that the nitrogen sorption method, the water desorption method and the gas pycnometer method can be applied to measure the total pore space and pore-size distribution. However, the Mercury Intrusion Porosimetry (MIP) method has been used as a reliable method to determine total pore spaces and pore-size distribution for a wide variety of porous solids (Diamond, 1970; Ritter and Drake, 1945). A number of researchers have previously attempted to compare MIP test data with soil-water characteristic curves. Purcell (1949) used the MIP test to predict the soil-water characteristic curve

for sandstone. Regab et al. (1982) compared the water desorption method and the MIP method for evaluating soil-water characteristic curve and water conductivity relationship. Prapaharan et al. (1985) also applied the MIP test to determine the SWCC of clayey road subgrade soils.

The basic theory used in the MIP test is similar to that used in the water desorption method in the pressure plate test. The amount and rate of incoming and outgoing water content at various matric suctions are related to the pore structure of the soil. The amount and distribution of pore space using a MIP test could be related to the SWCC of the soil. The objective of this paper is to determine the pore-size distribution of residual soils from the Bukit Timah granitic formation in Singapore at different weathering conditions and to relate the results of the porosimetry curve to the SWCC. By understanding the relation between pore-size distribution and SWCC, the gravimetric and volumetric water content at different matric suction could be estimated in a shorter period of time compared to the traditional method of determining the SWCC using a pressure plate.

COMPARISON OF TEST METHODS

There are some fundamental differences between the pressure plate test and the MIP test. The interface medium in the porosimetry test is a non-wetting liquid, mercury, whereas the interface medium in a pressure plate test is a wetting liquid, water. Schematic diagrams of an air-water interface and a mercury-air interface in a soil pore are shown in Figure 2. Although these two methods have different interface media, they have similar basic characteristics. The pressure plate test measures the amount of water outflow from the soil specimen due to applied air pressure and the MIP test measures the amount of intruded mercury into the evacuated pore

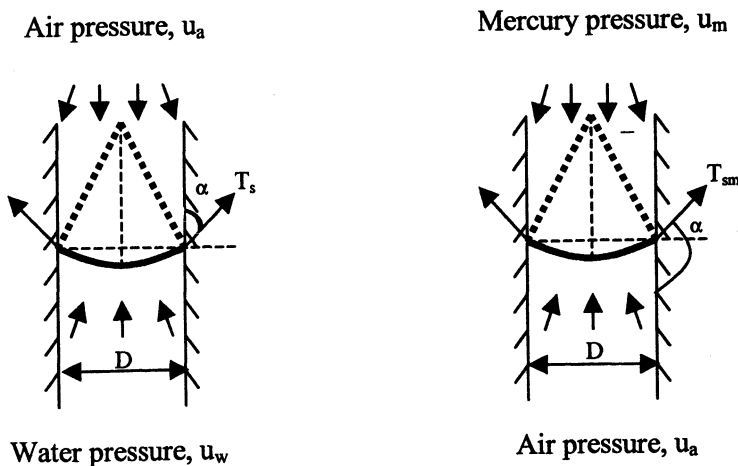


Figure 2. Schematic diagram of air-water interface and mercury-air interface.

spaces. Knowing the total pore space of the soil, the amount of air at different mercury intrusion pressures can be determined.

A pressure plate consists of a pressure vessel with a high-air entry ceramic disk. The high-air entry ceramic disk is used as an interface between air and water pressure. As long as the applied matric suction does not exceed the air entry value of the disk, air will not be able to pass through the saturated high-air entry disk. The axis-translation technique (Hilf, 1956) is employed in the pressure plate test to apply matric suction to soil specimens. Air pressure is supplied within the pressure vessel and the lower part of the high-air entry disk is connected to a burette of water under atmospheric pressure. Since the water pressure below the disk is atmospheric, the applied air pressure represents the applied matric suction.

By assuming that the soil pores can be treated as cylindrical flow channels, Kelvin's equation can be used to determine the equivalent pore diameter, D , at specific matric suction (Fredlund and Raharadjo, 1993). Kelvin's equation is given below:

$$\Delta P = \frac{4T \cos \alpha}{D} \quad (1)$$

where

ΔP = pressure difference between two interfaces

T = surface tension of the denser fluid

α = contact angle of fluid interface to solid

In the pressure plate test, the pressure difference between air and water interfaces is given by the applied matric suction, $(u_a - u_w)$. Atmospheric pressure is taken as zero gauge pressure. The contact angle, α , between the air-water interface and solid particles can be assumed to be zero. Therefore, the equivalent pore diameter corresponding to the air-water interface is given by:

$$(u_a - u_w) = \frac{4T_s}{D} \quad (2)$$

where T_s = surface tension of water (72.75×10^{-3} N/m at 20°C)

In the mercury intrusion porosimetry (MIP) test, the contact angle between mercury and soil particle, α , is more than 90°. Depending on the mineralogy of soil particle as well as its texture, the contact angle between mercury-air interface and soil particle, α , can vary from 100° to 170° (Penumadu and Dean, 1999). An average α of 130° has been used in the analysis. Absolute pressure is used to measure the mercury intrusion pressure into the evaluated pore space. Using Kelvin's equation, the equiv-

alent pore diameter in the porosimetry test (Diamond, 1970) is given in equation (3).

$$(u_m - u_a) = -\left(\frac{1}{D}\right)4T_{sm} \cos \alpha \quad (3)$$

where

D = pore diameter

$u_m - u_a$ = applied net mercury pressure

T_{sm} = surface tension of mercury (485×10^{-3} N/m at 20°C)

α = contact angle between mercury-air interface and solid

The negative sign is used in equation (3) because the α angle is greater than 90° (Prapaharan et al., 1985).

Methodology

SWCC and porosimetry tests were conducted for residual soils from the Bukit Timah granitic formation in Singapore. The soils are the weathering products of the Bukit Timah granite under the hot and humid tropical conditions. Due to the hilly terrain and deep groundwater table, the Bukit Timah granitic residual soils are generally unsaturated in nature. SWCC and porosimetry curve were obtained for soil samples at four different depths (4–6 m, 8.5–9.5 m, 13–17 m and 20.5–21.5 m) taken from a single borehole.

For pressure plate tests, soil specimens were cut to approximately 60 mm in diameter and 25 mm in thickness. The thicker the soil specimen, the longer the time required for the water content of the soil specimen to reach equilibrium at the applied matric suction. On the other hand, a thin specimen is difficult to handle during weighing. Therefore, 25 mm thick specimens were used in the pressure plate tests. These specimens were saturated using water-soaked cotton. The weight of each specimen, which absorbed water from the water-soaked cotton, was measured daily. The specimens were considered saturated when the weight of the specimen remained constant. Matric suctions ranging from 0 to 500 kPa were applied to the soil specimens since a 5 bar high-air entry disk was used in the pressure plate apparatus. The volumetric water contents of the soil specimen were determined at different matric suctions.

An Autopore III porosimetry machine was used to determine the porosity and pore-size distribution of the soils. Specimens were prepared by the freeze-drying method for quick removal of water. Griffiths and Joshi (1989, 1991) and Penumadu and Dean (1999) have recommended the use of the freeze-drying method for specimen preparation in order to minimise disturbance to the pore structure during the drying process.

The specimens prepared for Mercury Intrusion Porosimetry (MIP) test were weighed first before commencing the test. The weighed specimen was then put into

a penetrometer and mounted on the low-pressure port of the machine. An absolute pressure of 50 $\mu\text{m Hg}$ (i.e. close to vacuum) was applied to the specimen for 5 min in order to completely remove the moisture from the soil specimen. Subsequently, a low mercury pressure up to 207 kPa (30 psi) was intruded into the penetrometer. After the low pressurisation was completed, the penetrometer was taken out from the low-pressure port and weighed again. The penetrometer was then mounted on the high-pressure port and a pressure up to a maximum value of 414 MPa (60 000 psi) was applied to the specimen. The stepwise high-mercury pressurisation was controlled automatically by the computer and an equilibrium time of 10 s was used between pressure intervals. Intruded mercury volume and applied mercury pressure were recorded, and porosimetry curves were plotted.

Equivalent pore diameter due to mercury intrusion in the porosimetry tests (Equation 3) and pore diameter at various matric suctions in the pressure plates (Equation 2) can be calculated. Since these two equations originate from Kelvin's equation, the equivalent pore diameter should theoretically be equal for both tests (Equation 4).

$$D = \frac{4T_s}{(u_a - u_w)} = - \frac{T_{sm} \cos \alpha}{(u_m - u_a)} \quad (4)$$

The volume of air in the pore space was calculated by subtracting the volume of intruded mercury from the total pore space. Volumetric air contents were calculated using the volume of air at different pressures and total soil volume to determine the soil-air characteristic curves (SACC). Parameters of the SWCC and SACC were compared to study the possibility of determining a SWCC from porosimetry tests.

Results

Undisturbed samples were taken from the same borehole in the Bukit Timah granitic residual soil using a Mazier sampler (i.e., a triple tube core barrel). Index properties of the Bukit Timah granitic residual soils at four different depths are described in Table 1. The upper portion of the soil in the borehole (0–10 m) was weathered into residual soil, Grade VI (Little, 1969). The deeper portion (10–20 m) was com-

Table 1. Index properties of the Bukit Timah granitic residual soil.

Depth/Soil Classification (USCS)	4–6 m Clayey Silt (MH)	8.5–9.5 m Clayey Silt (MH)	13–17 m Silty Sand (SM)	20.5–21.5 m Silty Sand (SM)
Liquid Limit (LL)	62	67	51	78
Plastic Limit (PL)	41	42	32	37
Natural water content (w%)	54	63	29	20
Specific Gravity (G_s)	2.76	2.62	2.73	2.62
Total Density (ρ , Mg/m ³)	1.62	1.7	2.04	2.0
Porosity (n)	0.62	0.61	0.42	0.36

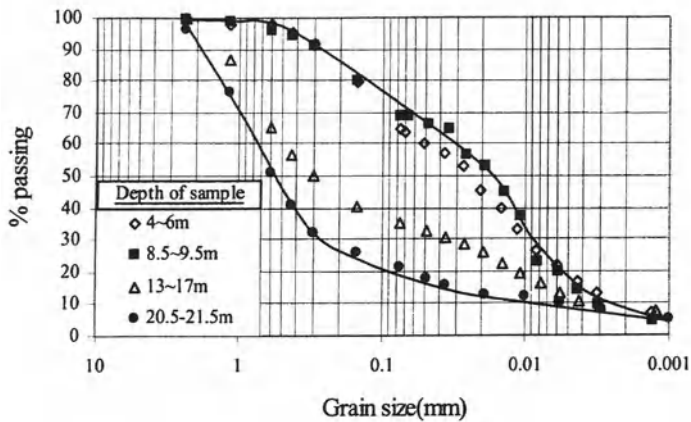


Figure 3. Grain size distribution of Bukit Timah granitic residual soil from different depths.

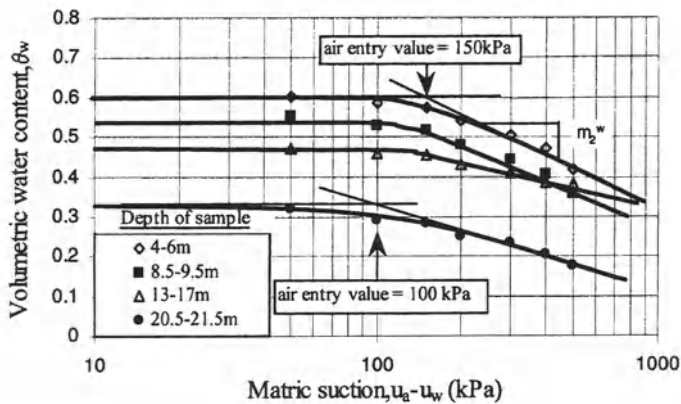


Figure 4. Soil-water characteristic curve for Bukit Timah granitic residual soil from different depths.

pletely weathered but small pieces of Bukit Timah granite could be seen (Grade V). The grain size distributions change with depth as shown in Figure 3. It can be seen that the grading becomes more coarse with depth.

Soil-water characteristic curves for the Bukit Timah granitic residual soil are shown in Figure 4. Air entry values of the SWCC were found to be 150 kPa for the soils at shallow depth. The soils at greater depth have a smaller air entry value of about 100 kPa. The slopes of the soil-water characteristic curve after the air entry value, m_2^w , were found to be constant up to the maximum value of suction of 500 kPa.

Porosimetry curves from the MIP tests are shown in Figure 5. Mercury was intruded from low to high pressures. A larger diameter corresponds to a smaller

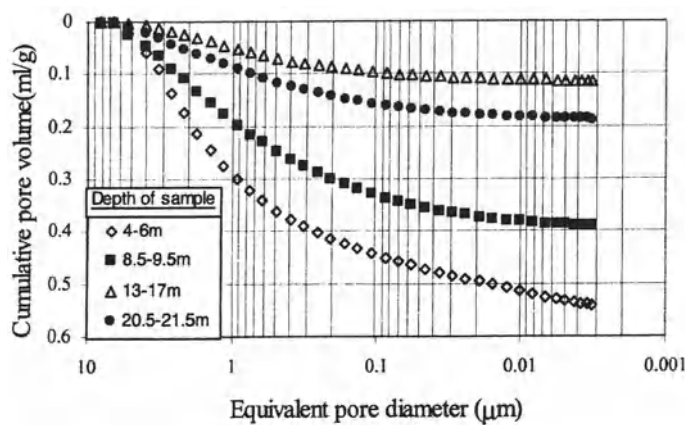


Figure 5. Porosimetry curves for Bukit Timah granitic residual soils from different depths.

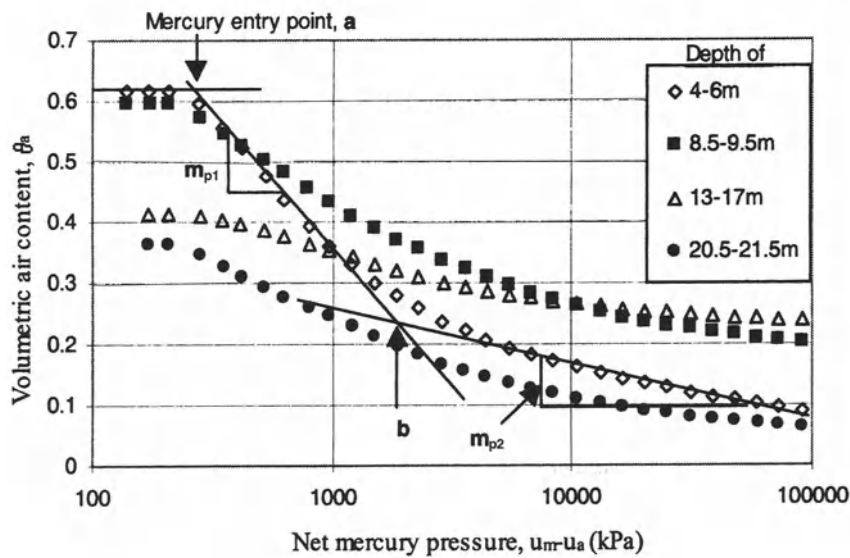


Figure 6. Soil-air characteristic curves for Bukit Timah granitic residual soils from different depths.

mercury pressure. Mercury starts to intrude significantly at diameters between 4 to 6 μm . Intruded mercury volume from the porosimetry curve were converted to volumetric air content (V_a/V_o) using the initial soil volume as V_o . The SACCs were drawn as shown in Figure 6.

Two inflection points, **a** and **b**, and two slopes, m_{p1} and m_{p2} , can be observed from the SACC. The point, **a**, corresponds to the mercury entry value. The amount of

intruded mercury was found to increase with the applied pressure after point **a**. The slope, m_{p1} , shows the change of volumetric air content with respect to pressure. As the pore size becomes smaller, the change of volumetric air content becomes less. Point **b**, determines the turning point towards residual volumetric air content. Slope, m_{p2} , determines the change in volumetric air content mercury at smaller pore size range.

SWCC, SACC and volumetric water and air contents versus equivalent pore diameter at different depths are compared in Figures 7 to 10. A comparison between the values of slopes, m_2^w , m_{p1} and m_{p2} are shown in Table 2. The relationship between m_2^w and m_{p1} are plotted in Figure 11.

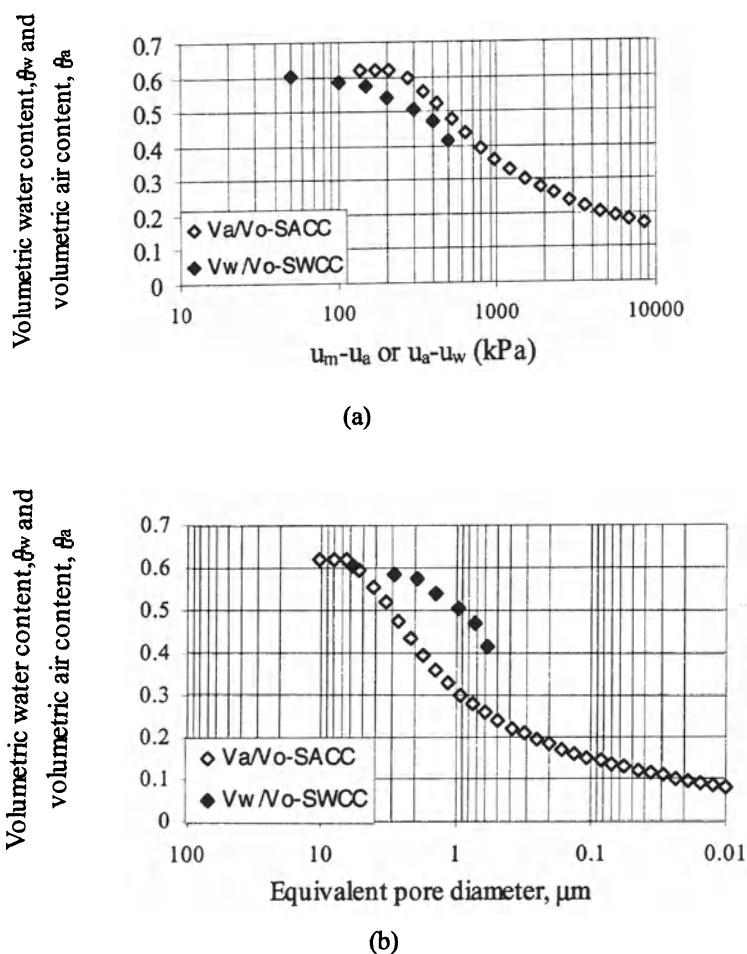
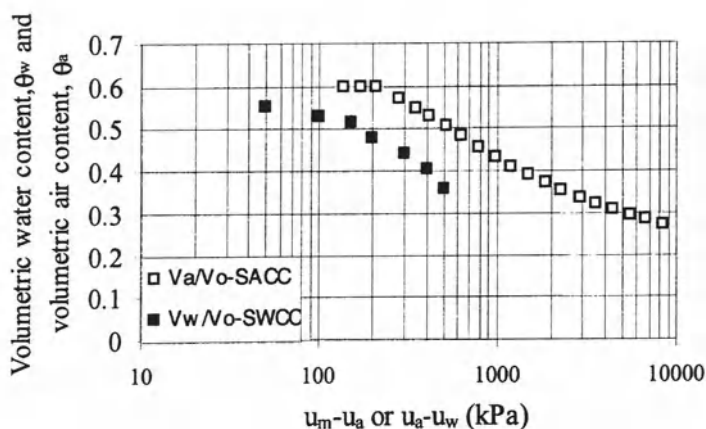
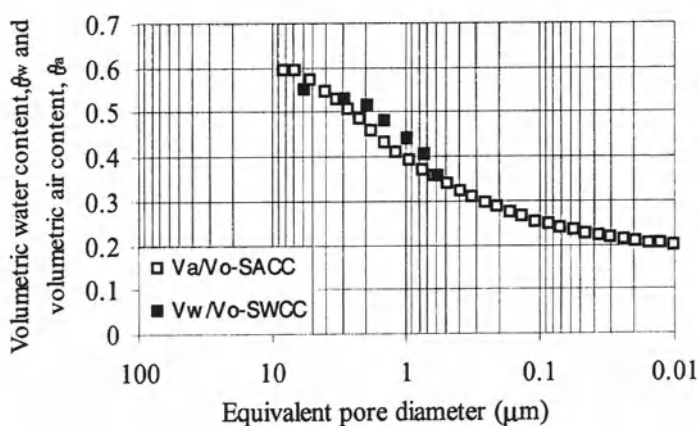


Figure 7. Comparison of (a) SWCC and SACC (b) Volumetric water and air contents versus equivalent pore diameter curve for the soil at 4–6 m depth.



(a)

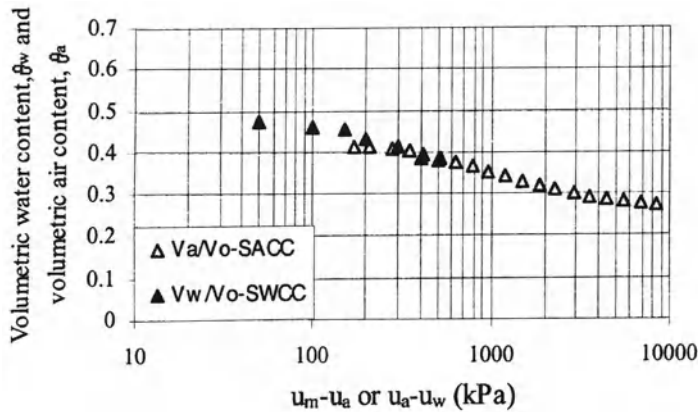


(b)

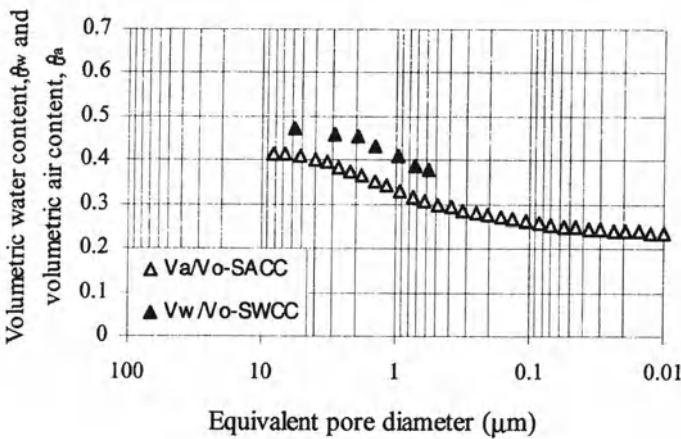
Figure 8. Comparison of (a) SWCC and SACC (b) Volumetric water and air contents versus equivalent pore diameter curve for the soil at 8.5–9.5 m depth.

Discussions

The air entry value of a SWCC depends on the grain size distribution of the soil. When the soil has a larger proportion of fine particles, intra-particle pore space between soil particles becomes smaller and the air entry value is higher. The soils at the shallower depth have fine contents from 60% to 70% (Figure 3) and their air entry values are around 150 kPa (Figure 4). The fine content of soils at greater depths is between 20% and 35% and their air entry values are less, around 100 kPa.



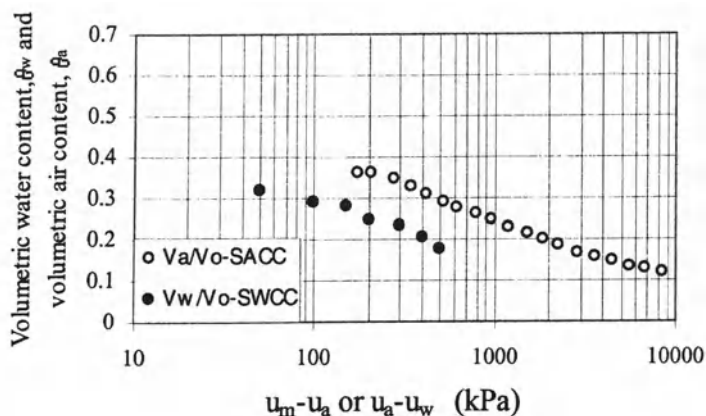
(a)



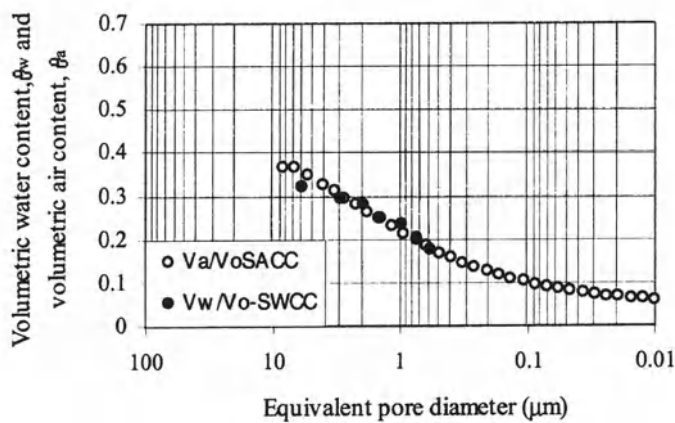
(b)

Figure 9. Comparison of (a) SWCC and SACC (b) Volumetric water and air contents versus equivalent pore diameter curve for the soil at 13–17 m depth.

Using equation (3), equivalent pore diameters at the air entry values are found to range from 2 to 3 μm . The rate of intrusion of mercury starts to change at pore diameters from 4 to 6 μm . This finding shows that the pore diameter at the threshold level of the porosimetry test and the air entry value of the SWCC is reasonably closely related. The small difference in pore diameter between the SWCC and the porosimetry test may be due to the disturbance of larger pore structures during sample preparation for the MIP test. In addition, clay mineralogy and specific surface have a more significant effect on measurements of pore diameter involving water as compared to the measurements using mercury (Prapaharan et al., 1985).



(a)



(b)

Figure 10. Comparison of (a) SWCC and SACC (b) Volumetric water and air contents versus equivalent pore diameter curve for the soil at 20.5–21.5 m depth.

For the same pore diameter, the mercury intrusion pressure in the porosimetry test and the applied matric suction are different due to the different interface media involved in the determination of SWCC and SACC. However, the slope of the SWCC and the SACC are found to be quite similar (Figures 7a–10a). When the volumetric water content and volumetric air content are plotted against equivalent pore diameter, the two curves seem in quite close agreement for depths of 8.5–9.5 m (Figure 8b) and 20.5–21.5 m (Figure 10b). However, the curves for depths of 4–6 m (Figure 7b) and 13–17 m (Figure 9b) show an offset, although the slopes are similar.

Table 2. Comparison between slope of SWCC (m_2^w) and slopes of SACC (m_{p1} and m_{p2}).

Depth (m)	Slope of SWCC (m_2^w)	Slope of SACC (m_{p1})	Slope of SACC (m_{p2})
4.0–6.0	0.352	0.458	0.055
8.5–9.5	0.327	0.258	0.030
13.0–17.0	0.126	0.100	0.023
20.5–21.5	0.176	0.186	0.015

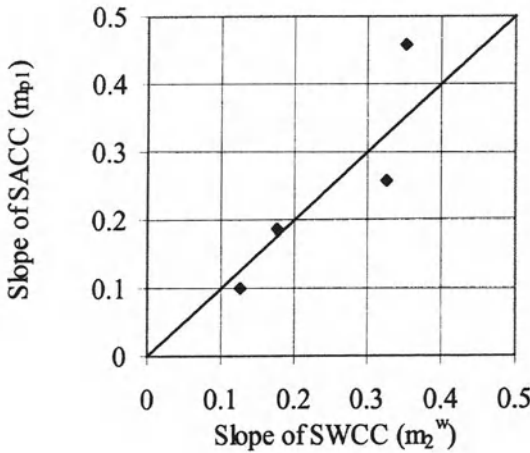


Figure 11. Relationship between slope of SWCC (m_2^w) and slope of SACC (m_{p1}).

The slopes of SWCC and SACC depend on the total amount of pores and their distribution in the smaller pore size range. Figure 11 shows the relation between the slopes of the SWCC (m_2^w) and the SACC (m_{p1}). The relationship between m_2^w and m_{p1} seems to be linear and equal. This linearity reflects the similarity of pore-size distributions predicted by the SWCC and the SACC.

The slopes of both the SWCC and SACC for the Bukit Timah granitic residual soil from different depths are generally found to decrease with depth (Table 2). The trends of change in slopes of the SWCC and the SACC for soil from different depths are shown in Figure 12. It indicates that the volume of pores for soil at shallower depth is larger and well distributed. The change of volumetric air and water content for soils at deeper depths is found to be less. This reflects the changes in grain size due to different degrees of weathering.

It is suggested that the mercury intrusion technique could be used to estimate a SWCC. The initial saturated volumetric water content in the SWCC, θ_s is equal to the initial porosity of the soil specimen. The pore diameters corresponding to the air entry value and the mercury entry value, a , are reasonably similar. The air entry value of the SWCC can be calculated from the pore diameter of soil corresponding to the mercury intrusion point using Equation 2. The slopes of the

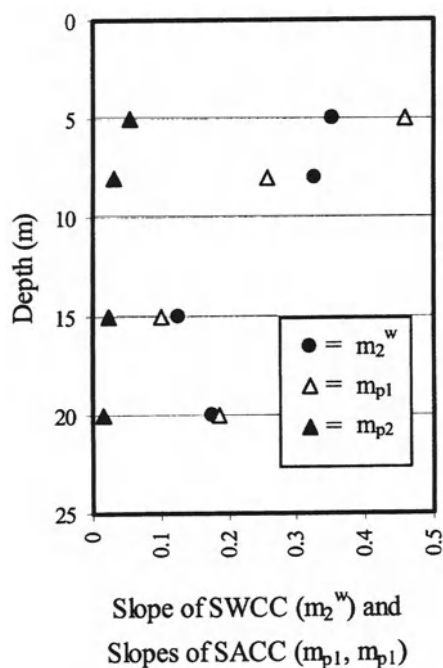


Figure 12. Variation of slopes of SWCC and SACC for the Bukit Timah granitic residual soil from different depths.

two curves have been shown to be equal. Therefore, by knowing the initial porosity, mercury entry value, a , and slope of the SACC, an estimate of the soil-water characteristic curve, SWCC, of a soil can be constructed from MIP test results.

Since a 5-bar pressure plate was used to determine the SWCCs in this study, comparison of parameters up to 500 kPa only was possible. SWCCs at higher matric suctions need to be performed and their results should be compared with parameters from porosimetry tests at high mercury intrusion pressures. The lower range of mercury intrusion pressures should also be used to determine more accurately the mercury entry value. Similar methods should be conducted on different types of unsaturated soils to further verify the validity of this method.

Conclusions

The results of mercury intrusion porosimetry tests on samples of residual soil from Singapore have been analysed to construct a soil-air characteristic curve (SACC). This is compared with the soil-water characteristic curves (SWCC) obtained from pressure plate tests. The pore diameter at air entry value determined from the SWCC is reasonably closely related to the pore diameter at the mercury entry value, a , of the SACC. The slope of the SWCC is also equal to the slope of the SACC. Since mercury

intrusion porosimetry tests can be done in a shorter time compared with pressure plate tests, it is suggested that the parameter of the SWCC can be determined from the porosimetry curve. However, it should be noted that the active interaction between water and clay particles in the pressure plate tests may cause a difference in the resulting SWCC as compared to that obtained from the mercury intrusion porosimetry test, since mercury is not reactive to clay particles. This difference may become more significant in soils with higher clay content.

Acknowledgements

This study is funded by the National Science and Technology Board of Singapore, NSTB 17/6/16: “Rainfall-induced slope failure”. The first author acknowledges the research scholarship provided by Nanyang Technological University.

References

- Croney, D., Coleman, J. D. and Bridge, P. M. (1951) The measurement of the suction of moisture held in porous materials and its relationship to moisture content, Report, Road Research Laboratory, Crowthorne, England.
- Danielson, R. E. and Sutherland, P. L. (1986) Porosity, *Methods of Soil Analysis, Physical and Mineralogical Methods*, Part 1, 2nd edition, Arnold Klute, ed., American Society of Agronomy, 443–460.
- Diamond, S. (1970) Pore size distributions in clays, *Clays and Clay Minerals*, **18**, 7–23.
- Fredlund, D. G. and Morgenstern, N. R. (1976) Constitutive relations for volume change in unsaturated soils, *Canadian Geotechnical Journal*, **13**, 261–276.
- Fredlund, D. G. and Rahardjo, H. (1993) *Soil Mechanics for Unsaturated Soil*, John Wiley and Sons Inc., New York.
- Fredlund, D. G., Xing, A., Fredlund, M. D. and Barbour, S. L. (1995) The relationship of the unsaturated soil shear strength to the soil-water characteristic curve, *Canadian Geotechnical Journal*, **32**, 440–448.
- Griffiths, F. J. and Joshi, R. C. (1989) Change in pore size distribution due to consolidation of clays, *Geotechnique*, **39**, 159–167.
- Griffiths, F. J. and Joshi, R. C. (1991) Change in pore size distribution owing to secondary consolidation of clays, *Canadian Geotechnical Journal*, **28**, 20–24.
- Hilf, J. W. (1956) An investigation of pore-water pressure in compacted cohesive soils, Ph.D. Dissertation, Tech. Memo. No. 654, U.S. Dept. of the Interior, Bureau of Land Reclamation, Design and Construction Div., Denver, CO.
- Little, A. L. (1969) The engineering classification of residual tropical soils, in *Proceedings 7th International Conference on Soil Mechanics and Foundation Engineering*, Mexico City, Mexico, **1**, 1–10.
- Penumadu, D. and Dean, J. (1999) Compressibility effect in evaluating the pore-size distribution of kaolin clay using mercury intrusion porosimetry, *Canadian Geotechnical Journal*, **37**, 393–405.
- Prapaharan, S., Altschaeffl, A. G. and Dempsey, B. J. (1985) Moisture curve of compacted clay: mercury intrusion method, *Journal of Geotechnical Engineering*, **111**(9), 1139–1142.
- Purcell, W. R. (1949) Capillary pressures, their measurement using mercury and the calculation of permeability therefrom, *Petroleum transactions, IME*, **186**, 39–48.

- Regab, R., Feyen, J. and Hillel, D. (1982) Effect of the method for determining pore size distribution on prediction of the hydraulic conductivity function and of infiltration, *Soil Science Society of America*, Proceeding 12: 141–145.
- Ritter, H. L. and Drake, L. C. (1945) Pore size distribution in porous materials: pressure porosimeter and determination of complete macropore size distributions, *Ind. Eng. Chem. Anal. Ed.* 17: 782–786.
- Vanapalli, S. K., Fredlund, D. G., Pufahl, D. E. and Clifton, A. W. (1996) Model for the prediction of shear strength with respect to soil suction, *Canadian Geotechnical Journal*, 33, 379–392.



Contents Volume 19 (2001)

No. 1

Papers

- H. A. ALAWAJI / Shear induced collapse settlement of arid soils 1–19
- JEONGI-GI UM and PINNADUWA H. S. W. KULATILAKE / Kinematic and Block Theory Analyses for Shiplock Slopes of the Three Gorges Dam Site in China 21–42
- FULVIO TONON, BERNARD AMADEI and ERNIAN PAN / Bayesian Estimation of Boundary Conditions with Application to Deep Tunneling 43–67

Technical Note

- AMER ALI AL-RAWAS, ABDULWAHID HAGO, HECTOR H. SUTHERLAND, ALI A. YOUSIF, MOHAMMED AL-SHIHI and BADR AL-SHIHI / A Comparative Quantitative Study of an Omani Soil Using X-Ray Diffraction Technique 69–84

Contents Volume 18 (2000) 85–86

Author index 87

Key word index 87–88

Instructions for authors 89–94

No. 2

Editorial

- DAVID G. TOLL / Editorial 95

Papers

- A. R. BYE and F. G. BELL / Geotechnical applications in open pit mining 97–117
- X. LI, T. S. LOK, D. A. SUMMERS, G. RUPERT and J. TYLER / Stress and energy reflection from impact on rocks using different indentors 119–136
- DAVID C. OYLER, CHRISTOPHER MARK, DENNIS R. DOLINAR and RUSSELL C. FRITH / A study of the ground control effects of mining longwall faces into open or backfilled entries 137–168
- 169–182

Technical Note

- SANJEEV KUMAR / Reducing liquefaction potential using dynamic compaction and construction of stone columns

Book Review 183–184

- C. E. AUGARDE / Modeling in geomechanics: M. Zaman, G. Gioda and J. Booker (eds.)

Nos. 3/4

Special Issue: UNSATURATED SOILS

Edited by D. G. TOLL

Preface	185–187
Papers	
A. TARANTINO and L. MONGIOVÌ / Experimental procedures and cavitation in tensiometer measurements	189–210
DAIZO KARUBE and KATSUYUKI KAWAI / The role of pore water in the mechanical behavior of unsaturated soils	211–241
W. SCOTT SILLERS, DELWYN G. FREDLUND and NOSHIN ZAKERZADEH / Mathematical attributes of some soil–water characteristic curve models	243–283
S. S. AGUS, E. C. LEONG and H. RAHARDJO / Soil–water characteristic curves of Singapore residual soils	285–309
E. ROMERO, A. GENS and A. LLORET / Temperature effects on the hydraulic behaviour of an unsaturated clay	311–332
SANDRA L. HOUSTON, WILLIAM N. HOUSTON, CLAUDIA E. ZAPATA and CHRIS LAWRENCE / Geotechnical engineering practice for collapsible soils	333–355
D. A. CAMERON / The extent of soil desiccation near trees in a semi-arid environment	357–370
H. RAHARDJO, X. W. LI, D. G. TOLL and E. C. LEONG / The effect of antecedent rainfall on slope stability	371–399
Technical Note	
K. K. AUNG, H. RAHARDJO, E. C. LEONG and D. G. TOLL / Relationship between porosimetry measurement and soil–water characteristic curve for an unsaturated residual soil	401–416
Contents Volume 19 (2001)	417–418
Author index	419
Key word index	419–420
Instructions for authors	421–426



Author index

- Agus, S. S., 285
Alawaji, H. A., 1
Al-Rawas, A. A., 69
Al-Shihi, B., 69
Al-Shihi, M., 69
Amadei, B., 43
Augarde, C. E., 183
Aung, K. K., 401
Bell, F. G., 97
Bye, A. R., 97
Cameron, D. A., 357
Dolinar, D. R., 137
Fredlund, D. G., 243
Frith, R. C., 137
Gens, A., 311
Hago, A., 69
Houston, S. L., 333
Houston, W. N., 333
Karube, D., 211
Kawai, K., 211
Kulatilake, P. H. S. W., 21
Kumar, S., 169
Lawrence, C., 333
Leong, E. C., 285, 371, 401
Li, X., 119
Li, X. W., 371
Lloret, A., 311
Lok, T. S., 119
Mark, C., 137
Mongiovi, L., 189
Oyler, D. C., 137
Pan, E., 43
Rahardjo, H., 285, 371, 401
Romero, E., 311
Rupert, G., 119
Sillers, W. S., 243
Summers, D. A., 119
Sutherland, H. H., 69
Tarantino, A., 189
Toll, D. G., 95, 371, 401
Tonon, F., 43
Tyler, J., 119
Um, J.-G., 21
Yousif, A. A., 69
Zakerzadeh, N., 243
Zapata, C. E., 333

Key word index

- Arid soils; collapse potential; direct shear; oedometer; shear strength, 1
Arid soils; collapsible soils; identification; mitigation; wetting, 333
Antecedent rainfall; landslide; numerical modelling; residual soil; seepage; slope stability; unsaturated, 371
Block theory; kinematic analysis; rock slope stability; shiplocks; Three Gorges project, 21
Cavitation; suction; tensiometer; unsaturated soil, 189
Coal mining; ground control; longwall; recovery room, 137
Constitutive equation; suction; unsaturated soil; water retention curve, 211
Design; expansive soil; soil drying; suction; trees, 357
Drillability; dynamic response; impact/penetration resistance; stress wave/energy reflection, 119
Dynamic compaction; earthquake; fine sands; liquefaction; size remediation, 169
Identification; Bayesian probability; tunneling monitoring, *in situ* stress; boundary conditions, 43
Multivariate; residual soil; soil–water characteristic curve; statistical analyses; suction, 285

Open pit mine production; slope stability; geotechnical control, 97

Permeability; retention curve; suction; temperature; unsaturated clay, 311

Pore size distribution; pressure plate test; soil suction; soil–water characteristic curve; unsaturated soil; water content, 243

Quantitative analysis; clays; X-ray diffraction; internal mineral standards, 69



Geotechnical and Geological Engineering

INSTRUCTIONS FOR AUTHORS

EDITOR

David G. Toll

University of Durham, School of Engineering, South Road, Durham, DH1 3LE, UK.

AIMS AND SCOPE

Geotechnical and Geological Engineering publishes papers in the areas of soil and rock mechanics as they relate to civil engineering, mining and offshore industries. The emphasis is on the practical aspects of geotechnical engineering and engineering geology, although papers on theoretical and experimental advances in soil and rock mechanics are also welcomed.

The Journal encompasses a broad range of geotechnical and geological engineering with the following areas given particular priority:

- Case histories describing ground engineering projects including contractual and logistical aspects
- Novel geotechnical construction techniques
- Pollution and environmental problems
- Tropical soil and rock engineering
- Ground investigation, engineering geological and hydrological appraisals
- Computer-aided geotechnical and geological engineering including the application of information technology.

Geotechnical and Geological Engineering publishes contributions in the form of original and review papers, or as short technical notes. A Book Review section informs the discerning reader of the type and quality of literature available to the geotechnical engineer and engineering geologist. Reports on recent meetings and symposia are included.

MANUSCRIPT SUBMISSION

Kluwer Academic Publishers prefer the submission of manuscripts and figures in electronic form in addition to a hard-copy printout. The preferred storage medium for your electronic manuscript is a 3½-inch diskette. Please label your diskette properly, giving exact details on the name(s) of the file(s), the operating system and software used. Always save your electronic manuscript in the word processor format that you use; conversions to other formats and versions tend to be imperfect. In general, use as few formatting codes as possible. For safety's sake, you should always retain a backup copy of your file(s). **After acceptance**, please make absolutely sure that you send the latest (i.e., revised) version of your manuscript, both as hard-copy printout and on diskette.

Kluwer Academic Publishers prefer articles submitted in word processing packages such as MS Word, WordPerfect, etc. running under operating systems MS DOS, Windows and Apple Macintosh, or in the file format LaTeX. Articles submitted in other software programs, as well as articles for conventional typesetting, can also be accepted.

For submission in LaTeX, Kluwer Academic Publishers have developed a Kluwer LaTeX class file, which can be downloaded from: www.wkap.nl/kaphtml.htm/IFAHOME. Use of this class file is highly recommended. Do not use versions downloaded from other sites. Technical support is available at: texhelp@wkap.nl. If you are not familiar with TeX/LaTeX, the class file will be of no use to you. In that case, submit your article in a common word processor format.

For the purpose of reviewing, articles for publication should be submitted as hard-copy printout (five-fold) and on diskette to:

The Journals Editorial Office
Geotechnical and Geological Engineering
Kluwer Academic Publishers
P.O. Box 990
3300 AZ Dordrecht
The Netherlands

For more detailed 'Instructions for Authors' please visit:
<http://www.wkap.nl/journals/gege>

MANUSCRIPT PRESENTATION

The journal's language is English. British English or American English spelling and terminology may be used, but either one should be followed consistently throughout the article. Manuscripts should range in length between 5000 and 10000 words (including references, tables and figures). Manuscripts should be printed or typewritten on A4 or US Letter bond paper, one side only, leaving adequate margins on all sides to allow reviewers' remarks. Please double-space all material, including notes and references. Quotations of more than 40 words should be set off clearly, either by indenting the left-hand margin or by using a smaller typeface. Use double quotation marks for direct quotations and single quotation marks for quotations within quotations and for words or phrases used in a special sense.

Number the pages consecutively with the first page containing:

- running head (shortened title)
- title
- author(s)
- affiliation(s)
- full address for correspondence, including telephone and fax number and e-mail address

Abstract

Please provide a short abstract of 100 to 250 words. The abstract should not contain any undefined abbreviations or unspecified references.

Key Words

Please provide 5 to 10 key words or short phrases in alphabetical order.

Abbreviations

Abbreviations should be explained at first occurrence.

Symbols and Units

ISSMGE units and symbols should be used. Where measurements are given in other systems, conversion factors or conversions should be inserted by the author.

Figures and Tables*Submission of electronic figures*

In addition to hard-copy printouts of figures, authors are encouraged to supply the electronic versions of figures in either Encapsulated PostScript (EPS) or TIFF format. Many other formats, e.g., Microsoft Postscript, PiCT (Macintosh) and WMF (Windows), cannot be used and the hard copy will be scanned instead.

Figures should be saved in separate files *without* their captions, which should be included with the text of the article. Files should be named according to DOS conventions, e.g., 'figure 1.eps'. For vector graphics, EPS is the preferred format. Lines should not be thinner than 0.25pts and in-fill patterns and screens should have a density of at least 10%. Font-related problems can be avoided by using standard fonts such as Times Roman and Helvetica. For bitmapped graphics, TIFF is the preferred format but EPS is also acceptable. The following resolutions are optimal: black-and-white line figures – 600–12 dpi; line figures with some grey or coloured lines – 600 dpi; photographs – 300 dpi; screen dumps – leave as is. Higher resolutions will not improve output quality but will only increase file size, which may cause problems with printing; lower resolutions may compromise output quality. Please try to provide artwork that approximately fits within the typeset area of the journal. Especially screened originals, i.e. originals with grey areas, may suffer badly from reduction by more than 10–15%.

AVOIDING PROBLEMS WITH EPS GRAPHICS

Please always check whether the figures print correctly to a PostScript printer in a reasonable amount of time. If they do not, simplify your figures or use a different graphics program.

If EPS export does not produce acceptable output, try to create an EPS file with the printer driver (see below). This option is unavailable with the Microsoft driver for Windows NT, so if you run Windows NT, get the Adobe driver from the Adobe site (www.adobe.com).

If EPS export is not an option, e.g., because you rely on OLE and cannot create separate files for your graphics, it may help us if you simply provide a PostScript dump of the entire document.

HOW TO SET UP FOR EPS AND POSTSCRIPT DUMPS UNDER WINDOWS

Create a printer entry specifically for this purpose: install the printer 'Apple Laserwriter Plus' and specify 'FILE': as printer port. Each time you send something to the 'printer' you will be asked for a filename. This file will be the EPS file or PostScript dump that we can use.

The EPS export option can be found under the PostScript tab. EPS export should be used only for single-page documents. For printing a document of several pages, select 'Optimise for portability' instead. The option 'Download header with each job' should be checked.

Submission of hard-copy figures

If no electronic versions of figures are available, submit only high-quality artwork that can be reproduced as is, i.e., without any part having to be redrawn or re-typeset. The letter size of any text in the figures must be large enough to allow for reduction. Photographs should

be in black-and-white on glossy paper. If a figure contains colour, make absolutely clear whether it should be printed in black-and-white or in colour. Figures that are to be printed in black-and-white should not be submitted in colour. Authors will be charged for reproducing figures in colour.

Each figure and table should be numbered and mentioned in the text. The approximate position of figures and tables should be indicated in the margin of the manuscript. On the reverse side of each figure, the name of the (first) author and the figure number should be written in pencil; the top of the figure should be clearly indicated. Figures and tables should be placed at the end of the manuscript following the Reference section. Each figure and table should be accompanied by an explanatory legend. The figure legends should be grouped and placed on a separate page. Figures are not returned to the author unless specifically requested.

In tables, footnotes are preferable to long explanatory material in either the heading or body of the table. Such explanatory footnotes, identified by superscript letters, should be placed immediately below the table.

Section Headings

Section headings should be numbered (e.g., 1., 1.1, 1.1.1, 2., 2.1, etc.)

Appendices

Supplementary material should be collected in an Appendix and placed before the Notes and Reference sections.

Notes

Please use endnotes rather than footnotes. Notes should be indicated by consecutive superscript numbers in the text. A source reference note should be indicated by means of an asterisk after the title. This note should be placed at the bottom of the first page.

Cross-Referencing

In the text, a reference identified by means of an author's name should be followed by the date of the reference in parentheses and page number(s) where appropriate. When there are more than two authors, only the first author's name should be mentioned, followed by 'et al.'. In the event that an author cited has had two or more works published during the same year, the reference, both in the text and in the reference list, should be identified by a lower case letter like 'a' and 'b' after the date to distinguish the works.

Examples:

Winograd (1986, p. 204)

(Winograd, 1986a, b)

(Winograd, 1986; Flores et al., 1988)

Acknowledgements

Acknowledgements of people, grants, funds, etc., should be placed in a separate section before the References.

References

References to books, journal papers, articles in collections and conference or workshop proceedings, and technical reports should be listed at the end of the article in alphabetical order following the Harvard system (see examples below). Articles in preparation or articles

submitted for publication, unpublished observations, personal communications, etc. should not be included in the reference list but should only be mentioned in the article text (e.g. T. Moore, personal communication).

References to books should include the author's name; year of publication; title; page numbers where appropriate; publisher; place of publication, in the order given in the example below.

Owen, D.R.J. (1980) *Finite Elements in Plasticity: Theory and Practice*, Pineridge Press, Swansea.

References to articles in an edited collection should include the author's name; year of publication; article title; editor's name; title of collection; first and last page numbers; publisher; place of publication, in the order given in the example below.

Quigley, R.M. (1983) Glaciolacustrine and glaciomarine clay deposition: A North American perspective. In *Glacial Geology: An Introduction for Engineers and Earth Scientists* (edited by N. Eyles), Pergamon Press, Oxford, pp. 140–167.

References to articles in conference proceedings should include the author's name; year of publication; article title; editor's name (if any); title of proceedings; first and last page numbers; place and date of conference; publisher and/or organization from which the proceedings can be obtained; place of publication, in the order given in the example below.

Cowland, J.W. and Carbray, A.M. (1988) Three cut slope failures on relict discontinuities in saprolitic soils, in *Proceedings of the Second International Conference on Geomechanics in Tropical Soils*, Singapore, Balkema, Rotterdam, Vol. 1, pp. 253–258.

References to articles in periodicals should include the author's name; year of publication; article title; full title of periodical; volume number (issue number where appropriate); first and last page numbers, in the order given in the example below.

Irfan, T.Y. (1994) Mechanism of creep in a volcanic saprolite, *Quarterly Journal of Engineering Geology*, **27**(3), 211–230.

References to technical reports or doctoral dissertations should include the author's name; year of publication; title of report or dissertation; institution, location of institution, in the order given in the example below.

Bement, R.A.P. (1996) Ground compaction due to vibrodriving of piles. PhD Thesis, University of Durham, U.K.

PROOFS

Proofs will be sent to the corresponding author. One corrected proof, together with the original, edited manuscript, should be returned to the Publisher within three days of receipt by mail (airmail overseas).

OFFPRINTS

50 offprints of each article will be provided free of charge. Additional offprints can be ordered by means of an offprint order form supplied with the proofs.

PAGE CHARGES AND COLOUR FIGURES

No page charges are levied on authors or their institutions. Colour figures are published at the author's expense only.

COPYRIGHT

Authors will be asked, upon acceptance of an article, to transfer copyright of the article to the Publisher. This will ensure that the widest possible dissemination of information under copyright laws.

PERMISSIONS

It is the responsibility of the author to obtain written permission for a quotation from unpublished material, or for all quotations in excess of 250 words in one extract or 500 words in total from any work still in copyright, and for the reprinting of figures, tables or poems from unpublished or copyrighted material.

ADDITIONAL INFORMATION

Additional information can be obtained from:

Drs. Petra D. van Steenbergen
Publishing Editor
Kluwer Academic Publishers
Spuiboulevard 50
P.O. Box 17
3300 AA Dordrecht
The Netherlands

Phone: (+31) 78 639 22 35

Fax: (+31) 78 639 23 88

E-mail: Petra.vanSteenbergen@wkap.nl